SEMI-ACTIVE ADAPTIVE CONTROL OF COUPLED STRUCTURES FOR SEISMIC HAZARD MITIGATION

A Dissertation

by

OMAR AHMED SALEH AL-FAHDAWI

Submitted to the Office of Graduate and Professional Studies of
Texas A&M University
in partial fulfillment of the requirements for the degree of

DOCTOR OF PHILOSOPHY

Chair of Committee,	Luciana R. Barroso
Committee Members,	John M. Niedzwecki
	Harry L. Jones
	H. Joseph Newton
Head of Department,	Robin Autenrieth

May 2019

Major Subject: Civil Engineering

ABSTRACT

The research presented in this dissertation examines innovative structures connected with smart control devices driven by adaptive control methods. The research focuses on understanding the dynamics of coupled structures and evaluating the merits of adaptive control in enhancing the seismic performance of these structures and dealing with uncertainties.

Coupled structures is recognized as an effective strategy to protect civil structures from seismic excitations. Coupling of adjacent structures has proved to offer functional benefits such as the potential for shifting the buildings' natural frequencies, likely leading to a reduction in the natural period of vibration. Structural performance is further enhanced by implementing energy-dissipative devices to connect adjacent buildings to minimize the seismic structural responses.

One of the main challenges to control civil structures is the high uncertainty involved throughout their lifetimes. Adaptive control promises to deal with changes in structures' characteristics, such as seismic-induced damage. The simple adaptive control method, which is a reference-model following scheme, is used in the current research to improve the seismic behavior of adjacent buildings connected by structural links where control devices are implemented. The philosophy of the simple adaptive control method is that an actual system (often called plant) can be forced to track the behavior of pre-determined trajectories through adjustable adaptive gains. The effectiveness of the simple adaptive controller in reducing the seismic responses is compared with other adaptive and

non-adaptive control methods. The results reveal that the simple adaptive controller is effective in alleviating the structural responses and dealing with uncertainties of coupled structures with both linear and nonlinear behavior. The results also show that the coupling strategy is viable for reducing the structural responses under seismic excitations.

DEDICATION

To my parents, my brothers and sisters, and all my friends

ACKNOWLEDGEMENTS

I would like to thank my committee chair, Dr. Barroso, and my committee members, Dr. Niedzwecki, Dr. Jones, and Dr. Newton, for their guidance and support throughout the course of this research.

Thanks also go to my friends and colleagues and the department faculty and staff for making my time at Texas A&M University a great experience.

Finally, thanks to my mother and father for their encouragement and to my brothers and sisters for their continuous support.

CONTRIBUTORS AND FUNDING SOURCES

Contributors

This work was supervised by a dissertation committee consisting of Dr. Luciana R. Barroso [advisor], Dr. John M. Niedzwecki, and Dr. Harry L. Jones of the Department of civil engineering at Texas A&M University and Dr. H. Joseph Newton of the Department of Statistics at Texas A&M University.

All work conducted for the dissertation was completed by the student independently.

Funding Sources

Graduate study was supported by a scholarship from the Higher Committee For Education Development (HCED) in Iraq.

TABLE OF CONTENTS

Page

Page

Page

LIST OF FIGURES

Page

Page

Page

Page

Page

Page

LIST OF TABLES

Page

CHAPTER I

INTRODUCTION AND LITERATURE REVIEW

Civil engineering structures are exposed to extreme hazards such as earthquakes, waves, and strong winds that may cause large-scale damage. Specifically, structural damage caused by earthquakes can be detrimental to the infrastructures and their human occupants. Protection of the structures demands structural safety and human survivability. As an example of earthquakes, Loma Prieta earthquake occurred in October 1989 in Northern California with 6.9 magnitude and IX intensity on the Mercalli intensity scale. The event caused 63 people to lose their lives and about 3,560 were injured. Even though the death toll was not high compared to other earthquakes, the impact on the infrastructures was devastating. The estimated damage cost caused by the quake was about $6 billion in property damage. The most impacted area was San Francisco and Oakland where more than 28,000 homes and businesses were collapsed and about four major highways were severely damaged (Stover, Coffman, & Scott, 1993). The second example is Northridge earthquake which occurred also in California in 1994 with 6.8 magnitude. The death toll was 60 people and the damage cost was estimated about $20 billion (Christenson & Spencer, 2001). Another example is Kobe earthquake which occurred in Japan 1995, with a magnitude of 6.9 on Richter scale. About 5,502 people were killed during the event and more than 36,000 were injured, and more than 200,000 buildings were either severely damaged or destroyed. The economic loss was estimated around $147 billion. Some of the

major earthquakes in terms of loss in lives and properties are listed in Table 1 (Christenson & Spencer, 2001).

Table 1: Loss of Life and economy for some major earthquakes.

Location	Date	Magnitude	Loss of Lives	Economic Loss
Northridge, USA	01/17/1994	6.8	60	$20 billion
Kocaeli, Turkey	08/17/1999	7.8	15,637	$6.5 billion
Chi-Chi, Taiwan	09/28/1999	7.7	2,400	$14 billion
Bhuj, India	01/26/2001	8.0	20,005	$4.5 billion

The above statistics remind us that our structures and their occupants are vulnerable to seismic hazards. Therefore, protection of people and infrastructures should be the highest priority for structural engineers.

1.1 Structural Control

Structural control for civil engineering structures was developed to provide safer and more efficient designs through dissipating the energy introduced by environmental loads such as earthquakes. Implementation of the control theory in structural engineering applications can reduce the unwanted vibrations, retrofitting existing structures, and developing a new design methodology based on structural motion. Structural control is usually carried out by using supplemental dissipative devices to modify the structural dynamics.

The structural control strategies are classified based on the class of control devices into three main categories: (1) passive, (2) active, and (3) semi-active. Passive devices do not require an external source of power to function, but they use the structural motion to

absorb energy. Since there is no external power supply, the passive devices do not have a potential to destabilize the structural systems. The second type of control devices is active which requires a significant amount of power to operate. The third type of supplemental devices is the semi-active which combines the desirable aspects of both passive and active devices. Semi-active devices require a very small amount of power which makes it possible to use batteries to keep these devices running during hazardous events as the power supply might fail.

1.1.1 Passive Control

Passive control systems are activated by the external input energy only with no need for additional power sources. Passive devices are usually attached to the structures. These devices have fixed characteristics and they require to be tuned to protect the structure under a particular type of loading (Christenson & Spencer, 2001). Therefore, passive devices might be ineffective when the structure is exposed to different types of dynamic loading. Passive devices include metallic yield dampers, friction dampers, visco-elastic dampers, viscous fluid dampers, base isolators, tuned liquid dampers, and tuned mass dampers (Housner et al., 1997). Passive control has been widely used because of its simplicity and inherent stability. However, the performance of passive control under seismic events is sometimes limited because of the impulsive nature of earthquakes which does not give enough time for passive devices to respond (Connor & Laflamme, 2014).

1.1.2 Active Control

Active control strategy imposes control forces on structures that counteract the earthquake-induced forces. Active systems require external power source and computer-controlled devices to determine appropriate control forces through closed-loop feedback action. Active control is more efficient than passive control and more complex since it requires computer control, sensors, feedback, and actuators. Sensors are required to measure either the structural responses or the external excitations, or both. Feedback is used when only the structural responses are measured and passed to the controller to make continual corrections on the generated control forces. Feedforward, on the other hand, refers to the case where the control forces are determined only by measuring the external excitation. Feedback-feedforward control is used where both the responses and excitations are measured (Spencer & Soong, 1999). Generally, active devices require a large amount of power which makes it difficult to provide them with an emergency source of power to keep the control system operable during earthquakes or immediately after. Another drawback of the active devices is that their performance may result in unstable system if the control system is not well designed. Some examples of active devices include active mass damper, active tuned liquid damper, active base isolation, and active bracing (Soong & Spencer, 2002; Spencer & Soong, 1999). To overcome the issues attributed to active control, hybrid control has emerged to alleviate some of the active control limitations. Hybrid control combines both passive and active control in one framework to reduce the latter energy requirements. Care still must be exercised to ensure that the structure is not

rendered unstable as a result of neglecting sensors' and/or actuators' dynamics (Housner et al., 1997).

Active control has been widely implemented in the last quarter of the previous century. For instance, the first full-scale active mass driver was installed in the Kyobashi Seiwa building in Tokyo, Japan, to increase its resilience against winds and moderate earthquakes (Kobori et al., 1993), as shown in Figure 1. Nearly 35 buildings and 15 bridges in Japan, China, Taiwan and Korea have been equipped with active and hybrid control devices. For a full list of active and hybrid control application, see (Spencer & Soong, 1999). Despite impressive success, structural engineers have not fully embraced active devices because of the large power requirement, system stability, and maintenance of the devices (Spencer & Sain, 1997).

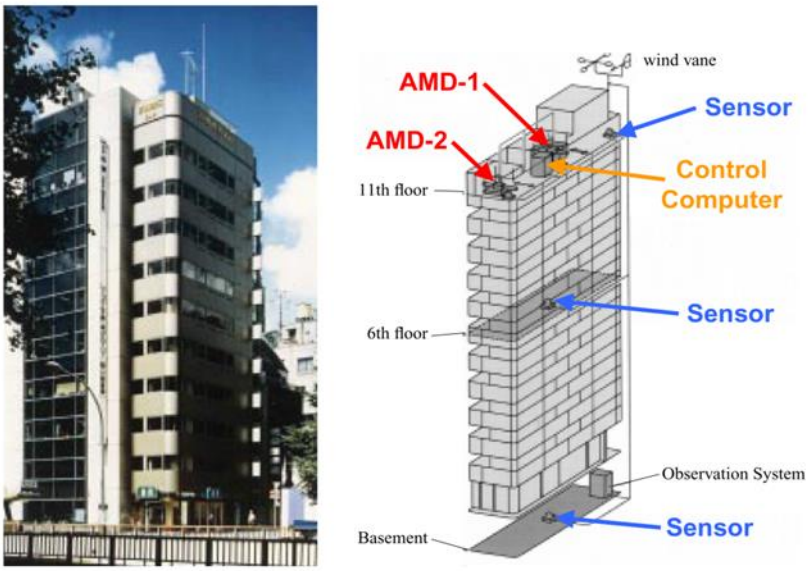

Figure 1: Kyobashi Seiwa building equipped with AMD in Japan (reprinted from Christenson & Spencer, 2001).

1.1.3 Semi-active Control

Semi-active control devices combine the best features of both passive and active control devices, as shown in Figure 2. Semi-active devices require very small external energy to operate, which makes it possible for batteries to be used to keep the control system running during hazardous events when the external power source may fail (Housner et al., 1997). Moreover, semi-active does not have a potential to render the structural systems unstable. Many studies have shown that appropriately used semi-active devices surpass the passive devices and have a potential to perform even better than the active devices (Dyke & Spencer, 1996). Some examples of semi-active control devices include variable stiffness devices, variable orifice fluid dampers, controllable fluid dampers, controllable friction devices, controllable-impact dampers, tuned liquid dampers, Magneto-rheological (MR), and Electro-rheological (ER) dampers (Housner et al., 1997).

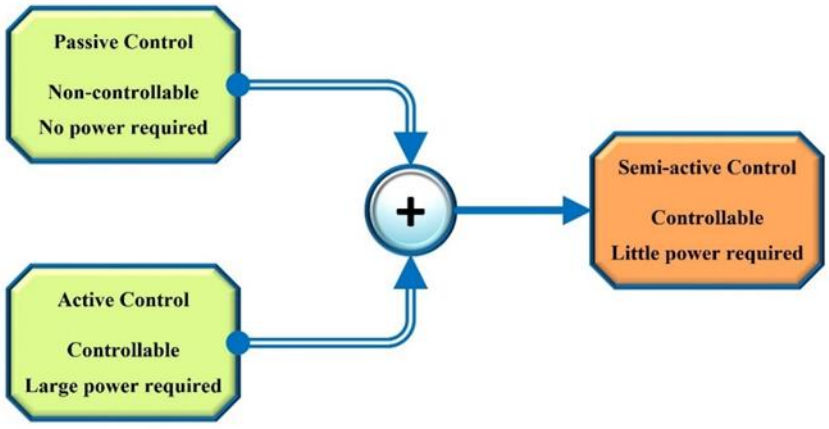

Figure 2: Main control strategies and associated devices.

Various control algorithms have been developed to regulate the hysteretic behavior of the semi-active devices. In fact, designing and practically implementing control algorithms is one of the most important and challenging tasks. Some examples of these algorithms are the bang-bang controller (McClamroch & Gavin, 1995; Mukai, Tachibana, Inoue, 1994), fuzzy control (Sun & Goto, 1994), Lyapunov theory-based algorithm (Brogan, 1991), modified Linear Quadratic Regulator, modulated homogeneous friction algorithm (Inaudi, 1997), and clipped-optimal control (Jansen & Dyke, 2000).

1.2 Coupled Buildings: Background

Protection of civil engineering structures from undesirable vibrations due to environmental events is crucial for maintaining structural integrity. Seismic events can induce severe plastic behavior in structures, threatening the human comfort in these structures and more seriously their safety. Some of structures have begun utilizing modern control technologies to help attenuate structural responses. Close-distance building construction is recognized as an effective strategy for utilizing limited land space within large cities. Coupling of adjacent structures has proved to offer architectural and functional benefits and to be a viable alternative for protecting close buildings (Seto, 1994). One functional-benefit example is the use of skywalks, as used at the Petronas Twin Towers in Malaysia and the World Trade Center in Bahrain, as shown in Figure 3 and Figure 4, respectively. The skywalks have been added to connect two or more structures to provide connections between these structures which may offer some architectural advantages. The skybridges serve as walkways for pedestrians from one building to

another which might serve, at the same time, as an escape way for people in case of disasters. Also, the skyways can be used to separate pedestrians from traffic in case where the connected buildings are on both sides of streets. Another advantage of using skybridges is that they add aesthetic feature to adjacent buildings which provides a spectacular view for people passing over these skywalks.

Another advantage of connecting buildings for functionality is the potential for shifting the buildings' natural frequencies, likely leading to a reduction in the natural period of vibration. The coupling theory utilizes non-identical adjacent buildings to impart forces on one building due to the other in such a way that structural responses might be alleviated. Structural performance can be further enhanced by implementing energy-dissipative devices to connect adjacent buildings, a proven effective approach to avoid pounding and minimize structural response (Bharti, Dumne, & Shrimali, 2010). Another advantage of the coupled systems theory appreciated by both architects and business owners is the use of control devices outside buildings, allowing more free space inside and likely minimizing the number of required control devices compared to classically separated buildings. The first proposals of connecting adjacent buildings were in the early 1970s by professor Klein (Klein, Cusano, & Stukel, 1973) in the United States and in 1976 by Kunieda in Japan (Kunieda, 1976). Coupled buildings theory gained more attention in Japan as full-scale applications began to appear. The coupling strategy of using full-scale devices to couple adjacent buildings was implemented in Japan for the Kajima Intelligent building complex in 1989 and for the Harumi Island Triton Square office complex in 2001 (Christenson et al., 2006).

In some cases where buildings lie in earthquake-prone areas, designers tend to divide structures totally with seismic joints. These joints are added to structures in order to reduce the higher modes effects and torsional loads (Kim, Ryu, & Chung, 2006). This structural requirement separates single buildings making them behave as different adjacent buildings.

Figure 3: Petronas Twin Tower Skybridge (reprinted from Rogers, 2017).

Figure 4: Bahrain World Trade Center (reprinted from Lomholt, 2018).

In the case of adjacent buildings, the clearance distance needs to be large enough to prevent pounding. Seismic pounding between adjacent buildings has been observed in most previous major earthquakes and has caused a significant amount of damage. The spatial variation of the ground motion and the difference in the dynamic properties of the adjacent buildings may lead them to vibrate out-of-phase, causing a collision if the separation gap between the buildings is not large enough. Regarding the spatial variation

of the ground motion, pounding occurs due to excessive liquefaction of soil, which has the potential to increase the magnitude of the relative responses between adjacent structures and thus increase the severity of the damage. The collided structures sustain large impact forces for a short time duration, which is not specifically considered in the design codes (Hao, 2015). The impact forces cause damage around the pounding areas and may worsen the overall structural responses. Moreover, pounding could cause huge damage in non-structural elements such as curtain walls, and in some extreme cases may lead to a total collapse. Figure 5 shows some pounding induced damage under different earthquakes.

(a)

(b)

Figure 5: Pounding damage: (a) 1999 Taiwan earthquake and (b) 2008 Wenchuan earthquake (reprinted from Hao, 2015).

In the following section, a review of publications dealing with the dynamic analysis and the structural control of coupled structures is presented. No claim is made that this review is fully comprehensive, but it could be said it is not lacking an essential line of research relevant to the subject matter.

1.3 Coupled Buildings: Literature Review

Interest in coupled buildings began in the U.S. in 1972 when Klein et al. proposed the concept of connecting two buildings. Four years later, Kunieda (1976) embraced the idea and expanded it to coupled multiple buildings. In the 1987, Klein and Healey proposed connecting adjacent structures with cables that could be released and tightened to provide control forces. It was observed in that research that for coupled buildings with a single link, the fundamental natural frequencies must be different to ensure controllability. Westermo (1989) suggested connecting adjacent floors by a hinge-ended beam to carry the axial force and to maintain the separation between these floors. In case of unaligned floors, the author suggested using a simply supported beam spread between two consecutive floors in one building connected to the corresponding floor in the other building. It was concluded that connecting adjacent buildings with a hinged link reduces the pounding effects but reverses the dynamic characteristics of the uncoupled structures, which may lead to some adverse torsional responses (Westermo, 1989).

Along with advancements in structural control in the early 1990's, interest in coupling strategy was accelerated. For instance, in 1994, both passive and active control strategies were employed to connect single-degree-of-freedom building models where the

LQR control method was utilized to drive the active devices (Graham, 1994). The study concluded that the active control strategy can further reduce the responses of the coupled system compared to the passive scheme. An enormous number of studies on using passive control to mitigate the responses of tall coupled buildings were conducted (Fukuda, Matsumoto, & Seto, 1996; Gurley et al., 1994; Sakai et al., 1999). Short to medium buildings were also considered in many publications (Ko, Ni, & Ying, 1999; Luco & Wong, 1994; Luco & De Barros, 1998; Xu, He, & Ko, 1999). All these papers reveal encouraging results in attenuating the structural responses due to wind and earthquakes.

More sophisticated control strategies for the coupled systems have been investigated. The active control strategy was studied for the connected structures in many publications. Seto (1999) proposed connecting four parallel high-rise buildings with hydraulic actuators to control the low frequency motion. The study was successful in controlling the first two modes of three connected building models both theoretically and experimentally (Christenson & Spencer, 2001). Many other studies utilizing active control were published during and after the 1990s in the subject (Fukuda, Matsumoto, Seto, 1996; Hori & Seto, 2000; Kamagata, Miyajima, & Seto, 1996; Matsumoto, 1998; Mitsuta et al., 1994; Ohkawa, 1990; Seto, Toba, & Matsumoto, 1995). Christenson et al. (2006) studied the effects of the configuration connector on the frequency and mode shapes of coupled buildings. Both passive and active control methods were considered and the effectiveness of the two strategies were compared over a range of building configurations. The two buildings were modeled as cantilever beams with different height, mass, and stiffness and the connector location was at the top floor of the shorter building. Tehrani and Gattulli

(2016) introduced a nonlinear damping to connect two adjacent linear oscillators subject to harmonic excitation. The model was chosen to represent different classes of engineering structures, specifically close tall buildings, and it was tested with different base excitation frequencies and amplitudes. The authors also conducted a parametric study to find the optimum damping ratio. The results show that the nonlinear damping model is more effective in terms of vibration control than the linear model.

The idea of connecting adjacent buildings with passive control devices to reduce earthquake-induced vibrations has received a great deal of attention from researchers. Richardson, Walsh, & Abdullah (2013) formulated closed-form equations of two close buildings connected with corresponding stiffness and damping elements. In that study, the fixed-point theory was introduced as it applied to connected buildings. The fixed-point parameters such as stiffness and damping were calculated through creating the transmissibility curves of the system. The upshot of the analysis shows that the displacement and acceleration of the coupled system were generally reduced compared to the uncoupled case. The efficacy of using the viscous dampers to connect two adjacent buildings was investigated (Bhaskararao & Jangid, 2007). The adjacent structures were modeled as single-degree-of-freedom systems connected with viscous damper and subjected to base harmonic acceleration and white noise process. An expression of the damping parameter of the device was derived, which was found to be as a function of mass and frequency of the coupled system. A significant amount of reduction in the seismic responses was observed as claimed by the authors.

Semi-active control was also implemented successfully to connect adjacent building structures in many studies. As an example, an analytical study was conducted on utilizing the mutual interaction of coupled buildings to mitigate the seismic responses (Zhu, Wen, & Iemura, 2001). In this study, one building was considered as the main building where the goal was to reduce its responses, and the second building was considered as an auxiliary. Both buildings were modeled as single-degree-of-freedom systems connected by a dashpot. In the past few years, the Magneto-rheological (MR) damper has been embraced by the researchers because of its promising features. Bharti, Dumne, Shrimali (2010) suggested connecting colinear floors of two adjacent buildings with Magneto-rheological (MR) dampers. The Lyapunov's direct algorithm was utilized in the study as a semi-active control algorithm, which involves the use of the well-known Lyapunov stability theory. The research shows that the used control scheme is effective in reducing the seismic responses of both buildings under different earthquake excitations. Abdeddaim (2017) investigated the case of retrofitting a weaker building by connecting it to another stronger building. The MR damper was used to connect the buildings at different levels. The fuzzy logic controller was used to provide the control device with the required voltage. The results were positive in reducing the drift, displacement, and base shear responses.

More studies investigating efficacy of different control strategies were conducted on coupled buildings utilizing different control devices (Amini & Doroudi, 2010; Bhaskararao & Jangid, 2004; Christenson et al., 2003; Kim, Ryu, Chung, 2006; Lee, Kim, & Ko, 2012; Matsagar & Jangid, 2005; Ok, Song, & Park, 2008; Uz & Hadi, 2014; Zhang

& Xu, 1999). These studies reveal encouraging results of using coupled structures theory in mitigating the structural responses under different types of dynamic loadings.

Some experimental studies were also carried out on coupled buildings in addition to the analytical studies mentioned above. Mitsuta et al. (1994) investigated experimentally the feasibility of coupling two single-degree-of-freedom and two two-degree-of-freedom building models coupled with an active actuator using displacement feedback measurement. Yamada et al. (1994) used a negative stiffness active device to experimentally couple a pair of two- and three-story building model. The test came up with a significant reduction in the peak displacements of both buildings. More experiments have been conducted on high-rise building models utilizing one or two active actuators with displacement feedback (Fukuda, Matsumoto, Seto, 1996; Hori & Seto, 2000; Kamagata, Miyajima, Seto, 1996; Seto, 1994; Seto, Toba, Matsumoto, 1995).

In addition to the theoretical and experimental studies, real full-scale applications were performed, particularly in Japan. Kajima Intelligent Building complex, which consists of two connected buildings, was constructed in Tokyo in 1989. The two buildings were connected at the fifth and ninth floors with passive devices (Christenson & Spencer, 2001). Konoike Headquarter buildings were also coupled with visco-elastic dampers in 1998. The complex consists of three nine-story buildings and the fourth is twelve-story building. Another example of coupled buildings located in Tokyo is the Triton Square office complex, as shown in Figure 6. The complex includes three tall buildings connected by 350 kN active actuators to mitigate the responses under wind and seismic events (Christenson et al., 2003).

Figure 6: Triton Building complex in Harumi, Tokyo, Japan (reprinted from http://harumi-triton.jp/en/).

1.4 Adaptive Control Strategy

Various types of control methods have been proposed to regulate the control devices. However, majority of these algorithms have fixed control parameters and cannot be adjusted to deal with uncertainties. As civil engineering structures exhibit a unique set of problems to control designers such as massively exogenous inputs and highly uncertain systems, structural engineers should embrace more sophisticated types of control methods to deal with these challenges. Such control methods are the adaptive controllers, which are emerging as a timely class of control systems, as reflected in many recent publications in the industry of control design.

Adaptive control possesses the ability to deal with inescapable challenges imposed by both internal and external uncertainties. Adaptive controllers are capable of adjusting their own parameters to achieve best possible performance. The term “adaptive” implies

that adaptive systems can provide continuous information of the current state, compare current performance to a desired trajectory, make a decision by changing a current system to achieve the desirable performance, and initiate a proper adjustment to force the controlled system to the optimum. The adaptation process involves choice of a controller, choice of reference performance, and online evaluation and adjustment (Housner et al., 1997). Other vocabularies for adaptive control were proposed by the IEEE committee in 1973 such as self-organizing control (SOC), performance-adaptive (SOC), and learning control systems (Åström & Wittenmark, 2013). Based on the performance, adaptive control, in general, can be classified into four types: gain scheduling, dual control, self-tuning regulators, and model-reference adaptive control (Åström & Wittenmark, 2013).

Adaptive control is more involved than the non-adaptive control methods, and it is generally used for uncertain plants (structures). Adaptive control is categorized as direct and indirect methods. Direct adaptive methods do not need parameters identification, but rather they are adjusted based on the error between the measured and desired outputs. On the other hand, indirect adaptive methods require estimation of the unknown plant and then the adaptive gains are generated based on the estimated plant. An example of the direct adaptive methods is the Model Reference Adaptive Control (MRAC) method. Figure 7 shows a schematic of MRAC. In this method, the output of the plant is forced to track the behavior of a reference-model where the parameters of the controller are adapted to continuously reduce the error between the plant and the reference-model. The output of an adaptive controller is always nonlinear and time-varying even when the system is linear and time-invariant. Hence, stability of the entire system becomes a great concern

(Kaufman, Barkana, & Sobel, 2012). Stability of MRAC was proved for “ideal” case assuming no external disturbances with no or very small “unmodeled dynamics”. In reality, these two assumptions do not exist, a case which might drive the adaptive algorithm to be unstable.

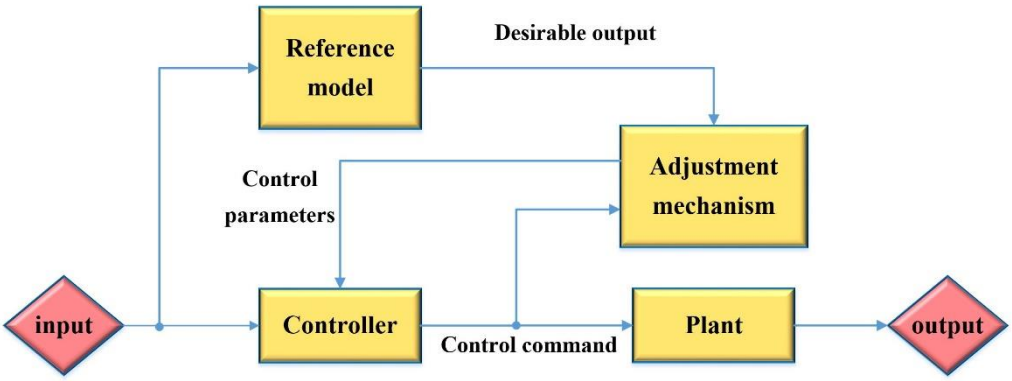

Figure 7: MRAC scheme.

MRAC has been successfully applied in structural engineering problems with the presence of uncertainties. However, MRAC requires “perfect-model tracking” condition to be satisfied, so that all the states of the plant must asymptotically track the states of the reference-model. In MRAC, the order of the reference-model must be the same order of the plant. In real-world applications, plants are usually very large systems in which the “unmodeled dynamics” must be considered. The developers of MRAC stipulated that the “unmodeled dynamics” is sufficiently small to make the use of this method feasible. Also, if one of the model states reaches a steady state case, some of the adaptive gains become dependent on different parameters, which raises the need for persistent excitation

(Barkana, 2014). All these conditions are required to guarantee the stability of the system before even controlling the performance, which make use of MRAC in civil engineering not that interesting.

Various solutions have been proposed to overcome some of the downsides of the MRAC method. One of these solutions is an output-model tracking controller. In the new development, only the outputs of the plant are required to follow the reference-model's outputs without prior knowledge of the plant parameters. The new controller seems to mitigate the problems that plagued MRAC such as unmodeled dynamics and persistent excitations. Since this method uses the reference-model as a command generator, it was first termed as "Adaptive Command Generator Tracker" (Kaufman, Barkana, & Sobel, 2012). However, since the reference-model is not required to be the same order of the plant, the term "simple" is used to refer to this merit. The method was ultimately called the simple adaptive control (SAC) method (Barkana, 2016). Chapter II of this dissertation includes a detailed discussion about SAC strategy.

1.5 Intelligent Control

Intelligent control is a control technique that uses various artificial intelligence computing approaches such as fuzzy logic, neural networks, machine learning, and genetic algorithms to sense, reason, plan, and learn in an intelligent manner (Burns, 2001). The term "intelligent control" was first proposed by Fu in 1971 to enhance the performance of automatic control systems and extend their applicability (Housner et al., 1997). Intelligent control is an adaptive control that has a capability to learn from the environment.

Intelligent control schemes, generally, comprise three main subsystems: (1) perception, (2) cognition, and (3) actuation. Perception process includes collecting information from the environment (plant) and processing it to be suitable to be used by the cognition system. Sensors are the main element in this process to provide information about the plant. Cognition subsystem includes reasoning, planning, and learning process through use of different algorithms such as fuzzy logic, neural networks, and adaptive search algorithms. Actuation subsystem includes actuators that receive information from the cognition process to drive the plant to a desirable state. Figure 8 shows the structure of intelligent control systems (Burns, 2001).

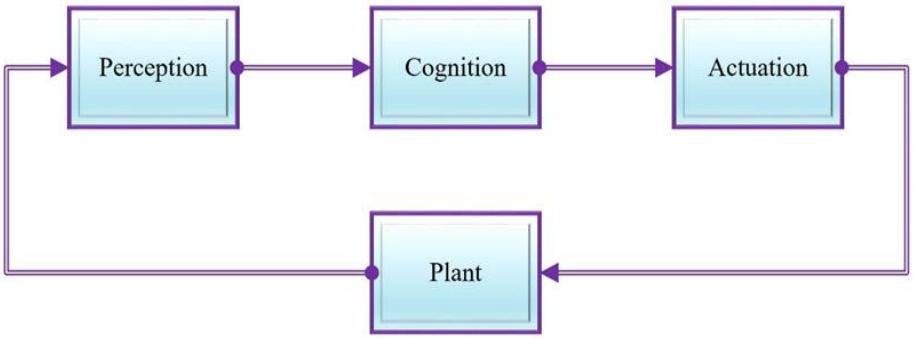

Figure 8: Intelligent control scheme.

1.6 Motivation and Significance of the Research

Protection of civil engineering structures requires structural engineers to explore more sophisticated control methods to mitigate the ramifications of the seismic events. Mutual-interaction between coupled buildings can be exploited to mitigate the seismic

responses. The coupling strategy of adjacent buildings is advantageous in different ways as summarized below:

1. Providing more control forces compared to the case where the links are fully passive, which will further reduce the seismic responses of the individual buildings. This strategy is also beneficial in avoiding pounding and retrofitting existing structures.
2. Freeing more space inside buildings since the control devices are implemented outside the buildings, which is appreciated by architects.
3. Utilizing the coupling strategy more likely decreases the number of the control devices compared to the case where each building is controlled individually.

The structural responses can be reduced by connecting closely-built buildings even with fully passive links. However, passive control was proved to be less effective under various dynamic loadings. Therefore, the efficacy of the links between adjacent buildings can be enhanced by implementing supplemental dissipative devices within these links. Therefore, the current research aims to investigate the efficiency of using control devices to connect adjacent buildings, and adaptive controllers are designed to drive these devices under different levels of seismic events.

The literature survey indicates that the classical control methods have been used extensively in structural engineering applications for the last four decades. However, all these methods cannot deal with changes in the controlled system characteristics. The parameter variations of the structural systems can be caused by the inelastic behavior under earthquakes or strong wind, fatigue, corrosion, or design parameter uncertainties.

The control strategy that has a capability to deal with any changes in the systems or presence of noise in the sensor measurements is the adaptive control strategy. In this strategy, the adaptive gains are adjusted according to the variation in the system characteristics. In the current research, two adaptive control strategies are developed for the coupled systems. The simple adaptive control (SAC) method is designed first, and its performance is compared with different classical methods. Then, the adaptive neuro-fuzzy control (ANFIS) strategy is also developed, and its performance is compared with SAC. ANFIS will be discussed further in the next chapter.

1.7 Goals and Objectives of the Research

The goal of this research is to develop and evaluate supplemental control strategies to mitigate the dynamic responses of coupled buildings with uncertain parameters.

To achieve the main goal of this research, several objectives are pursued and can be summarized as follows:

1. Designing and evaluating the performance of the simple adaptive control method in reducing the seismic responses of the connected structures. The performance of the adaptive controller is examined in the presence of noise and parametric changes. The evaluation process is accomplished by examining different control criteria and comparing the performance with other control methods such as the optimal control theory and the Lyapunov theory-based algorithm.

2. Designing and evaluating the performance of the simple adaptive control method in reducing the seismic responses of the connected structures with nonlinear behavior. A smooth and stable nonlinear restoring force-displacement relationship is adopted to model the nonlinear structural system. The formulation of the simple adaptive controller designed for the first objective is extended here to include the nonlinear behavior.
3. Designing and evaluating the performance of the adaptive neuro-fuzzy inference systems (ANFIS) strategy. The evaluation process is accomplished by using different performance metrics and comparing the performance with the simple adaptive control strategy.
4. Considering full three-dimensional coupled system to be controlled by the adaptive controllers designed earlier in order to identify their sensitivity to the structural modeling.

1.8 Overview of Dissertation

This dissertation investigates the effectiveness of using adaptive control to drive semi-active and active control devices connecting two adjacent buildings subjected to seismic excitations. Chapter 2 contains a review of the control devices used in this research. Following is a discussion of the control algorithms and their mathematical formulations.

Chapter 3 details a parametric study of a coupled system connected with active and semi-active control devices. The coupled system consists of two buildings with different

heights and connected at multiple levels. The simple adaptive controller is used to drive the control devices, and its performance is compared with the optimal control theory and Lyapunov stability theory-based algorithms.

In chapter 4, a semi-active control device (MR damper) is employed to connect two nonlinear buildings. A fully plastic model is used to represent the nonlinear behavior of the coupled structural system. The simple adaptive controller with displacement feedback is used, and its performance is compared with the optimal control theory.

Chapter 5 studies the effectiveness of the adaptive neuro-fuzzy inference systems, and its performance is compared with the simple adaptive control method. Different feedback schemes are examined such as displacement, velocity, acceleration, and velocity-acceleration feedbacks. The results of all schemes are discussed and commented upon.

Chapter 6 details the modeling process of three-dimensional coupled structures. x, y, and θ degrees-of-freedom for each floor are considered. Both the simple adaptive controller and the adaptive neuro-fuzzy inference systems are implemented to control the 3D coupled system under bi-directional seismic excitations.

Chapter 7 provides conclusions for the adaptively controlled coupled systems. Additionally, several research recommendations for future studies are recommended.

References

Abdeddaim, M. (2017). Retrofitting of a weaker building by coupling it to an adjacent stronger building using MR dampers. *Structural Engineering and Mechanics, 62*(2), 197-208.

Amini, F., & Doroudi, R. (2010). Control of a building complex with magneto-rheological dampers and tuned mass damper. *Structural Engineering and Mechanics, 36*(2), 181-195.

Åström, K. J., & Wittenmark, B. (2013). *Adaptive control*: Courier Corporation.

Barkana, I. (2016). Adaptive Control? But is so Simple! *Journal of Intelligent & Robotic Systems, 83*(1), 3-34.

Bharti, S., Dumne, S., & Shrimali, M. (2010). Seismic response analysis of adjacent buildings connected with MR dampers. *Engineering Structures, 32*(8), 2122-2133.

Bhaskararao, A. V., & Jangid, R. S. (2004). *Seismic response of adjacent buildings connected with dampers.* Paper presented at the 13th World Conference on Earthquake Engineering.

Bhaskararao, A. V., & Jangid, R. S. (2007). Optimum viscous damper for connecting adjacent SDOF structures for harmonic and stationary white-noise random excitations. *EARTHQUAKE ENGINEERING AND STRUCTURAL DYNAMICS, 36*, 563–571. doi:DOI: 10.1002/eqe.636

Brogan, W. L. (1991). *Modern control theory*: Pearson education india.

Burns, R. (2001). *Advanced control engineering*: Elsevier.

Christenson, R. E., & Spencer, B. F. (2001). *Semiactive control of civil structures for natural hazard mitigation: analytical and experimental studies.* directed by B. F. Spencer, for the Department of Civil Engineering and Geological Sciences. University of Notre Dame.

Christenson, R. E., Spencer, B. F., Hori, N., & Seto, K. (2003). Coupled Building Control Using Acceleration Feedback. Computer-Aided Civil and Infrastructure Engineering, 18(1), 4–18. doi:10.1111/1467-8667.00295.

Christenson, R. E., Spencer, B. F., Johnson, E. A., & Seto, K. (2006). Coupled Building Control Considering the Effects of Building/Connector Configuration. Journal of Structural Engineering, 132(6), 853–863. doi:10.1061/(asce)0733-9445(2006)132:6(853).

Connor, J., & Laflamme, S. (2014). *Structural motion engineering* (Vol. 493): Springer.

Dyke, S. J., & Spencer, B. F. (1996). Seismic response control using multiple MR dampers. In *Proceedings of the 2nd international workshop on structural control* (Vol. 2, pp. 163-173).

Fukuda, Y., Matsumoto, Y., & Seto, K. (1996). *Bending and torsional vibration control of flexible structures arranged in parallel.* Paper presented at the Proc., 3rd Int. Conf. on Motion and Vibration Control (MOVIC).

Graham, M. C. (1994). *Design strategies for coupling buildings.* (Master of Science), Massachusetts Institute of Technology,

Gurley, K., Kareem, A., Bergman, L., Johnson, E., & Klein, R. (1994). Coupling tall buildings for control of response to wind. *Structural Safety & Reliability, Balkema, Rotterdam*, 1553-1560.

Hao, H. (2015). Analysis of seismic pounding between adjacent buildings. *Australian Journal of Structural Engineering, 16*(3), 208-225.

Hori, N., & Seto, K. (2000). Vibration control of flexible space structures based on reduced order modeling method and filtered LQ control theory. *JSME International Journal Series C Mechanical Systems, Machine Elements and Manufacturing, 43*(3), 697-703.

Housner, G. W., Bergman, L. A., Caughey, T. K., Chassiakos, A. G., Claus, R. O., Masri, S. F., Yao, J. T. (1997). Structural control: past, present, and future. *Journal of engineering mechanics, 123*(9), 897-971.

Inaudi, J. A. (1997). Modulated homogeneous friction: a semi-active damping strategy. *Earthquake engineering & structural dynamics, 26*(3), 361-376.

Barkana, I. (2014). Simple adaptive control–a stable direct model reference adaptive control methodology–brief survey. *International Journal of Adaptive Control and Signal Processing, 28*(7-8), 567-603.

Jansen, L. M., & Dyke, S. J. (2000). Semiactive control strategies for MR dampers: comparative study. *Journal of engineering mechanics, 126*(8), 795-803.

Kamagata, K., Miyajima, K., & Seto, K. (1996). *Optimal design of damping devices for vibration control of parallel structures.* Paper presented at the Proc., 3rd Int. Conf. on Motion and Vibration Control (MOVIC).

Kaufman, H., Barkana, I., & Sobel, K. (2012). *Direct adaptive control algorithms: theory and applications*: Springer Science & Business Media.

Kim, J., Ryu, J., & Chung, L. (2006). Seismic performance of structures connected by viscoelastic dampers. *Engineering Structures, 28*(2), 183-195.

Klein, R., Cusano, C., & Stukel, J. (1973). *Investigation of a method to stabilize wind-induced oscillations in large structures.* Paper presented at the Mechanical Engineering.

Klein, R. E., & Healey, M. D. (1987). *Semi-Active Control of Wind Induced Oscillations in Structures*, Dordrecht.

Ko, J., Ni, Y., & Ying, Z. (1999). *Dynamic response of adjacent buildings coupled with nonlinear hysteretic dampers under random seismic excitation.* Paper presented at the Proc., Seminar on New Seismic Design Methodologies for Tall Buildings.

Kobori, T., Takahashi, M., Nasu, T., Niwa, N., & Ogasawara, K. (1993). Seismic response controlled structure with active variable stiffness system. *Earthquake engineering & structural dynamics, 22*(11), 925-941.

Kunieda, M. (1976). Earthquake prevent design and earthquake proof design for structures. *Journal of JSME, 79*(689), 86-91.

Lee, D. G., Kim, H. S., & Ko, H. (2012). Evaluation of coupling–control effect of a sky-bridge for adjacent tall buildings. *The Structural Design of Tall and Special Buildings, 21*(5), 311-328. doi:10.1002/tal.592.

Lomholt, I. (2018). World Trade Center Bahrain: Architecture, [web page]. Retrieved 12, January, 2019, from https://www.e-architect.co.uk/bahrain/bahrain-world-trade-centre.

Luco, J., & Wong, H. (1994). *Control of the seismic response of adjacent structures.* Paper presented at the Proceedings of the 1st World Conference on Structural Control.

Luco, J. E., & De Barros, F. C. P. (1998). Optimal damping between two adjacent elastic structures. *Earthquake engineering & structural dynamics*, *27*(7), 649-659.

Matsagar, V. A., & Jangid, R. S. (2005). Viscoelastic damper connected to adjacent structures involving seismic isolation. *Journal of civil engineering and management*, *11*(4), 309-322.

Matsumoto, Y. (1998). *Vibration control for multiple building structures connected with active bridges.* Paper presented at the Proceedings of the Second World Conference on Structural Control.

McClamroch, N. H., & Gavin, H. (1995). *Closed loop structural control using electrorheological dampers.* Paper presented at the American Control Conference, Proceedings of the 1995.

Mitsuta, S., Okawa, E., Seto, K., & Ito, H. (1994). Active vibration control of structures arranged in parallel. *JSME international journal. Ser. C, Dynamics, control, robotics, design and manufacturing*, *37*(3), 436-443.

Mukai, Y., Tachibana, E., & Inoue, Y. (1994). *Experimental study of active fin system for wind induced structural vibrations.* Paper presented at the Proc. of First World Conf. on Struct. Control.

Ohkawa, E. (1990). *Vibration control of flexible structure arranged in parallel (modeling the flexible structure by physical model).* Paper presented at the Proceedings of 1990 Dynamics and Design Conference B.

Ok, S.-Y., Song, J., & Park, K.-S. (2008). Optimal design of hysteretic dampers connecting adjacent structures using multi-objective genetic algorithm and stochastic linearization method. *Engineering Structures, 30*(5), 1240-1249. doi:https://doi.org/10.1016/j.engstruct.2007.07.019

Richardson, A., Walsh, K. K., & Abdullah, M. M. (2013). Closed-form equations for coupling linear structures using stiffness and damping elements. *Structural Control and Health Monitoring*, *20*(3), 259-281.

Rogers, S. (2017). Sky Bridges: 14 Ariel Structures that Span Skyscrapers, [web page]. Retrieved 28, January, 2019, from https://weburbanist.com/2013/09/16/sky-bridges-14-aerial-structures-that-span-skyscrapers/2/.

Sakai, D., Sugino, S., Seto, K., Christenson, R., & Spencer, B. F. (1999). *Vibration control of parallel structures connected with passive devices designed by GA.* Paper presented at the Proc. of DETC'99, 1999 ASME Design Engineering Technical Conferences.

Seto, K. (1994). *Vibration control method for flexible structures arranged in parallel.* Paper presented at the Proc. First World Conference on Structural Control.

Seto, K. (1999). Active vibration control of multiple buildings connected with active control bridges in response to large earthquakes. *Proceedings of the 1999 American Control Conference (Cat. No. 99CH36251), 2*, 1007.

Seto, M., Toba, Y., & Matsumoto, Y. (1995). *Reduced order modeling and vibration control methods for flexible structures arranged in parallel.* Paper presented at the American Control Conference, Proceedings of the 1995.

Soong, T., & Spencer, B. F. (2002). Supplemental energy dissipation: state-of-the-art and state-of-the-practice. *Engineering Structures, 24*(3), 243-259.

Spencer, B. F., & Sain, M. K. (1997). Controlling buildings: a new frontier in feedback. *IEEE Control Systems, 17*(6), 19-35.

Spencer, B. F., & Soong, T. (1999). *New applications and development of active, semi-active and hybrid control techniques for seismic and non-seismic vibration in the USA.* Paper presented at the Proceedings of International Post-SMiRT Conference Seminar on Seismic Isolation,

Passive Energy Dissipation and Active Control of Vibration of Structures, Cheju, Korea, August 23-25.

Stover, C. W., Coffman, J. L., & Scott, R. W. (1993). *Seismicity of the United States, 1568-1989 (revised) Rev. by Carl W. Stover and Jerry L. Coffman ; [edited by Richard W. Scott, Jr.]*: [Reston, Va.] : U.S. Dept. of the Interior, U.S. Geological Survey ;, 1993.

Sun, L., & Goto, Y. (1994). *Application of fuzzy theory to variable dampers for bridge vibration control.* Paper presented at the Proc. 1st World Conf. on Struct. Control.

Tehrani, M. G., & Gattulli, V. (2016). Vibration control using nonlinear damped coupling. *Journal of physics. Conference series, 744*(1).

Triton Building complex in Harumi, Tokyo, Japan [web page]. Retrieved December 22, 2018, from http://harumi-triton.jp/en/.

Uz, M. E., & Hadi, M. N. S. (2014). Optimal design of semi active control for adjacent buildings connected by MR damper based on integrated fuzzy logic and multi-objective genetic algorithm. *Engineering Structures, 69*, 135-148. doi:https://doi.org/10.1016/j.engstruct.2014.03.006

Westermo, B. D. (1989). The dynamics of interstructural connection to prevent pounding. *Earthquake engineering & structural dynamics, 18*(5), 687-699.

Xu, Y. L., He, Q., & Ko, J. M. (1999). Dynamic response of damper-connected adjacent buildings under earthquake excitation. *Engineering Structures, 21*(2), 135-148. doi:https://doi.org/10.1016/S0141-0296(97)00154-5

Yamada, Y., Ikawa, N., Yokoyama, H., & Tachibana, E. (1994). *Active control of structures using the joining member with negative stiffness.* Paper presented at the Proc. First World Conference on Structural Control.

Zhang, W., & Xu, Y. (1999). Dynamic characteristics and seismic response of adjacent buildings linked by discrete dampers. *Earthquake engineering & structural dynamics, 28*(10), 1163-1185.

Zhu, H., Wen, Y., & Iemura, H. (2001). A study on interaction control for seismic response of parallel structures. *Computers & Structures, 79*(2), 231-242.

CHAPTER II

CONTROL DEVICES AND ALGORITHMS

Structural control employs different types of supplemental control devices to help civil engineering structures withstand against hazardous events. As discussed in the previous chapter, the control devices are classified based on their controllability and power requirement as passive, active, and semi-active. Having the control devices selected, the other challenge is the choice of an effective control algorithm to regulate these devices. This chapter introduces two control devices: magneto-rheological (MR) damper and hydraulic actuator. The MR damper is a semi-active device while the hydraulic actuator is an active device. Following that an explanation is presented of the control algorithms that are used in this research: two adaptive controllers, simple adaptive controller (SAC) and adaptive neuro-fuzzy inference systems (ANFIS), and two non-adaptive controllers, linear quadratic regulator and Lyapunov stability theory-based algorithm.

2.1 Control Devices

2.1.1 Magneto-Rheological (MR) Damper

The MR damper represents a class of semi-active control since it uses a controllable fluid, as shown in Figure 9. The other class of semi-active control uses controllable valves instead to regulate the flow of the hydraulic fluid. In comparison with the controllable valve semi-active devices, the controllable fluid devices do not need many moving parts except one piston, which makes these devices reliable and quite simple

(Spencer & Soong, 1999). The most interesting feature of the controllable fluid is its ability to change from free flowing to semi-solid fluid, increasing its yield strength within milliseconds when exposed to a magnetic field as in the MR damper. The controllable fluid in the MR damper is called the MR fluid, which is a non-Newtonian fluid that is responsive to the magnetic field. The MR fluid contains tiny and magnetically polarizable particles suspended in an oil. Without a magnetic field, the liquid flows freely, but in the presence of a magnetic field, the iron particles line up in a chain form increasing the fluid thickness, as shown in Figure 10.

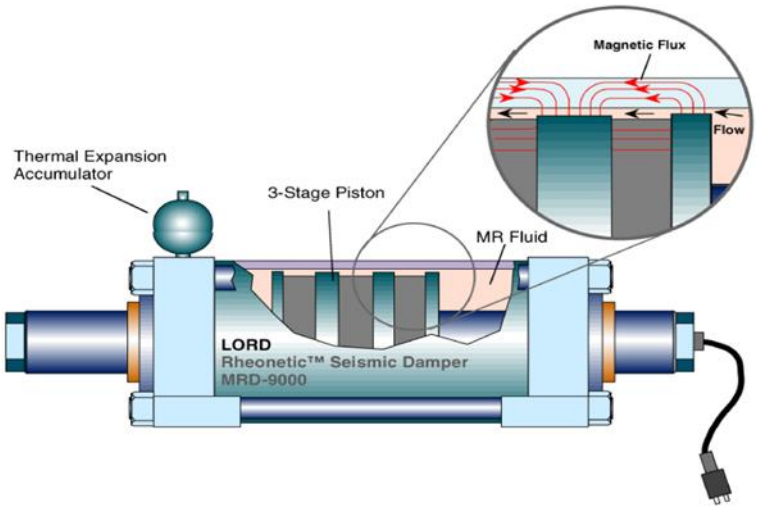

Figure 9: Schematic of 200 kN MR Damper (reprinted from Spencer & Soong, 1999).

The MR fluid can operate under a wide range of temperatures (-40 ^{o}C to +150 ^{o}C) with a small change in the yield strength (Weiss, Carlson, & Nixon, 1994). Moreover, the MR damper has the capability to operate with a low voltage and continue to work as a passive device in the case of the power supply or control algorithm failure.

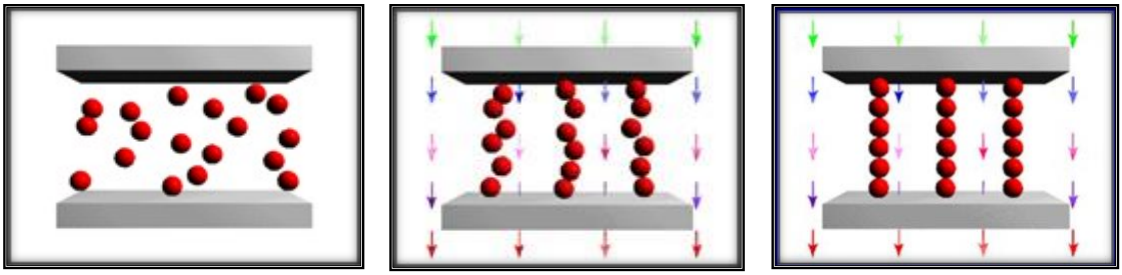

Figure 10: Chains formation process of the MR fluid in the presence of a magnetic field.

The prominent characteristics of the MR damper have received a great deal of attention from researchers. Many studies have been conducted to show the applicability of the MR damper in mitigating the seismic responses of the structural systems. Many theoretical and experimental studies show that the MR damper has a great potential in surpassing passive devices and competing well with fully active devices (Dyke et al., 1998; Jansen & Dyke, 2000; Spencer & Sain, 1997; Spencer, Christenson, & Dyke, 1998; Yoshida & Dyke, 2005). Other studies were carried out on the design of the MR damper to show its scalability to meet the civil engineering application needs (Carlson & Spencer, 1996).

First full-scale MR dampers were implemented in 2001 in the Nihon Kagaku Miraikan in the Tokyo National Museum of Emerging Science and Innovation, as shown in Figure 11. Two MR dampers with 30-ton capacity are positioned in the third and fifth floors of the building (Spencer & Nagarajaiah, 2003). Also, 40-ton MR dampers were installed in a residential building in Japan in 2003 along with a base isolation technique to enhance the seismic performance (Fujitani et al., 2003). In China, MR dampers were used

to mitigate the vibration of the Dongting Lake cable-stayed bridge. It was the first implementation of the MR damper for bridges where 312 MR dampers were installed to increase damping of 156 cables (Spencer & Nagarajaiah, 2003).

Figure 11: Nihon-Kagaku-Miraikan, Tokyo National Museum of Emerging Science and Innovation.

To evaluate the effectiveness of the MR damper in the civil engineering applications, a prototype of the device needs to be obtained through laboratory testing. Then, a representative model for use in the control design should be developed. Because the MR damper is highly nonlinear, creating a high-fidelity model becomes rather challenging. The Bouc-Wen model has been extensively used for modeling the hysteretic systems because of its mathematical tractability (Wen, 1976). The Bouc-Wen model

exhibits a capability to emulate the highly nonlinear behavior of the device over a wide range of inputs.

Utilizing the Bouc-Wen hysteretic model, researchers were able to model the MR damper with a high level of accuracy. One model is called the simple Bouc-Wen model, which has shown a great potential to track the nonlinear force-displacement curve producing well-predicted control forces. A schematic of the simple Bouc-model is shown in Figure 12. The control force predicted by this model is given as (Spencer et al., 1997):

$$F(t) = c_o \dot{x}(t) + \alpha z(t) \tag{2.1}$$

in which $z(t)$ is the evolutionary variable given by the following equation:

$$\dot{z}(t) = -\gamma \left| \dot{x}(t) \right| z(t) \left| z(t) \right|^{n-1} - \beta \dot{x}(t) \left| z(t) \right|^{n} + A\dot{x}(t) \tag{2.2}$$

where γ, β, A and n are constant parameters. The shape and sharpness of the force-displacement curves can be adjusted by tuning these parameters. The viscous damping parameters are varying as functions of the applied voltage as follows (Spencer et al., 1997):

$$\begin{aligned} c_o &= c_a + c_b u \\ \alpha &= \alpha_a + \alpha_b u \end{aligned} \tag{2.3}$$

where c_a, c_b, α_a and α_b are constants. The dynamics of the MR damper involving reaching rheological equilibrium is accounted according to the following first order filter:

$$\dot{u} = -\eta (u - v) \tag{2.4}$$

in which v is the applied voltage and η is a constant. It can be recognized from the above equations that there are many parameters need to be determined for the MR damper

prototype, which insinuates the complexity of the device behavior. The MR damper parameters are usually obtained through optimization studies such that the behavior of the damper matches the experimental data. Table 2 and Table 3 contain optimized MR damper parameters for 200 kN and 1000 kN capacities, respectively for the simple Bouc-Wen model (Yang et al., 2002; Yoshida & Dyke, 2005). The influence of these parameters was studied by Wong et al. (1994) and is compared to experimental data. The results showed that the proposed model matches the experimental data except near small velocities (Wong, Ni, & Lau, 1994).

The simple Bouc-Wen model depicts a highly nonlinear relationship between the predicted control force and the required voltage. In control design, it is sometimes beneficial to have a relationship that estimates the voltage required to provide the desired control forces. The inverse relationship of the MR damper can be determined by assuming the MR fluid is in the post-yielding region, the following approximate evolutionary variable, z_u, in its ultimate strength can be derived (Spencer, 1987) as follows:

$$z_u \approx \operatorname{sgn}(\dot{x})\left(\frac{A}{\gamma+\beta}\right)^{\frac{1}{n}} \tag{2.5}$$

By substituting equation (2.5) along with equation (2.3) back into equation (2.1) and solving for *u* yields the following equation (Tse & Chang, 2004):

$$u(t) \approx \frac{f(t) - c_a\dot{x}(t) - \alpha_a z_u}{c_b\dot{x}(t) + \alpha_b z_u} \tag{2.6}$$

where $f(t)$ in the equation is the predicted control force. Then the corresponding command voltage, *v*, can be numerically calculated from equation (2.4) as follows:

$$v = u + \frac{\dot{u}}{\eta} \tag{2.7}$$

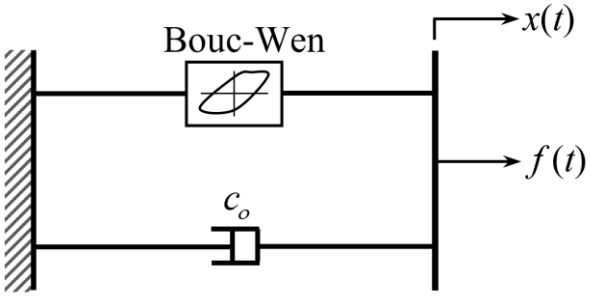

Figure 12: Simple Bouc-Wen model of the MR damper.

As mentioned earlier, the simple Bouc-Wen model behavior matches the experimental data except near low velocities. This shortcoming has been rectified by proposing a modified Bouc-Wen model, which contains new parameters to cope with low velocities (Spencer et al., 1997).

Table 2: Simple Bouc-Wen parameters of 200 kN capacity MR damper.

Parameter	Value	Parameter	Value
c_a	137,460 N.s/m	β	100.1 m^{-1}
c_b	12,553 N.s/m	A	833.45
α_a	103,690 N/m	n	2.39832
α_b	4,904 N/mV	η	31.4 s^{-1}
γ	3819.4 m^{-1}		

Table 3: Simple Bouc-Wen parameters of 1000 kN capacity MR damper.

Parameter	Value	Parameter	Value
c_a	440 N.s/m	β	300 m^{-1}
c_b	4400 N.s/m	A	1.2
α_a	1.0872×10^7 N/m	n	1
α_b	4.9615×10^7 N/mV	η	50 s^{-1}
γ	300 m^{-1}	V_{max}	10 V

Figure 13 shows a schematic of the modified Bouc-Wen model. The predicted forces on either side of the rigid bar are equated as follows (Spencer et al., 1997):

$$c_1\dot{y}(t) = k_o\left(\left(x(t)-x_o\right)\right)+c_o\left(\dot{x}(t)-\dot{y}(t)\right)+\alpha z(t) \tag{2.8}$$

in which the evolutionary variable, $z(t)$, is given by

$$\dot{z}(t) = -\gamma\left|\dot{x}(t)-\dot{y}(t)\right|z(t)\left|z(t)\right|^{n-1}-\beta\left(\dot{x}(t)-\dot{y}(t)\right)\left|z(t)\right|^{n}+A\left(\dot{x}(t)-\dot{y}(t)\right) \tag{2.9}$$

Solving equation (2.8) for $\dot{y}(t)$ gives

$$\dot{y}(t) = \frac{1}{\left(c_o+c_1\right)}\left[\alpha z(t)+k_o\left(x(t)-y(t)\right)+c_o\dot{x}(t)\right] \tag{2.10}$$

Finally, the total force generated by the device is determined by summing all the forces in both sections of the model depicted in Figure 13 as follows:

$$F(t) = k_o\left(\left(x(t)-x_o\right)\right)+c_o\left(\dot{x}(t)-\dot{y}(t)\right)+\alpha z(t)+k_1\left(x(t)-x_o\right) \tag{2.11}$$

where k_1 is the accumulator stiffness, c_o is a viscous damper due to large velocities, and c_1 is added variable to deal with low velocities.

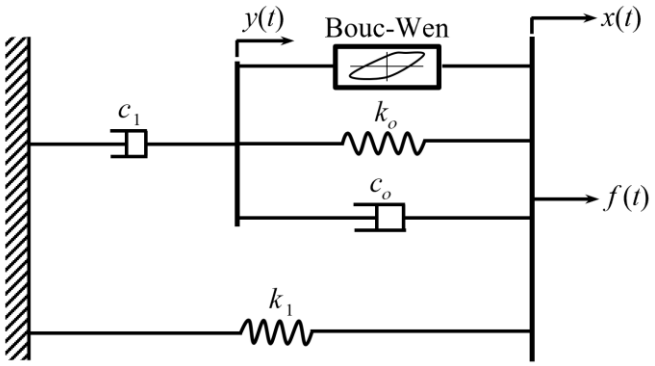

Figure 13: Modified Bouc-Wen model of the MR damper.

The parameters of the modified model, α, c_o, and c_1, are functions of the input current , *i*, in a form of cubic algebraic equations as follows (Yang et al., 2002):

$$\alpha(i) = 16566i^3 - 87071i^2 + 168326i + 15114 \tag{2.11}$$

$$c_o(i) = 437097i^3 + 1545407i^2 + 1641376i + 457741 \tag{2.12}$$

$$c_1(i) = -9363108i^3 + 5334183i^2 + 48788640i - 2791630 \tag{2.13}$$

The rest of the parameters of the modified Bouc-Wen model required to achieve 200 kN capacity MR damper are listed in Table 4 (Bitaraf, 2011). The inverse relationship of the modified model between the generated force and the required voltage is proposed (Tsang, Su, & Chandler, 2006) assuming negligible stiffnesses as follows:

$$i(t) = -\frac{2}{3}\ln\left[1 - \frac{-\left|F(t)\right| + \left|\tilde{F}_\eta(t)\right|}{1.5\times10^5}\right] \tag{2.14}$$

$$\tilde{F}_\eta(t) = \frac{c_o(t-\Delta t)c_1(t-\Delta t)}{c_o(t-\Delta t) + c_1(t-\Delta t)}\dot{x}(t) \tag{2.15}$$

where the evolutionary variable, $z(t)$, is assumed to reach the ultimate hysteretic strength as given in equation (2.5).

Table 4: Modified Bouc-Wen parameters of 1000 kN capacity MR damper.

Parameter	Value	Parameter	Value
c_a	440 N.s/m	β	647.46 m^{-1}
c_b	4400 N.s/m	A	2679
α_a	1.0872×10^7 N/m	n	10
α_b	4.9615×10^7 N/mV	η	31.4 s^{-1}
γ	647.46 m^{-1}	k_o	137,810 N/m
c_o	0.18 m	k_1	617.31 N/m

To evaluate the performance of the two models presented above, a comparison between the control forces generated by these two models is shown in Figure 14 under zero applied current and 2 amp., respectively. The external excitation is chosen as a sinusoidal force with 0.0254π amplitude and π rad/s frequency. It can be observed from Figure 14 that there is no significant difference between the behavior of the two models, especially the peaks of the control forces. Therefore, either model can be used to model the MR damper effectively in the structural engineering applications.

(a)

(b)

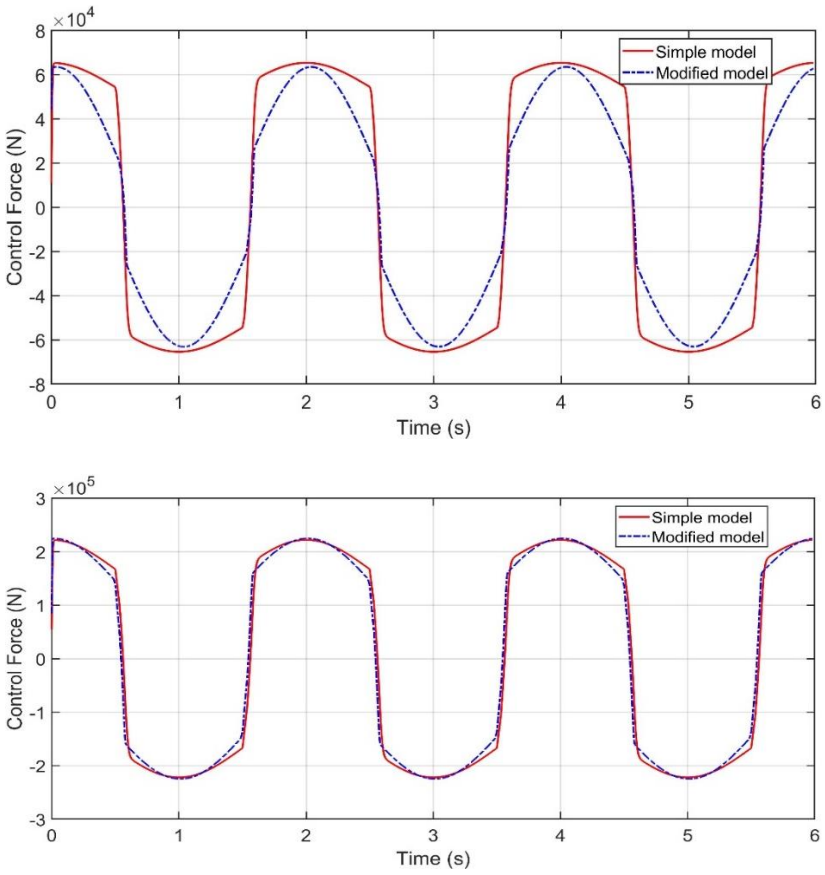

Figure 14: Control forces generated by the simple and modified Bouc-Wen models of the MR damper: (a) current = 0 and (b) current = 2 amp.

2.1.2 Hydraulic Actuator

The hydraulic actuator has three main components which are servo-valve, hydraulic actuator, and the feedback element (Tumanski, 2007). The servo-valve converts the electrical command into a spool displacement making the fluid flows into the actuator chamber, which results in the piston movement. DeSilva in 1989 derived equations for the servo-valve and the hydraulic actuator as follows (Tumanski, 2007):

$$\text{Servo-valve: } q_v(t) = k_q c - k_c \frac{f_{ha}(t)}{A_{ha}} \tag{2.16}$$

$$\text{Hydraulic actuator: } q_{ha}(t) = A_{ha}\dot{x}(t) + \frac{V_c}{2\mu A_{ha}}\dot{f}_{ha}(t) \tag{2.17}$$

where $q_v(t)$ and $q_{ha}(t)$ are the flow rate in the valve and hydraulic actuator, respectively; c is the valve input; k_q and k_c are system constants; $f_{ha}(t)$ is the force generated by the hydraulic actuator; A_{ha} is the cross-sectional area of the actuator; V_c is the volume of fluid chamber in the hydraulic actuator; $\dot{x}(t)$ is the actuator velocity; and μ is the bulk modulus of the fluid. Since the flow rate is the same in both the valve and the actuator, the above equations can be equated to obtain the following equation (Dyke et al., 1995).

$$\dot{f}_{ha}(t) = \frac{2\mu}{V_c}\left(A_{ha}k_q c - k_c f_{ha}(t) - A_{ha}^2\dot{x}(t)\right) \tag{2.18}$$

where c is the difference between the command signal to the actuator, u, and the displacement, $x(t)$ (Spencer, Christenson, & Dyke, 1998). Equation (2.18) can be written as follows:

$$\dot{f}_{ha}(t) = \lambda_1 u(t) - \lambda_1 x(t) - \lambda_2 \dot{x}(t) - \lambda_3 f_{ha}(t) \tag{2.19}$$

in which

$$\lambda_1 = \frac{2\mu k_q A_{ha}}{V_c}, \quad \lambda_2 = \frac{2\mu A_{ha}^2}{V_c}, \text{ and } \quad \lambda_3 = \frac{2\mu k_c}{V_c} \tag{2.20}$$

The above parameters were scaled up to achieve 1000 kN capacity (Dyke et al., 1995) as follows:

$$\begin{aligned} \lambda_1 &= 5.8128784\times10^9 \text{ N.s/m} \\ \lambda_2 &= 5.4641931\times10^7 \text{ N.s/m} \end{aligned} \tag{2.21}$$

$$\lambda_3 = 1.6210740 \times 10^3 \ \text{s}^{-1}$$

Equation (2.19) along with the parameters listed in equation (2.21) are used to model the dynamics of the hydraulic actuator in the current study.

2.2 Control Algorithms

2.2.1 Optimal Control Theory

Optimal control was first developed to operate the control systems at minimal cost. When a dynamic system is described by a set of linear differential equations and the cost by a quadratic function, the method is called linear quadratic regulator (LQR). LQR is a widely used technique in the control field because of its simplicity and effectiveness. In this method, an optimal feedback gain is calculated such that there is a control input that minimizes the following cost function (performance index):

$$J = \int_0^\infty \left\{ x_p(t)^T Q x_p(t) + u_p^T(t) R u_p(t) \right\} dt \tag{2.22}$$

where $u_p(t)$ is the control law which can determined as:

$$u_p(t) = -K x_p(t) \tag{2.23}$$

in which K is the controller gain calculated as follows:

$$K = R^{-1} B_p^T P \tag{2.24}$$

where P is a unique positive-semidefinite matrix, and it can be found by solving the following Riccati algebraic equation:

$$A_p^T P + P A_p - B_p P R^{-1} B^T P + Q = 0 \tag{2.25}$$

where Q and R are weighting matrices, which are chosen to allow for tradeoffs between the rate of convergence and the control effort. The first term in the equation (2.22) implicitly measures the rate of convergence of the states, while the second term penalizes any aggressive use of the control energy. The better choice of Q could enhance the structural performance, while the choice of R can regulate the total control energy of the structure.

The gain matrix, K, in equation (2.23) can be found by MATLAB built-in function "lqr.m". The challenge of the control designer is to specify the parameters of the performance index, Q and R, that makes the performance reach a specified design criterion. That means the design of the control system is an iterative process until a target performance is achieved. The process of finding the right weighting parameters for the controller sometimes limits the use of LQR in real-world applications.

2.2.2 Lyapunov Stability Theory-Based Algorithm

In this algorithm, the Lyapunov direct approach to stability analysis is employed to design the feedback controller (Brogan, 1982). The algorithm requires the use of a positive definite Lyapunov function of the states of the system. According to the theory, if the rate of change of the Lyapunov function is negative, the system is asymptotically stable. Leitmann (1994) used the Lyapunov theory to design a semi-active algorithm for a system represented by the following state-space:

$$\dot{x}(t) = Ax(t) + Bu(t)$$
$$y(t) = Cx(t) + D(t) \tag{2.26}$$

where $x(t)$ is the state vector. The following function was chosen to be the Lyapunov function candidate (Leitmann, 1994):

$$L = \frac{1}{2}\left\|x(t)\right\|_p \tag{2.27}$$

where $\left\|x(t)\right\|_p$ is the P-norm of the system's states, which can be defined as:

$$\left\|x(t)\right\|_p = \left(x(t)^T P_L x(t)\right)^{1/2} \tag{2.28}$$

in which P_L is a unique positive semidefinite solution of the Lyapunov algebraic equation, which takes the form

$$A^T P_L + P_L A + Q_L = 0 \tag{2.29}$$

where Q_L is a positive semidefinite matrix that can be chosen by trial and error. The derivative of the Lyapunov function of the solution of the state-space is

$$\dot{L} = -\frac{1}{2}x(t)^T Q_L x(t) + x(t)^T P_L B f_m(t) + x(t)^T P_L E \ddot{x}_g(t) \tag{2.30}$$

In order to develop the control law, the rate of change of the Lyapunov function $\left(\dot{L}\right)$ should be negative. From equation (2.30), one can realize that the only term that can be controlled is the second term, which contains the control inputs vector. Thus, the control algorithm is formulated in a way that keeps $\left(\dot{L}\right)$ negative as follows (Jansen & Dyke, 2000):

$$v_i = V_{\max} H\left(-x_p(t)^T P_L B f_m(t)\right) \tag{2.31}$$

where H[.] is the Heaviside function and $f_m(t)$ is the control forces vector. It is obvious from equation (2.31), that this method is an on-off algorithm since the voltage provided to the control device is either V_{max}, when the term between the parentheses is greater than zero, or zero otherwise.

2.2.3 Simple Adaptive Controller

The simple adaptive control (SAC) method is a direct adaptive scheme, which neither requires explicit parameters identification nor full-state feedback. SAC was developed by Sobel, Kaufman, and Mabius and extended by Barkana and Kaufman (BarKana & Kaufman, 1993) as a novel version of the Model Reference Control Method (MRAC) to overcome the drawbacks that the MRAC had, as discussed in the previous chapter. SAC was successfully implemented in such diverse applications as flight control (Barkana, 2005; Belkharraz & Sobel, 2007; Fradkov, Andrievsky, & Peaucelle, 2008; Morse & Ossman, 1990; Yossef, Shaked, & Yaesh, 1998), spacecrafts (Hu & Zhang, 2015; Maganti & Singh, 2007), autopilot (Rusnak, Weiss, & Barkana, 2014), power systems (Barkana & Fischl, 1992; Ritonja, Dolinar, & Grcar, 1995), robotics (Barkana & Guez, 1991; Ulrich, Sasiadek, & Barkana, 2012, 2014), motor control (Barkana & Kaufman, 1993; Shibata et al., 1996; Sun, Shibata, & Maruoka, 2000), satellite mission life extension (Hu, Jia, & Xu, 2013a, 2013b, 2014), quadrotor helicopter (Chen et al., 2015), and civil engineering (Bitaraf, Barroso, & Hurlebaus, 2010; Bitaraf, Hurlebaus, & Barroso, 2012; Bitaraf et al., 2010).

In this method, the desirable behavior is defined by an output of a priori designed reference-model that meets standard specifications such as settling time, rise time, steady-state error, and overshoot (Kaufman, Barkana, & Sobel, 2012). Then, the performance is evaluated by monitoring the error between the output of the plant and the output of the reference-model. The process of computing the error is easy and instantaneous, and then it leads to the process of adjusting the adaptive gains based on the computed error. The need for an adjustable controller in the structural engineering is quite important in order to cope with high uncertainties involved in the structural systems as well as the external disturbances. SAC is based on matching the behavior of a plant to that of a reference-model. The inputs to the plant include the states of the reference-model, the reference-model inputs, and the computed error between the plant and the reference-model output. If the control system is well designed, the control command generated from these inputs will drive the plant output to match the reference-model behavior.

If the governing equations of the plant are written as a state-space formulation as follows:

$$\begin{aligned} \dot{x}_p(t) &= A_p x_p(t) + B_p u_p(t) + d_i(t) \\ y_p(t) &= C_p x_p(t) + D_p u_p(t) + d_o(t) \end{aligned} \tag{2.32}$$

where A_p, B_p, and C_p are the plant, input, and output matrices, respectively. $x_p(t)$ is the $R^n \times 1$ state vector of the plant and $u_p(t)$ is the $R^n \times 1$ plant output vector. $y_p(t)$ is the $R^n \times 1$ plant output vector. $d_i(t)$ and $d_o(t)$ are the external disturbances and output noise,

respectively. According to SAC philosophy, the goal is to find a control command, $u_p(t)$, such that $y_p(t)$ tracks the following reference-model:

$$\dot{x}_m(t) = A_m x_m(t) + B_m u_m(t)$$
$$y_m(t) = C_m x_m(t) + D_m u_m(t) \tag{2.33}$$

where A_m, B_m, and C_m are the plant, input, and output matrices, respectively. $x_m(t)$ is the $R^m \times 1$ state vector of the plant and $u_m(t)$ is the $R^m \times 1$ plant output vector. $y_m(t)$ is the $R^m \times 1$ plant output vector. It is to be noted that the order of the reference-model could be less than the order of the plant, but the dimension of the measured output of the plant, $y_p(t)$, must be the same as the reference-model output vector, $y_m(t)$.

If the output tracking error is measured according to the following equation

$$e_y(t) = y_m(t) - y_p(t) \tag{2.34}$$

and used to generate the adaptive gains, as defined in equation (2.35), the tracking error will be minimized.

$$u_p(t) = K_e(t) e_y(t) + K_x(t) x_m(t) + K_u(t) u_m(t) \tag{2.35}$$

where $K_e(t)$ is unknown stabilizing feedback output matrix. $K_x(t)$ and $K_u(t)$ are unknown gains added to improve the adaptation. These adaptive gains are written as differential equations as follows (Barkana, 2016):

$$\dot{K}_e(t) = e_y(t) e_y^T(t) \Gamma_e \tag{2.36}$$

$$\dot{K}_x(t) = e_y(t) x_m^T(t) \Gamma_x \tag{2.37}$$

$$\dot{K}_u(t) = e_y(t) u_m^T(t) \Gamma_u \tag{2.38}$$

in which Γ_e, Γ_x, and Γ_u are tuning matrices. A schematic of SAC is shown in Figure 15.

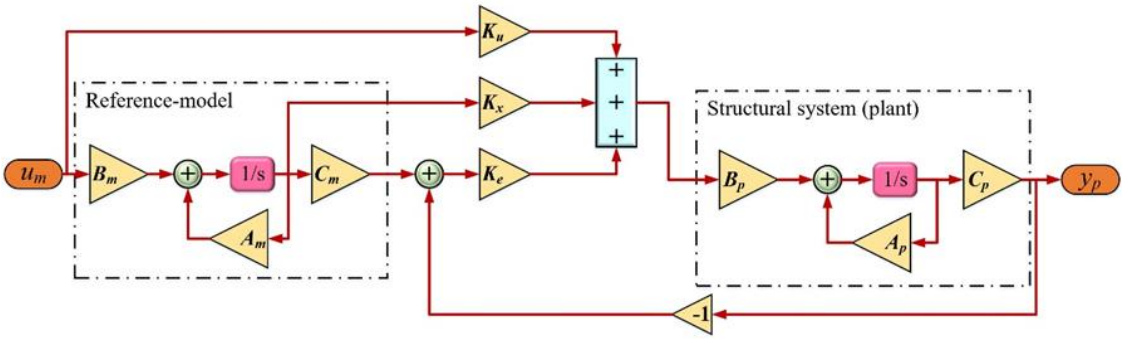

Figure 15: SAC block diagram.

The stability of SAC was extensively studied by the developers to show its robustness (Barkana, 2013, 2014b, 2015; Barkana & Fischl, 1992). The priori condition of stability is that the controlled plant is an almost strictly positive real (ASPR) system. The ASPR condition to be satisfied for a linear time-invariant system with the state-space realization [*A, B, C*], there two positive-symmetric-definite matrices, *P* and *Q*, and a gain matrix, $\tilde{K}$, such that the following two equations are simultaneously satisfied:

$$\begin{aligned} P\left(A - B\tilde{K}C\right) + \left(A - B\tilde{K}C\right)^T P &= -Q \\ PB &= C^T \end{aligned} \tag{2.39}$$

According to the above two conditions, if the plant is in minimum-phase and the matrical product *CB* is positive symmetric definite, the plant can be stabilized with some positive definite feedback (Barkana, 2016). In real-world systems, however, it is not

uncommon that the ASPR condition is not satisfied. In such systems, the parallel feedforward configuration (PFC) can be employed to allow the system to satisfy the ASPR condition (Barkana, 1987). It is to be warned that the additional term utilized by the PFC should be small in order not to drive the system performance away from the optimum trajectory. In fact, it was proven that the PFC renders ASPR always exists for any stable/unstable, SISO/MIMIO, or minimum/non-minimum phase systems (Barkana, 2016).

In the last part of this section, a practical implantation of SAC for a simple three-degree-of-freedom building is examined. The system considered for the numerical simulation is a shear-building model to represent a three-story building provided with three MR dampers, as shown Figure 16. The mass, stiffness, and damping matrices of the system are as follows:

$$M = 10^3 \times \begin{pmatrix} 478 & 0 & 0 \\ 0 & 478 & 0 \\ 0 & 0 & 478 \end{pmatrix} \text{ kg} \tag{2.40}$$

$$K = 10^8 \times \begin{pmatrix} 3.3966 & -1.6983 & 0 \\ -1.6983 & 3.3966 & -1.6983 \\ 0 & -1.6983 & 1.6983 \end{pmatrix} \text{ N/m} \tag{2.41}$$

$$C = 10^5 \times \begin{pmatrix} 5.4420 & -2.130 & 0 \\ -2.130 & 5.4420 & -2.130 \\ 0 & -2.130 & 3.3120 \end{pmatrix} \text{ N.s/m} \tag{2.42}$$

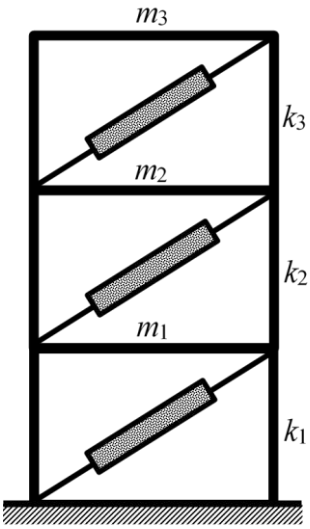

Figure 16: Three-story building model.

In the analysis of the current example, two cases are considered. The first case assumes that the control devices are “ideal”, meaning they can provide all the amount of the required forces produced by SAC no matter how large. The second case employs actual MR devices with upper and lower limits imposed on the control forces. Kobe earthquake with 6.9 magnitude and PGA = 1.810 m/s^2 is selected as an external excitation for the time-domain simulations.

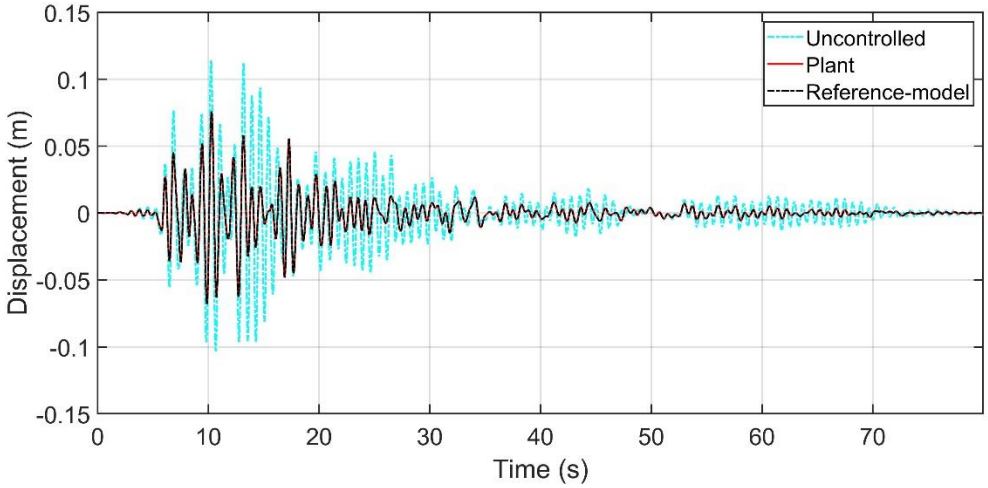

Figure 17: SAC with ideal device showing almost perfect tracking.

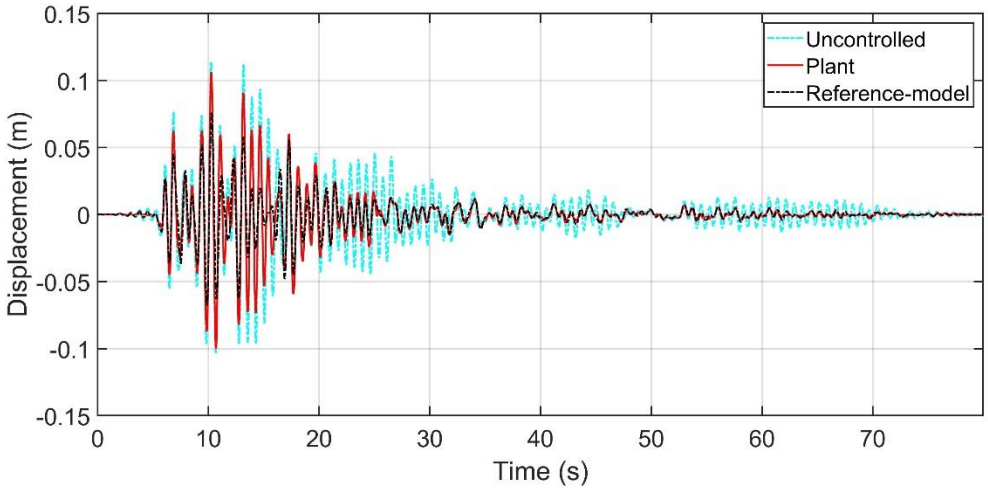

Figure 18: SAC with three MR dampers 200kN capacity each.

From Figure 17, it can be realized that the tracking is almost perfect, while in Figure 18 there is a significant error between the reference-model and the plant. The reason is that in the former figure it was assumed that the control devices are perfect and can

provide all the control forces required by SAC to match the behavior of the plant and the reference-model. In Figure 18, actual MR dampers are implemented with upper and lower limits on the produced control forces as +200kN and -200kN, respectively. Since the saturated control forces are less than these produced by SAC, the tracking cannot be perfect.

2.2.4 Adaptive Neuro-Fuzzy Control

Adaptive neuro-fuzzy inference systems (ANFIS) combines the fuzzy inference characteristics of the fuzzy logic controller (FLC) with the learning capability of the artificial neural networks (ANN). Therefore, ANFIS has a potential to surpass the classical FLC or ANN. The philosophy of employing ANFIS scheme is to utilize the ANN learning capabilities to continuously upgrade the rules or the membership functions of the FLC (Burns, 2001). Since FLC and ANN are the essential elements of ANFIS, it is important to discuss these two algorithms separately.

Fuzzy logic was first proposed by Zadeh (1965) based on fuzzy sets theory as a means of representing uncertainty. Fuzzy logic is used to model imprecise and vague information through “soft” computing techniques to infer control actions. The main concept of fuzzy logic is the partial membership functions between 0 and 1. Membership functions can have different shapes such as triangles, trapezoids, Gaussian and bell shapes. As shown in Figure 19, the fuzzy logic control (FLC) method consists of four main processes: (1) fuzzification, (2) fuzzy rule-base, (3) fuzzy inference, and (4) defuzzification (Burns, 2001). Fuzzification process includes mapping input (crisp) data

into fuzzy membership values along the universe of discourse. In this process, number and shape of fuzzy membership functions, and size of the universe of discourse need to be decided. Fuzzy rule-base process includes a set of IF-THEN rules usually called "Mamdani" type. The rule-base is commonly constructed based on expert knowledge in which no mathematical model is required. Fuzzy inference process includes mapping the values of the input membership functions to the output windows passing through the rule-base process. Defuzzification process, which is the final step in FLC, produces a non-fuzzy (crisp) control output from the inferred fuzzy control signals in the output window. The center of area method is most-used in the defuzzification technique, which represents the sum of first moments of the areas divided by the sum of the areas (Burns, 2001).

Fuzzy controllers have been utilized extensively for control. For instance, Sun and Goto (1994) employed FLC to obtain the optimum damping of a viscous-damper to control bridges subjected to environmental loads. Use of optimization theory to determine the optimal membership functions was conducted by Yamada et al. (1994). Guclu and Yazici (2008) used FLC and PD controllers to attenuate earthquake-induced vibrations on a multi-degree-freedom system provided with active tuned mass damper.

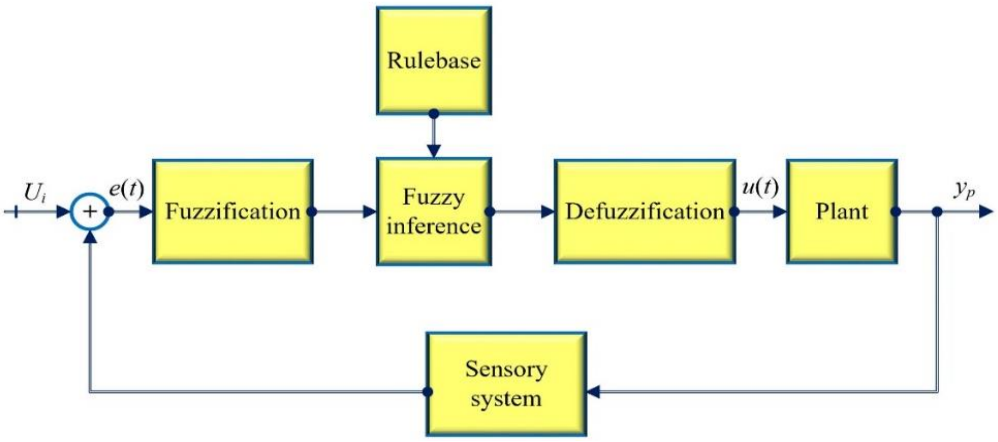

Figure 19: Fuzzy Logic Controller scheme.

Artificial neural networks were developed to emulate the biological neuron in the human brain, resulting in systems with learning capabilities. A neuron has a cell that is connected to several dendrites and a single axon, which is attached to other neurons via "synapses". The synapse generates a reaction to counteract the exogenous inputs. Then, the neuron "fires" if the sum of the reactions are large enough (Burns, 2001). Each neuron often has three layers: an input layer, a hidden layer, and an output layer. Each layer is randomly connected to the other layers as shown in Figure 20.

In Figure 20, $x_1 \cdots x_i$ represent the inputs, $w_{j1} \cdots w_{ji}$ are the weights, and y_i is the output. The activation (transfer) function can take different forms such as unit step, ramp, hyperbolic tangent, and sigmoid function. Generally, the sigmoid function (S-shaped) is the most used for applications because it is more appropriate for propagation algorithms (Burns, 2001). The sigmoid function takes the form:

$$f(x) = \frac{1}{1+e^{-x}} \tag{2.43}$$

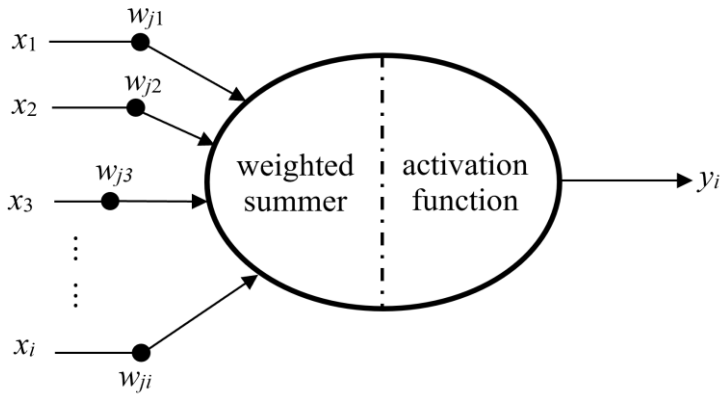

Figure 20: Artificial single neuron connections.

Artificial neural networks were first introduced to the control field in the early 1960s (Widrow & Lehr, 1990). In 1986, Rumelhart and McClelland have written a book on the revival interest in the artificial neural networks. After that, two books were written by Miller et al. (1990), and Brown and Harris (1994) to highlight the effectiveness of artificial neural networks specifically for control (Housner et al., 1997). An extensive use of the neural networks has been implemented in structural control since the late 1990s (Adeli & Jiang, 2006; Bani-Hani & Ghaboussi, 1998; Chang & Zhou, 2002; Jiang & Adeli, 2005; Kim, Jung, & Lee, 2000; Li, Song, & Ou, 2010; Omidvar & Elliott, 1997).

Hence, ANFIS provides the fuzzy modeling scheme with a method that can learn from a data set. ANFIS was first implemented by Jang (1993) where the Sugeno-fuzzy

model was employed. More about ANFIS including the mathematical formulation is discussed in Chapter V.

References

Adeli, H., & Jiang, X. (2006). Dynamic fuzzy wavelet neural network model for structural system identification. Journal of Structural Engineering, 132(1), 102-111.

Bani-Hani, K., & Ghaboussi, J. (1998). Nonlinear structural control using neural networks. Journal of engineering mechanics, 124(3), 319-327.

Barkana, I. (1987). Parallel Feedforward and Simple Adaptive Control of Flexible Structures: First-Order Pole Instead of Collocated Velocity Sensors? Journal of aerospace engineering, 29(2), 04015039.

Barkana, I. (2005). Classical and simple adaptive control for nonminimum phase autopilot design. Journal of Guidance, Control, and Dynamics, 28(4), 631-638.

Barkana, I. (2013). Extensions in adaptive model tracking with mitigated passivity conditions. Chinese Journal of Aeronautics, 26(1), 136-150.

Barkana, I. (2014a). The beauty of simple adaptive control and new developments in nonlinear systems stability analysis. AIP Conference Proceedings, 1637, 89-113.

Barkana, I. (2014b). Defending the beauty of the Invariance Principle. International journal of control, 87(1), 186-206.

Barkana, I. (2015). The new theorem of stability - Direct extension of Lyapunov theorem. Mathematics in Engineering, Science & Aerospace (MESA), 6(3), 519-550.

Barkana, I. (2014). Simple adaptive control–a stable direct model reference adaptive control methodology–brief survey. International Journal of Adaptive Control and Signal Processing, 28(7-8), 567-603.

Barkana, I. (2016). Adaptive Control? But is so Simple! Journal of Intelligent & Robotic Systems, 83(1), 3-34.

Barkana, I. (2016). Robustness and perfect tracking in simple adaptive control. International Journal of Adaptive Control and Signal Processing, 30(8-10), 1118-1151. doi:10.1002/acs.2573

Barkana, I., & Fischl, R. (1992). A simple adaptive enhancer of voltage stability for generator excitation control. Paper presented at the American Control Conference, 1992.

Barkana, I., & Guez, A. (1991). Simplified techniques for adaptive control of robotic systems. In Control and Dynamic Systems (Vol. 40, pp. 147-203): Elsevier.

BarKana, I., & Kaufman, H. (1993). Simple adaptive control of large flexible space structures. IEEE transactions on aerospace and electronic systems, 29(4), 1137-1149.

Belkharraz, A. I., & Sobel, K. (2007). Simple adaptive control for aircraft control surface failures. IEEE transactions on aerospace and electronic systems, 43(2).

Bitaraf, M. (2011). Enhancing the Structural Performance with Active and Semi-active Devices Using Adaptive Control Strategy (Ph.D), Texas A&M,

Bitaraf, M., Barroso, L. R., & Hurlebaus, S. (2010). Adaptive Control to Mitigate Damage Impact on Structural Response. Journal of Intelligent Material Systems and Structures, 21(6), 607-619. doi:10.1177/1045389x10361993

Bitaraf, M., Hurlebaus, S., & Barroso, L. R. (2012). Active and Semi-active Adaptive Control for Undamaged and Damaged Building Structures Under Seismic Load. Computer-Aided Civil and Infrastructure Engineering, 27(1), 48-64. doi:10.1111/j.1467-8667.2011.00719.x

Bitaraf, M., Ozbulut, O. E., Hurlebaus, S., & Barroso, L. (2010). Application of semi-active control strategies for seismic protection of buildings with MR dampers. Engineering Structures, 32(10), 3040-3047. doi:https://doi.org/10.1016/j.engstruct.2010.05.023

Brogan, W. L. (1982). Modern control theory. Prentice-Hall: Englewood Cliffs, N.J.

Burns, R. (2001). Advanced control engineering: Elsevier.

Carlson, J., & Spencer. (1996). Magneto-rheological fluid dampers for semi-active seismic control. Paper presented at the Proc. 3rd Int. Conf. on Motion and Vibration Control, 1996-9.

Chang, C.-C., & Zhou, L. (2002). Neural network emulation of inverse dynamics for a magnetorheological damper. Journal of Structural Engineering, 128(2), 231-239.

Chen, F., Wu, Q., Jiang, B., & Tao, G. (2015). A reconfiguration scheme for quadrotor helicopter via simple adaptive control and quantum logic. IEEE Transactions on Industrial Electronics, 62(7), 4328-4335.

Dyke, S., Spencer, B. F., Sain, M., & Carlson, J. (1998). An experimental study of MR dampers for seismic protection. Smart materials and structures, 7(5), 693.

Dyke, S. J., Spencer, B. F., Quast, P., & Sain, M. K. (1995). Role of Control-Structure Interaction in Protective System Design. Journal of Engineering Mechanics, 121(2), 322.

Dyke, S. J., Yi, F., Frech, S., & Carlson, J. D. (1999). Application of magnetorheological dampers to seismically excited structures. Paper presented at the SPIE proceedings series.

Fradkov, A. L., Andrievsky, B., & Peaucelle, D. (2008). Adaptive control design and experiments for laas "helicopter" benchmark. European Journal of Control, 14(4), 329-339.

Fujitani, H., Sodeyama, H., Tomura, T., Hiwatashi, T., Shiozaki, Y., Hata, K., . . . Soda, S. (2003). Development of 400kN magnetorheological damper for a real base-isolated building. Paper presented at the Smart Structures and Materials 2003: Damping and Isolation.

Guclu, R., & Yazici, H. (2008). Vibration control of a structure with ATMD against earthquake using fuzzy logic controllers. Journal of Sound and Vibration, 318(1-2), 36-49.

Housner, G. W., Bergman, L. A., Caughey, T. K., Chassiakos, A. G., Claus, R. O., Masri, S. F., . . . Yao, J. T. (1997). Structural control: past, present, and future. Journal of engineering mechanics, 123(9), 897-971.

Hu, Q., Jia, Y., & Xu, S. (2013a). Recursive dynamics algorithm for multibody systems with variable-speed control moment gyroscopes. Journal of Guidance, Control, and Dynamics, 36(5), 1388-1398.

Hu, Q., Jia, Y., & Xu, S. (2013b). Simple adaptive control for vibration suppression of space structures using control moment gyroscopes as actuators. Paper presented at the AIAA Guidance, Navigation, and Control (GNC) Conference.

Hu, Q., Jia, Y., & Xu, S. (2014). Adaptive suppression of linear structural vibration using control moment gyroscopes. Journal of Guidance, Control, and Dynamics, 37(3), 990-996.

Hu, Q., & Zhang, J. (2015). Attitude control and vibration suppression for flexible spacecraft using control moment gyroscopes. Journal of aerospace engineering, 29(1), 04015027.

Inaudi, J. A. (1997). Modulated homogeneous friction: a semi-active damping strategy. Earthquake engineering & structural dynamics, 26(3), 361-376.

Ioannou, P., & Kokotovic, P. (1983). Adaptive Systems with Reduced Models. Springer-Verlag, Berlin.

Jang, J. S. (1993). ANFIS: adaptive-network-based fuzzy inference system. IEEE transactions on systems, man, and cybernetics, 23(3), 665-685.

Jansen, L. M., & Dyke, S. J. (2000). Semiactive control strategies for MR dampers: comparative study. Journal of engineering mechanics, 126(8), 795-803.

Jiang, X., & Adeli, H. (2005). Dynamic wavelet neural network for nonlinear identification of highrise buildings. Computer-Aided Civil and Infrastructure Engineering, 20(5), 316-330.

Kaufman, H., Barkana, I., & Sobel, K. (2012). Direct adaptive control algorithms: theory and applications: Springer Science & Business Media.

Kim, J.-T., Jung, H.-J., & Lee, I.-W. (2000). Optimal structural control using neural networks. Journal of engineering mechanics, 126(2), 201-205.

Leitmann, G. (1994). Semiactive control for vibration attenuation. Journal of Intelligent Material Systems and Structures, 5(6), 841-846.

Li, L., Song, G., & Ou, J. (2010). Nonlinear structural vibration suppression using dynamic neural network observer and adaptive fuzzy sliding mode control. Journal of Vibration and Control, 16(10), 1503-1526.

Maganti, G. B., & Singh, S. N. (2007). Simplified adaptive control of an orbiting flexible spacecraft. Acta Astronautica, 61(7-8), 575-589.

Morse, W., & OSSMAN, A. (1990). Model following reconfigurable flight control system for the AFTI/F-16. Journal of Guidance, Control, and Dynamics, 13(6), 969-976.

Mukai, Y., Tachibana, E., & Inoue, Y. (1994). Experimental study of active fin system for wind induced structural vibrations. Paper presented at the Proc. of First World Conf. on Struct. Control.

Omidvar, O., & Elliott, D. L. (1997). Neural systems for control: Elsevier.

Ritonja, J., Dolinar, D., & Grcar, B. (1995). Combined conventional-adaptive power system stabilizer. Paper presented at the Stockholm Power Tech, Proceedings of the International Symposium on Electric power engineering, and power systems.

Rusnak, I., Weiss, H., & Barkana, I. (2014). Improving the performance of existing missile autopilot using simple adaptive control. International Journal of Adaptive Control and Signal Processing, 28(7-8), 732-749.

Shibata, H., Li, D., Fujinaka, T., & Maruoka, G. (1996). Discrete-time simplified adaptive control algorithm and its application to a motor control. Paper presented at the Industrial Electronics, 1996. ISIE'96., Proceedings of the IEEE International Symposium on.

Spencer, B. F., & Sain, M. K. (1997). Controlling buildings: a new frontier in feedback. IEEE Control Systems, 17(6), 19-35.

Spencer, B. F., & Soong, T. (1999). New applications and development of active, semi-active and hybrid control techniques for seismic and non-seismic vibration in the USA. Paper presented at the Proceedings of International Post-SMiRT Conference Seminar on Seismic Isolation.

Spencer, B. F., & Nagarajaiah, S. (2003). State of the Art of Structural Control. Journal of Structural Engineering, 129(7), 845-856.

Spencer, B. F. (1987). Reliability of randomly excited hysteretic structures. Journal of Sound and Vibration, 119(3), 590-591.

Spencer, B. F., Christenson, R. E., & Dyke, S. J. (1998). Next generation benchmark control problem for seismically excited buildings. Paper presented at the Proceedings of the Second World Conference on Structural Control.

Spencer, B. F., Dyke, S., Sain, M., & Carlson, J. (1997). Phenomenological model for magnetorheological dampers. Journal of engineering mechanics, 123(3), 230-238.

Sun, L., & Goto, Y. (1994). Application of fuzzy theory to variable dampers for bridge vibration control. Paper presented at the Proc. 1st World Conf. on Struct. Control.

Sun, Y., Shibata, H., & Maruoka, G. (2000). Discrete-time Simplified Adaptive Control of a DC Motor Based on Asymptotic Output Tracker Theory. IEEJ Transactions on Industry Applications, 120(2), 254-261.

Tsang, H., Su, R., & Chandler, A. (2006). Simplified inverse dynamics models for MR fluid dampers. Engineering Structures, 28(3), 327-341.

Tse, T., & Chang, C. (2004). Shear-mode rotary magnetorheological damper for small-scale structural control experiments. Journal of Structural Engineering, 130(6), 904-911.

Tumanski, S. (2007). Sensors and Actuators - Control System Instrumentation (de Silva, C.W.; 2007) [book review]. IEEE Instrumentation & Measurement Magazine, 10(6), 56-56.

Ulrich, S., Sasiadek, J. Z., & Barkana, I. (2012). Modeling and direct adaptive control of a flexible-joint manipulator. Journal of Guidance, Control, and Dynamics, 35(1), 25-39.

Ulrich, S., Sasiadek, J. Z., & Barkana, I. (2014). Nonlinear adaptive output feedback control of flexible-joint space manipulators with joint stiffness uncertainties. Journal of Guidance, Control, and Dynamics, 37(6), 1961-1975.

Weiss, K. D., Carlson, J. D., & Nixon, D. A. (1994). Viscoelastic properties of magneto- and electro-rheological fluids. Journal of Intelligent Material Systems and Structures, 5(6), 772-775.

Wen, Y.-K. (1976). Method for random vibration of hysteretic systems. Journal of the engineering mechanics division, 102(2), 249-263.

Widrow, B., & Lehr, M. A. (1990). 30 years of adaptive neural networks: perceptron, madaline, and backpropagation. Proceedings of the IEEE, 78(9), 1415-1442.

Wong, C., Ni, Y., & Lau, S. (1994). Steady-state oscillation of hysteretic differential model. I: Response analysis. Journal of Engineering Mechanics, 120(11), 2271-2298.

Yamada, Y., Ikawa, N., Yokoyama, H., & Tachibana, E. (1994). Active control of structures using the joining member with negative stiffness. Paper presented at the Proc. First World Conference on Structural Control.

Yang, G., Spencer Jr, B., Carlson, J., & Sain, M. (2002). Large-scale MR fluid dampers: modeling and dynamic performance considerations. Engineering Structures, 24(3), 309-323.

Yoshida, O., & Dyke, S. J. (2005). Response Control of Full-Scale Irregular Buildings Using Magnetorheological Dampers. Journal of Structural Engineering, 131(5), 734-742. doi:10.1061/(ASCE)0733-9445(2005)131:5(734)

Yossef, T., Shaked, U., & Yaesh, I. (1998). Simplifed adaptive control of F16 aircraft pitch and angle-of-attack loops. Paper presented at the Proceedings of 44Th israel annual conference on aerospace sciences.

Zadeh, L. A. (1965). Fuzzy sets. Information and control, 8(3), 338-353.

CHAPTER III

ADAPTIVE CONTROL FOR COUPLED BUILDINGS CONSIDERING PARAMETER VARIATIONS*

The effectiveness of using the simple adaptive control method in the presence of noise and parameter variation in mitigating the seismic structural responses of two coupled adjacent buildings is investigated in this chapter. The coupled system is formed of two buildings having different heights and the equations of motion are formulated as two multi-degree of freedom shear-type model buildings connected at different levels with control devices. The magneto-rheological damper and the hydraulic actuator are used as semi-active and active control devices, respectively in the current chapter. A suite of five major earthquakes are chosen to perform the dynamic analysis in the time domain. The advantage of using the adaptive controller is that it can deal with any change in the dynamic characteristics of a structural system as it deteriorates during seismic events. The change in the structural characteristics is reflected as a reduction in the system's mass and stiffness as an outcome of the damage potential in the two buildings. The simple adaptive control method is optimized for the undamaged system and extended to control the damaged one. The amount of damage is assumed to occur evenly throughout the system while the control devices' connectors are assumed to stay undamaged. The performance

* Reprinted with permission from "Simple adaptive control method for mitigating the seismic responses of coupled adjacent buildings considering parameter variations" by Al-Fahdawi, O. A. S., Barroso, L. R., and Soares, R. W., 2019. *Journal of Engineering Structures*, Vol. 186, pp 369–381, Copyright 2019 Elsevier.

of the adaptive method is compared with different control strategies such as LQR, and Lyapunov theory-based algorithm. The results show that using the adaptive controller to drive the control devices connecting two adjacent buildings is effective in alleviating the seismic responses. The proposed control scheme is shown to be promising for reducing the seismic responses and dealing with the structural parameter variations.

3.1 Prelude

Close-distance building construction is recognized as an effective strategy for utilizing limited land space within large cities. Various control algorithms have been developed to regulate the behavior of the magneto-rheological (MR) damper. Due to the invertible dynamics between the produced force and applied voltage, predicting the required voltage that produces the desired control force is difficult, and therefore, different voltage algorithms have emerged to overcome this problem (Motra, Malik, & Chandiramani, 2011). Dyke et al. (1996) employed the acceleration feedback Linear Quadratic Gaussian (LQG) controller with the modified Bouc-Wen model to obtain the optimal control force. Chang and Zhou (Chang & Zhou, 2002) utilized the Linear Quadratic Regulator (LQR) and the modified Bouc-Wen model, with the neural network algorithm to determine the required voltage. Many other semi-active control algorithms have been proposed to control the MR damper such as the decentralized bang-bang, Lyapunov, clipped-optimal controller, maximum energy dissipation, and modulated homogenous friction control.

A significant weakness in all prior research of supplemental control of coupled buildings has been the lack of consideration of parametric uncertainty and variation during the life of the structure, which is inherent in real-world problems where the structural systems are quite uncertain. Adaptive control seems to be the natural solution for the real-world applications (Barkana, 2014) because it can deal with the parameter variations during hazardous events like earthquakes. It is quite known that during major earthquakes, structures experience damage and the amount of the damage depends on the severity of the seismic forces and the dynamic characteristics of the structure itself. The adaptive control approach can adjust the control command online in order to reduce the effects of the unknown parameters (Kaufman, Barkana, & Sobel, 2012).

One of the promising adaptive control methods is the simple adaptive controller (SAC) in which a physical system (plant) is forced to follow the behavior of a reference-model with desired trajectories (Al-Fahdawi, Barroso, Soares, 2019; Soares, Barroso, & Al-Fahdawi, 2018). SAC is a direct (implicit) scheme in which the adaptive gains can be computed directly without a need for parameters' identification (Al-Fahdawi, Barroso, & Soares, 2018; Soares, Barroso, & Al-Fahdawi, 2018).

The focus of this chapter is the investigation of the effectiveness of using SAC for mitigating the seismic structural responses of coupled adjacent buildings in the presence or parameter changing. The variations in parameters are taken as a percentage of the nominal design value, and they can represent variations due to damage or fluctuations due to environmental effects. Consideration of effectiveness under parametric variation is especially critical and has not been investigated in coupled systems. A suite of five major

earthquakes is chosen to perform the dynamic analysis in the time domain. To test the efficacy of SAC with different types of devices, one representative semi-active device, an MR damper, and one representative active device, a hydraulic actuator, were investigated, as these are common devices being studied for civil engineering applications. The performance of the adaptive method is compared with different control algorithms to benchmark its effectiveness against other known strategies.

3.2 Structural Systems Modeling

Two adjacent buildings are idealized as linear shear-type buildings where the masses of the floors are assumed to be concentrated at the centers of the floors. The number of stories of the buildings is different, but the corresponding floors of the two buildings are collinear. The number of the unconnected floors is n_1 while n_2 is the number of the connected floors. Therefore, Building 1 has (n_1+n_2) stories and Building 2 has n_2 stories as shown in Figure 21. The coupled system will then be having (n_1+2n_2) degrees of freedom. The two buildings are assumed to be symmetric in terms of their planes' alignment and dynamics characteristics. However, the number of stories is different. The system is assumed to be subjected to same unidirectional earthquake excitation with neglecting the spatial variation of the ground motion, and any effect due to soil-structure interaction is also neglected. The control devices are assumed to be rigidly connected between the collinear floors to maintain its performance.

The governing equation of motion of the combined system can be written in a compact form as

$$[M_s]\{\ddot{x}(t)\}+[C_s]\{\dot{x}(t)\}+[K_s]\{x(t)\}=[J]\{f_m(t)\}-[M_s]\{\Lambda\}\ddot{x}_g(t) \tag{3.1}$$

where $f_m(t)$ is the vector of the control forces; J is the location matrix of the control devices; $x(t)$, $\dot{x}(t)$, and $\ddot{x}(t)$ are the relative displacement, velocity, and acceleration vectors, respectively. $\{\Lambda\}$ is a vector with all elements equal ones; $\ddot{x}_g(t)$ is the ground acceleration vector. M_s, C_s, and K_s are the mass, damping and stiffness matrices of the coupled system, respectively.

The structural mass matrix of the coupled system can be explicitly defined as

$$M_{s(n_1+2n_2,n_1+2n_2)}=\begin{bmatrix} M_{1(n_1+n_2,n_1+n_2)} & 0_{(n_1+n_2,n_2)} \\ 0_{(n_2,n_1+n_2)} & M_{2(n_2,n_2)} \end{bmatrix} \tag{3.2}$$

in which 0's are null matrices with zero elements.

M_1 and M_2 are diagonal individual mass matrices for Building 1 and 2, respectively as follows:

$$M_1=\begin{bmatrix} m_{11} & 0 & \cdots & 0 \\ 0 & m_{21} & 0 & 0 \\ \vdots & 0 & \ddots & 0 \\ 0 & 0 & 0 & m_{(n_2+n_1)1} \end{bmatrix}$$

$$M_2=\begin{bmatrix} m_{12} & 0 & \cdots & 0 \\ 0 & m_{22} & 0 & 0 \\ \vdots & 0 & \ddots & 0 \\ 0 & 0 & 0 & m_{(n_2)2} \end{bmatrix} \tag{3.3}$$

where m_{i1} and m_{i2} are the floor mass in Building 1 and 2, respectively.

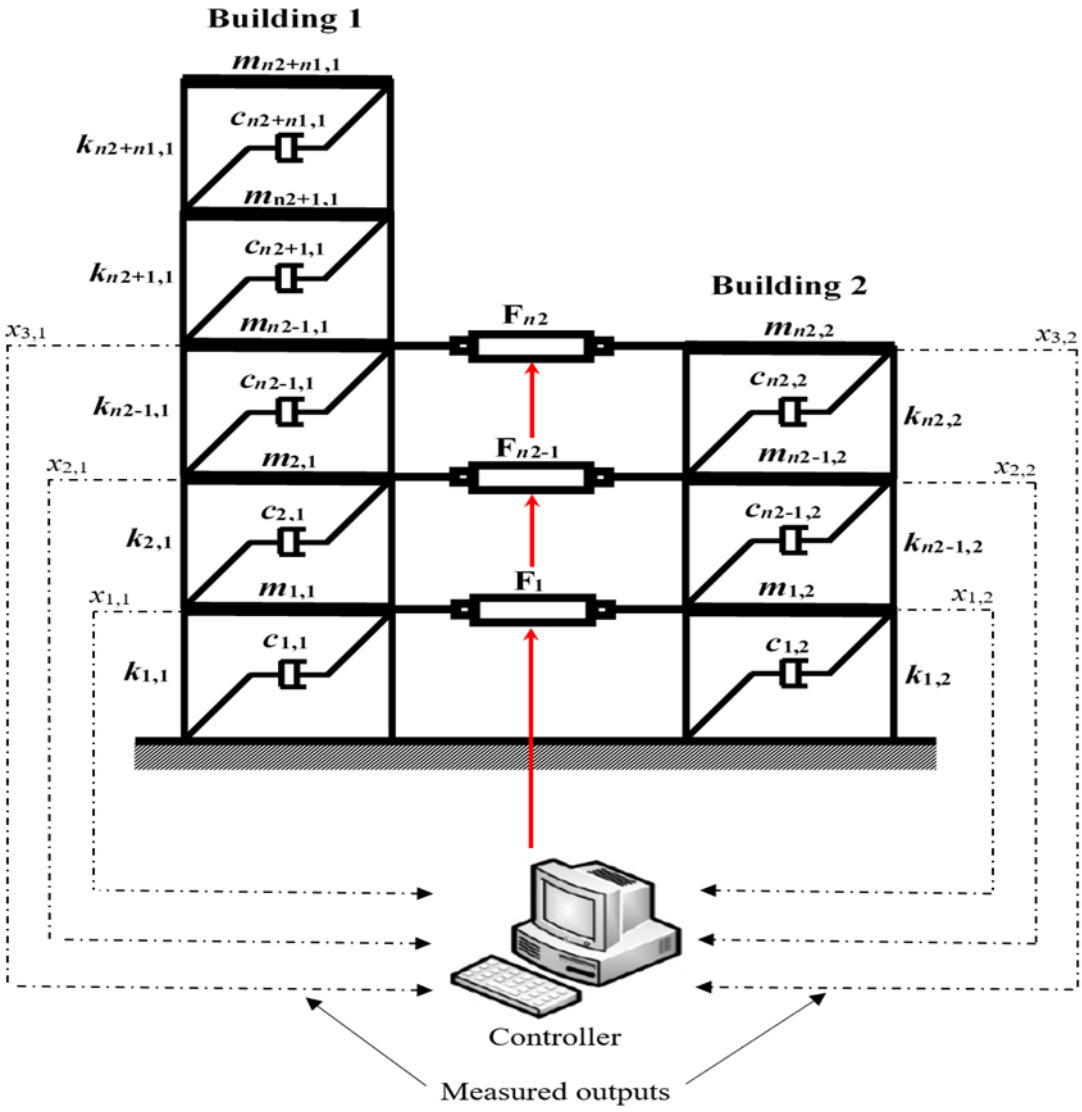

Figure 21: Coupled buildings model with the control layout.

The stiffness matrix, K_s, and damping matrix, C_s, of the coupled system are written as:

$$K_s = K_0 + K_c \tag{3.4}$$

$$C_s = C_0 + C_c \tag{3.5}$$

where K_0 and C_0 are the stiffness and damping matrices without the coupling effects. K_c and C_c are the stiffness and damping matrices of the connectors used to support the control devices. K_0 can be defined as follows:

$$K_{o(n_1+2n_2,n_1+2n_2)} = \begin{bmatrix} K_{1(n_1+n_2,n_1+n_2)} & 0_{(n_1+n_2,n_2)} \\ 0_{(n_2,n_1+n_2)} & K_{2(n_2,n_2)} \end{bmatrix} \tag{3.6}$$

where K_1 and K_2 are the individual tridiagonal stiffness matrices for Building 1 and 2, respectively and they are written as:

$$K_1 = \begin{bmatrix} k_{11}+k_{21} & -k_{21} & 0 & 0 \\ -k_{21} & k_{21}+k_{31} & -k_{31} & 0 \\ 0 & -k_{31} & \ddots & -k_{(n_2+n_1)1} \\ 0 & 0 & -k_{(n_2+n_1)1} & k_{(n_2+n_1)1} \end{bmatrix}$$

$$K_2 = \begin{bmatrix} k_{12}+k_{22} & -k_{22} & 0 & 0 \\ -k_{22} & k_{22}+k_{32} & -k_{32} & 0 \\ 0 & -k_{32} & \ddots & -k_{(n_2)2} \\ 0 & 0 & -k_{(n_2)2} & k_{(n_2)2} \end{bmatrix} \tag{3.7}$$

where k_{i1} and k_{i2} are the floor stiffness in Building 1 and 2, respectively. The damping matrix, C_0, for the uncoupled system is formulated by using the Rayleigh formula which can be written as:

$$C_0 = a_\circ M_s + a_1 K_s \tag{3.8}$$

The resulting damping matrix without considering the coupling effects can be given as:

$$C_{o(n_1+2n_2,n_1+2n_2)} = \begin{bmatrix} C_{1(n_1+n_2,n_1+n_2)} & 0_{(n_1+n_2,n_2)} \\ 0_{(n_2,n_1+n_2)} & C_{2(n_2,n_2)} \end{bmatrix} \tag{3.9}$$

where C_1 and C_2 are the individual tridiagonal damping matrices for Building 1 and 2, respectively and they are defined as:

$$C_1 = \begin{bmatrix} c_{11}+c_{21} & -c_{21} & 0 & 0 \\ -c_{21} & c_{21}+c_{31} & -c_{31} & 0 \\ 0 & -c_{31} & \ddots & -c_{(n_2+n_1)1} \\ 0 & 0 & -c_{(n_2+n_1)1} & c_{(n_2+n_1)1} \end{bmatrix}$$

$$C_2 = \begin{bmatrix} c_{12}+c_{22} & -c_{22} & 0 & 0 \\ -c_{22} & c_{22}+c_{32} & -c_{32} & 0 \\ 0 & -c_{32} & \ddots & -c_{(n_2)2} \\ 0 & 0 & -c_{(n_2)2} & c_{(n_2)2} \end{bmatrix} \tag{3.10}$$

where c_{i1} and c_{i2} are the floor stiffness in Building 1 and 2, respectively. Coupling effects are reflected in K_c and C_c matrices which they can formulated as follows:

$$K_{c(n_1+2n_2,n_1+2n_2)} = \begin{bmatrix} K_{d(n_2,n_2)} & 0_{(n_2,n1)} & -K_{d(n_2,n_2)} \\ 0_{(n_1,n_2)} & 0_{(n_1,n_1)} & 0_{(n_1,n_2)} \\ -K_{d(n_2,n_2)} & 0_{(n_2,n1)} & K_{d(n_2,n_2)} \end{bmatrix} \tag{3.11}$$

$$C_{c(n_1+2n_2,n_1+2n_2)} = \begin{bmatrix} C_{d(n_2,n_2)} & 0_{(n_2,n1)} & -C_{d(n_2,n_2)} \\ 0_{(n_1,n_2)} & 0_{(n_1,n_1)} & 0_{(n_1,n_2)} \\ -C_{d(n_2,n_2)} & 0_{(n_2,n1)} & C_{d(n_2,n_2)} \end{bmatrix} \tag{3.12}$$

in which the K_d and C_d are matrices to map the link stiffness and damping properties into the global stiffness and damping matrices of the whole system. These matrices can be defined as:

$$K_{d(n_2,n_2)} = \begin{bmatrix} k_{c1} & 0 & 0 & 0 \\ 0 & k_{c2} & 0 & 0 \\ 0 & 0 & \ddots & 0 \\ 0 & 0 & 0 & k_{c(n_2)} \end{bmatrix} \tag{3.13}$$

$$C_{d(n_2,n_2)} = \begin{bmatrix} c_{c1} & 0 & 0 & 0 \\ 0 & c_{c2} & 0 & 0 \\ 0 & 0 & \ddots & 0 \\ 0 & 0 & 0 & c_{c(n_2)} \end{bmatrix} \tag{3.14}$$

where the k_{ci} and c_{ci} are the stiffness and damping properties of the *i*th link, respectively. The location matrix, *J*, is written as:

$$J_{(n_1+2n_2,n_1+2n_2)} = \begin{bmatrix} [I]_{(n_2,n_2)} & [0]_{(n_2,n_1+n_2)} \\ [0]_{(n_1,n_2)} & [0]_{(n_1,n_1+n_2)} \\ [0]_{(n_2,n_1+n_2)} & -[I]_{(n_2,n_2)} \end{bmatrix} \tag{3.15}$$

Rewriting the governing equation of motion, equation (3.1), in the state-space formulation yields the following:

$$\dot{y}(t) = Ay(t) + Bf_m(t) + E\ddot{x}_g(t) \tag{3.16}$$

where *y* is the state vector, *A* is the system matrix, *B* is the distribution matrix of the control forces and *E* is the distribution matrix to map the excitation to all degrees of freedoms. The matrices *y*, *A*, *B*, and *E* are expressed below:

$$y(t) = \begin{Bmatrix} \{x(t)\} \\ \{\dot{x}(t)\} \end{Bmatrix} \qquad A = \begin{bmatrix} [0]_{(n_1+2n_2,n_1+2n_2)} & [I]_{(n_1+2n_2,n_1+2n_2)} \\ -[M_s]^{-1}[K_s] & -[M_s]^{-1}[C_s] \end{bmatrix} \tag{3.17}$$

$$B = \begin{Bmatrix} [0]_{(n_1+2n_2,\, n_1+2n_2)} \\ [M_s]^{-1}[J] \end{Bmatrix} \qquad E = \begin{Bmatrix} [0]_{(n_1+2n_2,1)} \\ [-\Lambda]_{(n_1+2n_2,1)} \end{Bmatrix}$$

where [0] and [I] are null and identity matrices, respectively.

To perform the numerical simulations in the time domain and to scrutinize the robustness of the proposed control methods, five earthquake recordings are adopted to represent the external excitations, see Table 5. Figure shows the acceleration and velocity response spectra for the selected recordings. The damping ratio is taken as 2% for the SDOF systems required to construct the response spectra.

Table 5: Earthquakes suite characteristics.

Earthquake	% Exceedance	PGA (g)	PGV (m/s^2)	Duration (s)
landers 1992 (LA10)	10	0.360	0.603	80.00
Northridge 1994 (LA16)	10	0.360	1.007	14.95
Loma Preita 1989 (LA23)	2	0.418	0.7376	25.00
artificial (LS19F)	10	0.784	0.974	81.92
Tabas 1978 (NF01)	Near-field	0.899	1.100	50.00

(a)

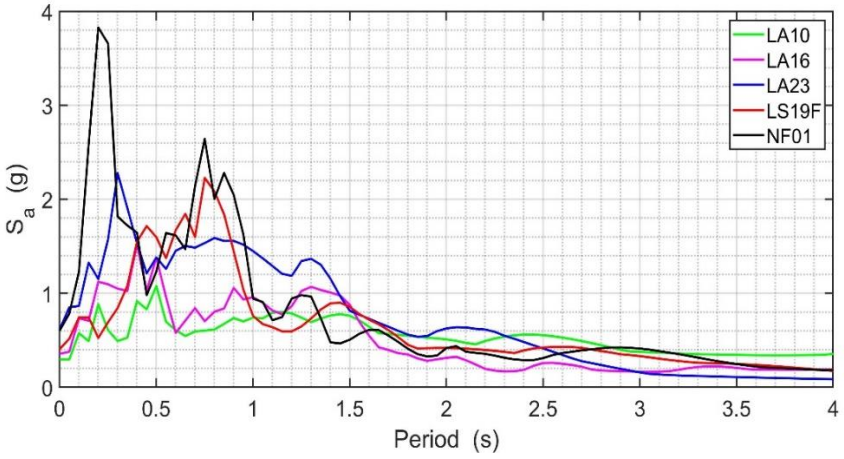

Figure 22: Response spectra for the selected five earthquakes: (a) acceleration spectra (S_a) and (b) velocity spectra (S_v).

(b)

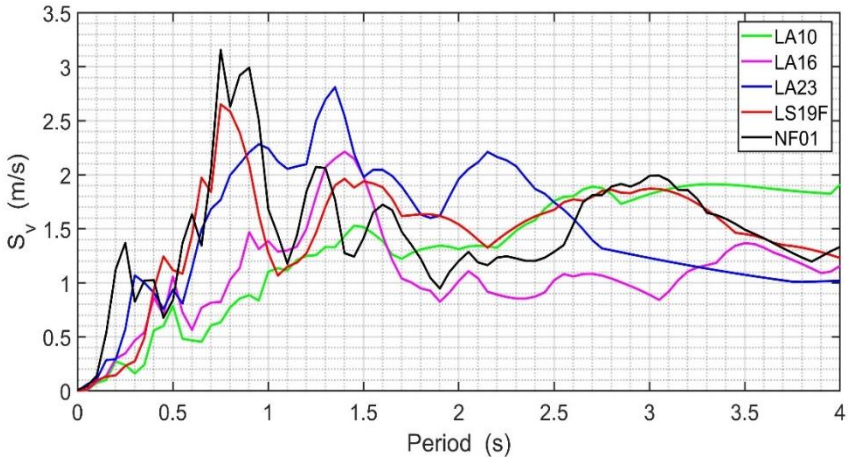

Figure 22: Continued.

3.3 Simple Adaptive Control

As explained in the previous chapter, SAC is a direct control method that it does not need a system identification to compute the adaptive gains. Moreover, this algorithm is an output feedback scheme which requires neither adaptive identifiers nor full state feedback, but the plant must satisfy the almost strictly positive real (ASPR) condition (Kaufman, Barkana, & Sobel, 1994). The ASPR condition is discussed in the previous chapter. If the coupled system described above and the reference-model are represented by equation (3.18) and (3.19), respectively as:

$$\begin{aligned} \dot{x}_p(t) &= A_p x_p(t) + B_p u_p(t) + d_i(t) \\ y_p(t) &= C_p x_p(t) + D_p u_p(t) + d_o(t) \end{aligned} \tag{3.18}$$

where A_p and B_p are the plant and input matrices, respectively. C_p is the plant output matrix, $x_p(t)$ is the state vector, $y_p(t)$ is the plant output vector, $u_p(t)$ is the control input vector, $d_i(t)$ and $d_o(t)$ are bounded input and output plant disturbances, respectively.

$$\dot{x}_m(t) = A_m x_m(t) + B_m u_m(t)$$
$$y_m(t) = C_m x_m(t) + D_m u(t) \tag{3.19}$$

where A_m and B_m are the model and input matrices, respectively. C_m is the model output matrix, $x_m(t)$ is the state vector, $y_m(t)$ is the model output vector, $u_m(t)$ is the control input vector into the model. SAC attempts to match the behavior of the plant and the reference-model both described in equation (3.18) and (3.19), respectively by monitoring the error according to the following equation:

$$e_y(t) = y_m(t) - y_p(t) \tag{3.20}$$

The adaptive controller minimizes the error above continuously to reach the perfect tracking level. If the plant perfectly tracks the model, i.e. $e_y(t) = 0$, the control is termed as "ideal" which is not known if it is possible (Kaufman, Barkana, & Sobel, 1994). The output of the adaptive controller, the control command, is the input into the plant which can be calculated as :

$$u_p(t) = K(t) r(t) \tag{3.22}$$

where $r(t)$ is the reference vector and $K(t)$ is the gain matrix which they can be determined as follows:

$$r(t)^T = \left[e_y{}^T(t) \;\; x_m^T(t) \;\; u_m^T(t) \right] \tag{3.23}$$

$$K(t) = \left[K_e(t) \;\; K_x(t) \;\; K_u(t) \right] \tag{3.24}$$

The adaptive gains $K_e(t)$, $K_x(t)$, and $K_u(t)$ are defined in equations (2.36) through (2.18) in chapter II. They are repeated here for convenience

$$\dot{K}_e(t) = e_y(t) e_y(t)^T \Gamma_e \tag{2.36}$$

$$\dot{K}_x(t) = e_y(t) x_m(t)^T \Gamma_x \tag{2.37}$$

$$\dot{K}_u(t) = e_y(t) u_m(t)^T \Gamma_u \tag{2.38}$$

The adaptive gains above can be written in an alternative form as (I. Barkana, 2016):

$$K(t) = K_I(t) + K_p(t) \tag{3.25}$$

where K_I (t) and K_p (t) are the integral and proportional gains which are computed as follows:

$$\dot{K}_I(t) = e_y(t) r^T(t) T - \sigma K_I(t) \tag{3.26}$$

$$K_p(t) = e_y(t) r^T(t) \bar{T} \tag{3.27}$$

where T and $\bar{T}$ are "selected" positive definite symmetric and positive semi-definite scaling matrices, respectively. Both matrices are chosen to adjust the adaptation rate. The integral gain is needed for the stability of the control system adaptation and speeding up the convergence. The proportional gain is introduced because it can enhance the plant performance and facilitate the perfect output tracking by adding immediate penalty on large errors. The σ-term in equation (3.26) is added to keep the integral gain away from divergence especially in the presence of disturbances and it can be a very small value (Ioannou & Kokotovic, 1983).

The performance of SAC is compared with Lyapunov theory-based algorithm and the Linear Quadratic Regulator (LQR) both explained in the previous chapter. For LQR, the following parameters are chosen since they give better results:

$$Q = \frac{1}{2}\begin{bmatrix} K_s & 0 \\ 0 & M_s \end{bmatrix} \tag{3.28}$$

$$R = \rho I_{(n_1+2n_2,\, n_1+2n_2)}; \quad \rho = 1\times 10^{-5} \tag{3.29}$$

In equations (3.28) and (3.29), Q and R are taken to be as same order as the plant. However, all the gains are zeroed in the SIMULINK model for the unconnected floors where no control devices provided. It is also to be noted here that the LQR algorithm is used in this study to obtain the desired trajectories of the reference-model in the adaptive controller, SAC, while keeping the dynamic characteristics of the reference-model same as in the plant.

3.4 Control Devices

Two devices are used in the current chapter. The first is the MR damper as a semi-active control device. Modeling of the MR damper is a critical step to accurately predict the behavior of the controlled system. The simple Bouc-Wen model, depicted in Figure 12, has been shown to accurately emulate the highly nonlinear behavior of the device over a wide range of inputs (Dyke et al., 1999; Yi et al., 1999). The equations governing the damper force predicted by this model are listed in chapter II. However, they are repeated here for convenience as:

$$f(t) = c_o \dot{x}(t) + \alpha z(t) \tag{2.1}$$

$$\dot{z}(t) = -\gamma \left| \dot{x}(t) \right| z(t) \left| z(t) \right|^{n-1} - \beta \dot{x}(t) \left| z(t) \right|^{n} + A\dot{x}(t) \tag{2.2}$$

where $f(t)$ is the control force generated by the MR damper and $z(t)$ is the evolutionary variable which accounts for the hysteretic behavior of the device. The SIMULINK model for calculating the evolutionary variable, $z(t)$, is depicted in Figure 23. In the current study, the relative velocities between the colinear floors need to be implemented in equations (2.1) and (2.2). Therefore, these equations can be written in a modified form as

$$f(t) = c_o \left[\dot{x}_{B1}(t) - \dot{x}_{B2}(t) \right] + \alpha z(t) \tag{3.30}$$

$$\begin{aligned} \dot{z}(t) = -\gamma & \left| \left[\dot{x}_{B1}(t) - \dot{x}_{B2}(t) \right] \right| z(t) \left| z(t) \right|^{n-1} - \beta \left[\dot{x}_{B1}(t) - \dot{x}_{B2}(t) \right] \left| z(t) \right|^{n} \\ & + A \left[\dot{x}_{B1}(t) - \dot{x}_{B2}(t) \right] \end{aligned} \tag{3.31}$$

where $\dot{x}_{B1}(t)$ and $\dot{x}_{B2}(t)$ are the velocity vectors of the connected floors in the first and second building, respectively. The parameters of the MR damper needed to scale up its capacity to 1000 kN are listed in Table 3.

As we have seen, the output of SAC represents the control forces required to make the plant perfectly follow the reference-model. Therefore, the output of SAC cannot be supplied directly to the MR damper before converting it to voltage. The inverse model of the MR damper can be used to determine the required voltage based on the control command provided by SAC. The inverse model of the MR damper was detailed in the previous chapter.

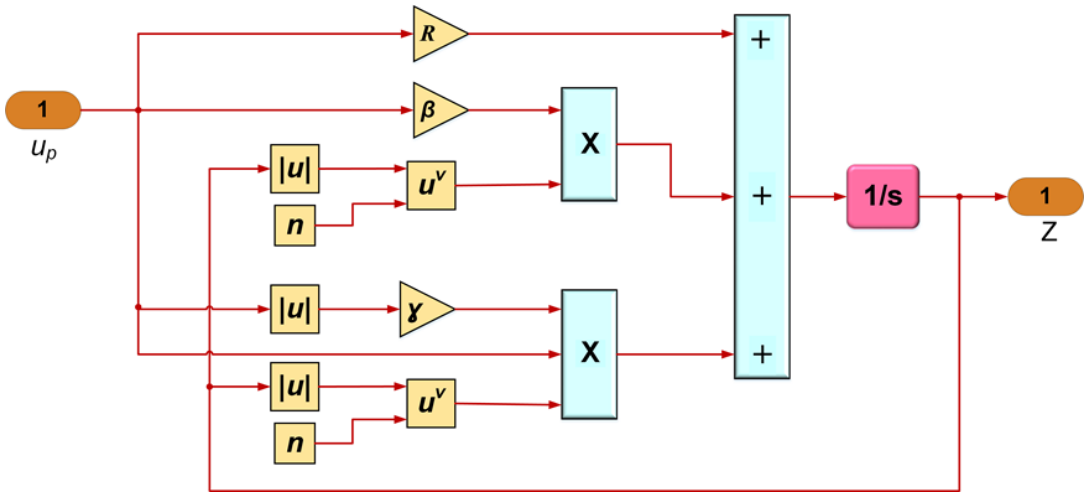

Figure 23: Evolutionary variable SIMULINK model.

The second device is the hydraulic actuator, which represents the active control class. The governing equation of the hydraulic actuator is mentioned in the previous chapter and it is repeated here for convenience (Dyke et al., 1995):

$$\dot{f}_{ha} = \frac{2\mu}{V_c}\left(A_{ha}k_q c_{ha} - k_c f_{ha} - A_{ha}^2 \dot{x}\right) \tag{2.18}$$

where c_{ha} is the difference between the command signal to the ith actuator, u_i, and the displacement of the ith actuator, x_i (Spencer, Christenson, & Dyke, 1998). Equation (2.18) is modified to accommodate the behavior of the current complex system as follows:

$$\dot{f}_{ha_{(i)}} = \lambda_1 u_i - \lambda_1 \left[x_{B1} - x_{B2}\right]_i - \lambda_2 \left[\dot{x}_{B1} - \dot{x}_{B2}\right]_i - \lambda_3 f_{ha(i)} \tag{3.32}$$

in which λ_1, λ_2, and λ_3 are listed in equation (2.21) for a hydraulic actuator with 1000 kN capacity.

Equation (3.32) along with the parameters listed in equation (2.21) are used to model the dynamics of the hydraulic actuator in the current study. The SIMULINK model for the hydraulic actuator is shown in Figure 24 below.

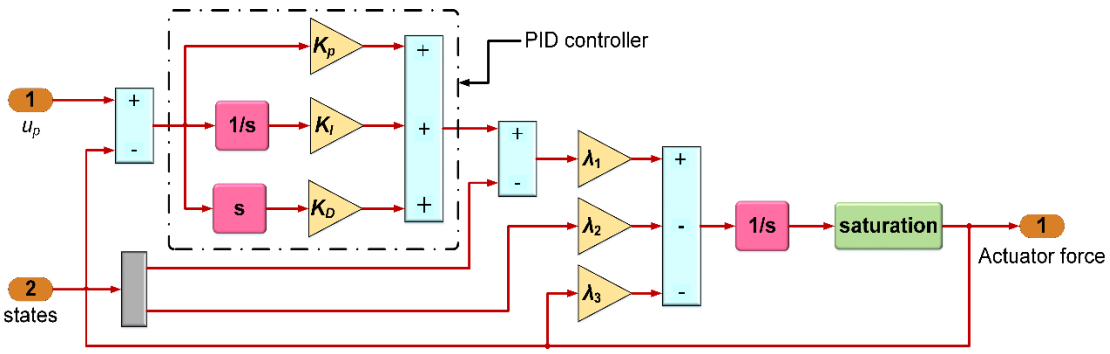

Figure 24: SIMULINK block diagram for the hydraulic actuator.

3.5 Numerical Study

The system considered in this study consists of two buildings (Building 1 and Building 2) connected at three levels as shown in Figure 21. Building 1 is five-stories tall in which $n_1 = 2$ and $n_2 = 3$, while Building 2 is a three-stories tall in which $n_2 = 3$. The two buildings are modeled as linear shear type buildings where the floors' masses are assumed to be lumped at the centers of the floors. The mass and stiffness of each floor of Building 1 and 2 are 478×10^3 kg and 1.6983×10^8 N/m, respectively. The total stiffness is 8.4915×10^8 N/m and 5.0949×10^8 N/m for Building 1 and 2, respectively. The mass and stiffness matrices of the two buildings were chosen to give the fundamental natural periods of the Building 1 and 2 as 1.35 s and 0.86 s, respectively. Having these different fundamental periods, the modes of the two buildings are well separated. It is worth

mentioning here that since the wave form of earthquakes is neglected as it is usually the case in the civil engineering applications, the dominant frequencies of the two buildings must not coincide; otherwise, the link would sway synchronously with the buildings making the use of the control devices within the links unfeasible. The damping matrix of the combined system is determined by using the Rayleigh damping formula with 2% damping ratio for both the lower and higher modes.

3.6 Results and Discussions

The simulations are carried out for both undamaged with clean measurements structure and damaged structure with noisy measurements. The damaged system cases considered in the current study are labeled as "Case 2" and "Case 3", respectively as shown in Table 6 below where the reductions are evenly applied throughout the coupled system.

Matlab R2017b and SIMULINK are interactively used to perform all the numerical simulations in the time domain. The built-in function ode45 is selected to be the primary solver. The initial conditions are assumed to be $\dot{x}(0) = 0$ (at rest), $u(0) = 0$ (no initial voltage), and $z(0) = 0$ (no initial hysteretic behavior). Noise signal is added to the actual measurements by generating a random signal using "Random Source" block in SIMULINK where the noise is bounded between 0.01 to -0.01 m. For SAC strategy, the tuning matrices T and $\bar{T}$ are chosen respectively to be $10^3[I]_{25\times25}$ and $10^{10}[I]_{25\times25}$ and σ is taken as 0.1. Six sensors are required to measure the output displacements of the

connected floors for both buildings. Since the control devices used in this study need to be provided with velocity, the measured displacements are differentiated to determine the corresponding velocities. The LQR and Lyapunov-based algorithms both require full-state availability; therefore, an observer has been designed to estimate the rest of the states from the measured data. The PID controller embedded in the hydraulic actuator has proportional, integral, and derivative parameters need to be tuned for the current system. The PID Tuner App built-in MATLAB is used to automatically tune these parameters. The tuned parameters are 1.50×10^{-6}, 0.0055, and -3.05×10^{-11} for the proportional, integral, and derivative, respectively.

Table 6: Mass and stiffness reductions.

	Mass Reduction (%)	Stiffness Reduction (%)
Case 1	0	0
Case 2	5	20
Case 3	7	30

The desired trajectories of the reference-model are determined by using an ideal (no device involved) LQR approach. The control command generated by SAC for Case 1, 2 and 3, respectively are depicted in Figure 25. Also, the resulting voltage, for Case 2 determined by the inverse model under LA16 and LA23 earthquakes are shown in Figure 26. The plots in Figure 25 show the amount of control forces required to force the plant to track the reference-model. However, since the capacity of the control device is limited to 1000 kN, the tracking cannot be perfect. It can be visualized from Figure 25 that when the

plant's parameters were changed in Case 2 and 3, the control command provided by SAC was adjusted accordingly to keep the tracking quality at the same level.

(a)

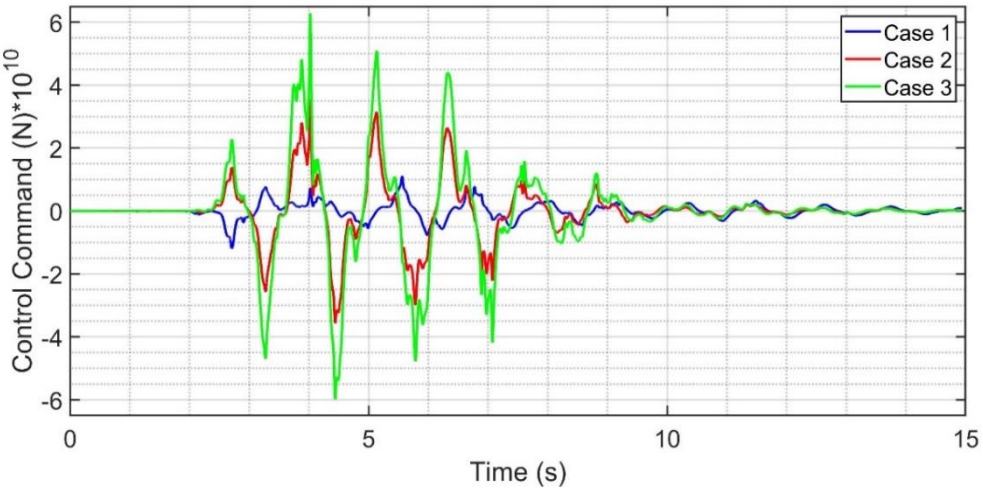

(b)

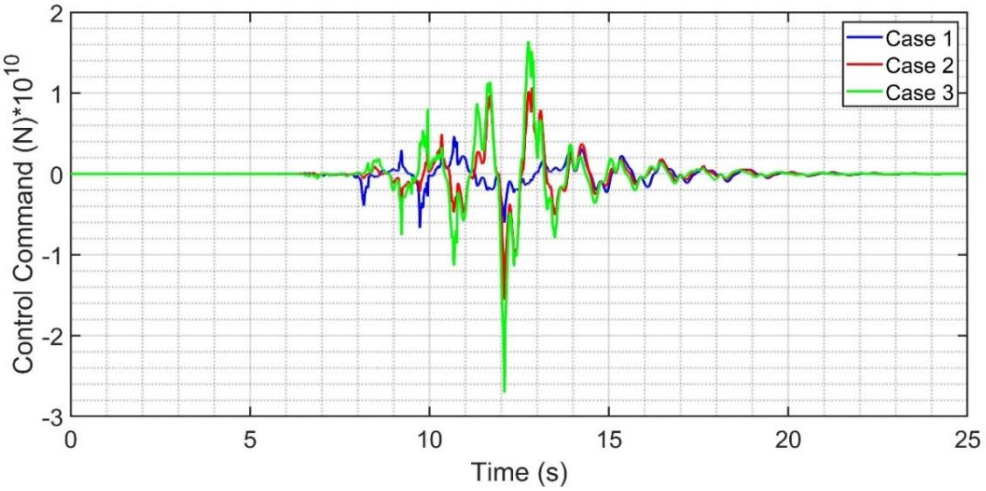

Figure 25: Control command generated by SAC for the third floor of Building 1 for both cases under: (a) LA16 earthquake, and (b) LA23 earthquake.

(a)

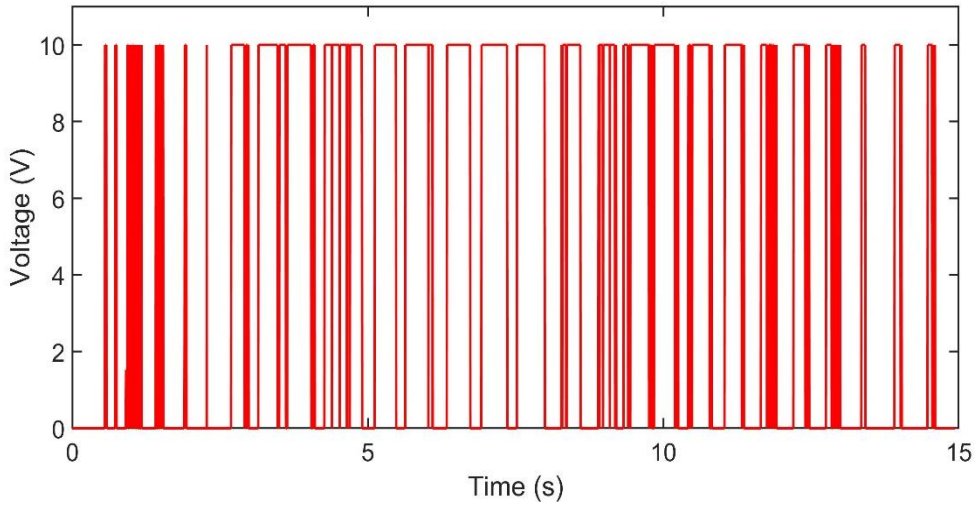

(b)

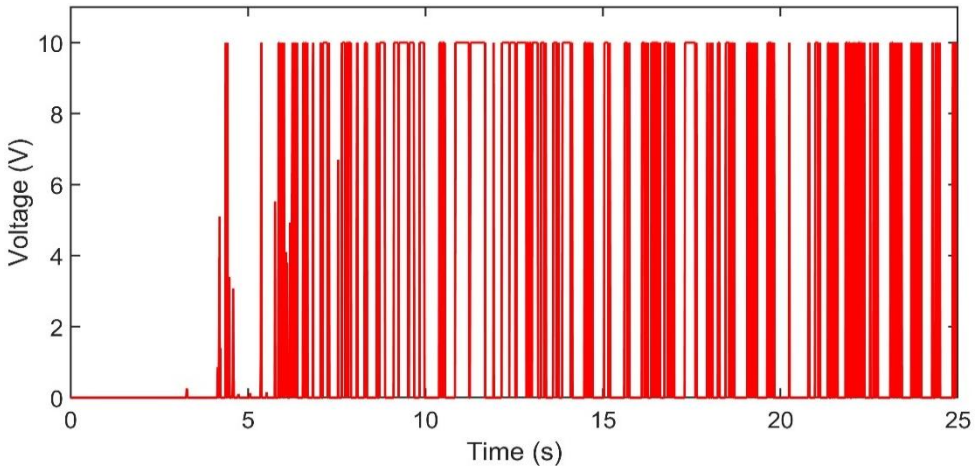

Figure 26: Applied voltage time history of the third floor of Building 1 for Case 2 under: (a) La16 earthquake, and (b) LA23 earthquake.

Figure 27 through Figure 29 show comparisons between SAC (MR) and LQR (MR) of the displacement time histories of the top floors of both buildings under LA10 earthquake for Case 1, 2, and 3, respectively. In Figure 27, the maximum displacement occurs at 17.68s for SAC (MR) and 17.96s for LQR (MR) for Building 1 and at 19.48s for SAC (MR) and 19.01s for LQR (MR) for Building 2. In Figure 28 and Figure 29 where

the damaged system with noise is considered, the peak displacement of the top floor of Building 1 controlled by SAC (MR) occurs at 17.69s and 17.75s for Case 2 and 3, respectively. on the other hand, the maximum displacement of the controlled top floor of Building 1 by LQR (MR) occurs 19.75s and 19.85 for Case 2 and 3, respectively. It can be noted that the peak displacements of the top floor of Building 1 for Case 1, 2, and 3 occur almost at the same time when SAC (MR) is used, which means that the adaptive controller maintains the performance even in the presence of noise and parameters changes. Though, this conclusion is not applicable for Building 2 as it is highly affected by the motion of the heavier building (Building 1).

Figure 30 and Figure 31 show a comparison of the peak inter-story drifts of the coupled system under LA10 and LA16 earthquakes for Case 1. Figure 30 shows the peak inter-story drifts of Building 1 and 2 for Case 1 under LA10 earthquake. It can be noticed from the above figure that SAC (MR) competes very well with LQR (MR) for Building 2's first floor where they give close results while for Building 1, LQR (MR) achieves more reduction for the first story. In contracts, the other schemes amplify the maximum drifts for both buildings.

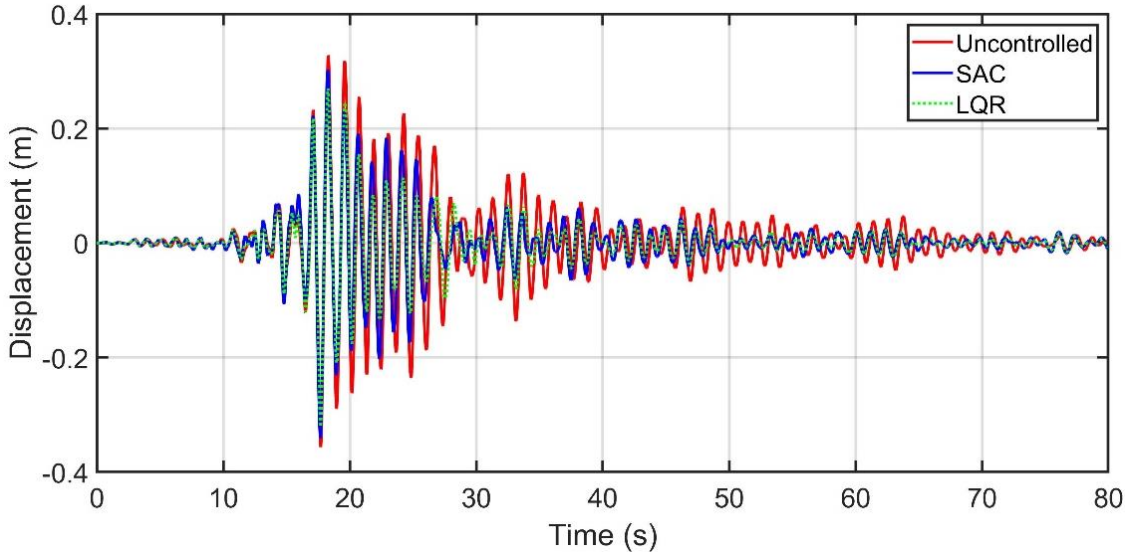

(a)

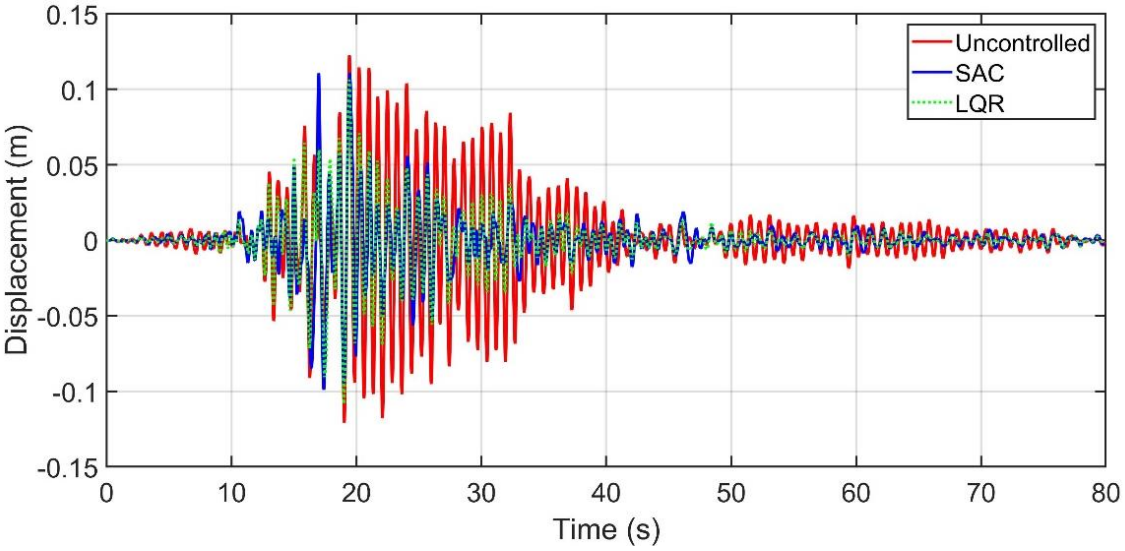

(b)

Figure 27: Displacement time history of the top floors for Case 1 under LA10 earthquake: (a) Building 1 and (b) Building 2.

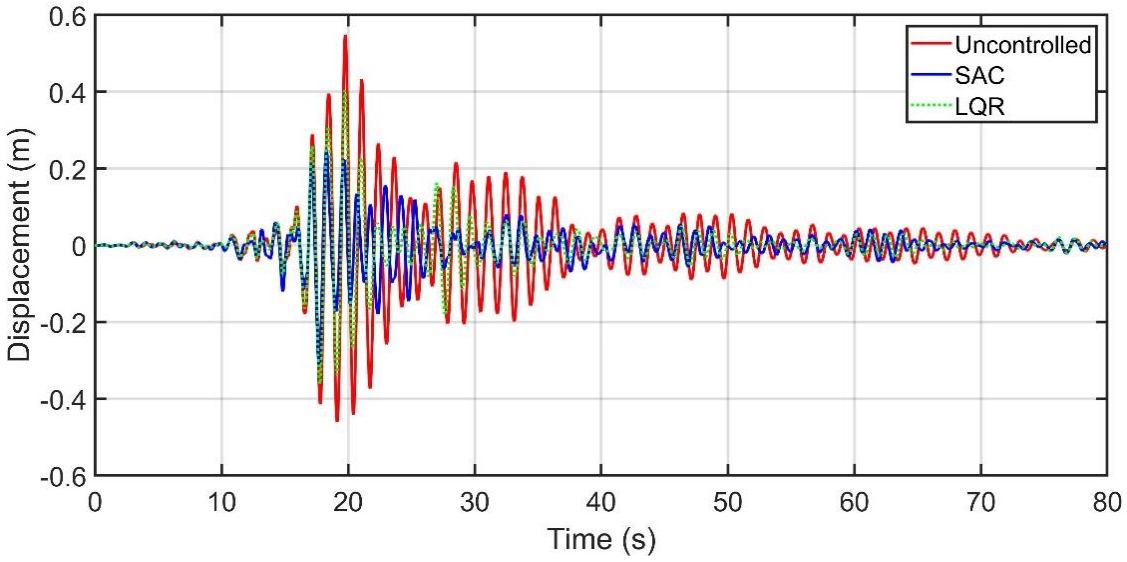

(a)

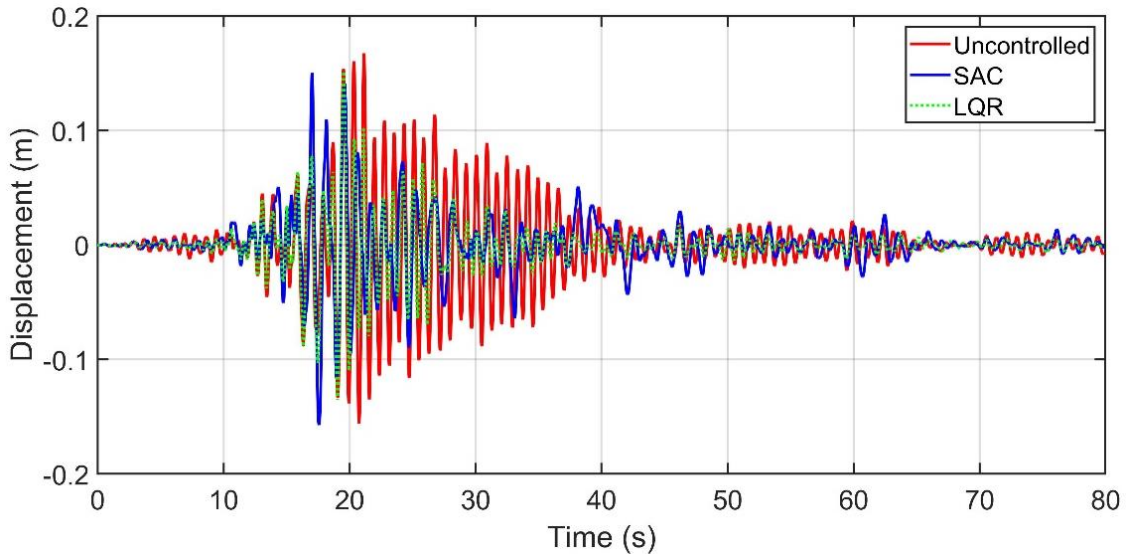

(b)

Figure 28: Displacement time history of the top floors for Case 2 under LA10 earthquake: (a) Building 1 and (b) Building 2.

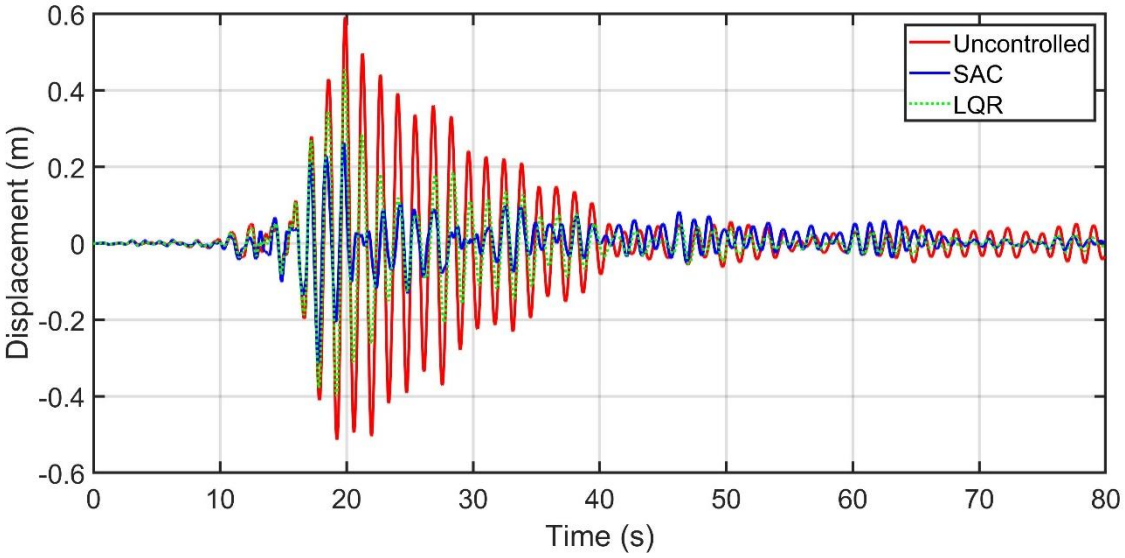

(a)

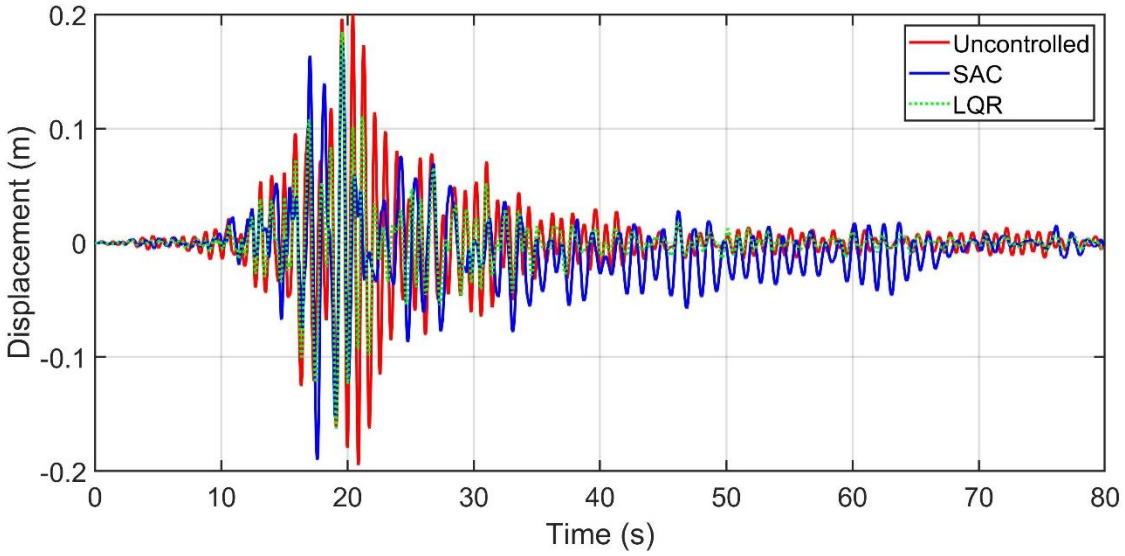

(b)

Figure 29: Displacement time history of the top floors for Case 3 under LA10 earthquake: (a) Building 1, and (b) Building 2.

Figure 31 depicts the maximum drift profiles under LA16 earthquake for Case 1. This figure shows that SAC (MR) achieves the biggest reduction for Building 2 compared to the other control strategies while for Building 1, LQR (MR) and LQR (HA) performs better than SAC (MR). The discrepancy in the performance of each controller between Figure 30 and Figure 31 for Building 1 and 2 should be understood in the context of the complexity of the coupled system's dynamics and the frequency content of each ground motion.

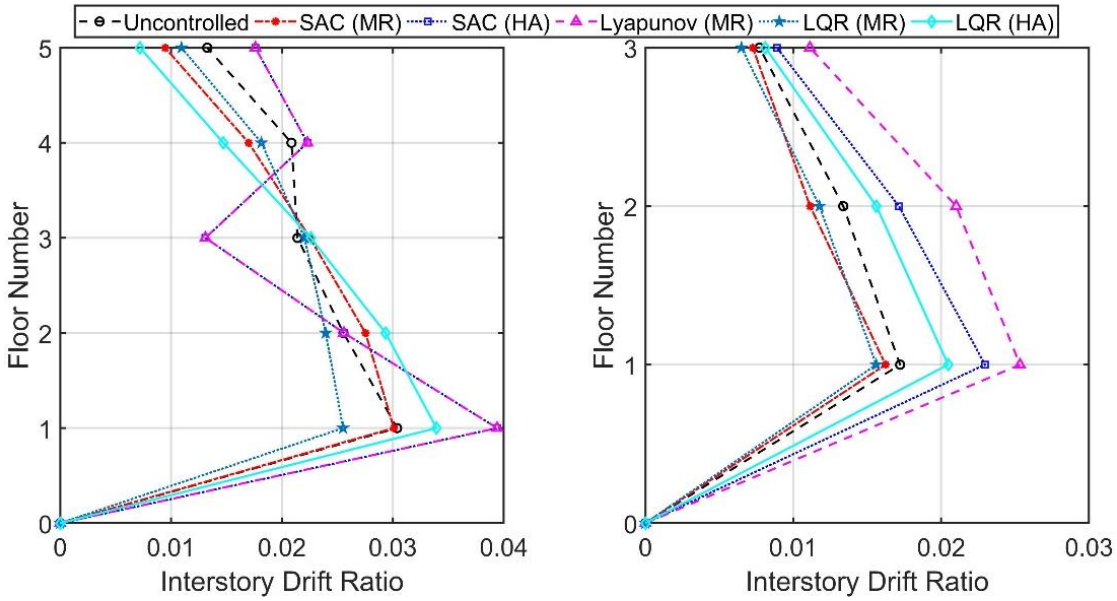

Figure 30: Maximum inter-story drift for Case 1 under LA10 excitation for Building 1 (left) and Building 2 (right).

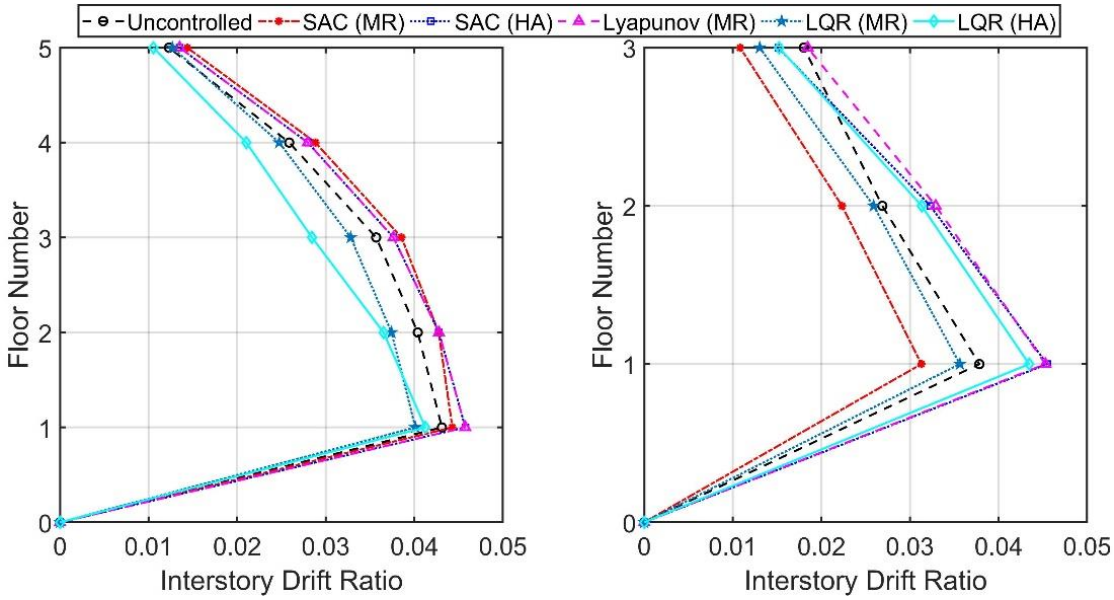

Figure 31: Maximum inter-story drift for Case 1 under LA16 excitation for Building 1 (left) and Building 2 (right).

Figure 32 through Figure 35 depict the peak inter-story drift profiles for the damaged cases, Case 2 and 3, respectively. Figure 32 shows the peak inter-story drifts of Building 1 and 2 for Case 2 under LA10 earthquake. It can be seen from the above figure that using the SAC (MR) reduces the maximum inter-story drift for Building 1 by 36.37% and LQR (MR) reduces it by 22.7% while the other schemes behave far worse. Under LA16, Figure 33, the reduction in the peak drift for the first floor achieved by SAC (MR) is 46.6% and 33.3% for Building 1 and 2, respectively while the LQR (MR) reduces the peak drift by 30.10% and 35.0% for Building 1 and 2, respectively. For Case 3, SAC(MR) significantly reduces the maximum inter-story drifts of Building 1 and performs relatively good in Building 2, as shown in Figure 34 and Figure 35, respectively.

Different evaluation criteria were developed for the benchmark problem in structural control to assess the performance of control strategies for buildings (Spencer et al., 1998). The set of these criteria listed in equation (3.33) below is used in the current study to evaluate the performance of the controlled coupled system as follows:

$$J_1 = \max\left\{\frac{\max\left|x_i^c(t)\right|}{\left|x_{\max}^{un}\right|}\right\} \qquad J_2 = \max\left\{\frac{\max\left|\ddot{x}_i^c(t)\right|}{\left|\ddot{x}_{\max}^{un}\right|}\right\}$$

$$J_3 = \max\left\{\frac{\max\dfrac{\left|d_i^c(t)\right|}{h_i}}{\left|d_{\max}^{un}\right|}\right\} \qquad J_4 = \max\left\{\frac{\left|m_i\ddot{x}_i^c(t)\right|}{\left|m_i\ddot{x}_i^{un}(t)\right|}\right\} \tag{3.33}$$

where the superscripts *c* and *un* represent the controlled and uncontrolled responses, respectively. J_1, J_2, J_3, and J_4 are the displacement, acceleration, drift, and base shear criteria, respectively. The d_i and h_i are the inter-story drift and height of the *i*th floor, respectively.

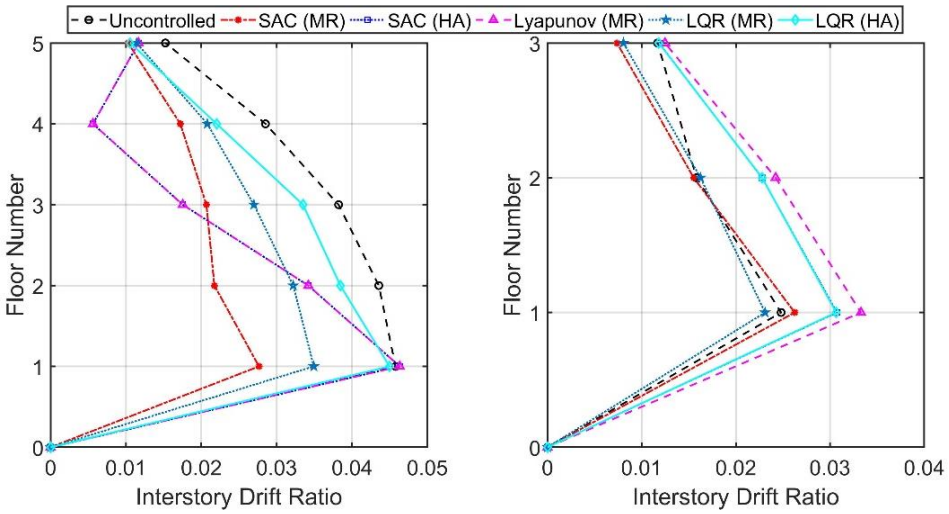

Figure 32: Maximum inter-story drift for Case 2 under LA10 excitation for Building 1 (left) and Building 2 (right).

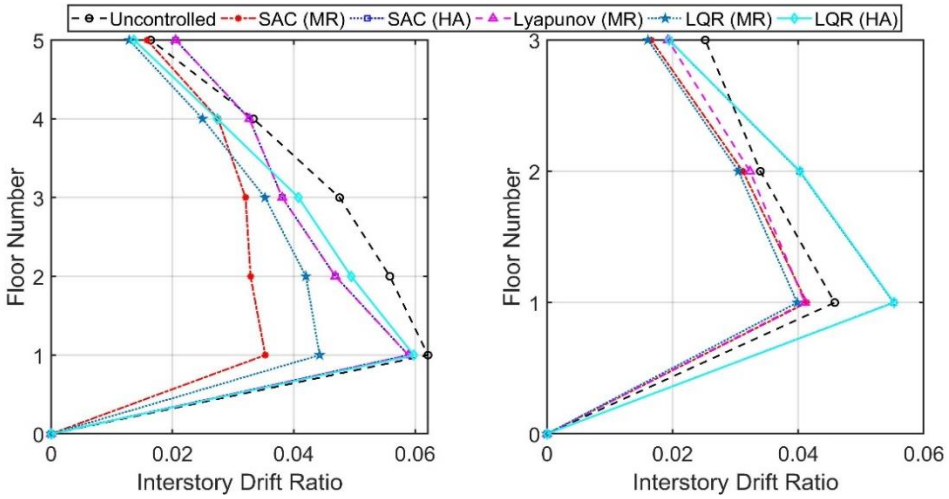

Figure 33: Maximum inter-story drift for Case 2 under LA16 excitation for Building 1 (left) and Building 2 (right).

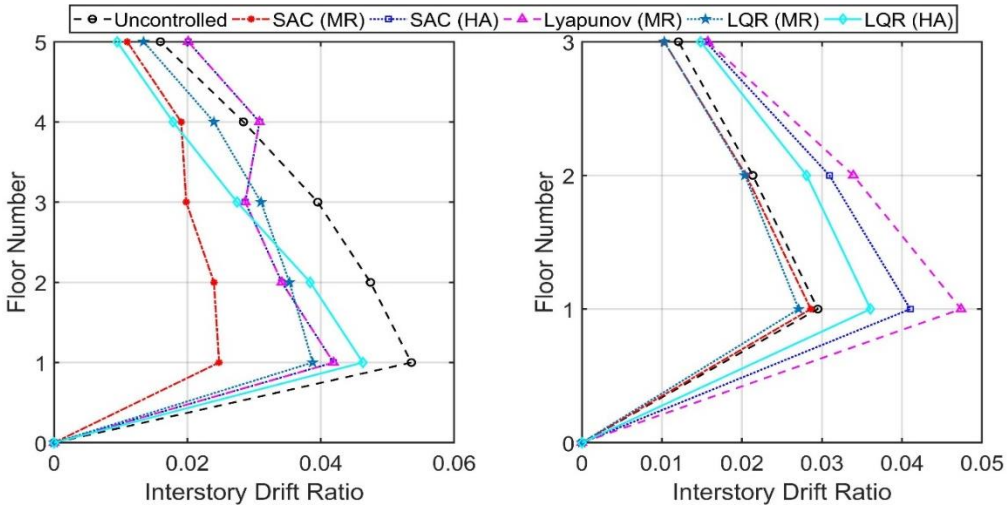

Figure 34: Maximum inter-story drift for Case 3 under LA10 excitation for Building 1 (left) and Building 2 (right).

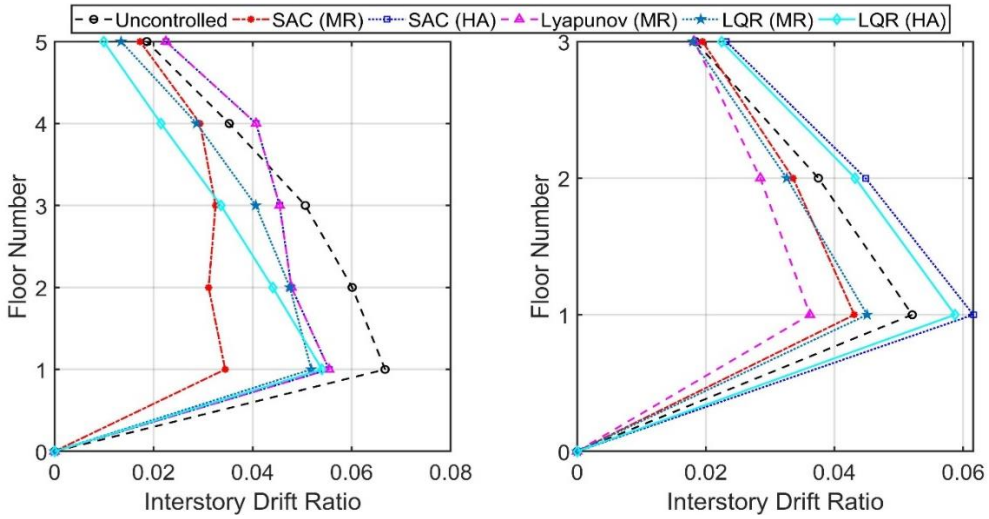

Figure 35: Maximum inter-story drift for Case 3 under LA16 excitation for Building 1 (left) and Building 2 (right).

The evaluation criteria for the coupled system for all cases under five ground motions are listed in Table 7. For Case 1, the results indicate that the hydraulic actuator

(HA) exhibits response amplification for most excitations. Also, Lyapunov (MR) increases the indices J_1, J_2, and J_4 specifically for most excitations. The LQR (MR) performs quite good in reducing the peak displacements, accelerations, and inter-story drift, but it increases the base shear for both buildings under almost all the excitations. The more sustainable performance is SAC (MR) under all the excitations considered in this study. SAC (MR) reduces the peak displacements for Building 2 and with some exceptions for Building1 as under LA16 and LS19F, specifically. It is interesting that SAC (MR) performs well in reducing the acceleration as well as the displacement and inter-story drift. Moreover, SAC (MR) performs better than the other methods in reducing the inter-story drifts and base shear.

For Case 2 and 3, both SAC (HA) and Lyapunov (MR) introduces undesirable behavior by increasing the peak responses for Building 1 and/or Building 2 under some excitations as LA16, LA23, and LS19F. LQR (MR) and LQR (HA) both make the base shear much worse than the uncontrolled system. SAC (MR) performs quite well in almost all cases under different earthquakes. In contrast to the LQR, SAC (MR) decreases the base shear significantly.

Table 7: Evaluated Performance criteria for Building 1.

		Control Method	J_1	J_2	J_3	J_4
LA10	Case 1	LQR (MR)	0.902	0.825	0.825	0.839
		LQR (HA)	0.967	0.831	0.829	1.117
		SAC (MR)	0.956	0.809	0.749	0.990
		SAC (HA)	1.008	0.957	0.965	1.244
		Lyapunov (MR)	1.058	1.645	1.643	1.297
	Case 2	LQR (MR)	0.737	0.730	0.732	0.763
		LQR (HA)	0.872	0.784	0.791	0.982
		SAC (MR)	0.569	0.764	0.694	0.603
		SAC (HA)	0.872	0.881	0.792	0.982
		Lyapunov (MR)	0.673	1.283	1.303	1.012
	Case 3	LQR (MR)	0.770	0.794	0.796	0.723
		LQR (HA)	0.754	0.638	0.631	0.864
		SAC (MR)	0.533	0.759	0.653	0.462
		SAC (HA)	0.789	0.876	0.765	0.934
		Lyapunov (MR)	0.841	1.562	1.573	0.782
LA23	Case 1	LQR (MR)	0.946	0.819	0.815	0.640
		LQR (HA)	1.042	0.907	0.899	0.694
		SAC (MR)	0.972	1.040	1.102	1.088
		SAC (HA)	1.087	1.062	1.016	0.703
		Lyapunov (MR)	1.125	1.957	1.955	1.074
	Case 2	LQR (MR)	0.827	0.792	0.791	0.614
		LQR (HA)	1.059	0.898	0.890	0.896
		SAC (MR)	0.572	0.805	0.808	0.526
		SAC (HA)	1.058	0.969	0.889	0.895
		Lyapunov (MR)	0.966	1.530	1.537	0.740
	Case 3	LQR (MR)	0.842	0.792	0.794	0.732
		LQR (HA)	0.968	0.899	0.925	0.908
		SAC (MR)	0.474	0.877	0.735	0.399
		SAC (HA)	0.999	1.178	1.101	0.984
		Lyapunov (MR)	0.986	2.011	2.036	0.882

Table 7: Continued.

		Control Method	J_1	J_2	J_3	J_4
LS19F	Case 1	LQR (MR)	0.893	0.869	0.871	1.495
		LQR (HA)	0.951	0.917	0.917	1.878
		SAC (MR)	0.999	1.038	0.941	0.961
		SAC (HA)	0.951	1.017	0.918	1.879
		Lyapunov (MR)	0.937	1.151	1.158	1.566
	Case 2	LQR (MR)	0.737	0.906	0.903	1.154
		LQR (HA)	0.859	0.910	0.906	1.509
		SAC (MR)	0.690	1.028	0.935	0.582
		SAC (HA)	0.859	0.912	0.907	1.510
		Lyapunov (MR)	0.844	1.307	1.313	1.420
	Case 3	LQR (MR)	0.729	0.836	0.832	1.058
		LQR (HA)	0.818	0.758	0.756	1.271
		SAC (MR)	0.697	1.043	0.990	0.675
		SAC (HA)	0.871	0.801	0.844	1.349
		Lyapunov (MR)	0.867	1.298	1.303	1.426
NF01	Case 1	LQR (MR)	0.799	0.811	0.810	1.230
		LQR (HA)	1.086	0.960	0.968	1.816
		SAC (MR)	0.774	0.819	0.655	0.657
		SAC (HA)	1.086	1.091	0.971	1.818
		Lyapunov (MR)	0.835	1.324	1.327	1.599
	Case 2	LQR (MR)	0.817	0.799	0.808	1.106
		LQR (HA)	0.880	1.051	1.046	1.119
		SAC (MR)	0.535	0.917	0.682	0.500
		SAC (HA)	0.881	1.054	1.048	1.120
		Lyapunov (MR)	0.814	1.172	1.164	1.096
	Case 3	LQR (MR)	0.886	0.920	0.908	0.960
		LQR (HA)	0.786	0.789	0.798	0.822
		SAC (MR)	0.640	0.940	0.943	0.688
		SAC (HA)	0.832	1.067	0.888	0.892
		Lyapunov (MR)	0.977	1.373	1.364	1.205

Table 7: Continued.

		Control Method	J_1	J_2	J_3	J_4
LA16	Case 1	LQR (MR)	0.939	0.829	0.823	1.320
		LQR (HA)	0.875	0.770	0.773	1.357
		SAC (MR)	1.072	0.981	0.998	1.027
		SAC (HA)	1.072	0.963	0.860	1.457
		Lyapunov (MR)	1.065	1.201	1.206	1.506
	Case 2	LQR (MR)	0.740	0.782	0.786	0.967
		LQR (HA)	0.887	0.793	0.810	1.306
		SAC (MR)	0.666	0.933	0.834	0.568
		SAC (HA)	0.666	0.883	0.809	1.304
		Lyapunov (MR)	0.915	1.310	1.317	1.286
	Case 3	LQR (MR)	0.787	0.871	0.867	0.967
		LQR (HA)	0.704	0.611	0.608	1.007
		SAC (MR)	0.625	0.885	0.814	0.516
		SAC (HA)	0.625	0.825	0.683	1.090
		Lyapunov (MR)	0.915	1.415	1.425	1.034

3.7 Epilogue

The effectiveness of the simple adaptive control (SAC) method in mitigating the seismic responses of the coupled system was investigated in this study. The coupled system consists of two buildings with different heights and connected by MR dampers or hydraulic actuators at three levels. The aim of using the adaptive controller was to enhance the structural performance by reducing the displacements and inter-story drifts during the seismic excitations. The SAC method is compared with optimal control theory and Lyapunov stability theory-based algorithm. The numerical simulations' results show that SAC is quite effective in reducing the displacements and the inter-story drifts even with the presence of noise while reducing the peak absolute acceleration for most of the excitations considered. The effectiveness of the SAC is more notable when the parameter

variations was introduced to the structural system. SAC proved to be more interesting than the other classical control methods since it can adapt itself with any change in the system parameters which makes it a good fit for the earthquake engineering applications where the damage is highly expected under even moderate earthquakes. The results also show that the MR damper is more effective in reducing the structural responses than the hydraulic actuator which amplifies the responses under different excitations. It can be concluded from the current study that SAC with the MR damper has more effective and sustainable performance under different earthquakes and in the presence of noise and parameter variations.

References

Barkana, I. (2016). Robustness and perfect tracking in simple adaptive control. International Journal of Adaptive Control and Signal Processing, 30(8-10), 1118-1151. doi:10.1002/acs.2573

Chang, C.-C., & Zhou, L. (2002). Neural network emulation of inverse dynamics for a magnetorheological damper. Journal of Structural Engineering, 128(2), 231-239.

Dyke, S. J., Spencer, B. F., Sain, M. K., & Carlson, J. D. (1996). Modeling and control of magnetorheological dampers for seismic response reduction. *Smart materials and structures*, *5*(5), 565.

Dyke, S. J., Spencer, B. F., Quast, P., & Sain, M. K. (1995). Role of Control-Structure Interaction in Protective System Design. Journal of Engineering Mechanics, 121(2), 322–338. doi:10.1061/(asce)0733-9399(1995)121:2(322).

Dyke, S. J., Yi, F., Frech, S., & Carlson, J. D. (1999). Application of Magnetorheological Dampers to Seismically Excited Structures,# 361. In *Proceedings of the 17th International Modal Analysis Conference* (Vol. 3727, p. 410).

Ioannou, P., & Kokotovic, P. (1983). Adaptive Systems with Reduced Models. Springer-Verlag, Berlin.

Barkana, I. (2014). Simple adaptive control–a stable direct model reference adaptive control methodology–brief survey. International Journal of Adaptive Control and Signal Processing, 28(7-8), 567-603.

Kaufman, H., Barkana, I., & Sobel, K. (1994). Direct Adaptive Control Algorithms: Theory and Applications. doi:10.1007/978-1-4684-0217-9

Motra, G. B., Mallik, W., & Chandiramani, N. K. (2011). Semi-active vibration control of connected buildings using magnetorheological dampers. *Journal of intelligent material systems and structures*, *22*(16), 1811-1827.

Al-Fahdawi, O. A. S., Barroso, L. R., & Soares, R. W. (2018). Utilizing the Adaptive Control in Mitigating the Seismic Response of Adjacent Buildings Connected with MR Dampers. 2018 Annual American Control Conference (ACC). doi:10.23919/acc.2018.8431135.

Al-Fahdawi, O. A. S., Barroso, L. R., & Soares, R. W. (2019). Simple adaptive control method for mitigating the seismic responses of coupled adjacent buildings considering parameter variations. Engineering Structures, 186, 369–381. doi:10.1016/j.engstruct.2019.02.025.

Soares, R. W., Barroso, L. R., & Al-Fahdawi, O. A. S. (2018). Simple Adaptive Control Strategy Applied to Reduce Response of Bridge Structure Subjected to Changes in Plant. 2018 Annual American Control Conference (ACC). doi:10.23919/acc.2018.8431623

Spencer, B. F., Christenson, R. E., & Dyke, S. J. (1998). Next generation benchmark control problem for seismically excited buildings. In *Proceedings of the Second World Conference on Structural Control* (Vol. 2, pp. 1135-1360). Japan: Kyoto.

Yi, F., Dyke, S. J., Caicedo, J. M., & Carlson, J. D. (1999). Seismic response control using smart dampers. In Proceedings of the 1999 American Control Conference (Cat. No. 99CH36251) (Vol. 2, pp. 1022-1026). IEEE.

CHAPTER IV

ADAPTIVE CONTROL FOR NONLINEAR COUPLED BUILDINGS

The efficacy of using the simple adaptive control method for alleviating the seismic responses of two nonlinear adjacent buildings connected at multiple levels with magneto-rheological dampers is investigated in this chapter. The connected system is formed by two shear-type model buildings that are of the same height but have different dynamic characteristics so that the fundamental frequencies of the individual buildings do not coincide. A stable hysteretic behavior of the structural system is considered in the current study, which captures the variation in flexibility and energy loss under various intensity levels of seismic events. The Bouc-Wen's nonlinear differential equation is utilized to model the hysteretic behavior of the restoring force-displacement smooth curve of the developed nonlinear structural system which is then integrated into a semi-active adaptive control system. The advantage of using the Bouc-Wen model is that it has the ability to mathematically track various shapes of the force-displacement curves by adjusting its non-dimensional parameters. The proposed nonlinear model is validated through a finite element model. Adaptive control is well suited to handle the nonlinear behavior because the adaptive control gains can be adjusted depending on the situation through a closed-loop action to yield better performance. The results presented in this chapter show that using the adaptive controller to drive the magneto-rheological dampers connecting two adjacent nonlinear buildings can be used to effectively alleviate the

seismic responses and reduce permanent deformations. However, the performance improvement is not the same under all ground motions considered in this study.

4.1 Prelude

Civil engineering structures may experience large-scale damage due to hazardous events such as earthquakes. This urges civil engineers to explore different strategies to mitigate the ramifications of these events. One of these strategies is interconnecting adjacent buildings with single or multiple links. The coupling of adjacent structures has proven to be both architecturally and functionally beneficial. Structural performance can be enhanced by implementing devices that dissipate energy in adjacent buildings. In the last few decades, significant advances have been made in this technology to alleviate the seismic responses of structures subjected to moderate to severe earthquakes. However, much of this research has been performed on highly simplified linear systems that do not provide any information about the nonlinear and/or plastic responses.

Engineers have been aware of the importance of coupling adjacent buildings in order to mitigate the structural responses to earthquakes and hurricanes since the 1970s. Since then, many studies have been published on connecting adjacent buildings with fully passive links (Richardson, Walsh, & Abdullah, 2013; Westermo, 1989). Implementation of active control strategies began in the 1990s. For example, few studies proposed using the active control strategy to connect adjacent high-rise buildings with hydraulic actuators (Mitsuta et al., 1994; Seto, 1999). In addition to the analytical studies conducted on

coupled buildings, there has been few experimental studies on the subject (Mitsuta et al., 1994; Yamada et al., 1994).

Due to the drawbacks of the active control such as high-power demand and potential for instability, the semi-active control method has been embraced by researchers because it is free of both the drawbacks of the other technique. One of the more advanced and effective semi-active devices is the magneto-rheological (MR) damper which requires only minimal power, and moreover, it continues to work as a passive device when there is no electricity during hazardous events. Many studies have been carried out on using MR dampers to connect adjacent buildings to attenuate seismic responses

In recent years, there has been an increasing demand for solving civil engineering problems using nonlinear time history analysis. Most of the nonlinear dynamic problems are either computationally intensive or very difficult; therefore, numerical solutions are the best practical method for solving these problems (Tedesco, McDougal, & Ross, 1999). There are two sources of nonlinearities: geometric and material. The former is based on the fact that the equilibrium equations are derived based on the deformed geometry, which includes P-Δ effects. This type of nonlinearity is vital for tall buildings that must withstand high axial forces. In this study, the focus is on the material nonlinearity in which the structures are pushed beyond their elastic limit where the stress-strain relationship is nonlinear and plastic. The analysis of such problems can be simplified by assuming bilinear behavior. More realistic representation of the nonlinear behavior is represented as linear up to the yielding point, where the first yielding occurs. The constituent cross sections of the system plasticize as the load increases and plastic hinges form when full

plastification of a cross section is attained. When unloading, the curve rebounds in a linear fashion leaving a permanent displacement. If the loading is reversed, the hysteretic curve will be reversed accordingly. The hysteretic loop continues until all energy in the system has dissipated. In the following section, a smooth hysteretic model is adopted to represent the behavior of a materially nonlinear system. In such a system, it is crucial that the chosen controller can handle this inevitable nonlinear behavior.

Despite the impressive achievements of classical control design, the performance of the classical control methods seems to be limited since these methods cannot cope with nonlinearities and time-varying parameters in real-world applications (Barkana, 2014). Therefore, the adaptive control strategy promises to be more suitable for such systems because it applies the right control commands to the right situations. Under seismic excitations, civil structures experience damage where the amount of the damage depends on the severity of the seismic forces and the dynamic characteristics of the structure itself. Therefore, using an adaptive control method that can deal with the structural damage is paramount. In the adaptive control approach, the control command can be adjusted online in order to reduce the effects of uncertain parameters (Kaufman, Barkana, & Sobel, 1994).

While there are few studies on using the adaptive control in enhancing the performance of conventional buildings, no previous work has been done to utilize the adaptive control for nonlinear coupled buildings. To this end, the purpose of this chapter is to fill this gap by using SAC to alleviate the seismic structural responses of two nonlinear adjacent buildings connected with MR dampers. The performance of the coupled system is studied under three major earthquakes with different intensity levels.

4.2 Hysteretic Model

Various hysteretic models have been developed to emulate the restoring force-displacement relationship of inelastic systems. One of the most popular models is the Bouc-Wen (Wen, 1976) which includes several parameters enabling a mathematical tractability for expressing a variety of hysteretic patterns. The model is governed by a single nonlinear differential equation that can be applied to a variety of engineering problems. According to the Bouc-Wen model, the restoring force, F_s, can be decomposed into two components, F_e and F_h, representing the elastic and hysteretic restoring forces, respectively. Therefore, the restoring force can be expressed as:

$$F_s\left(x,\dot{x},t\right)=F_e\left(t\right)+F_h\left(t\right)=\alpha K_e x\left(t\right)+\left[1-\alpha\right]K_e z\left(t\right) \tag{4.1}$$

where K_e is the pre-yielding stiffness and K_h is the stiffness associated with the nonlinear behavior. $x(t)$ is the relative displacement vector and α is the ratio of the post-yielding to pre-yielding stiffness for each time step which can be calculated as:

$$\alpha=\frac{K_{post}}{K_e}=\frac{1}{K_e}\frac{F_{s\,i+1}-F_{s\,i}}{x_{i+1}-x_i} \tag{4.2}$$

where K_{post} is the post-yielding stiffness that represents the slope of the force-displacement curve at each time step. The subscripts i and i+1 in equation (4.2) refer to the beginnings and ends of the time steps.

The vector $z(t)$, in equation (4.1), is the hysteretic displacement that is governed by the following equation with zero initial condition [$z(0) = 0$]:

$$\dot{z}\left(t\right)=\dot{x}\left(t\right)\left[A-\left(\beta+\gamma\,\mathrm{sgn}\left(\dot{x}\left(t\right)z\left(t\right)\right)\right)\left|z\left(t\right)\right|^n\right] \tag{4.3}$$

where A, β, and γ are parameters that control the general shape of the hysteretic loop while the sharpness of the force-displacement curve is controlled by the parameter n (Wen, 1976). *sgn*(.) is the signum function. By adjusting the parameter n, the elastic-perfectly plastic model can be achieved by taken $n = \infty$ (Wen, 1976). Various restoring force-displacement curves are plotted in Figure 36 for different values of n. Assuming the yield displacement $Y = (\beta + \gamma)^{1/n}$ and taking β and γ as equal (Barroso, Hunt, & Chase, 2002), equation (4.2) can be written as:

$$\dot{z}(t) = \dot{x}(t)\left[A - 0.5\left(1 + \operatorname{sgn}\left(\dot{x}(t)\, z(t)\right)\right)\left|\frac{z(t)}{Y}\right|^{n} \right] \tag{4.4}$$

In order to reduce the model to a formulation with well-defined properties, Constantinou and Adnane (1987) suggested imposing the following constraint:

$$\frac{A}{\beta + \gamma} = 1 \tag{4.5}$$

A system with a materially nonlinear behavior can now be solved by substituting the above hysteretic model, equation (4.4), in an equation of motion of that system and then using any number of numerical algorithms.

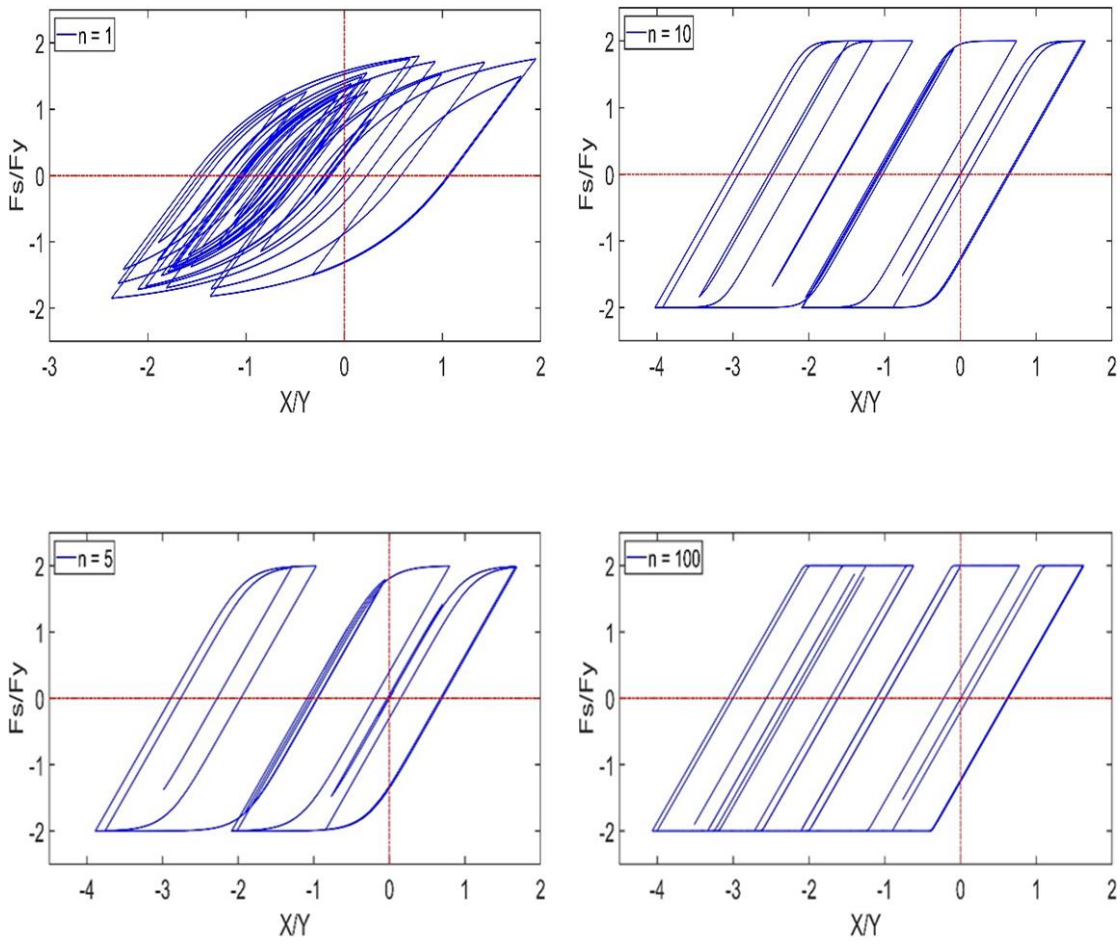

Figure 36: Portion of hysteretic loops for different values of the exponent, *n*.

4.3 Hysteretic Model Verification

To validate the model described in the previous section, an idealized one-story building shown in Figure 37 is considered. The equation of motion of the system is written as:

$$m\ddot{x}(t) + c\dot{x}(t) + F_s(x, \dot{x}, t) = -m1\ddot{x}_g(t) \tag{4.6}$$

in which *m* and *c* are the mass and damping parameters of the system. $F_s\left(x,\dot{x},t\right)$ is the restoring force defined in equation (4.1) and $\ddot{x}_g\left(t\right)$ is the ground acceleration vector. By substituting equation (4.1) into (4.6) and re-arranging yields the following equation:

$$\ddot{x}\left(t\right)=-1\ddot{x}_g\left(t\right)-\frac{c}{m}\dot{x}\left(t\right)+\alpha\frac{k_e}{m}\left[z\left(t\right)-x\left(t\right)\right]-\frac{k_e}{m}z\left(t\right) \tag{4.7}$$

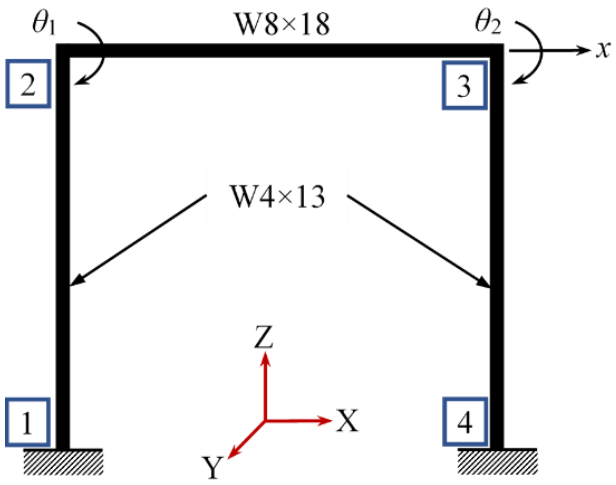

Figure 37: Single-story frame with three degrees-of-freedom.

MATLAB and SIMULINK are used to solve equation (4.7) in the time domain. The built-in function ode45 from the MATLAB ode suite is used as a primary solver. Ode45 is a variable time step integration algorithm that is suitable for non-stiff differential equations. The solution is compared with the finite element solution. SAP2000 software is chosen to perform the finite element analysis of the nonlinear system where the force-displacement relationship is modeled as a bilinear curve. The inelastic behavior is assumed to occur at the ends of each member where plastic hinges are inserted. The minimum yield

stress of the columns and the girder is 3.447×10^8 N/m^2. Concentrated mass equals 1.5×10^5 kg was added at node 2 and 3, respectively. The system is modeled as a 2-D frame with two rotational degrees of freedom and one translational. The proportional damping ratio was set to 2% of the first and second modes. Figure 38 shows a comparison of the translational displacement time history between the finite element method and the Bouc-Wen model. The results show that there is a significant difference when the parameter *n* is relatively small, and the results become closer and closer as *n* increases. The reason is that as *n* increases, the restoring force-displacement curve becomes bilinear as in the finite element software.

4.4 Structural System Model

Two adjacent buildings are idealized as nonlinear shear-type buildings where the masses of the floors are assumed to be concentrated at the centers of these floors. The number of stories of the two buildings are the same and the corresponding floors of the two buildings are collinear. The number of the floors is n_1 and n_2 for Building 1 and 2, respectively as shown in Figure 39. The two buildings are assumed to be symmetric in terms of their planes' alignment and asymmetric in their dynamic's characteristics. The system is assumed to be subjected to the same unidirectional earthquake excitation with negligence of the waveform of the ground motion, and any effect due to soil-structure interaction is also neglected. The MR dampers connecting the two buildings are assumed to be rigidly connected between the inline floors.

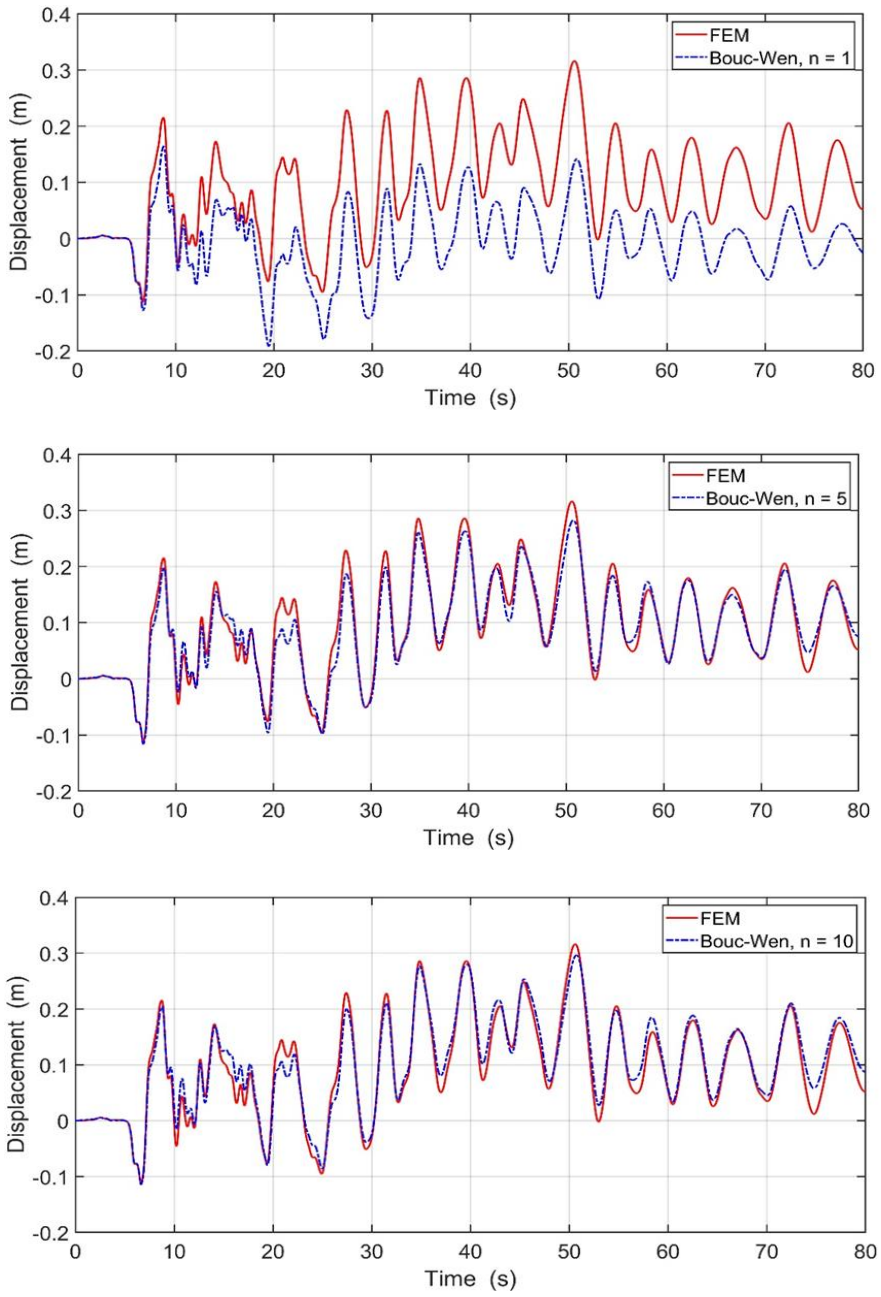

Figure 38: Translational displacement time histories with different values of the exponent, *n*.

The governing equation of motion of the combined nonlinear system can be written in a compact form as:

$$[M_s]\{\ddot{x}(t)\}+[C_s]\{\dot{x}(t)\}+F_s(x,\dot{x},t)=[J]\{f_m(t)\}-[M_s][r]\{\ddot{x}_g(t)\} \tag{4.8}$$

where M_s, C_s, and K_s are the mass, damping and stiffness matrices of the coupled system, respectively. $f_m(t)$ is the control forces vector; J is the location matrix of the control devices; $x(t)$, $\dot{x}(t)$, and $\ddot{x}(t)$ are the relative displacement, velocity, and acceleration vectors, respectively. r is a vector with all elements equal ones; $\ddot{x}_g(t)$ is the ground acceleration vector. $F_s(x,\dot{x},t)$ is as defined in equation (4.1).

The structural mass, stiffness, and damping matrices of the coupled system can be explicitly defined as:

$$M_{s(2n_1,2n_2)}=\begin{bmatrix}[M_1]_{(n_1,n_1)} & [0]_{(n_1,n_1)}\\ [0]_{(n_2,n_2)} & [M_2]_{(n_2,n_2)}\end{bmatrix} \tag{4.9}$$

$$K_s=\begin{bmatrix}[K_1]_{(n_1,n_1)} & [0]_{(n_1,n_1)}\\ [0]_{(n_2,n_2)} & [K_2]_{(n_2,n_2)}\end{bmatrix}+\begin{bmatrix}K_{d(n_1,n_1)} & -K_{d(n_1,n_1)}\\ -K_{d(n_2,n_2)} & K_{d(n_2,n_2)}\end{bmatrix} \tag{4.10}$$

$$C_s=\begin{bmatrix}[C_1]_{(n_1,n_1)} & [0]_{(n_1,n_1)}\\ [0]_{(n_2,n_2)} & [C_2]_{(n_2,n_2)}\end{bmatrix}+\begin{bmatrix}C_{d(n_1,n_1)} & -C_{d(n_1,n_1)}\\ -C_{d(n_2,n_2)} & C_{d(n_2,n_2)}\end{bmatrix} \tag{4.11}$$

where M_1 and M_2, K_1 and K_2, and C_1 and C_2 are mass, stiffness, and damping matrices for Building 1 and 2, respectively. K_d and C_d are matrices utilized to map the link stiffness and damping properties into the global stiffness and damping matrices of the peripheral structures.

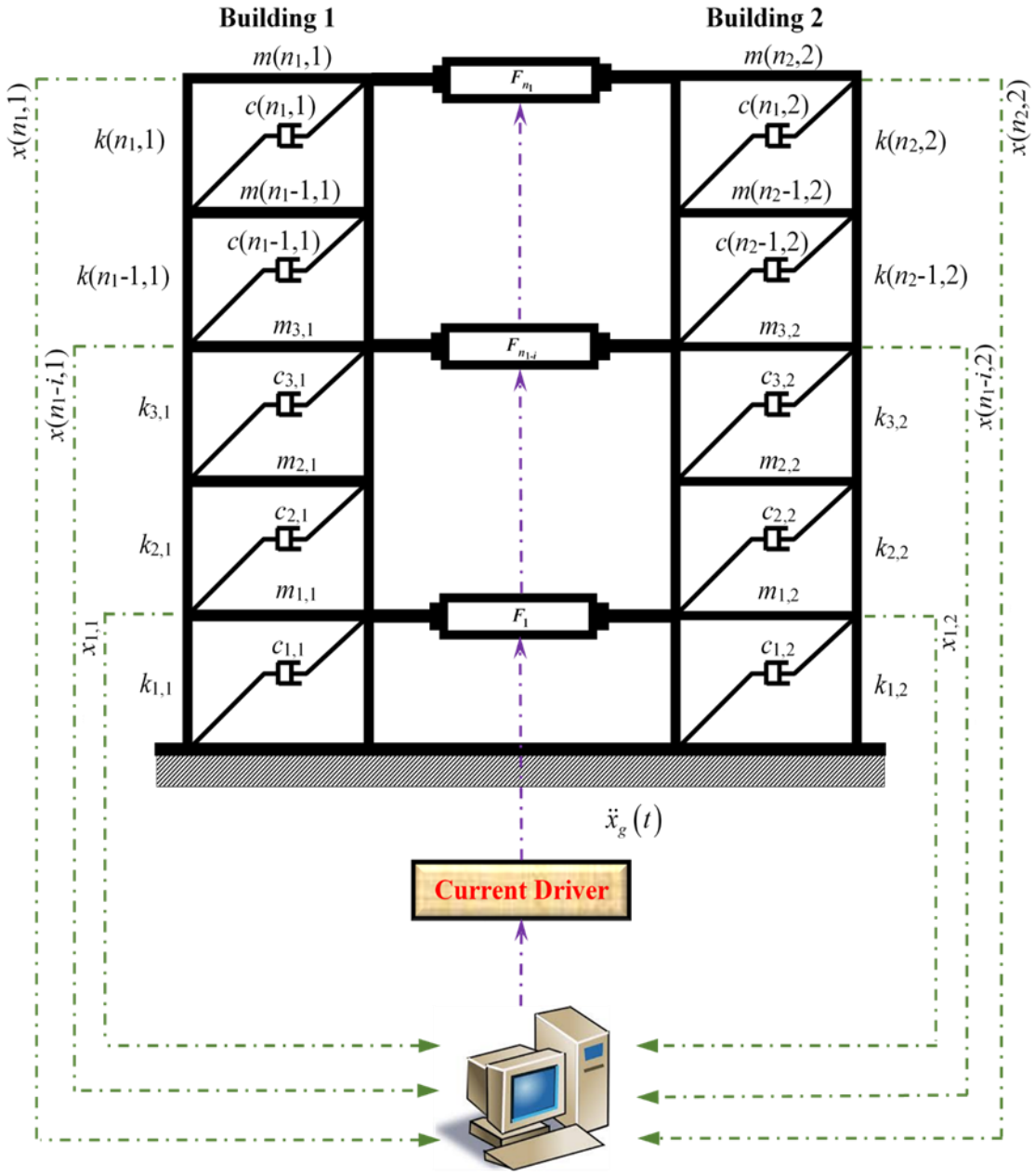

Figure 39: Structural system along with the control scheme.

Assuming all the adjacent floors are connected, K_d and C_d can be written as:

$$K_{d(n_1,n_1)} = \begin{bmatrix} k_{c1} & 0 & 0 & 0 \\ 0 & k_{c2} & 0 & 0 \\ 0 & 0 & \ddots & 0 \\ 0 & 0 & 0 & k_{c(n_2)} \end{bmatrix}$$

$$C_{d(n_1,n_1)} = \begin{bmatrix} c_{c1} & 0 & 0 & 0 \\ 0 & c_{c2} & 0 & 0 \\ 0 & 0 & \ddots & 0 \\ 0 & 0 & 0 & c_{c(n_2)} \end{bmatrix} \tag{4.12}$$

where the k_{ci} and c_{ci} are the stiffness and damping coefficients of the *i*th link, respectively. It is assumed in this study that the material of the connectors does not yield, i.e., it keeps its linear elastic behavior during the hazardous events. Finally, the location matrix of the control forces, *J*, is written as follows:

$$J_{(2n_1,2n_2)} = \begin{bmatrix} [I]_{(n_1,n_1)} & [0]_{(n_1,n_1)} \\ [0]_{(n_2,n_2)} & -[I]_{(n_2,n_2)} \end{bmatrix} \tag{4.13}$$

where the $[I]$ is identity matrix. The negative sign in equation (4.13) indicates that the control forces act in opposite direction on Building 2 with respect to Building 1.

4.5 SAC Algorithm for Nonlinear Systems

In this method, the behavior of the nonlinear system (plant) is characterized by pre-determined trajectories of a reference-model. To ensure that the plant tracks the behavior of the reference-model, SAC adjusts the control command by monitoring the error between the plant and the reference-model. Figure 40 shows the block diagram of SAC with feedforward configuration. Considering the equation of motion of the nonlinear

system derived in equation (4.10), the system can be formulated in a nonlinear state-space representation as follows:

$$\begin{Bmatrix} \dot{x}(t) \\ \ddot{x}(t) \\ \dot{z}(t) \end{Bmatrix} = \begin{bmatrix} [0] & [I] & [0] \\ -[M_s]^{-1}[K_s] & -[M_s]^{-1}[C_s] & -(1-\alpha)[K_s]\{z\} \\ 0 & \left[1-0.5\left(1+\mathrm{sgn}\left(\dot{x}z\right)\right)\left|\frac{z}{Y}\right|^n\right] & 0 \end{bmatrix} \begin{Bmatrix} x(t) \\ \dot{x}(t) \\ z(t) \end{Bmatrix} + \begin{Bmatrix} 0 \\ [M_s]^{-1} \\ 0 \end{Bmatrix} - [M_s]\{\ddot{x}_g(t)\} \tag{4.14}$$

It is obvious from the above equation that the internal parameters of the plant change as a function of the state variables. The output of the nonlinear system represented in equation (4.14) is required to track the output of the reference-model represented by the following state-space formulation:

$$\begin{aligned} \dot{x}_m(t) &= A_m(x_m)x_m(t) + B_m(x_m)u_m(t) \\ y_m(t) &= C_m(x_m)x_m(t) + D_m(x_m)u_m(x_m) \end{aligned} \tag{4.15}$$

The reference-model is chosen to represent the desired output of the plant, yet it does not have to be the result of the prior modeling of the plant (Barkana & Guez, 1990). Equation (4.15) represents the nonlinear reference-model for sake of generality, but it could be chosen as a linear time-invariant model.

SAC adjusts the control command, $u_p(t)$ to bring the error, $e_y(t) = y_m(t) - y_p(t)$, to zero. $u_p(t)$ is determined as follows:

$$u_p(t) = K(t)r(t) \tag{4.16}$$

where $r(t)$ is the reference vector and $K(t)$ is the gain matrix where they can be determined as follows:

$$r^T(t) = \left[\left(y_m(t) - y_p(t) \right)^T \quad x_m^T(t) \quad u_m^T(t) \right] \tag{4.17}$$

$$K(t) = K_I(t) + K_p(t) \tag{4.18}$$

where $K_I(t)$ and $K_p(t)$ are the integral and proportional adaptive gains which are defined as follows:

$$\dot{K}_I(t) = e_y(t)r(t)^T T - \sigma K_I(t) \tag{4.19}$$

$$K_p(t) = e_y(t)r(t)^T \bar{T} \tag{4.20}$$

in which T and $\bar{T}$ are tuning matrices need to be tuned by the designer to adjust the adaptation rate. The σ-term in equation (4.19) was omitted or restricted in later works (Barkana, 1987; Barkana, 2016); therefore, it will be set to zero in the current chapter.

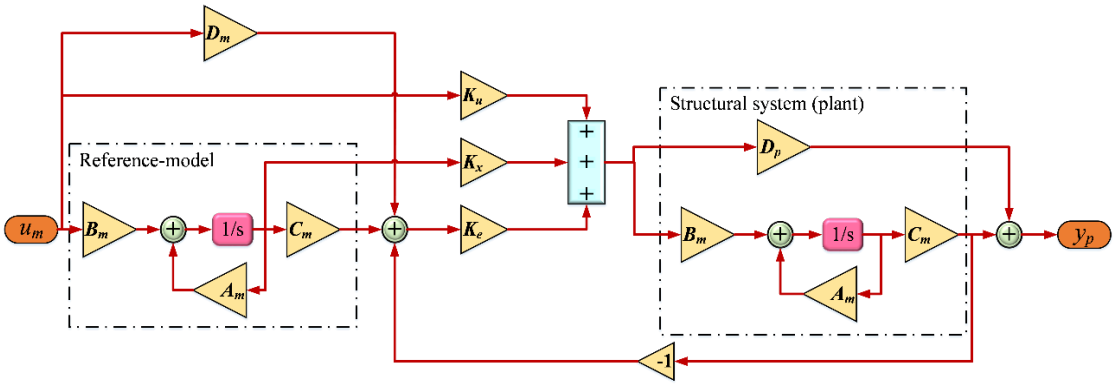

Figure 40: Block diagram of adaptive control system for nonlinear problem .

4.6 Numerical Study

The system considered for the numerical implementation consists of two buildings (Building 1 and Building 2) connected at three levels. Both buildings are five-stories tall; thus, $n_1 = n_2 = 5$. The two buildings are modeled as shear-type model buildings where the floors' masses are assumed to be lumped at the centers of the floors. The mass and stiffness of each floor of Building 1 are 4.78×10^5 kg and 1.6983×10^8 N/m, respectively. The stiffness of each floor of Building 2 is 1.019×10^8 N/m while keeping the mass as of Building 1. The total mass and stiffness of Building 1 are 23.9×10^5 kg and 8.4915×10^8 N/m, respectively and the total stiffness of Building 2 is 5.0949×10^8 N/m. The mass and stiffness matrices of the two buildings were chosen to give the fundamental natural periods of the Building 1 and 2 as 1.17 s and 1.51 s, respectively. As stated earlier, the dominant frequencies of the two individual buildings must not coincide; otherwise, the link would sway synchronously with the buildings making the use of the control devices within the links unfeasible. The damping matrix of the combined system is determined by using the Rayleigh damping formula with 2% damping ratio for both the lower and higher modes. This implies that the damping is assumed to be constant with time regardless the stiffness variations. In the current numerical study, the connected floors are the fifth, fourth, and third floors which renders the equation (4.12) to take the form:

$$K_{d(5,5)} = \begin{bmatrix} 0 & 0 & 0 & 0 & 0 \\ 0 & 0 & 0 & 0 & 0 \\ 0 & 0 & k_{c_3} & 0 & 0 \\ 0 & 0 & 0 & k_{c_4} & 0 \\ 0 & 0 & 0 & 0 & k_{c_5} \end{bmatrix}; \quad C_{d(5,5)} = \begin{bmatrix} 0 & 0 & 0 & 0 & 0 \\ 0 & 0 & 0 & 0 & 0 \\ 0 & 0 & c_{c_3} & 0 & 0 \\ 0 & 0 & 0 & c_{c_4} & 0 \\ 0 & 0 & 0 & 0 & c_{c_5} \end{bmatrix} \tag{4.21}$$

It is to be noted that the Bouc-Wen's nonlinear differential equation that describes the hysteretic behavior appears in both sides of the equation of motion derived in equation (4.10), but with different parameters. This renders the equation of motion to be highly nonlinear.

4.7 Simulations and Analyses

The reference-model output in the SAC scheme is chosen to have a specific range of outputs as follows:

$$y_m(t) = \frac{1}{3}.y_p(t) \tag{4.22}$$

Thus, the goal of using the adaptive control method is to decrease the error between the system's response, $y_p(t)$, and the reference-model's, $y_m(t)$, as possible. However, since the control system is not perfect and has limitations, the system's output tracks the reference-model's only up to a certain limit.

For SAC strategy, the tuning matrices T and $\bar{T}$ are chosen respectively to be $10^3[I]_{31\times31}$ and $10^8[I]_{31\times31}$. Six sensors are required to measure the output displacements of the connected floors for both buildings. Since the control devices used in this study need to be provided with velocity, the measured displacements are differentiated to determine the corresponding velocities as follows:

$$X_p(t) = \begin{Bmatrix} x_p(t) \\ \frac{d}{dt}\left[x_p(t)\right] \end{Bmatrix} = \begin{Bmatrix} Y_p(t) \\ \frac{d}{dt}\left[Y_p(t)\right] \end{Bmatrix} \tag{4.23}$$

where $X_p(t)$ and $Y_p(t)$ are the state and output vectors of the plant, respectively.

The results drawn from SAC is compared with the LQR controller. The LQR is designed by choosing the Q_{lqr} and R_{lqr} matrices as in the equations below:

$$Q_{lqr} = \frac{1}{2}\begin{bmatrix} K_s & 0 \\ 0 & M_s \end{bmatrix} \tag{4.24}$$

$$R_{lqr} = \rho I_{(2n_1, 2n_1)}; \quad \rho = 1\times 10^{-5} \tag{4.25}$$

The performance of the proposed system is investigated when the structure is subjected to Kobe, Northridge, and Whittier earthquakes with different intensity levels (0.5, 1.0, and 1.5 times the PGA of each recording). The characteristics of these three earthquakes are listed in Table 8. To highlight the nonlinear behavior of the structural system, the hysteretic loops of the top floors of both buildings under Kobe earthquake are depicted in Figure 41. This figure shows the hysteretic behavior of the uncontrolled versus controlled systems. It can be recognized that the hysteretic loops are smaller in magnitude for the controlled system than the uncontrolled one and/or faster in dissipating the energy.

Figure 42, Figure 43, and Figure 44 depict the time histories of Building 1's top floor displacement and acceleration of both the controlled and uncontrolled systems under the selected earthquakes with intensity equals 1. It could be seen that the permanent (plastic) deformations were occurred under all these earthquakes. As shown in these figures, the permanent deformations are significantly reduced by using SAC, which means that SAC considerably reduces the structural damage. In contrast, LQR strategy worsen the permanent drift and/or displacement under Kobe and Northridge.

(a)

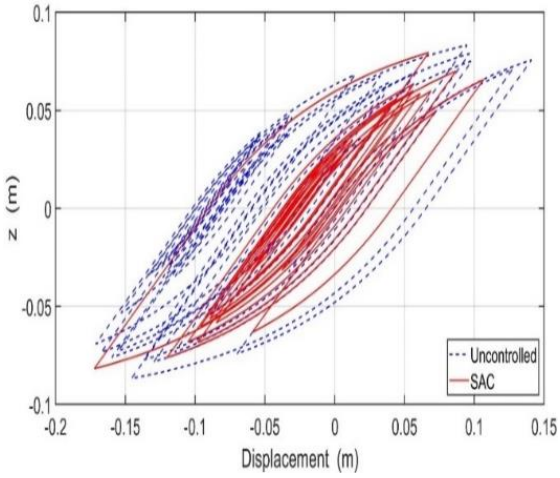

(b)

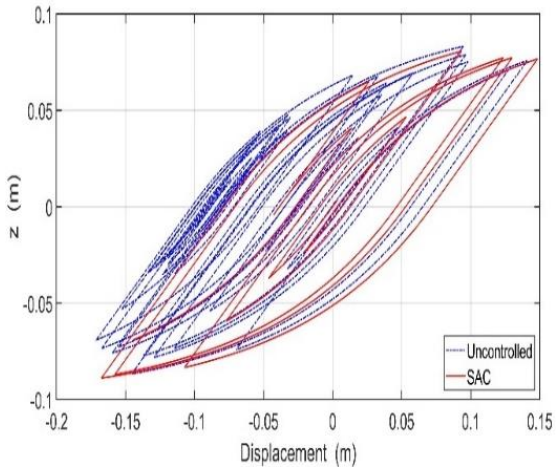

Figure 41: Portion of the hysteretic behavior of the top floors of Building 1 under Kobe earthquake (intensity = 1): (a) Building 1 and (b) Building 2.

Permanent deformations can make the structural systems dysfunctional or unserviceable; therefore, decreasing the inelastic structural responses is crucial. From the above figures, SAC reduces the peak displacements by 48% and 23% under Northridge and Whittier, respectively while small increase in the peak displacement has occurred under Kobe by 2%. On the other hand, a reduction achieved by LQR as 20.5% and 28%

under Northridge and Whittier, respectively, while 14.3% increase in the peak displacement under Kobe earthquake. Interestingly, SAC reduced the peak acceleration of the top floor under Kobe earthquake by 26.3%, but with increasing the maximum acceleration by 21% and 7.6% under Northridge and Whittier, respectively. LQR performs relatively well in attenuating the peak accelerations by 25% and 39% under Kobe and Northridge, respectively, but with small increase, about 0.5%, under Whittier earthquake.

Table 8: Ground Motions Characteristics for nonlinear dynamics.

Earthquake	Station	Magnitude	PGA (m/s^2)
Kobe	Fukushima	6.9	1.8105
Whittier	Alhambra School	5.9	2.8418
Northridge	Fermont School	6.69	0.9913

Figure 43 shows the time histories of Building 2 top floor's displacement and acceleration under Kobe earthquake with intensity equals 1. Again, tremendous reduction in the permanent displacement is achieved by using SAC while LQR amplifies both significantly. However, SAC increases the peak displacement by 34%, while a significant reduction in the peak acceleration by 29%. On the other hand, 20% reduction in the peak acceleration by using LQR, but with 48.5% increase in the peak displacement. In general, it can be seen from the above discussion that the proposed control scheme is more effective for Building 1 than Building 2. This behavior can be understood in the context of transferring the energy and momentum from the stronger building (Building 1) to the weaker one (Building 2) during the motion.

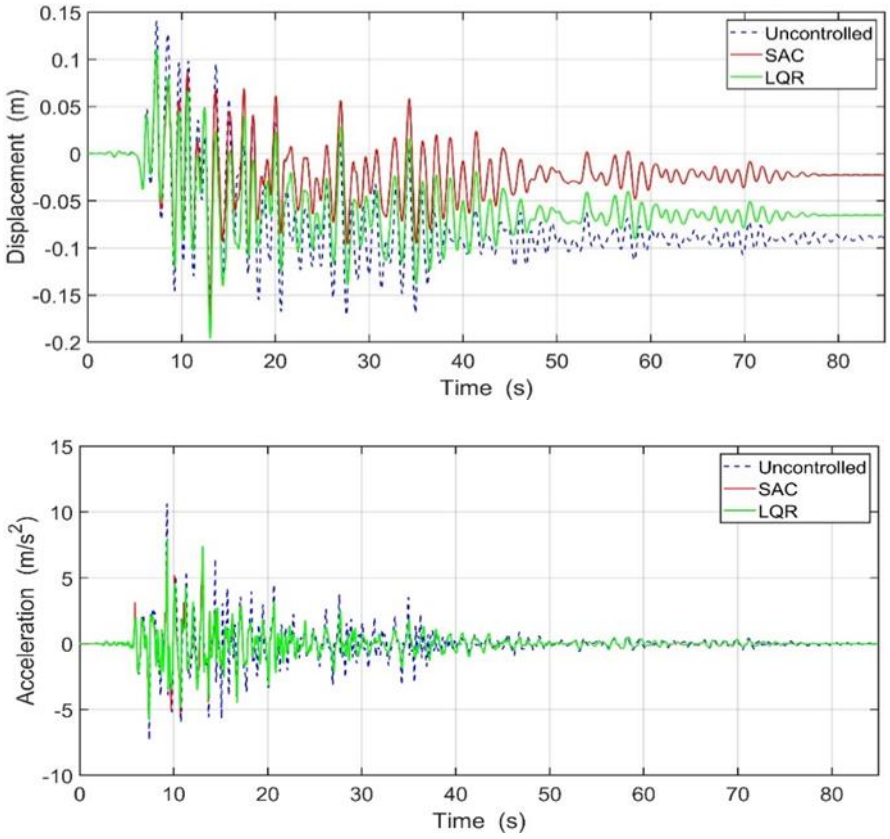

Figure 42: Uncontrolled and controlled time histories of Building 1's top floor displacement and acceleration under Kobe earthquake (intensity = 1).

The profiles of the maximum inter-story drift of both the uncontrolled and controlled systems under the selected earthquakes' suite are depicted in Figure 46 through Figure 48. It can be noticed that SAC decreases the maximum inter-story drift for Building 1 for all exciting conditions except for Northridge with intensity equals 1.5. Also, under Kobe with 1.5 intensity level, very small reduction for the drift of the first floor was achieved while some increase has occurred for the higher floors. On the other hand, LQR performs good in reducing the maximum drifts of Building 1 under all excitations

considered except Kobe with 0.5 and 1.0 intensity levels where a noticeable increase has occurred.

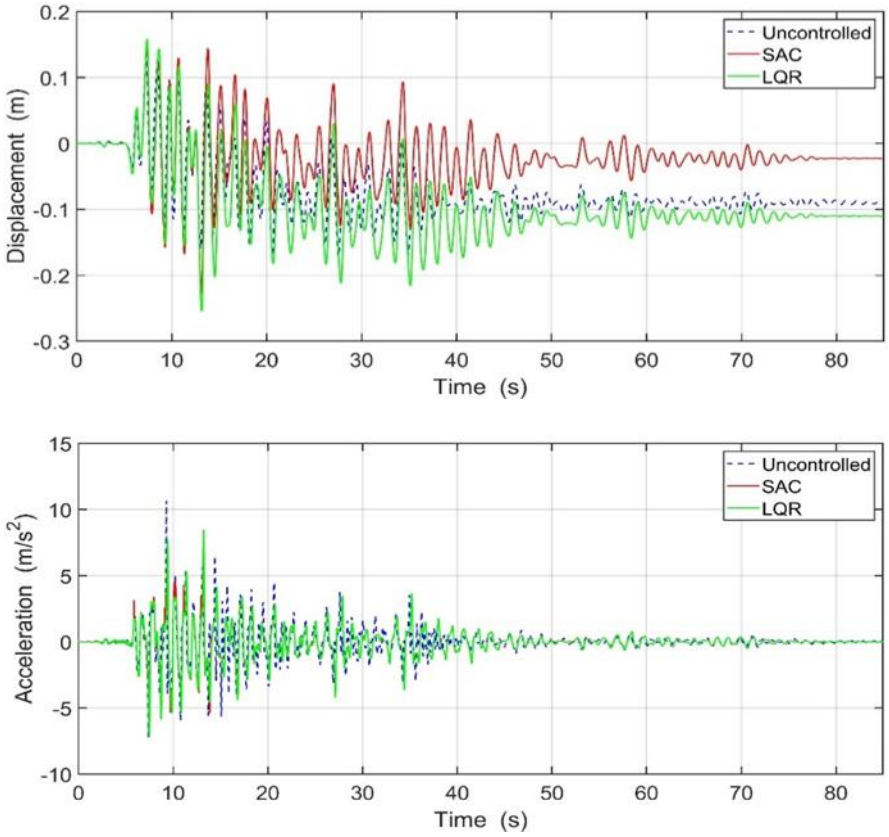

Figure 43: Uncontrolled and controlled time histories of Building 2's top floor displacement and acceleration under Kobe earthquake (intensity = 1).

For Building 2, in general, the control schemes are not as effective for Building 1. For instance, the maximum drift has been increased by SAC under Kobe with intensity levels 1.0 and 1.5, respectively. Noticeable reduction can be seen when the system was subject to Northridge earthquake, Figure 48, with all intensity levels while for Whittier case, significant reduction was achieved for some higher floors while always we have a

small increase in the maximum drift for the first floor. LQR performs far worse under all the exciting conditions. Again, the discrepancy between the performance quality for Building 1 and Building 2 is because of the complex dynamics due to the coupling effects.

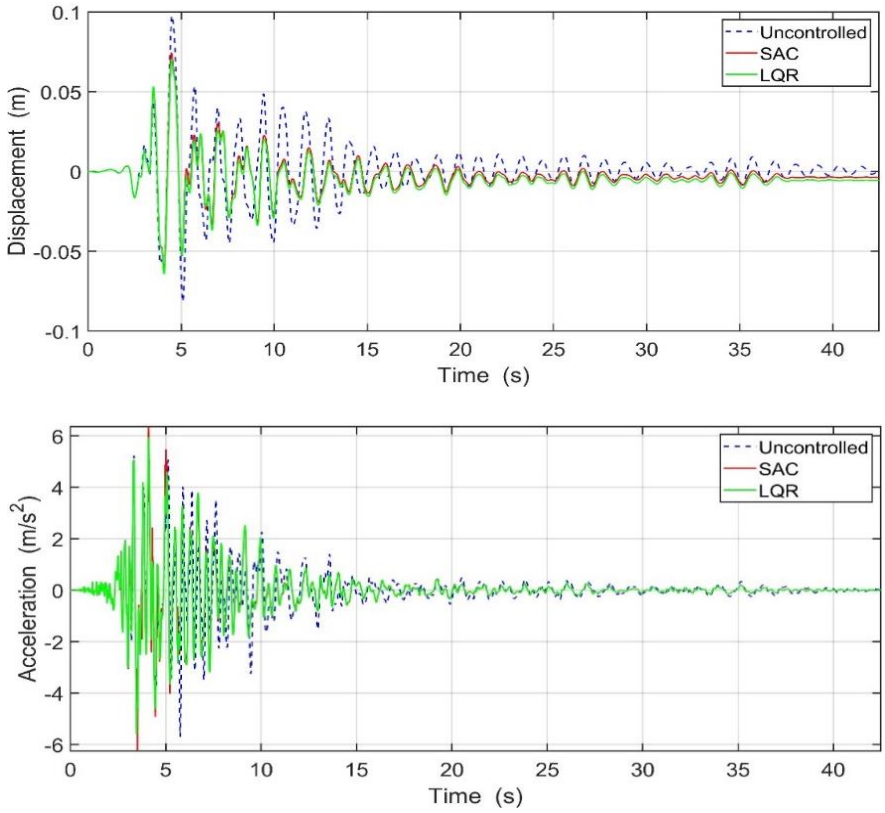

Figure 44: Uncontrolled and controlled time histories of Building 1's top floor displacement and acceleration under Whittier earthquake (intensity = 1).

To assess the performance of SAC and LQR, the following evaluation indices defined for the benchmark problem (Ohtori et al., 2004) are utilized:

$$J_1 = \max\left\{\frac{|x_i(t)|_c}{|x_i(t)|_{un}}\right\} \qquad J_2 = \max\left\{\frac{|\ddot{x}_i(t)|_c}{|\ddot{x}_i(t)|_{un}}\right\} \qquad J_3 = \left\{\frac{RMS[x_i(t)]_c}{RMS[x_i(t)]_{un}}\right\} \tag{4.26}$$

$$J_4 = \max\left\{\frac{\left|\sum m_i \ddot{x}_i(t)\right|}{F_b^{\max}}\right\} \qquad J_5 = permanent\left\{\frac{|x_i|_c}{|x_i|_{un}}\right\}$$

where J_1, J_2, J_3, J_4, and J_5 are the displacement, acceleration, RMS response, base shear and permanent drift, respectively. The RMS response is calculated as the square root of the mean squares of a discrete series of time values as follows:

$$x_{RMS} = \left(\frac{1}{N}\sum_{i=1}^{N}|x_i|^2\right)^{1/2} \tag{4.27}$$

Table 9 below presents all the evaluation criteria where the values in bold are for Building 1.

(a)

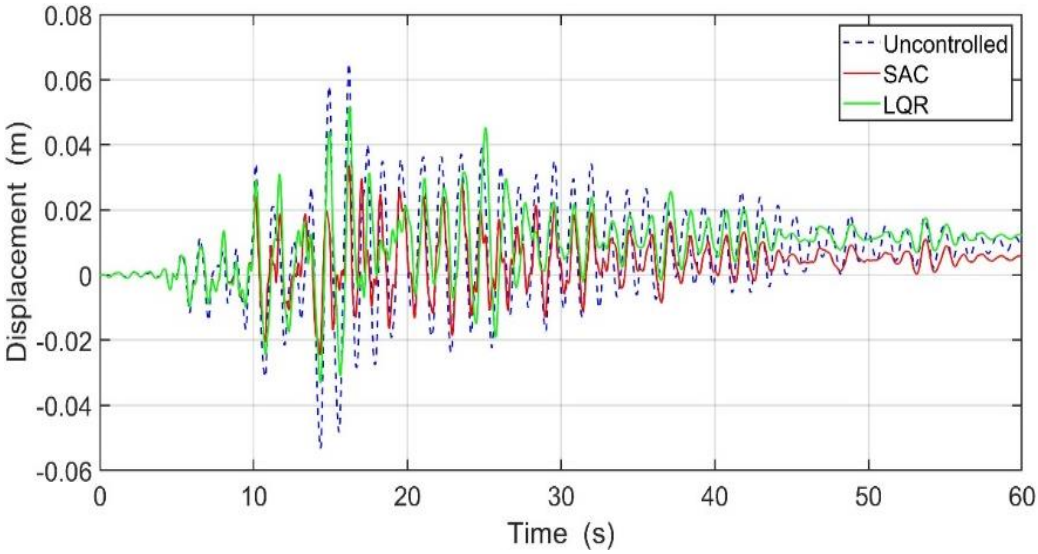

(b)

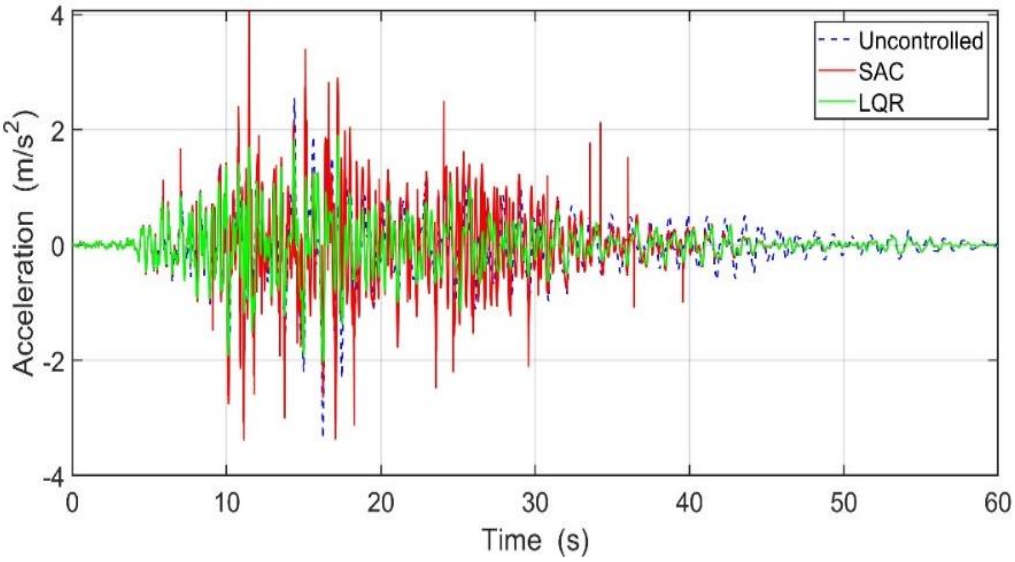

Figure 45: Uncontrolled and controlled time histories of Building 1 top floor's displacement and acceleration under Northridge earthquake (intensity = 1).

(a)

(b)

(c)

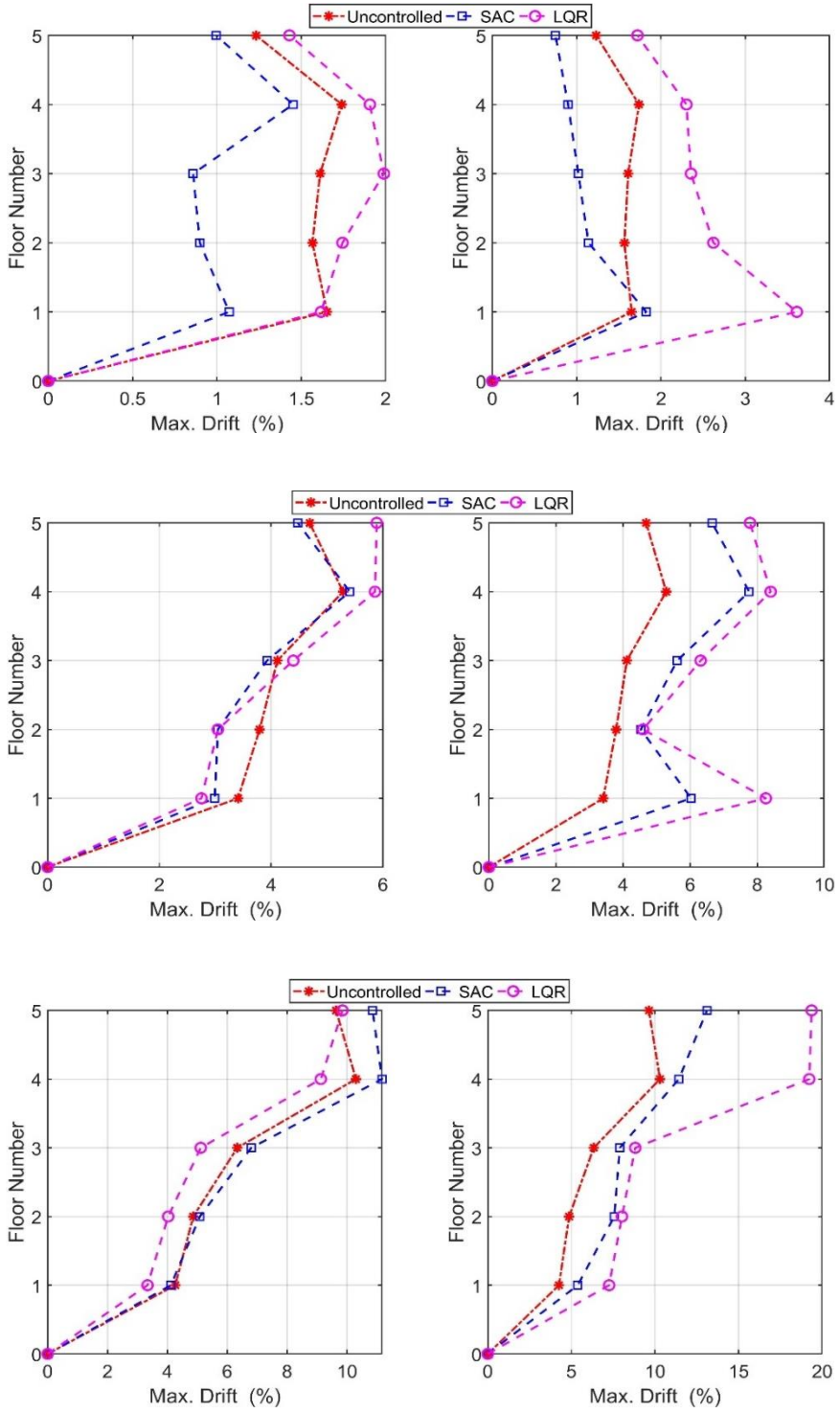

Figure 46: Maximum drift profile for Building 1(left) and Building 2 (right) under Kobe earthquake: (a) intensity = 0.5, (b) intensity = 1, and (c) intensity = 1.5.

(a)

(b)

(c)

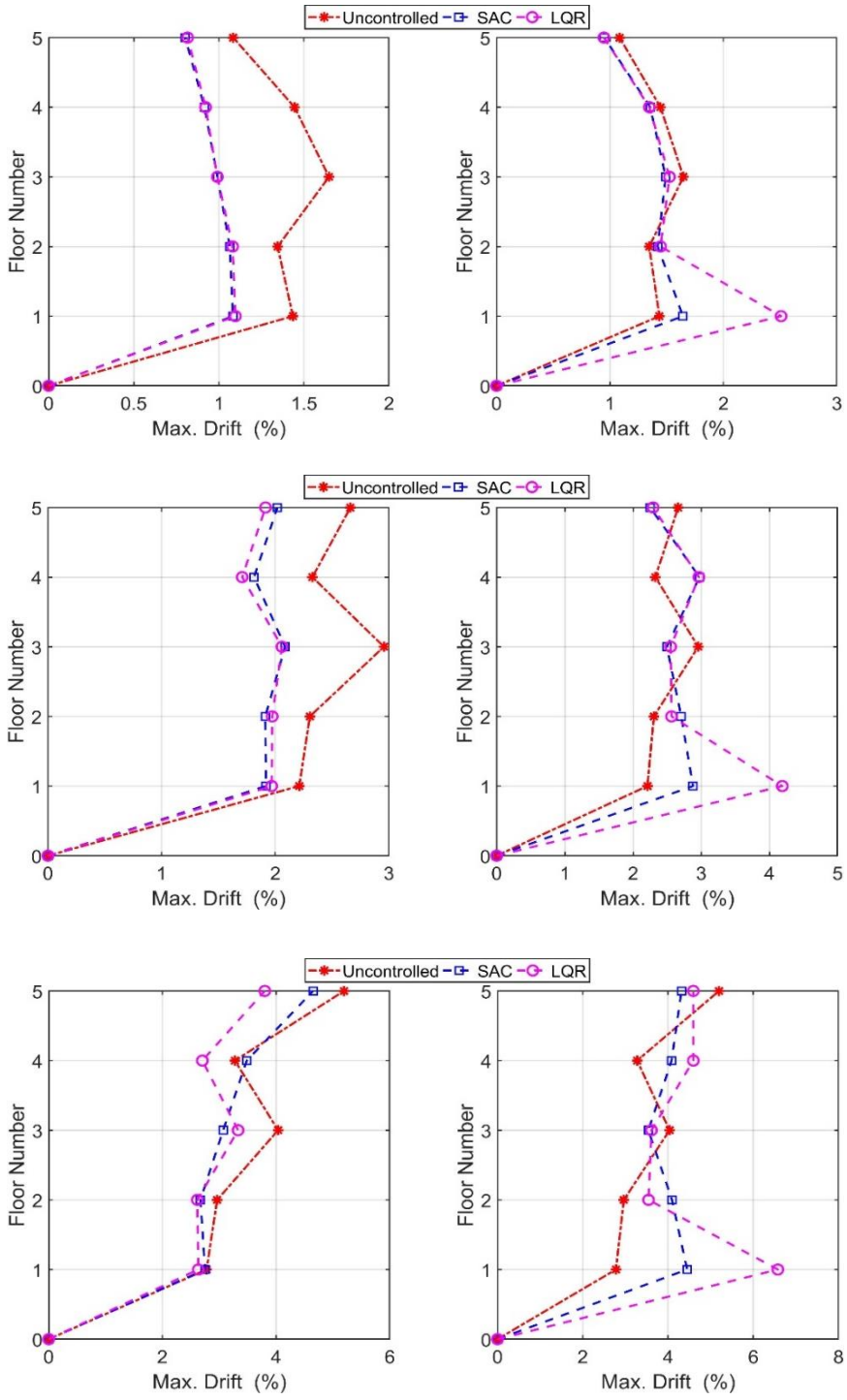

Figure 47: Maximum drift profile for Building 1(left) and Building 2 (right) under Whittier earthquake: (a) intensity = 0.5, (b) intensity = 1, and (c) intensity = 1.5.

(a)

(b)

(c)

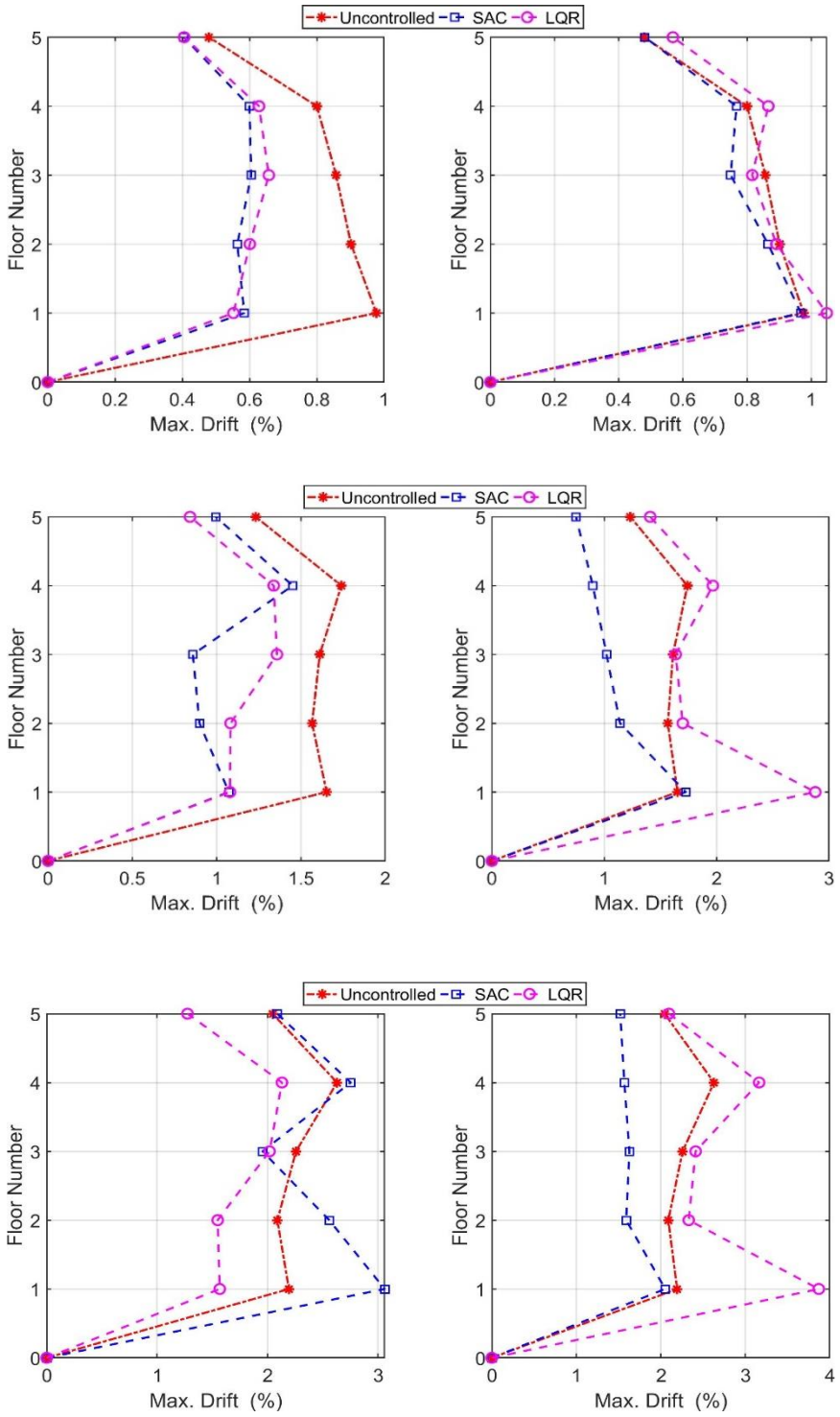

Figure 48: Maximum drift profile for Building 1(left) and Building 2 (right) under Northridge earthquake: (a) intensity = 0.5, (b) intensity = 1, and (c) intensity = 1.5.

Table 9: Evaluation criteria of the top floors of the coupled system.

		Kobe			Whittier			Northridge		
		0.5	1.0	1.5	0.5	1.0	1.5	0.5	1.0	1.5
J_1	SAC	**0.877**	**1.005**	**0.942**	**0.684**	**0.763**	**0.955**	**0.687**	**0.518**	**0.833**
		1.112	1.327	1.032	0.982	1.012	1.077	0.924	0.675	0.615
	LQR	**0.877**	**1.143**	**0.904**	**0.698**	**0.719**	**0.742**	**0.772**	**0.794**	**0.819**
		1.128	1.484	1.530	1.010	1.033	1.137	0.999	1.058	1.182
J_2	SAC	**1.11**	**0.736**	**0.89**	**1.022**	**1.076**	**1.203**	**0.938**	**1.129**	**2.157**
		0.959	0.711	0.815	0.605	0.815	1.149	1.027	0.874	1.024
	LQR	**0.884**	**0.745**	**0.764**	**1.02**	**1.005**	**0.99**	**0.763**	**0.607**	**0.61**
		0.972	0.796	0.811	0.569	0.775	0.880	0.767	0.704	0.704
J_3	SAC	**0.963**	**0.458**	**0.283**	**0.583**	**0.787**	**0.966**	**0.684**	**0.548**	**0.56**
		1.333	0.600	0.282	0.801	1.122	1.406	0.958	0.742	0.617
	LQR	**0.921**	**0.775**	**0.626**	**0.521**	**0.698**	**0.65**	**0.662**	**0.795**	**0.894**
		1.333	1.264	1.611	0.697	0.957	1.317	0.995	1.268	1.493
J_4	SAC	**0.713**	**0.809**	**0.966**	**0.754**	**0.867**	**0.99**	**0.598**	**0.649**	**1.395**
		1.096	1.051	1.340	0.941	1.128	1.263	1.048	0.836	1.084
	LQR	**0.714**	**0.807**	**0.782**	**0.764**	**0.89**	**0.947**	**0.565**	**0.653**	**0.714**
		1.096	1.043	1.241	0.941	1.112	1.224	1.059	1.188	1.187
J_5	SAC	**0.692**	**0.689**	**0.146**	**0.197**	**0.478**	**0.735**	**0.598**	**0.299**	**0.645**
		0.181	0.550	0.367	0.034	0.556	0.565	1.048	0.634	0.357
	LQR	**0.749**	**1.089**	**0.793**	**0.209**	**0.342**	**0.507**	**0.865**	**0.408**	**0.421**
		0.208	1.123	2.183	0.037	0.663	0.678	2.751	1.651	1.430

4.8 Epilogue

In this chapter, the efficacy of using the simple adaptive controller (SAC) in enhancing the performance of the nonlinear adjacent buildings connected with MR dampers was investigated. The Bouc-Wen model was utilized to model the nonlinear behavior of the structural system as well as the hysteretic behavior of the MR damper. The numerical simulations indicated that using SAC to drive MR dampers connecting two adjacent buildings was effective in mitigating the structural responses of the complex system under elevated intensity levels of seismic excitations. The results showed that SAC

was more effective than LQR in reducing the permanent displacement and permanent drift, which means that SAC is more effective in preserving the structure's serviceability and functionality during earthquakes. It can be concluded that the proposed control scheme was more effective for Building 1 than Building 2, especially for inter-story drifts.

References

Barkana, I., & Guez, A. (1990). Simple adaptive control for a class of non-linear systems with application to robotics. International journal of control, 52(1), 77-99. doi:10.1080/00207179008953525

Barkana, I. (2014). The beauty of simple adaptive control and new developments in nonlinear systems stability analysis. AIP Conference Proceedings, 1637, 89-113.

Barroso, L. R., Hunt, S., & Chase, J. G. (2002). Application of magneto-rheological dampers for multi-level seismic hazard mitigation of hysteretic structures. Paper presented at the 15th ASCE engineering mechanics conference, Columbia University, New York.

Constantinou, M. C., & Adnane, M. A. (1987). Evaluation of two models for yielding systems. Drexel University.

Kaufman, H., Barkana, I., & Sobel, K. (1994). Direct Adaptive Control Algorithms: Theory and Applications. doi:10.1007/978-1-4684-0217-9.

Mitsuta, S., Okawa, E., Seto, K., & Ito, H. (1994). Active Vibration Control of Structures Arranged in Parallel. JSME International Journal. Ser. C, Dynamics, Control, Robotics, Design and Manufacturing, 37(3), 436–443. doi:10.1299/jsmec1993.37.436

Richardson, A., Walsh, K. K., & Abdullah, M. M. (2011). Closed-form equations for coupling linear structures using stiffness and damping elements. Structural Control and Health Monitoring, 20(3), 259–281. doi:10.1002/stc.490.

Tedesco, J. W., McDougal, W. G., Ross, C. A. (1999). Structural dynamics: theory and applications: Addison-Wesley Menlo Park, CA.

Wen, Y. K. (1976). Method for random vibration of hysteretic systems. Journal of the engineering mechanics division, 102(2), 249-263.

Westermo, B. D. (1989). The dynamics of interstructural connection to prevent pounding. Earthquake engineering & structural dynamics, 18(5), 687-699.

Yamada, Y., Ikawa, N., Yokoyama, H., & Tachibana, E. (1994). Active control of structures using the joining member with negative stiffness. Paper presented at the Proc. First World Conference on Structural Control.

CHAPTER V

ADAPTIVE NEURO-FUZZY AND SIMPLE ADAPTIVE CONTROL METHODS FOR CONNECTED BUILDINGS

This chapter describes two adaptive control methods for mitigating the seismic responses of two adjacent buildings connected with MR dampers at multiple levels. The first method developed in this chapter is the adaptive neuro-fuzzy controller which consists of a fuzzy logic controller provided with a learning algorithm based on adaptive neural networks. The learning algorithm is implemented to adjust the parameters of the fuzzy logic controller such that its outputs track the behavior of predetermined training data. The second method is the simple adaptive controller, which falls into the category of model-following adaptive strategies. In this method, a plant is commanded to follow a well-designed reference-model with desirable trajectories through a closed loop action. The coupled system is formed by two shear-type model buildings having different heights in order to separate the mode shapes of the individual buildings. Different types of feedbacks such as displacement, velocity, and acceleration are employed to identify their impacts on the performance of the developed adaptive controllers. Numerical analyses are carried out for the complex system assuming no change in the nominal design parameters and then for the system where a change in these parameters is introduced. The results reveal that using the adaptive controllers used in this chapter to drive the magneto-rheological dampers connecting two adjacent buildings can successfully alleviate the seismic responses under various types and intensities of earthquakes.

5.1 Prelude

Protection of civil engineering structures from undesirable vibrations due to environmental events is crucial for maintaining structural integrity. One of the creative ideas to withstand these events is interconnecting adjacent buildings with single or multiple links. The coupling of adjacent structures has proven to be both architecturally and functionally beneficial. Structural performance of coupled structures can be enhanced by implementing control devices within these links to dissipate energy in adjacent buildings, an approach that has been proven effective for minimizing structural responses. In the last few decades, significant advances have been made in this technology to alleviate the seismic responses of structures subjected to moderate to severe earthquakes.

In civil engineering applications, control studies are usually divided into two categories: those which focus on safety and those which main concern is functionality. For the former type, the goal is to use the dissipative devices to reduce displacement and inter-story drifting. However, when functionality is the concern as in the design of tall and slender buildings, control is used to mitigate structural acceleration in order to increase occupant comfort during relatively mild events (Barroso, Breneman, & Smith, 1998).

Enhancing the structural performance of coupled buildings has been reported in the use of passive links. More advanced strategies were implemented by using active control devices to connect adjacent high-rise buildings such as hydraulic actuator. In addition to the analytical studies conducted on coupled buildings, there has been few experimental studies on the subject. Because of the high-power demand and instability potential associated with active devices, semi-active devices have been embraced by

researchers. Semi-active devices have a potential to remedy the issues that the former had, which make them ideal for civil engineering applications (Schurter & Roschke, 2001a). One of the most advanced and effective semi-active devices is the magneto-rheological (MR) damper, which shows a great potential for use in vibration control of large-scale structures. Many studies have been carried out on using MR dampers to connect adjacent buildings to attenuate seismic responses. The device has the capability to operate with a small amount of power and continues to work as a passive device in case of the failure of the power supply or the control algorithm. Also, the MR damper is capable of modifying its yield strength by changing the intensity of the magnetic field through controlling the current in the coil (Gong et al., 2014). The simple Bouc-Wen model is used to model the hysteretic behavior of the MR damper. This model combines linear dashpot element and the Bouc-Wen element, which describes the hysteretic behavior of the MR damper. The performance of the simple Bouc-Wen model was studied by Wong et al. (1994) and compared to experimental data. The results showed that the proposed model matches the experimental data except near small velocities. Spencer et al. (1997) rectified this shortcoming by proposing a modified model in which additional parameters were added to deal with low velocities. However, one of the challenges of implementing the MR damper is the choice of an appropriate control algorithm.

Despite the impressive achievements of classical control design, the performance of the classical control methods seems to be limited since these methods cannot cope with uncertainties and time-varying parameters in real-world applications (Barkana, 2014). Therefore, the adaptive control strategy promises to be more suitable for such systems

because it applies the right control command to the right situation. The adaptive control command is adjusted online in order to reduce the effects of uncertain parameters.

In this chapter, the adaptive neuro-fuzzy inference systems (ANFIS) and the simple adaptive controller (SAC) are used. ANFIS, as an intelligent control scheme, based on Sugeno-fuzzy model combines the fuzzy logic controller (FLC) and the adaptive neural networks in one framework. This method has a set of rules corresponding to fuzzy IF-THEN statements with learning capabilities to simplify nonlinear relations into simplistic verbose statements. In particular, the fuzzy logic controller has been used in research to regulate semi-active devices (Choi et al., 2004; Symans & Kelly, 1999). The learning capability of ANFIS comes from the artificial neural networks, which attempt to emulate the biological neurons of the human brain (Burns, 2001). SAC, however, is one of the model-following adaptive methods in which an uncertain system is forced to track the behavior of a reference-model with pre-determined trajectories (Al-Fahdawi, Barroso, & Soares, 2018; Soares, Barroso, & Al-Fahdawi, 2018; Al-Fahdawi, Barroso, & Soares, 2019). SAC was implemented in different fields. For example, in aerospace engineering, SAC was used by Ulrich et al. (2014) to address the problem of the adaptive feedback in the spacecrafts under unknown external perturbation and parametric uncertainties. In civil engineering, few studies have used SAC for conventional buildings to deal with parameter changes under hazardous events (Amini et al., 2018; Bitaraf, Hurlebaus, Barroso, 2012).

The purpose of this chapter is to investigate the efficiency of the adaptive control such as ANFIS and SAC in alleviating the seismic structural responses of two adjacent buildings connected with MR dampers. Different feedback types for both ANFIS and SAC

are examined to identify the impact of each feedback type on the performance of each method. The following feedback schemes are investigated in this chapter:

1.1. Displacement feedback for both ANFIS and SAC which is labeled as "ANFIS1" and "SAC1", respectively.

1.2. Velocity feedback for both ANFIS and SAC which is labeled as "ANFIS2" and "SAC2", respectively.

1.3. Acceleration feedback for both ANFIS and SAC which is labeled as "ANFIS2" and "SAC2", respectively.

1.4. Combined velocity and acceleration feedback for ANFIS which is labeled as "ANFIS3".

5.2 Modeling of the Coupled System

Two adjacent buildings are idealized as shear-type buildings where the masses of the floors are assumed to be concentrated at the center of each floor. The number of stories of the two buildings are different, but the corresponding floors of the two buildings are in-line. The number of unconnected floors is n_1 and the number of connected floors is n_2. Therefore, the total number of floors in the coupled system is $n_1 + 2n_2$, as shown in Figure 21. The two buildings are assumed to be symmetric in terms of their planes' alignment and their dynamic characteristics. The system is assumed to be subjected to the same unidirectional earthquake excitation where the waveform of the ground motion is neglected, and any effect due to soil-structure interaction is also neglected. The MR

dampers connecting the two buildings are assumed to be rigidly connected between the inline floors.

The governing equation of motion of the combined system can be written in a compact form as:

$$[M_s]\{\ddot{x}(t)\}+[C_s]\{\dot{x}(t)\}+[K_s]\{x(t)\}=[J]\{f_m(t)\}-[M_s][r]\{\ddot{x}_g(t)\} \tag{5.1}$$

where M_s, C_s, and K_s are the mass, damping and stiffness matrices of the coupled system, respectively. $f_m(t)$ is the control forces vector; J is the location matrix of the control devices; $x(t)$, $\dot{x}(t)$, and $\ddot{x}(t)$ are the relative displacement, velocity, and acceleration vectors, respectively. r is a vector with all elements equal ones; $\ddot{x}_g(t)$ is the ground acceleration vector.

The structural mass, stiffness, and damping matrices of the coupled system can be explicitly defined as (Al-Fahdawi, Barroso, & Soares, 2019):

$$M_{s(n_1+2n_2,n_1+2n_2)}=\begin{bmatrix}[M_1]_{(n_1+n_2,n_1+n_2)} & [0]_{(n_1+n_2,n_2)}\\ [0]_{(n_2,n_1+n_2)} & [M_2]_{(n_1+n_2,n_1+n_2)}\end{bmatrix} \tag{5.2}$$

$$K_{s(n_1+2n_2,n_1+2n_2)}=\begin{bmatrix}[K_1]_{(n_1+n_2,n_1+n_2)} & [0]_{(n_1+n_2,n_2)}\\ [0]_{(n_2,n_1+n_2)} & [K_2]_{(n_1+n_2,n_1+n_2)}\end{bmatrix}+[K_c] \tag{5.3}$$

$$C_{s(n_1+2n_2,n_1+2n_2)}=\begin{bmatrix}[C_1]_{(n_1+n_2,n_1+n_2)} & [0]_{(n_1+n_2,n_2)}\\ [0]_{(n_2,n_1+n_2)} & [C_2]_{(n_1+n_2,n_1+n_2)}\end{bmatrix}+[C_c] \tag{5.4}$$

where M_1 and M_2, K_1 and K_2, and C_1 and C_2 are mass, stiffness, and damping matrices for Building 1 and 2, respectively. K_c and C_c are matrices utilized to map the link stiffness

and damping properties into the global stiffness and damping matrices of the peripheral structures and can be written as (Al-Fahdawi, Barroso, & Soares, 2019):

$$K_{c(n_1+2n_2,n_1+2n_2)} = \begin{bmatrix} [K_d]_{(n_2,n_2)} & [0]_{(n_2,n_1)} & -[K_d]_{(n_2,n_2)} \\ [0]_{(n_1,n_2)} & [0]_{(n_1,n_1)} & [0]_{(n_1,n_2)} \\ -[K_d]_{(n_2,n_2)} & [0]_{(n_2,n_1)} & [K_d]_{(n_2,n_2)} \end{bmatrix} \tag{5.5}$$

$$C_{c(n_1+2n_2,n_1+2n_2)} = \begin{bmatrix} [C_d]_{(n_2,n_2)} & [0]_{(n_2,n_1)} & -[C_d]_{(n_2,n_2)} \\ [0]_{(n_1,n_2)} & [0]_{(n_1,n_1)} & [0]_{(n_1,n_2)} \\ -[C_d]_{(n_2,n_2)} & [0]_{(n_2,n_1)} & [C_d]_{(n_2,n_2)} \end{bmatrix} \tag{5.6}$$

where the K_d and C_d are matrices contain stiffness and damping coefficients of the links. It is assumed in this study that the dynamic characteristics of the connectors do not change. Finally, the location matrix of the control forces, J, is written as follows:

$$J_{(n_1+2n_2,n_1+2n_2)} = \begin{bmatrix} [I]_{(n_2,n_1+2n_2)}; & [0]_{(n_1,n_2+2n_2)} \\ [0]_{(n_2,n_1+n_2)}, & -[I]_{(n_2,n_2)} \end{bmatrix} \tag{5.7}$$

where $[I]$ is identity matrix. The negative sign in equation (5.7) indicates that the control forces act in opposite direction on Building 2 with respect to Building 1.

5.3 Adaptive Control

Adaptive control strategy has a capability to adjust its own parameters automatically based on an operative situation. The advantage of using the adaptive control is to improve the structural performance in the presence of uncertainties and parameter

variations. This chapter introduces a new adaptive control method that is developed to drive MR dampers connecting two adjacent buildings.

5.3.1 Adaptive Neuro-Fuzzy Inference system

The effectiveness of the fuzzy logic controller is dependent on verbose rules needed to define the correlation between the inputs and outputs. These rules most of the times are determined based on expert knowledge. Adaptive Neuro-Fuzzy Inference system (ANFIS) is utilized to facilitate the adaptation and learning ability of the adaptive system in a way that makes the system less reliant on expert knowledge. The architecture of ANFIS consists of a number of fuzzy IF-THEN statements that are written based on Sugeno model as follows (Jang, 1993; Jang, Sun, & Mizutani, 1997):

Rule 1. If x is A_1 and y is B_1 then $f_1 = p_1 x + q_1 y + r_1$

Rule 2. If x is A_2 and y is B_2 then $f_2 = p_2 x + q_2 y + r_2$

Rule n. If x is A_n and y is B_n then $f_n = p_n x + q_n y + r_n$

where x and y are the inputs and $A_1 \ldots A_n$ and $B_1 \ldots B_n$ are fuzzy membership functions. $f_1 \ldots f_n$ are the outputs within the fuzzy region specified by the fuzzy rules. p_i, q_i, and r_i are parameters that are defined during the training process. The inputs x and y are antecedent variables, and f_i is a consequent variable of the rule i. The rules above are implemented in ANFIS as in Figure 49 in which the squares represent adaptive nodes and circles represent stationary (fixed) nodes. ANFIS utilizes a hybrid learning technique to establish an input–output mapping based on the input–output data pairs collected from

simulation. The hybrid strategy uses a combination of steepest-descent method and least-squares estimation technique to adjust the fuzzy membership functions.

In the first layer of Figure 49 represented by squared nodes, ANFIS maps the inputs (crisp) to the fuzzy membership functions and the outputs of this layer is determined as follows:

$$\begin{aligned} Q_i^1 &= \mu_{A_i}(x_i), \; i = 1,2, \\ Q_i^1 &= \mu_{B_{i-2}}(y_i), \; i = 3,4, \end{aligned} \tag{5.8}$$

where μ is a weight obtained from the fuzzy membership function. In the second layer, simple multiplication of the outputs of layer 1 as follows:

$$Q_i^2 = w_i = \mu_{A_i}(x_i)\,\mu_{B_i}(y_i), \; i = 1,2, \tag{5.9}$$

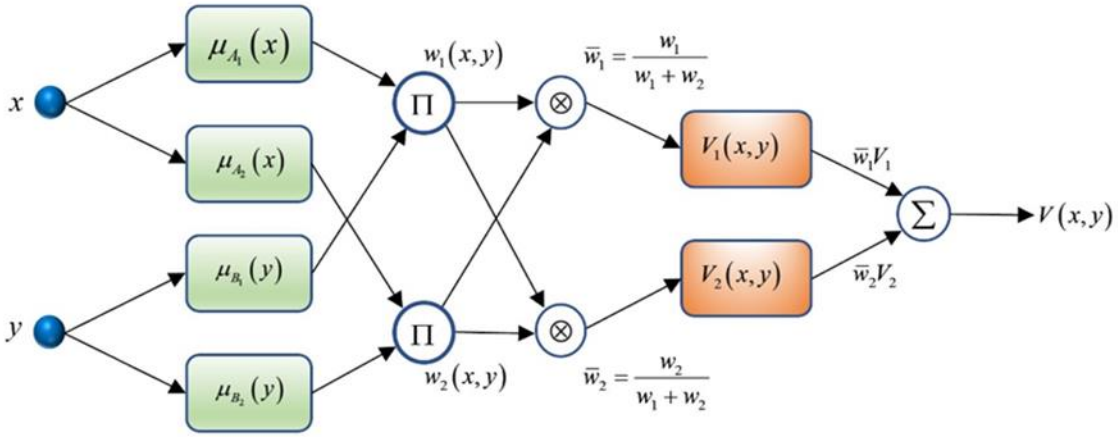

Figure 49: ANFIS architecture.

A normalization of the outputs of the second layer is conducted in the third layer. The outputs of this layer can be represented as follows:

$$Q_i^3 = \bar{w}_i = \frac{w_i}{w_1 + w_2}, \; i = 1,2, \tag{5.10}$$

The fourth layer represents the product of the outputs of the third layer and a first order Sugeno model. The outputs of this layer can be given by:

$$Q_i^4 = \bar{w}_i V_i = \bar{w}_i \left(p_i x + q_i y + r_i \right), \; i = 1,2, \tag{5.11}$$

The fifth layer is only one fixed node which performs the summation of all coming signals. Hence, the output of this layer represents the overall output of the model as follows:

$$Q_i^5 = \sum_{i=1}^{2} \bar{w}_i V_i = \frac{\sum_{i=1}^{2} w_i V_i}{w_1 + w_2} \tag{5.12}$$

The adaptive neural network (learning algorithm) task is to tune all the fuzzy logic controller parameters (p_i, q_i, and r_i) until the error between the fuzzy model and the input (e.g. acceleration) – output (voltage) data pairs (training data) is sufficiently small or attain a predefined epoch.

The training data are produced by using Linear Quadradic Regulator (LQR) designed for this purpose assuming full-state feedback. The training data should be representative of different situations under different excitations during the operation of the controller (Schurter & Roschke, 2001a). Also, there must be enough training data available for the fuzzy controller; otherwise, the mount of interpolation by the fuzzy controller would be excessive (Schurter & Roschke, 2001b). The external disturbance used to create the training data set should accommodate the range and frequency content of actual excitations where the fuzzy controller is employed to handle. The disturbance

used by the target controller is created through band-limited Gaussian white noise built in SIMULINK with a duration of 80 s. The parameters of the LQR are chosen as follows:

$$Q_{(2n_1+2n_2,2n_1+2n_2)} = \frac{1}{2}\begin{bmatrix} [K_s]_{(n_1+2n_2,n_1+2n_2)} & [0]_{(n_1+2n_2,n_1+2n_2)} \\ [0]_{(n_1+2n_2,n_1+2n_2)} & [M_s]_{(n_1+2n_2,n_1+2n_2)} \end{bmatrix} \tag{5.13}$$

$$R_{(2n_1,2n_1)} = \rho I_{(2n_1,2n_1)};\quad \rho = 1\times 10^{-5}$$

where K_s and M_s are the stiffness and mass matrices of the coupled system. The primary fuzzy logic controller developed in the current chapter employs one and two inputs, respectively to infer the command voltage. Seven Gaussian membership functions are defined for each input, as shown in Figure 50. The fuzzy sets for the input variables are PL = positive large, PM = positive medium, PS = positive small, ZE = zero, NL = negative large, NM = negative medium, NS = negative small. The fuzzy sets for the output (voltage) variable are ZE = zero, M = medium, and L = large. The maximum applied voltage for the MR damper is saturated to 10 V. Since different inputs considered in this study, range of the universe of discourse will vary based on the input type. For instance, if the input variable is the displacement, the range is defined from -1 to 1. On the other hand, if the input is the acceleration, the range is chosen to be from -15 to 15. If the range of the universe of discourse does not accommodate all values of the input variable, the software will return error message.

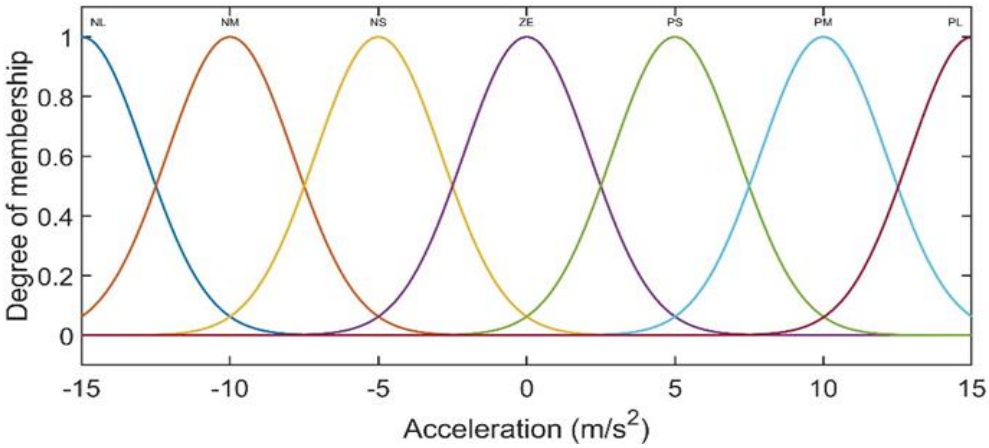

Figure 50: Input membership functions for the FLC.

5.4 Numerical Study

The system considered for the numerical implementation consists of two buildings (Building 1 and Building 2) connected at three levels. Building 1 has five stories and Building 2 consists of three stories. Number of unconnected floors is n_1 and number of connected floors is n_2. Therefore, the total number of floors in the coupled system is $n_1 + 2n_2$. The mass and stiffness of each floor of both buildings are 4.78×10^5 kg and 1.6983×10^8 N/m, respectively. The total mass and stiffness of Building 1 are 23.9×10^5 kg and 8.4915×10^8 N/m, respectively and the total stiffness of Building 2 is 5.0949×10^8 N/m. The mass and stiffness matrices of the two buildings were chosen to give the fundamental natural periods of the Building 1 and 2 as 1.171 s and 0.749 s, respectively. Thus, the dominant frequencies of the two individual buildings are well separated as it is required to make the coupling strategy feasible. The damping matrix of the combined system is determined by using the Rayleigh damping formula with 2% damping ratio for both the

lower and higher modes. In the current numerical study, the connected floors are the first, second, and third floor.

Three MR dampers are used to connect the two buildings. The equations governing the damper force predicted by the simple Bouc-Wen model for the coupled system are as follows (Al-Fahdawi, Barroso, & Soares, 2018; Al-Fahdawi, Barroso, & Soares, 2019):

$$f(t) = c_o\left[\dot{x}_{B1}(t) - \dot{x}_{B2}(t)\right] + \alpha_o z(t) \tag{5.21}$$

$$\begin{aligned}\dot{z}(t) = &-\gamma\left|\left[\dot{x}_{B1}(t) - \dot{x}_{B2}(t)\right]\right| z(t)\left|z(t)\right|^{n-1} - \beta\left[\dot{x}_{B1}(t) - \dot{x}_{B2}(t)\right]\left|z(t)\right|^{n} \\ &+ A\left[\dot{x}_{B1}(t) - \dot{x}_{B2}(t)\right]\end{aligned} \tag{5.22}$$

$$c_o = c_a + c_b u(t) \tag{5.23}$$

$$\alpha_o = \alpha_a + \alpha_b u(t) \tag{5.24}$$

$$\dot{u}(t) = -\eta\left[u(t) - \mathrm{v}\right] \tag{5.25}$$

5.5 Simulations and Analyses

The performance of the proposed system is investigated when the structure is subjected to a suite of five different earthquakes representing the external disturbances. The characteristics of the five earthquakes are listed in Table 5. Time history analyses of the complex system are conducted in MALAB/SIMULINK R2018a environment. The Dormand-Prince (ode45) solver with variable time step size is used as a primary solver. This method is one of the Runge-Kutta family of ordinary differential equation solvers which uses six function evaluations per step to calculate higher order precise solutions.

For the adaptive neuro-fuzzy control method, the number of the input membership functions of the primary fuzzy logic controller is chosen to be seven in Gaussian shape as shown in Figure 50. These membership functions along with their parameters will be adjusted by the adaptive neural networks to match the training data. For SAC method, the tuning values of σ, T and $\bar{T}$ are chosen to be 0.1, $10^3\left[I\right]_{31\times31}$, and $10^{10}\left[I\right]_{31\times31}$, respectively.

The performance of both adaptive control methods is evaluated based on the peak values as well as the overall responses. The peak values of the floor displacement, absolute acceleration, inter-story drift, and base shear are monitored. To assess the peak responses, four evaluation metrics are utilized, as listed in equation (5.26).

$$J_1 = \frac{\max\left|x_i(t)\right|}{x^{\max}} \qquad J_2 = \frac{\max\left|\ddot{x}_i(t)\right|}{\ddot{x}^{\max}}$$

$$J_3 = \frac{\max\left\{\left|d_i(t)/h_i\right|\right\}}{\delta^{\max}} \qquad J_4 = \frac{\max\left\{\sum_i^n k_i x_i(t)\right\}}{F_b^{\max}} \tag{5.26}$$

where J_1, J_2, J_3, and J_4 address the peak displacement, absolute acceleration, inter-story drift, and base shear, respectively. The subscript i is the story level and h_i is the height of the associated floor. $x^{\max}$ and $\ddot{x}^{\max}$ are the maximum displacement and absolute acceleration of the uncontrolled system, respectively. $\delta^{\max}$ and $F_b^{\max}$ are the peak values of the inter-story drift and base shear of the uncontrolled system, respectively. It is obvious that when these criteria are less than unity meaning a reduction in the peak responses has occurred, otherwise, when they are greater than unity, there is an amplification in the peak responses compared to the uncontrolled ones. To evaluate the overall responses of the system, the

root-mean-square (RMS) of the structural responses of both buildings is calculated. RMS of a vector is calculated according to the following formula:

$$\| . \| = \left(\frac{1}{t_f} \int_0^{t_f} [.]^2 \, dt \right)^{1/2} \tag{5.27}$$

The goal of using SAC is to decrease the error between the system's response, $y_p(t)$, and the reference-model's, $y_m(t)$, as possible even with the presence of parameters changing. Similarly, the adaptive neural networks in the ANFIS strategy attempts to monitor the error between the system's responses and the training data and then adjust the parameters of the fuzzy logic controller to decrease the error accordingly. However, since the control system is not perfect and has limitations, the system's outputs would never perfectly match the reference-model's (or training data) trajectories.

5.6 Results and Discussion

The time history analyses are conducted on the coupled system considering two cases. First case assumes that the system preserves its dynamic characteristics during the earthquakes which sometimes termed in this study as "undamaged" structure. Second case assumes that the structure experiences some parametric changes during the earthquakes which is sometimes labeled as "damaged" structure. The change in the parameters could be as a result of damage due seismic events, fatigue, temperature fluctuations, … etc. The "damaged" case is reflected in the analysis by reducing the mass by 5% and stiffness by 20%.

Figure 51 and Figure 52 display the time histories of Building 1's top floor displacement and acceleration of the undamaged structure with SAC3, ANFIS3, and ANFIS4, respectively subjected to the far-field, LA10, and near-field, NF01, earthquakes, respectively. The results of the undamaged uncontrolled system are also provided as a measure of performance assessment of the proposed schemes. SAC1, SAC2, ANFIS1, and ANFIS3 are intentionally suppressed in these figures for sake of clarity. It can be observed from these figures that the proposed schemes are effective in reducing both the peak displacements and accelerations under both, LA10 NF01 ground motions.

Figure shows the performance metrics of the undamaged Building 1 for each control scheme under the seismic events. It can be observed that the performance is different from scheme to the other. For instance, the performance of SAC2 and SAC3 with respect to displacements, J_1, is different based on the feedback type. While SAC performs surprisingly good in reducing J_1 with acceleration feedback, SAC3, under all earthquakes, it exacerbates the peak displacements with displacement feedback, SAC1, under LA16 and with velocity feedback, SAC2, under and LA16 and LA23. SAC3 also surpasses all ANFIS schemes in reducing J_1.

(a)

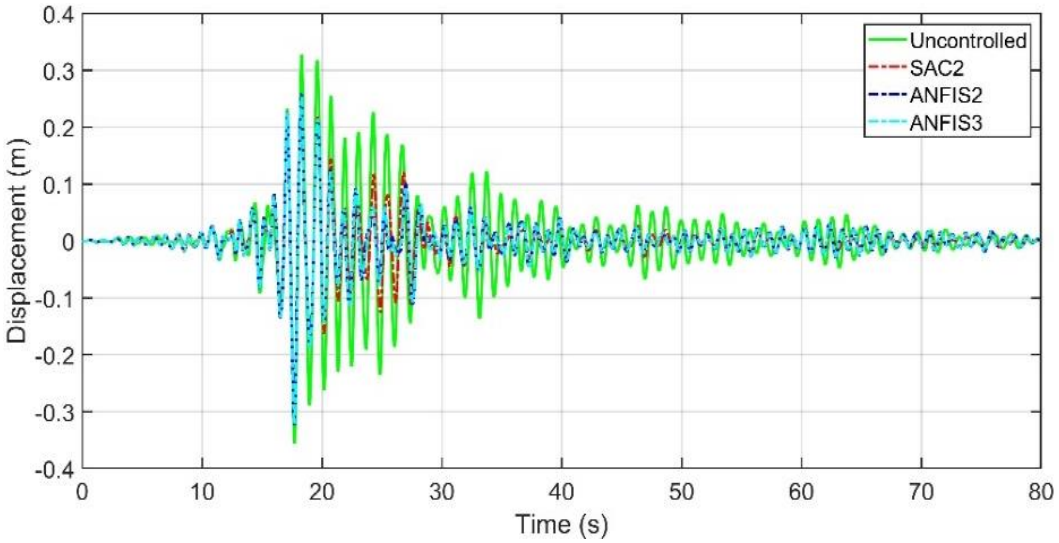

(b)

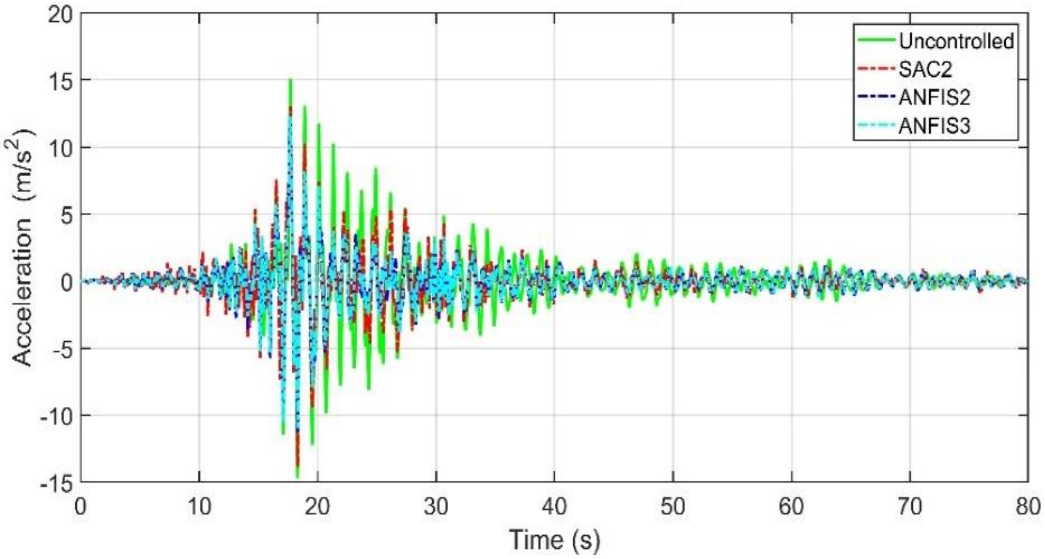

Figure 51: Displacement and acceleration time histories of the undamaged structure under LA10: (a) Building 1 and (b) Building 2.

(a)

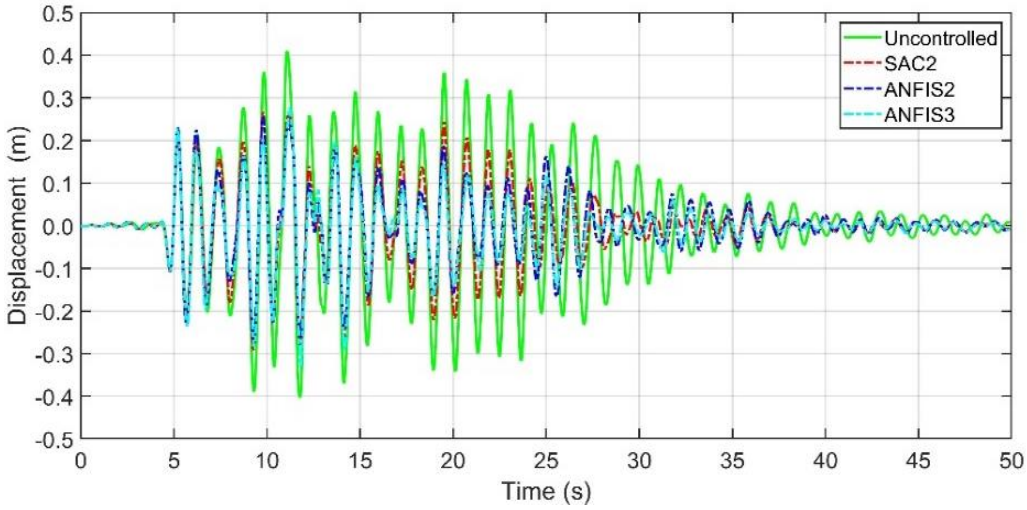

(b)

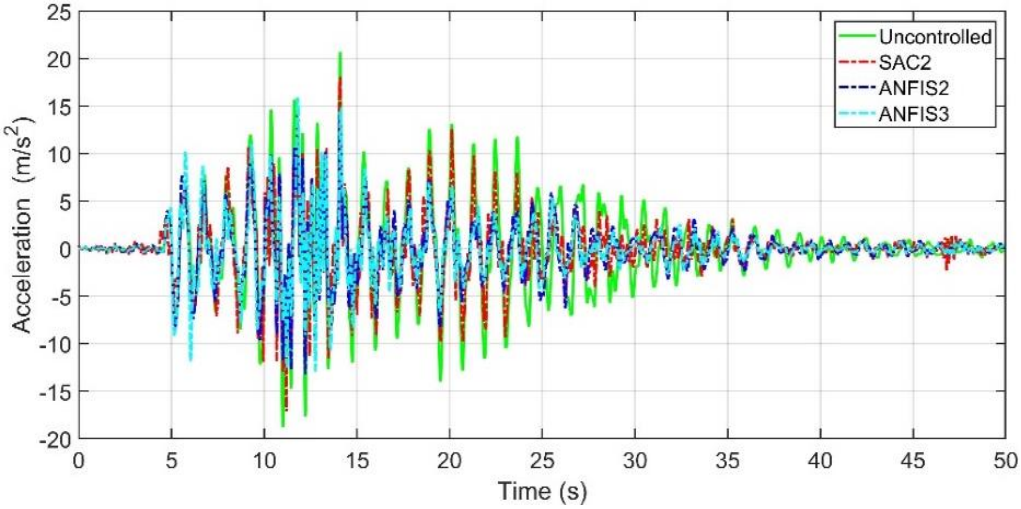

Figure 52: Displacement and acceleration time histories of the undamaged structure under NF01: (a) Building 1 and (b) Building 2.

Regarding the absolute acceleration, SAC1 worsen the index J_2 under LA23 and LS19F while SAC2 increases J_2 under all the ground motions except NF01. SAC3, on the other hand, performs much better and sustain the performance under all excitations. ANFIS1 and ANFIS3 reduce J_2 quite well in all cases except under LA23 where there is

a small increase in the peak acceleration. Other ANFIS schemes did poorly under some earthquakes. SAC2 and ANFIS4 produce one data point greater than unity associated with peak drift and peak base shear, respectively under LA23. SAC1 performs poorly under many earthquakes in reducing J_3 and J_4. The rest of data points for all schemes are less than unity meaning that there is a reduction in the peak values of inter-story drift and base shear, respectively. It can be observed that SAC3 is the only scheme that never exacerbated the peak responses for the undamaged structure while the other schemes sometimes perform better than SAC3 and other times much worse.

Figure displays the performance indices of Building 1 for the case associated with parameter change. SAC with displacement feedback, SAC1, surpasses all other schemes in reducing J_1, J_2, and J_3. Moreover, the other control cases reflect an enhancement in the displacement criteria, J_1, except SAC2 under LA23 where there is an increase in the peak displacement. ANFIS schemes perform better than SAC2 and SAC3 in reducing the peak displacement for the damaged structure. For the absolute acceleration index, J_2, SAC2, and ANFIS4 perform poorly under some earthquakes while they enhance the performance under other excitations. In reducing the peak acceleration, ANFIS1 and ANFIS2 seem to surpass all other schemes for this case. For the inter-story drift index, J_3, SAC2 is the only scheme that has one data point off the threshold under LA23 earthquake regarding J_3 and J_4, respectively while all other schemes perform quite well in minimizing these indices.

In order to further evaluate the performance of the proposed adaptive control methods, RMS of the top floors' displacements of Building 1 and 2 is calculated and depicted in Figure 55 and Figure 56, respectively. Figure 55 shows RMS responses for the

undamaged structure. In this figure, the results indicate that all the proposed control schemes are successful in reducing the overall responses under all earthquakes considered in the current study. ANFIS4 performs better than the other schemes in reducing the overall responses of both buildings and sustaining the performance under all earthquakes. SAC2 competes well with ANFIS4, except under LA10, in Building 1, but the latter scheme significantly outweighs the scale in Building 2. SAC1 does not perform that good compared with the other schemes. The performance of the other schemes is not the same from one building to the other. Fluctuation of the control schemes performances between Building 1 and 2 comes from the fact that the dynamics of each building is highly impacted by the motion of the other building.

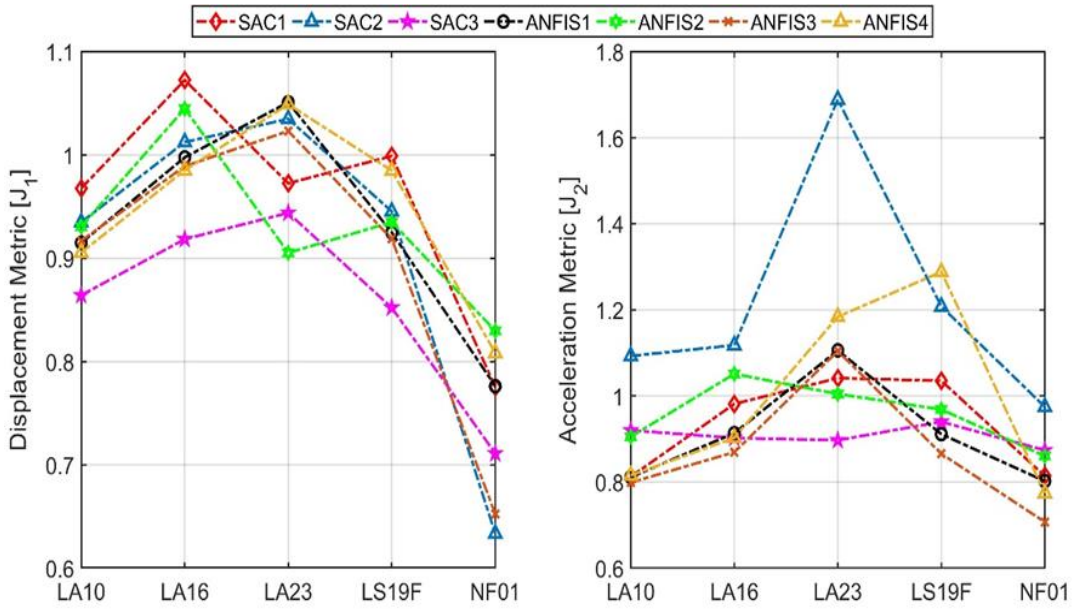

Figure 53: Building 1 performance indices without parameter changes.

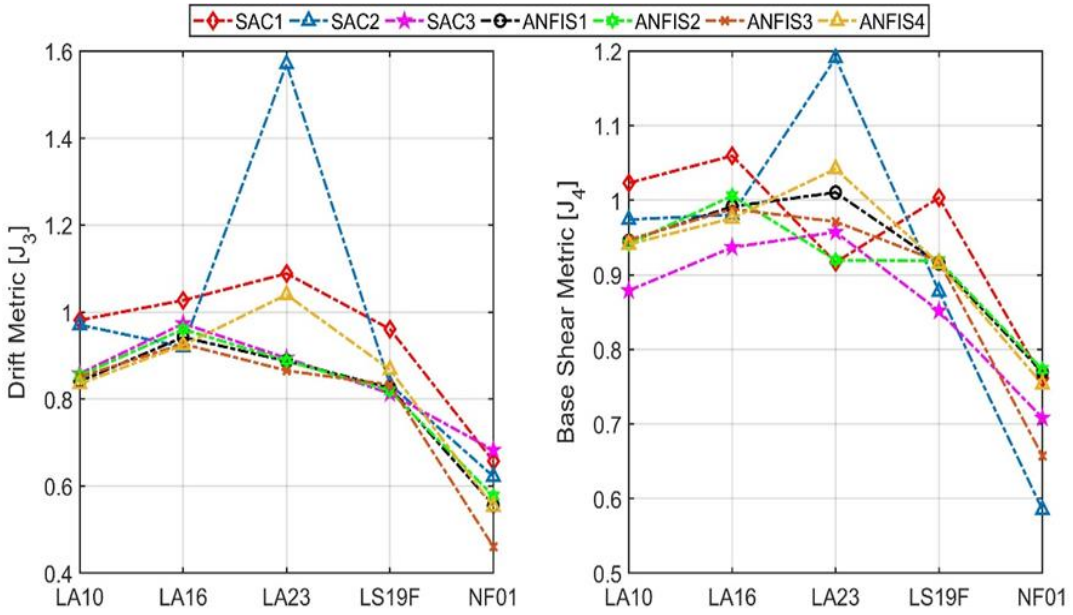

Figure 53: Continued.

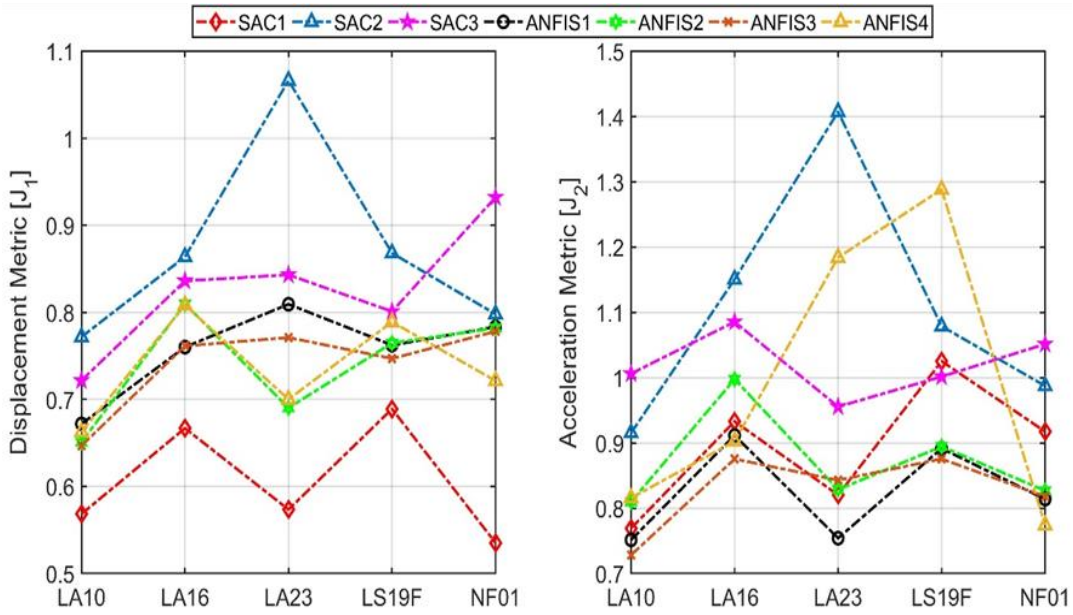

Figure 54: Building 1 performance indices with a reduction in the mass and stiffness.

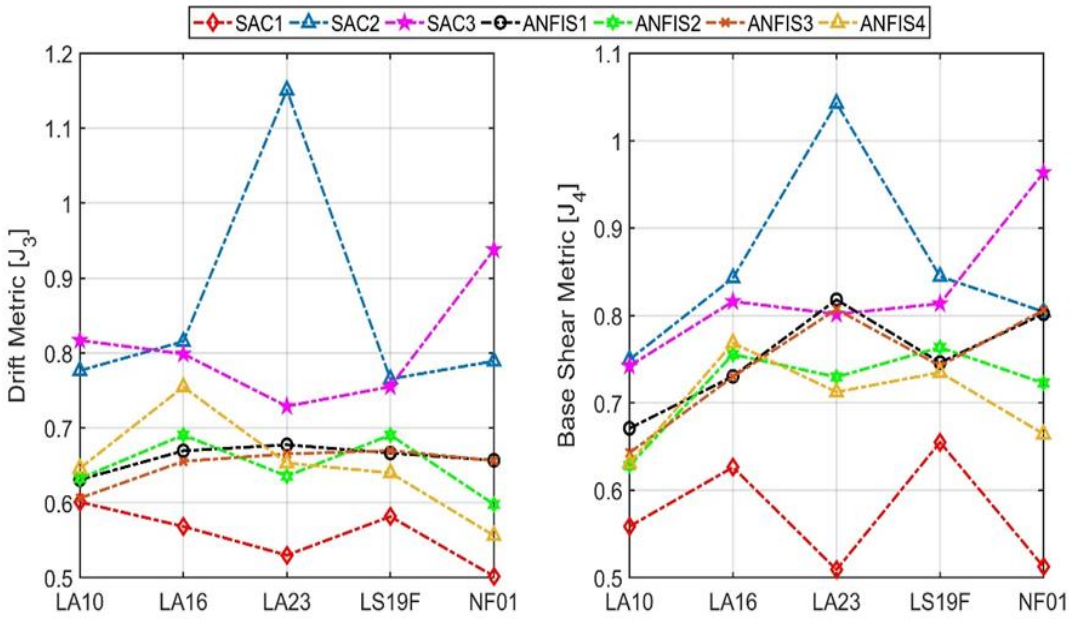

Figure 54: Continued.

Figure 56 shows RMS responses for the damaged structure. Again, this figure shows that all the proposed control schemes are capable to attenuate the overall responses of both buildings under all earthquakes. However, SAC1 surpasses the other schemes in mitigating RMS displacements of Building 1 while ANFIS2 performs better for Building 2.

To evaluate all the schemes considered in the current study, the mean value of each scheme under all excitations is computed and listed in Table 10 and Table 11, respectively. For the undamaged structure, Table 10, the results of all control cases reveal a significant reduction in the seismic responses. For example, the maximum reduction of floor displacement of Building 1 is achieved by SAC3 with 85.8% for J_1 index. However, ANFIS3 achieves maximum overall reduction for J_2 index with 86.9%. on the other hand,

for the damaged structure, Table 11, minimum J_1 is achieved by SAC1 with 60.7% while ANFIS1 performs better in minimizing J_2 with 82.5% reduction.

Table 10: Average reductions of all schemes for Building 1 (undamaged).

	J_1	J_2	J_3	J_4	RMS-B1	RMS-B2
SAC1	0.957	0.937	0.943	0.953	0.801	0.530
SAC2	0.912	1.217	0.984	0.922	0.715	0.490
SAC3	0.858	0.907	0.844	0.867	0.709	0.656
ANFIS1	0.933	0.909	0.810	0.927	0.646	0.497
ANFIS2	0.929	0.958	0.820	0.912	0.571	0.481
ANFIS3	0.900	0.869	0.787	0.896	0.576	0.453
ANFIS4	0.947	0.993	0.844	0.925	0.597	0.487

Table 11: Average reductions of all schemes for Building 1 (damaged).

	J_1	J_2	J_3	J_4	RMS-B1	RMS-B2
SAC1	0.607	0.893	0.557	0.572	0.419	0.586
SAC2	0.874	1.108	0.860	0.857	0.770	0.543
SAC3	0.827	1.020	0.808	0.827	0.731	0.701
ANFIS1	0.757	0.825	0.660	0.754	0.581	0.539
ANFIS2	0.740	0.871	0.649	0.720	0.541	0.519
ANFIS3	0.741	0.828	0.651	0.746	0.543	0.513
ANFIS4	0.736	0.982	0.650	0.702	0.477	0.523

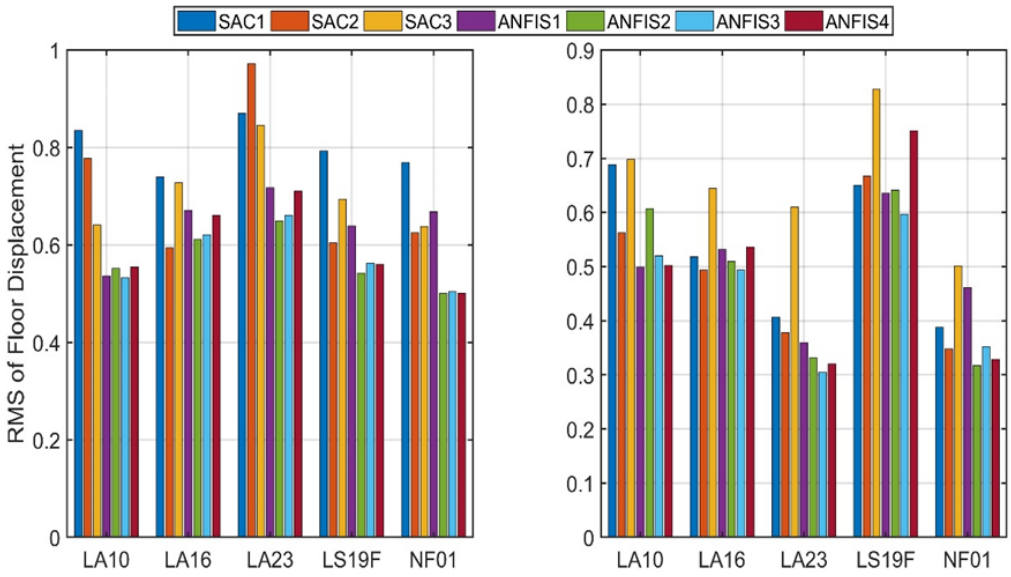

Figure 55: RMS of the undamaged top floors displacements of Building 1 (left) and Building 2 (right).

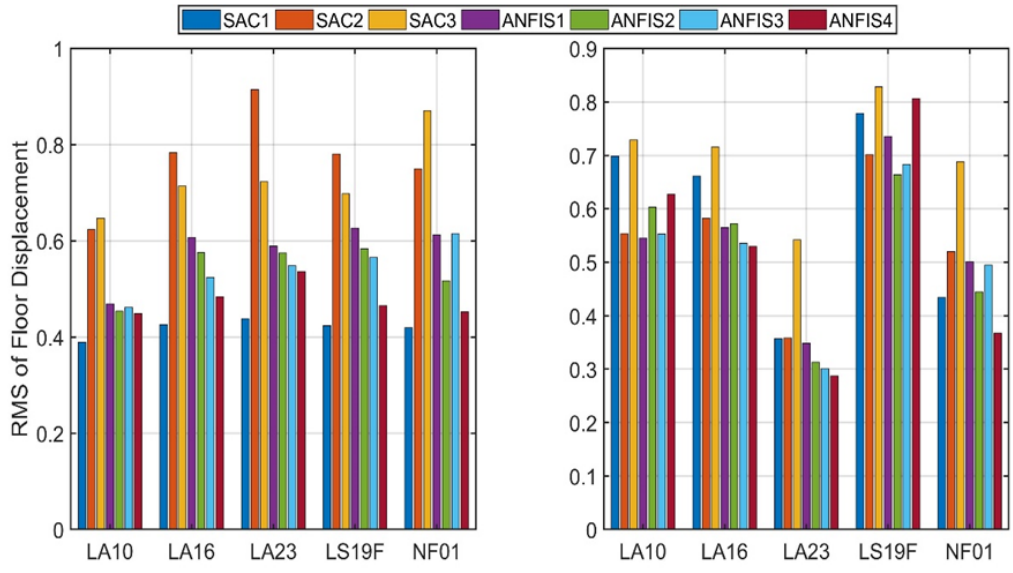

Figure 56: RMS of the damaged top floors displacements of Building 1 (left) and Building 2 (right).

The evaluation criteria for the undamaged and damaged Building 2 under all earthquakes are listed in Table 12. The values in the parentheses represent the results of the damaged structure.

Table 12: Metrics for Building 2 (parentheses represent the damaged structure).

Earthquake	Scheme	J_1	J_2	J_3	J_4
LA10	SAC1	0.923 (0.947)	1.205 (1.077)	1.036 (0.977)	0.927 (1.034)
	SAC2	0.815 (0.840)	1.391 (1.094)	1.118 (0.842)	0.825 (0.837)
	SAC3	1.207 (0.915)	1.690 (1.190)	1.356 (0.983)	1.209 (0.975)
	ANFIS1	0.943 (0.893)	1.127 (0.868)	1.134 (0.887)	0.956 (0.923)
	ANFIS2	1.313 (1.100)	1.368 (1.053)	1.349 (1.069)	1.317 (1.099)
	ANFIS3	0.998 (0.893)	1.147 (0.862)	1.155 (0.880)	0.996 (0.912)
	ANFIS4	0.882 (1.105)	1.034 (1.005)	1.049 (1.023)	0.897 (1.154)
LA16	SAC1	0.779 (0.849)	0.786 (0.789)	0.674 (0.659)	0.823 (0.898)
	SAC2	0.836 (0.782)	0.845 (0.740)	0.702 (0.717)	0.877 (0.825)
	SAC3	0.947 (0.842)	0.978 (0.909)	0.782 (0.936)	0.998 (0.888)
	ANFIS1	0.860 (0.766)	0.669 (0.597)	0.695 (0.620)	0.904 (0.809)
	ANFIS2	0.833 (0.731)	0.704 (0.556)	0.734 (0.581)	0.878 (0.783)
	ANFIS3	0.860 (0.766)	0.655 (0.581)	0.659 (0.587)	0.911 (0.809)
	ANFIS4	0.843 (0.720)	0.669 (0.825)	0.664 (0.585)	0.890 (0.770)
LA23	SAC1	0.501 (0.528)	0.509 (0.493)	0.520 (0.481)	0.498 (0.542)
	SAC2	0.533 (0.499)	0.554 (0.527)	0.584 (0.457)	0.522 (0.507)
	SAC3	0.735 (0.727)	0.750 (0.779)	0.765 (0.775)	0.729 (0.717)
	ANFIS1	0.513 (0.517)	0.508 (0.530)	0.503 (0.524)	0.515 (0.515)
	ANFIS2	0.553 (0.511)	0.553 (0.445)	0.555 (0.448)	0.557 (0.525)
	ANFIS3	0.479 (0.450)	0.493 (0.503)	0.486 (0.500)	0.476 (0.440)
	ANFIS4	0.552 (0.441)	0.661 (0.485)	0.673 (0.479)	0.556 (0.434)
LS19F	SAC1	0.981 (1.012)	1.102 (1.053)	1.039 (1.034)	0.972 (1.005)
	SAC2	1.067 (1.004)	1.193 (1.088)	1.101 (1.017)	1.071 (1.000)
	SAC3	1.194 (1.066)	1.288 (1.164)	1.160 (1.094)	1.198 (1.060)
	ANFIS1	1.099 (1.005)	1.086 (1.002)	1.101 (1.012)	1.096 (1.002)
	ANFIS2	1.137 (0.974)	1.168 (1.003)	1.183 (1.015)	1.128 (0.964)
	ANFIS3	1.072 (0.968)	1.014 (0.959)	1.036 (0.969)	1.079 (0.966)
	ANFIS4	1.155 (1.038)	1.189 (1.142)	1.200 (1.131)	1.145 (1.020)

Table 12: Continued.

Earthquake	Scheme	J_1	J_2	J_3	J_4
NF01	SAC1	0.554 (0.482)	0.829 (0.632)	0.658 (0.464)	0.524 (0.500)
	SAC2	0.429 (0.539)	0.713 (0.653)	0.539 (0.594)	0.411 (0.533)
	SAC3	0.623 (0.719)	0.902 (0.888)	0.733 (0.723)	0.604 (0.727)
	ANFIS1	0.600 (0.563)	0.690 (0.597)	0.691 (0.580)	0.585 (0.567)
	ANFIS2	0.439 (0.504)	0.523 (0.527)	0.524 (0.529)	0.429 (0.505)
	ANFIS3	0.515 (0.548)	0.634 (0.624)	0.633 (0.609)	0.494 (0.553)
	ANFIS4	0.478 (0.409)	0.510 (0.423)	0.499 (0.427)	0.464 (0.432)

5.7 Epilogue

The objective of the current chapter is to investigate the efficacy of two adaptive control methods that were utilized to drive MR dampers connecting two adjacent buildings subjected to seismic excitations. The first controller is the adaptive neuro-fuzzy control method which is used to determine the command voltage of the MR damper according to the intensity of ground motion. The adaptive neuro-fuzzy controller exploits the capability of the artificial neural networks to adjust the parameters of the fuzzy logic controller in order to reduce the error between the measured and training data. The second controller is the simple adaptive controller which produces optimum control forces to make a structure tracks the behavior of a well-designed reference-model. The aim of the developed adaptive control schemes was to alleviate the peak seismic responses as well as the overall responses of the coupled structure. The numerical simulations of several ground motions show that driving MR dampers connecting two adjacent buildings by the adaptive controllers developed in this chapter can effectively alleviate the seismic responses of the complex system. However, the structural performance is not the same in Building 1 and Building 2 and/or under all ground motions. Also, the results show that the type of

feedback significantly impacts the performance of both adaptive methods considered in the current chapter.

References

Al-Fahdawi O.A.S., Barroso, L. R., & Soares, R. W. (2018). Utilizing the Adaptive Control in Mitigating the Seismic Response of Adjacent Buildings Connected with MR Dampers. 2018 Annual American Control Conference (ACC). IEEE, 912-917.

Al-Fahdawi, O. A. S., Barroso, L. R., & Soares, R. W. (2019). Simple adaptive control method for mitigating the seismic responses of coupled adjacent buildings considering parameter variations. Engineering Structures, 186, 369–381. doi:10.1016/j.engstruct.2019.02.025.

Amini, F., Bitaraf, M., Eskandari Nasab, M. S., & Javidan, M. M. (2018). Impacts of soil-structure interaction on the structural control of nonlinear systems using adaptive control approach. Engineering Structures, 157, 1–13. doi:10.1016/j.engstruct.2017.11.071.

Barkana, I., (2014) The beauty of simple adaptive control and new developments in nonlinear systems stability analysis. AIP Conference Proceedings 1637: 89-113.

Barroso, L.R., Breneman, S. E., & Smith, H. A. (1998) Evaluating the effectiveness of structural control within the context of performance-based engineering. Proceedings of the Sixth US National Conference on Earthquake Engineering, Seattle, Washington, Earthquake Engineering Research Institute.

Bitaraf, M., Hurlebaus, S., & Barroso, L. R. (2012) Active and Semi-active Adaptive Control for Undamaged and Damaged Building Structures Under Seismic Load. Computer-Aided Civil and Infrastructure Engineering 27: 48-64.

Burns, R. (2001) Advanced control engineering: Elsevier.

Choi, K.-M., Cho, S.-W., Jung, H.-J., & Lee, I.-W. (2004). Semi-active fuzzy control for seismic response reduction using magnetorheological dampers. Earthquake Engineering & Structural Dynamics, 33(6), 723–736. doi:10.1002/eqe.372.

Gong, X., Ruan, X., Xuan, S., Yan, Q., & Deng, H. (2014). Magnetorheological Damper Working in Squeeze Mode. Advances in Mechanical Engineering, 6, 410158. doi:10.1155/2014/410158

Jang, J-S. (1993) ANFIS: adaptive-network-based fuzzy inference system. IEEE transactions on systems, man, and cybernetics 23: 665-685.

Jang, J-SR, Sun C-T and Mizutani E. (1997) Neuro-fuzzy and soft computing; a computational approach to learning and machine intelligence.

Soares, R. W., Barroso, L. R., & Al-Fahdawi, O. A. S. (2018). Simple Adaptive Control Strategy Applied to Reduce Response of Bridge Structure Subjected to Changes in Plant. 2018 Annual American Control Conference (ACC). doi:10.23919/acc.2018.8431623.

Schurter KC and Roschke PN. (2001a) Neuro-fuzzy control of structures using acceleration feedback. Smart materials and structures 10: 770.

Schurter KC and Roschke PN. (2001b) Neuro-fuzzy control of structures using magnetorheological dampers. American Control Conference, 2001. Proceedings of the 2001. IEEE, 1097-1102.

Symans, M. D., & Kelly, S. W. (1999). Fuzzy logic control of bridge structures using intelligent semi-active seismic isolation systems. Earthquake engineering & structural dynamics 28: 37-60.

Ulrich, S., Hayhurst, D. L., Saenz Otero, A., Miller, D., & Barkana, I. (2014). Simple Adaptive Control for Spacecraft Proximity Operations. AIAA Guidance, Navigation, and Control Conference. doi:10.2514/6.2014-1288.

Wong, C. W., Ni, Y. Q., & Ko, J. M. (1994). Steady-State Oscillation of Hysteretic Differential Model. II: Performance Analysis. Journal of Engineering Mechanics, 120(11), 2299–2325. doi:10.1061/(asce)0733-9399(1994)120:11(2299).

CHAPTER VI

ADAPTIVE CONTROL FOR THREE-DIMENSIONAL COUPLED BUILDINGS

The attenuation of three-dimensional coupled buildings under bi-directional seismic excitations using semi-active control devices is pursued in this chapter. Multiple magneto-rheological (MR) dampers are employed to connect two adjacent buildings at multiple levels for real-time control of the structural responses. The MR dampers are managed by adaptive neuro-fuzzy inference systems (ANFIS) and simple adaptive control (SAC) methods. The displacement feedback type is used for both control methods to design the closed-loop action. The structural system modeled as two three-dimensional buildings connected by frame elements in which the MR dampers are implemented. The equations of motions of the three-dimensional model are formulated by assuming that each floor diaphragm is rigid in its own plane but flexible in the vertical coordinate. Each link is assumed to have three degrees-of-freedom two translational and one rotational at its ends. The adaptive neuro-fuzzy inference system is designed based on Sugeno-type model. Seven triangular membership functions are chosen to fuzzify the input crisp data in the fuzzy logic controller built-in Matlab Fuzzy Logic Toolbox. The training data for ANFIS are generated by utilizing the LQR under white-noise excitation. For SAC, LQR is also used to generate the desired trajectories of the reference-model. Numerical simulations are carried out for both symmetrical and asymmetrical coupled buildings under eleven pairs of major earthquakes. The results show that both ANFIS and SAC can deal very successfully with modeling complexities associated with full three-dimensional

models. In terms of seismic responses reduction, both methods have shown a great potential in enhancing the structural performance under bi-directional earthquakes.

6.1 Prelude

Nowadays, there is a trend to construct buildings in close proximity as connected building systems. Such systems are usually connected by horizontal links such as skybridges. There is an extensive research on the seismic responses of simplified coupled building models. However, very limited studies on the seismic responses utilizing three-dimensional models can be found in the literature. For instance, Song and Tse (2014) investigated the effects of the skybridges on the wind-induced vibrations of a coupled system considering three-dimensional model. The above paper considers only a system consisting of two identical buildings connected by a structural element (Song & Tse, 2014). However, the case of identical buildings cannot be considered for implementing control devices within the links as explained in the previous chapters. Lim et al. (2011) described analytical modeling of twin buildings connected by a structural element. The structural element of the coupled buildings was modeled by introducing 6DOFs at its ends (Lim, Bienkiewicz, & Richards, 2011). The effect of introducing single or multiple skybridges on the dynamics of a connected two buildings considering three-dimensional space frames was studied by Atheer (2017). It was concluded by the author that multiple links highly influence the modal characteristics of the coupled system (Atheer, 2017).

Regrading structural control, the aforementioned studies address only the dynamic behavior of three-dimensional coupled systems without control devices. Also, these

studies consider only symmetrical buildings with no torsional motion expected for each individual building. It should be noted that the symmetrical buildings assumption cannot be applied to asymmetrical building systems because, in such systems, excitation in one direction causes motion in all other directions. As a result, it is necessary to develop a 3D model of connected symmetrical and asymmetrical buildings to identify the sensitivity of the adaptive control methods with such systems. Therefore, in this chapter, both simple adaptive control (SAC) method and adaptive neuro-fuzzy inference systems (ANFIS) are used to enhance the seismic behavior of three-dimensional symmetrical and asymmetrical coupled system subjected to bi-directional earthquakes.

6.2 Analytical Model of Coupled Buildings

6.2.1 Coupled Symmetrical Buildings

Two identical buildings with multiple links are considered in this section. Both buildings are assumed to be symmetric about the *x*, *y*, and *z* axes, respectively. The floors of both buildings are considered as rigid diaphragms with same elevations to be connected by horizontal links, as shown if Figure 57. The number of floors of Building 1 and 2 is n_1 and n_2, respectively. in this section, the center of the lumped mass of each floor in both buildings is assumed to coincide with the center of the stiffness to eliminate the effects of eccentricities. This assumption is made to highlight the effect of structural coupling on the control system. The individual buildings are modeled as multi-degree-of-freedom systems where each floor has three motions, i.e. two translations along *x* and *y* axes and one

rotational about the vertical axis, *z*. The links are modeled as frame members rigidly connected to the peripheral buildings.

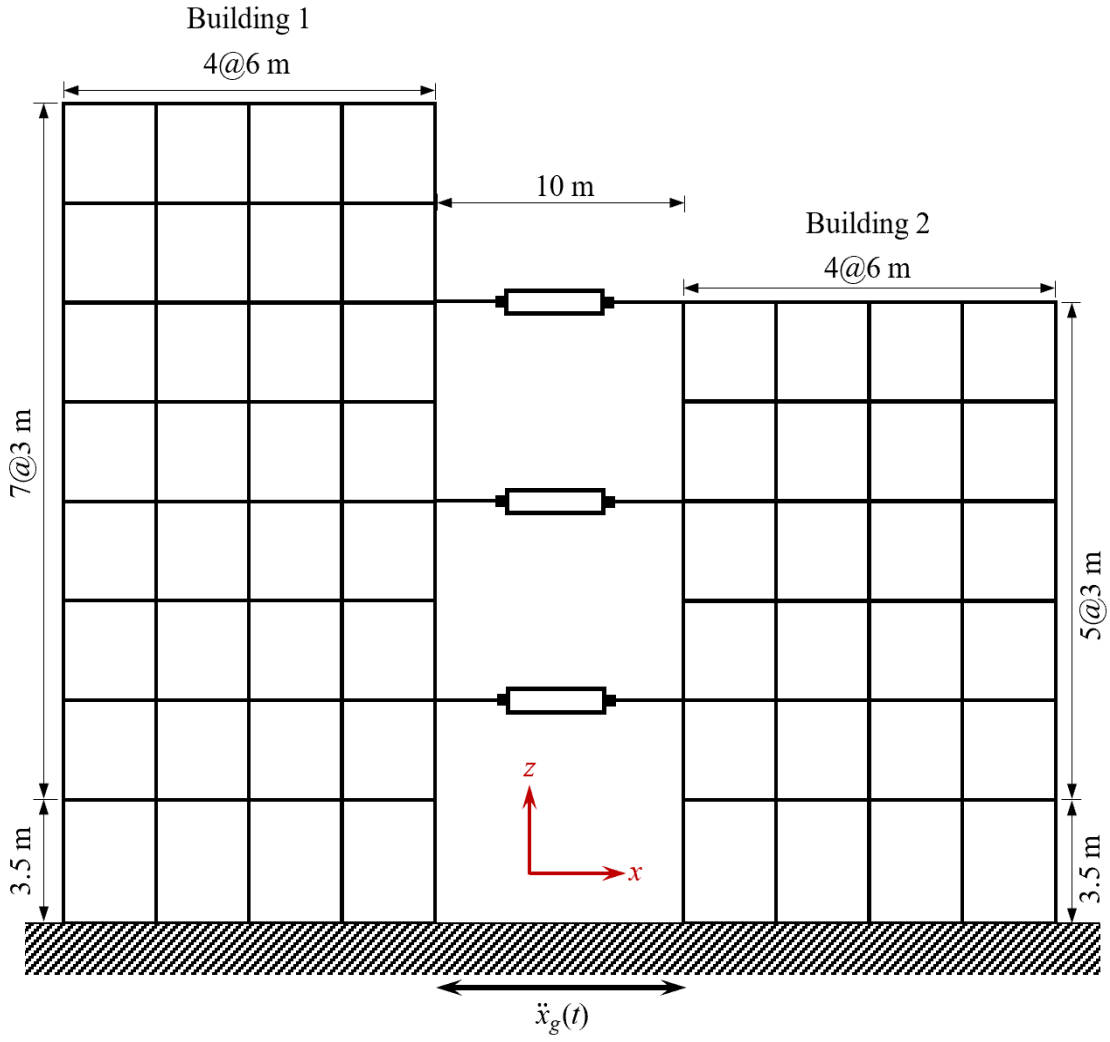

Figure 57: Placement of the control devices along *x* direction.

The equation of motion of 3-dimensional individual buildings can be found in structural dynamics textbooks (Chopra, 2012; Paultre, 2013). The total number of the

degrees of freedom of the coupled system can be determined as $3n_1 + 3n_2$. Accordingly, the equation of motion of the coupled system subjected to seismic excitation can be written as

$$\left[M + M_L\right]\ddot{x}(t) + \left[C + C_L\right]\dot{x}(t) + \left[K + K_L\right]x(t) = -\left[M + M_L\right]\ddot{x}_g(t) \tag{6.1}$$

where M, C, and K are the mass, damping, and stiffness matrices of the individual buildings; M_L, C_L, and K_L are additional mass, damping, and stiffness matrices due to the structural coupling; $\ddot{x}_g(t) = \left\{\ddot{x}_{g1x}(t),\ \ddot{x}_{g1y}(t),\ \ddot{x}_{g1\theta}(t),\ \ddot{x}_{g2x}(t),\ \ddot{x}_{g2y}(t),\ \ddot{x}_{g2\theta}(t)\right\}^T$ is the seismic load vector. $\ddot{u}_{g1\theta}$ and $\ddot{u}_{g2\theta}$ are the rotational accelerations of the bases of Building 1 and 2, respectively about their vertical axes. The rotational acceleration is usually taken equal to zero in most civil engineering applications because it cannot be recorded by strong-motion accelerographs (Chopra, 2012). M, C, and K matrices of the coupled system are defined as follows:

$$M_{(3n_1,3n_2)} = \begin{bmatrix} M_{1(3n_1,3n_1)} & 0_{(3n_1,3n_2)} \\ 0_{(3n_2,3n_1)} & M_{2(3n_2,3n_2)} \end{bmatrix} \tag{6.2}$$

$$K_{(3n_1,3n_2)} = \begin{bmatrix} K_{1(3n_1,3n_1)} & 0_{(3n_1,3n_2)} \\ 0_{(3n_2,3n_1)} & K_{2(3n_2,3n_2)} \end{bmatrix} \tag{6.3}$$

$$C_{(3n_1,3n_2)} = \begin{bmatrix} C_{1(3n_1,3n_1)} & 0_{(3n_1,3n_2)} \\ 0_{(3n_2,3n_1)} & C_{2(3n_2,3n_2)} \end{bmatrix} \tag{6.4}$$

where M_1 and M_2 are the individual mass matrices of Building 1 and 2, respectively, and can be written as:

$$M_1 = M_2 = \begin{bmatrix} M_x & 0 & 0 \\ 0 & M_y & 0 \\ 0 & 0 & I_{xy} \end{bmatrix} \tag{6.5}$$

where M_x and M_y are the mass matrices in the x and y directions, respectively. These matrices are the same in the current study. I_{xy} is the matrix of the mass moment of inertia of floor diaphragms. The stiffness matrix of an individual building considering coupled three-degrees-of-freedom is defined as:

$$K_1 = K_2 = \begin{bmatrix} K_{xx} & K_{xy} & K_{x\theta} \\ K_{yx} & K_{yy} & K_{y\theta} \\ K_{\theta x} & K_{\theta y} & K_{\theta\theta} \end{bmatrix} \tag{6.6}$$

The stiffness matrix of two buildings connected with a link is derived based on Figure 58, but the stiffness matrix of the link needs to be defined first. Since the link is modeled as a frame member, the stiffness matrix of such member can be written as follows (Paz, 2012):

$$\begin{Bmatrix} F_{1x} \\ F_{1y} \\ M_1 \\ F_{2x} \\ F_{2y} \\ M_2 \end{Bmatrix} = \frac{EI}{L^3} \begin{bmatrix} AL^2/I & 0 & 0 & -AL^2/I & 0 & 0 \\ 0 & 12 & 6L & 0 & -12 & 6L \\ 0 & 6L & 4L^2 & 0 & -6L & 2L^2 \\ -AL^2/I & 0 & 0 & AL^2/I & 0 & 0 \\ 0 & -12 & -6L & 0 & 12 & -6L \\ 0 & 6L & 2L^2 & 0 & -6L & 4L^2 \end{bmatrix} \begin{Bmatrix} u_{1x} \\ u_{1y} \\ \theta_1 \\ u_{2x} \\ u_{2y} \\ \theta_2 \end{Bmatrix} \tag{6.7}$$

where E is the modulus of elasticity of the link material; L is the link length; I is the moment of inertia of the link; A is the cross-sectional area of the link.

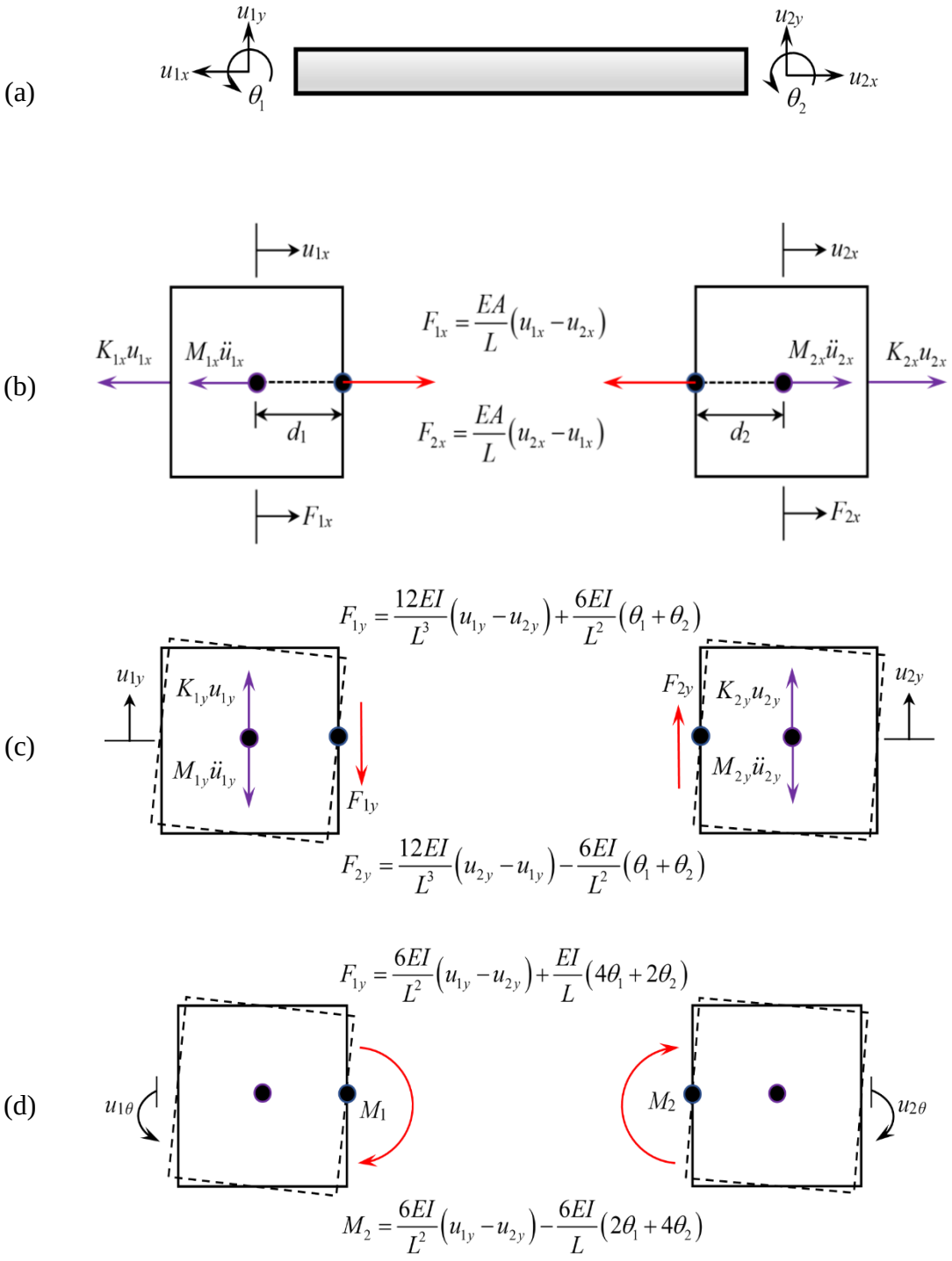

Figure 58: Forces and associated deformations at the ends of the link; (a) Link's DOFs, (b) *x*-motion, (c) *y*-motion, and (d) θ-motion.

From equation (6.7), the local stiffness matrix of the link, K'_{Link}, can be written as follows:

$$K'_{Link} = \frac{EI}{L^3}\begin{bmatrix} AL^2/I & 0 & 0 & -AL^2/I & 0 & 0 \\ 0 & 12 & 6L & 0 & -12 & 6L \\ 0 & 6L & 4L^2 & 0 & -6L & 2L^2 \\ -AL^2/I & 0 & 0 & AL^2/I & 0 & 0 \\ 0 & -12 & -6L & 0 & 12 & -6L \\ 0 & 6L & 2L^2 & 0 & -6L & 4L^2 \end{bmatrix} \tag{6.8}$$

The mass of the link is lumped at its ends while the masses of the adjacent floors are lumped at the center of each floor. Therefore, a transformation matrix is required to assemble the mass matrix of the link with the mass matrices of the peripheral buildings. It is worth to be mentioned here that no transformation is needed when dealing with the motion along *x*-axis since the mass of the link is in alignment with the masses of Building 1 and 2, respectively and the same situation applies for the rotational motion. The transformation matrix is needed when dealing with the motion along y-direction as the mass of the link would develop an overturning moment about the lumped mass of the adjacent buildings. The transformation matric can be written as follows (Song & Tse, 2014):

$$K_{Link} = T^T K'_{Link} T \tag{6.9}$$

where T is the transformation matrix which can be defined as:

$$T_{(6,6)} = \begin{bmatrix} T_{1(3,3)} & 0_{(3,3)} \\ 0_{(3,3)} & T_{2(3,3)} \end{bmatrix} \tag{6.10}$$

in which

$$T_{1(3,3)} = \begin{bmatrix} 1 & 0 & 0 \\ 0 & 1 & d_1 \\ 0 & 0 & 1 \end{bmatrix} \tag{6.11}$$

$$T_{2(3,3)} = \begin{bmatrix} 1 & 0 & 0 \\ 0 & 1 & -d_2 \\ 0 & 0 & 1 \end{bmatrix} \tag{6.12}$$

where d is the distance between the end of the link and the center of the mass of the building as shown in Figure 58b above. Performing the transformation given in equation (6.9) gives the following global stiffness matrix of the link:

$$K_L = \frac{EI}{L^3} \begin{bmatrix} AL^2/I & 0 & 0 & -AL^2/I & 0 & 0 \\ 0 & 12 & 12d_1+6L & 0 & -12 & 12d_2+6L \\ 0 & 12d_1+6L & d_1(12+12L) & 0 & -12d_1-6L & 12d_1+12Ld_2+2L^2 \\ -AL^2/I & 0 & 0 & AL^2/I & 0 & 0 \\ 0 & -12 & -12d_1-6L & 0 & 12 & -12d_2-6L \\ 0 & 12d_2+6L & 12d_2+6L(d_1+d_2)+2L^2 & 0 & -12d_2-6L & d_2(12+12L)+4L^2 \end{bmatrix} \begin{Bmatrix} x_1 \\ y_1 \\ \theta_1 \\ x_2 \\ y_2 \\ \theta_2 \end{Bmatrix} \tag{6.13}$$

or

$$K_L = \frac{EI}{L^3} \begin{bmatrix} AL^2/I & -AL^2/I & 0 & 0 & 0 & 0 \\ -AL^2/I & AL^2/I & 0 & 0 & 0 & 0 \\ 0 & 0 & 12 & -12 & 12d_1+6L & 12d_2+6L \\ 0 & 0 & -12 & 12 & -12d_1-6L & -12d_2-6L \\ 0 & 0 & 12d_1+6L & -12d_1-6L & d_1(12+12L) & 12d_1+12Ld_2+2L^2 \\ 0 & 0 & 12d_2+6L & -12d_2-6L & 12d_2+6L(d_1+d_2)+2L^2 & d_2(12+12L)+4L^2 \end{bmatrix} \begin{Bmatrix} x_1 \\ x_2 \\ y_1 \\ y_2 \\ \theta_1 \\ \theta_2 \end{Bmatrix} \tag{6.14}$$

Figure 58b indicates that the equation of motion along x-direction is uncoupled with other motions when the peripheral buildings are symmetrical. However, when the

buildings are none-symmetrical, the *x*-motion is coupled with the *y* and θ motions as we will see in the next section.

After defining the global stiffness matrix of the link, the parameters of the generic equation of motion (6.1) are defined in equation (6.15) and (6.16), respectively. The damping matrix, *C*, of both buildings is determined by using Rayleigh formula with 2% damping ratio for both lower and higher modes. The parameters related to the links should be added to the parameters of the buildings to complete the formulation of the equation of motion defined in equation (6.1). In the current study, the masses of the links are neglected, i.e. $M_L = 0$, because they are very small compared to the masses of the adjacent buildings. The damping properties of each link is assumed to be proportional to its global stiffness matrix.

$$M_{(3n_1+3n_2,3n_1+3n_2)} = \begin{bmatrix} M_{1x(n_1,n_1)} & 0 & 0 & 0 & 0 & 0 \\ 0 & M_{2x(n_2,n_2)} & 0 & 0 & 0 & 0 \\ 0 & 0 & M_{1y(n_1,n_1)} & 0 & 0 & 0 \\ 0 & 0 & 0 & M_{2y(n_2,n_2)} & 0 & 0 \\ 0 & 0 & 0 & 0 & I_{1xy(n_1,n_1)} & 0 \\ 0 & 0 & 0 & 0 & 0 & I_{2xy(n_2,n_2)} \end{bmatrix} \quad (6.15)$$

$$K_{(3n_1+3n_2,3n_1+3n_2)} = \begin{bmatrix} K_{1x(n_1,n_1)} & 0 & 0 & 0 & 0 & 0 \\ 0 & K_{2x(n_2,n_2)} & 0 & 0 & 0 & 0 \\ 0 & 0 & K_{1y(n_1,n_1)} & 0 & 0 & 0 \\ 0 & 0 & 0 & K_{2y(n_2,n_2)} & 0 & 0 \\ 0 & 0 & 0 & 0 & K_{1\theta(n_1,n_1)} & 0 \\ 0 & 0 & 0 & 0 & 0 & K_{2\theta(n_2,n_2)} \end{bmatrix} \quad (6.16)$$

6.2.2 Coupled Asymmetrical Buildings

In the previous section, the equations of motions of two coupled buildings with symmetrical planes were derived. It has been shown that when the individual buildings are symmetrical, the x-motion is uncoupled from the y and θ motions. Therefore, considering only the x-motion in the previous chapters to conduct parametric studies is justifiable. In this section, a case of asymmetrical buildings about their principal coordinates is investigated. We start the derivation by considering only one asymmetrical building, say Building 1, to derive the coupled equations of motion and then the coupling effects between the two buildings will be added to model the whole system. The model considered earlier is preserved in this section while imposing an eccentricity about both x and y coordinates located as shown in Figure 59. The eccentricities along x and y coordinates are labeled as e_x and e_y, respectively. The masses, M_{1x}, M_{1y} are concentrated at the center of each floor level. Therefore, the inertia forces on the mass components are uncoupled and can be written as :

$$M_1 = \begin{bmatrix} M_{1x} & 0 & 0 \\ 0 & M_{1y} & 0 \\ 0 & 0 & I_{1xy} \end{bmatrix} \tag{6.17}$$

The force-deformation relations are determined by applying external static forces on the stiffness components following the direct equilibrium strategy. The lateral stiffness of the building along x and y coordinates are K_{1x} and K_{1y}, respectively while the rotational stiffness about z axis is $K_{1\theta}$.

The stiffness matrix of Building 1 is determined by imposing a unit displacement successively in each degree-of-freedom and the stiffness coefficients are determined by

statics. The details of the process are depicted in Figure 60 where the figure should be self-explanatory. The resulting stiffness matrix for Building 1 is

$$K_1 = \begin{bmatrix} K_{xx} & 0 & e_y K_{xx} \\ 0 & K_{yy} & e_x K_{yy} \\ e_y K_{xx} & e_x K_{yy} & e_y^2 K_{xx} + e_x^2 K_{yy} \end{bmatrix} \tag{6.18}$$

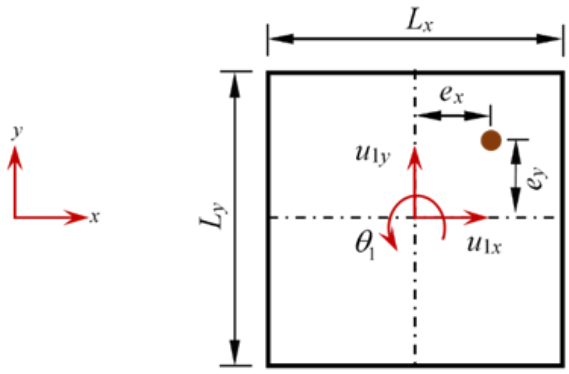

Figure 59: Plan view of Building 1 showing the imposed eccentricity.

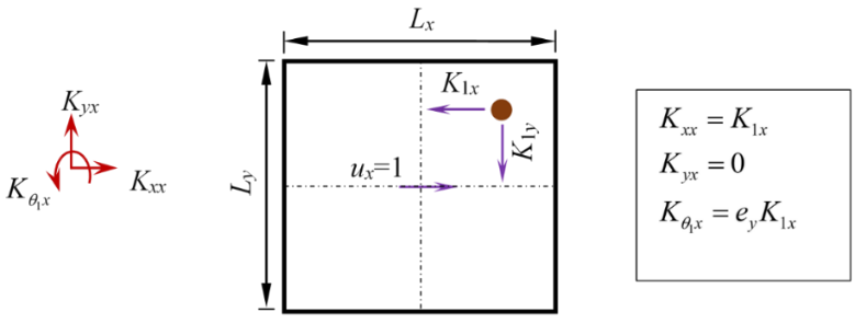

$$u_x = 1,\ u_y = u_{\theta_1} = 0$$

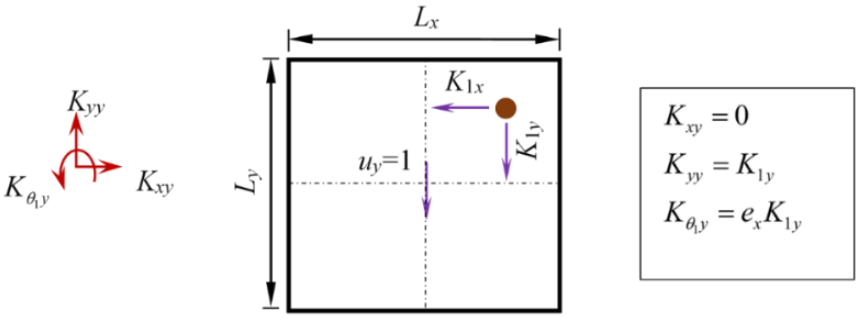

$$u_y = 1,\ u_x = u_{\theta_1} = 0$$

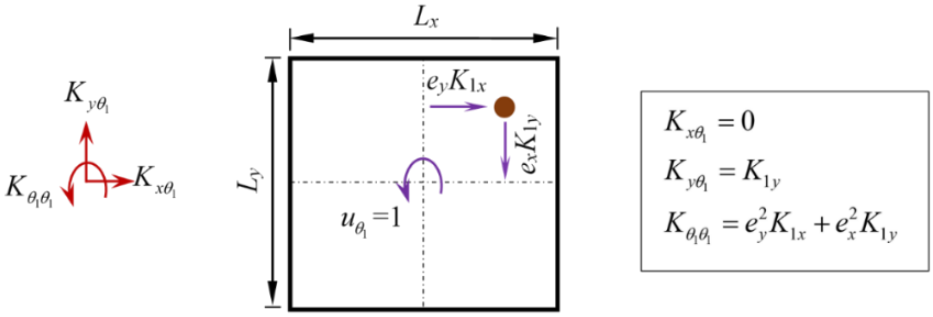

$$u_{\theta_1} = 1,\ u_x = u_y = 0$$

Figure 60: Evaluation of the stiffness matrix coefficients of Building 1.

6.3 Numerical Study

In this section, the coupled system considered for the numerical simulations consisting of two buildings connected at three levels. Building 1 has eight stories and Building 2 has six stories. Each building is modeled as a multi-degree-of-freedom system with rigid floor diaphragm as explained earlier in this chapter. The floor plan of each building is (24×24) m. The height of each floor in both buildings is taken as 3.0 m except the ground floor which is assumed to be 3.5 m. Each building has four bays in each direction with twenty columns in each floor. The eccentricities, e_x and e_y, are taken equal to 3m. The columns on the perimeter are assumed to be moment-resisting while the interior columns are assumed fixed-hinged columns. The column properties designed for Building 1 and Building 2 are listed in Table 13 and Table 14, respectively. The second, fourth, and sixth floor of both buildings are connected by two MR dampers at each level. Two girders (W12×30) are used to support the MR dampers at each floor. Each floor slab is assumed to be 6 inches (15 cm) thick. The mass of each floor is 3×10^5 kg and the mass moment of inertia of each floor is calculated as $(1/12)\times\left(L_x^{\,2}+L_y^{\,2}\right)$. The damping matrix of the combined system is determined by using the Rayleigh damping formula with 2% damping ratio for both the lower and higher modes. The equations governing the control forces produced by the MR dampers are (5.21) through (5.25).

Table 13: Columns properties for Building 1.

Column	I_x	I_y	Floors
W12×112	716	236	1-2
W12×85	455	154	3-5
W12×49	272	93.4	6-8

Table 14: Columns properties for Building 2.

Column	I_x	I_y	Floors
W12×112	716	236	1-2
W12×85	455	154	3-6

6.4 Simulations and Analyses

Numerical simulations for both controlled and uncontrolled of symmetrical and asymmetrical coupled buildings are carried out using MATLAB and SIMULINK R2018a. ode45 function with variable time steps is selected as a primary solver. The primary fuzzy logic controller developed in the current chapter employs the measured displacement vector to infer the command voltage. Seven triangular membership functions are defined for each input as shown in Figure 61. The fuzzy sets for the input variables are PL = positive large, PM = positive medium, PS = positive small, ZE = zero, NL = negative large, NM = negative medium, NS = negative small. The maximum applied voltage for the MR damper is saturated to 10 V to conform with the scaled parameters of 1000kN capacity listed in Table 3.

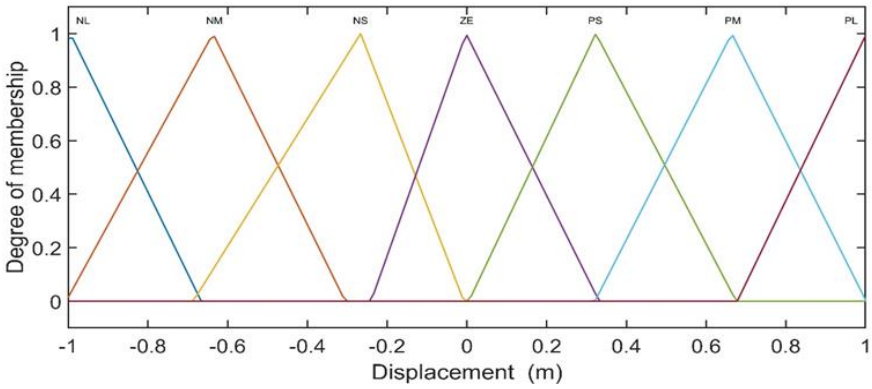

Figure 61: Membership functions for the primary FLC inputs.

Eleven pairs of major earthquakes have been chosen to represent the external disturbances on the coupled system under consideration. Each earthquakes pair consists of two components applied along both *x* and *y* directions simultaneously. The characteristics of the ground accelerations in both directions are listed in Table 15.

In the current numerical analyses, two strategies of placing the control devices have been employed. The first strategy is depicted in Figure 57 is achieved by connecting the two adjacent buildings along *x*-direction by the MR dampers. In contrast, it is assumed that there are no adjacent buildings along *y*-direction and; therefore, the MR dampers are placed inside the buildings in that direction, as shown in Figure 62. Employing these two strategies for one system is advantageous since the performance of each strategy can be manifested and a comparison between the two strategies can be made. It is also relevant to be mentioned here that placing control devices along *y*-direction within the links is unfeasible strategy. The reason is that the control forces produced along *y*-direction cause the adjacent buildings to rotate producing high torsional responses.

Table 15: Ground motions characteristics.

Earthquake	Magnitude	Component	PGA (m/s^2)	Time Step (s)	Duration (s)
Chi-Chi, Taiwan, 1999	7.62	N-S	2.347	0.004	149.996
	7.62	E-W	1.347	0.004	149.996
Big-Bear, CA, 1992	6.46	N-S	4.723	0.010	60.040
	6.46	E-W	5.344	0.010	60.040
Denali, Alaska, 2002	7.90	N-S	0.121	0.005	171.995
	7.90	E-W	0.225	0.005	171.995
Ducze, Turkey, 1999	7.14	N-S	0.372	0.005	86.195
	7.14	E-W	0.264	0.005	86.195
El-Centro, CA, 1940	6.90	N-S	3.421	0.020	53.460
	6.90	E-W	2.100	0.020	53.460
Landers, CA, 1992	7.28	N-S	1.128	0.004	9.996
	7.28	E-W	1.433	0.004	9.996
Loma Prieta, CA, 1989	6.93	N-S	1.540	0.005	39.995
	6.93	E-W	0.863	0.005	39.995
Kobe, Japan, 1995	6.90	N-S	1.810	0.010	79.990
	6.90	E-W	2.110	0.010	79.990
Niigata, Japan, 2004	6.63	N-S	0.421	0.010	186.990
	6.63	E-W	0.475	0.010	186.990
Northridge, CA, 1994	6.69	N-S	3.385	0.020	39.980
	6.69	E-W	3.019	0.020	39.980
San-Fernando, CA, 1971	6.61	N-S	0.252	0.004	56.156
	6.61	E-W	0.407	0.004	56.156

6.4.1 Simulations for Symmetrical Buildings

This section investigates the effectiveness of using adaptive control to attenuate the seismic responses of two connected symmetrical buildings. Figure through Figure depict the time histories of the Building 1's top floor *x* and *y* translational displacements as well as the rotational motions about the vertical axis.

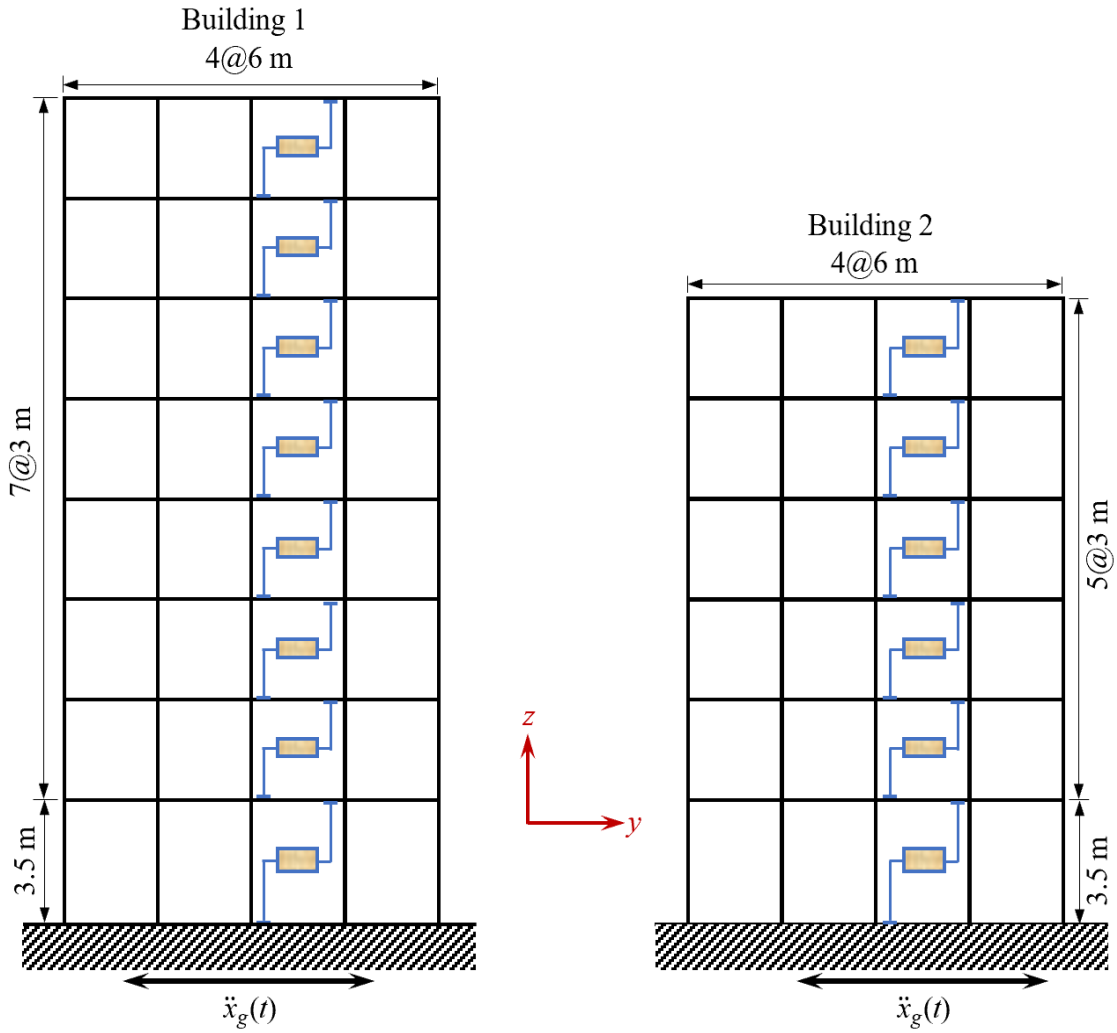

Figure 62: Placement of the control devices along *y* direction.

From Figure through Figure, it can be seen that the bi-directional seismic displacements have been significantly attenuated by the adaptive controllers. However, the performance of each controller is not the same from one building to another and from one earthquake to another. The discrepancy in performance between the two buildings can be justified by understanding the complex dynamics involved in the coupled systems by transferring the energy from one building to another through the coupling links. Moreover,

the random nature and difference in frequency content of each earthquake causes the discrepancy in the performance under different earthquakes. For instance, a significant reduction is achieved by both SAC and ANFIS under Chi-Chi earthquake along *x*-direction while it is not that good along *y* and θ directions. Also, Figure, the displacement time history along *y*-direction is greatly attenuated by SAC while it is not that effective by ANFIS. In contrast, Figureb shows a great reduction is achieved by using ANFIS compared to SAC.

(a)

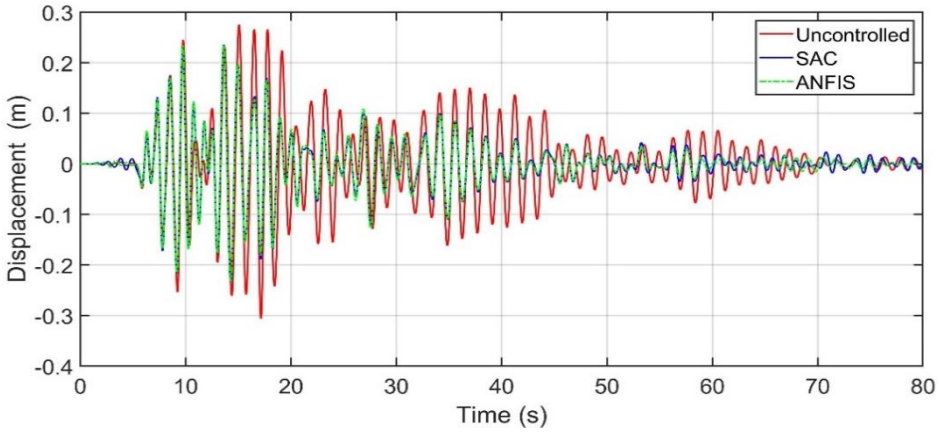

(b)

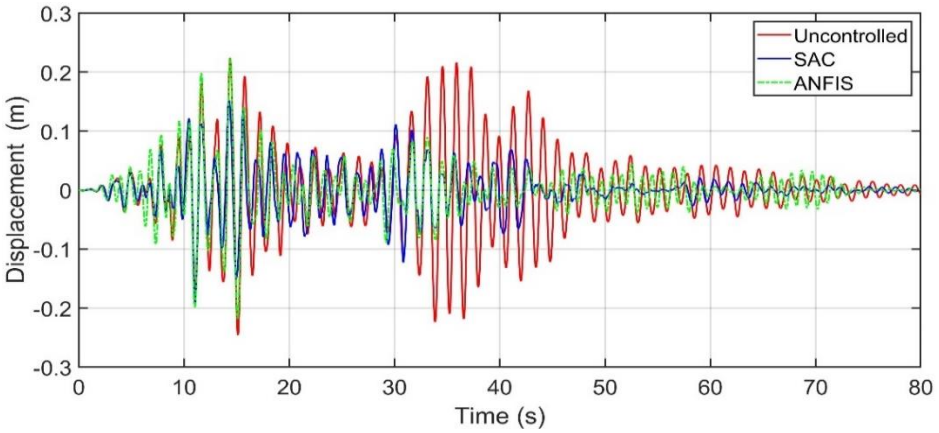

Figure 63: Time histories of the Building 1's top floor displacements under Kobe earthquake: (a) *x*-direction, (b) *y*-direction, and (b) rotation.

(c)

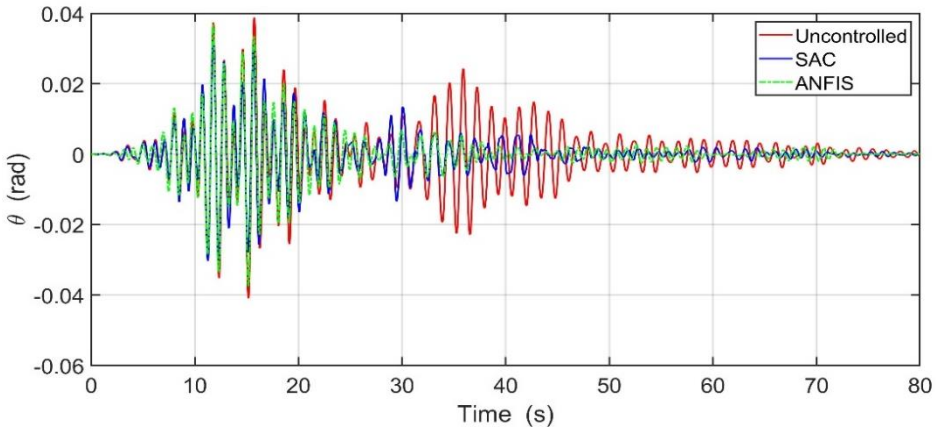

Figure 63: Continued.

(a)

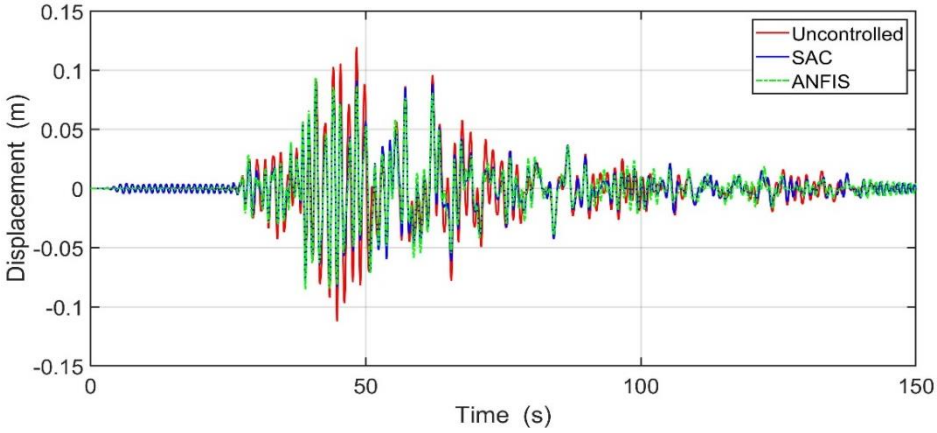

(b)

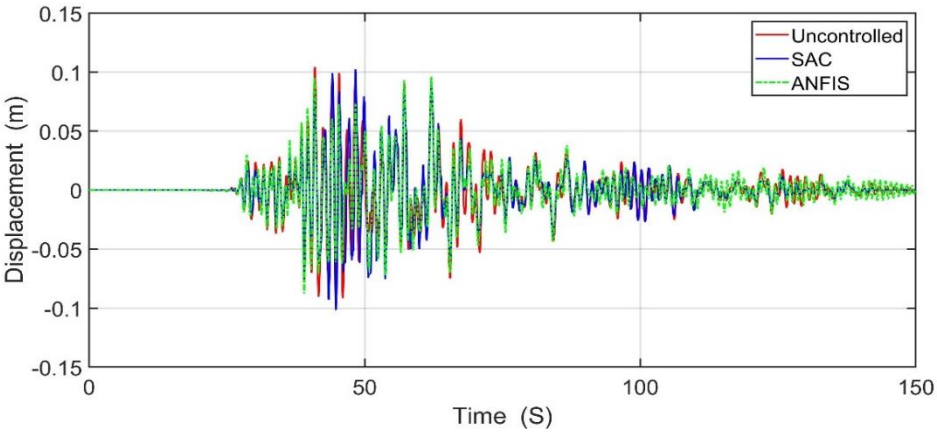

Figure 64: Time histories of the Building 1's top floor displacements under Chi-Chi earthquake: (a) *x*-direction, (b) *y*-direction, and (b) rotation.

(c)

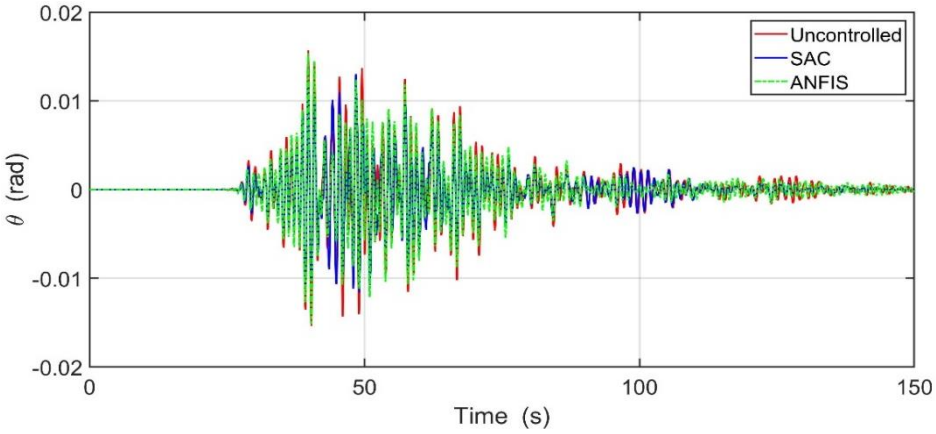

Figure 64: Continued.

(a)

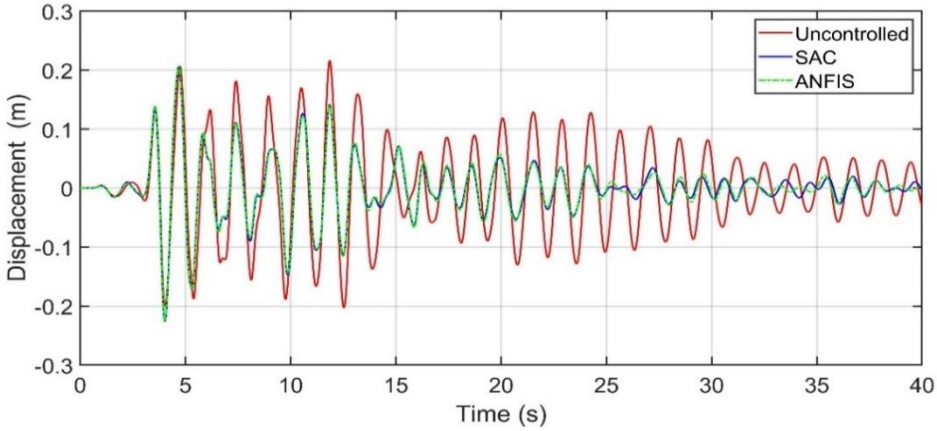

(b)

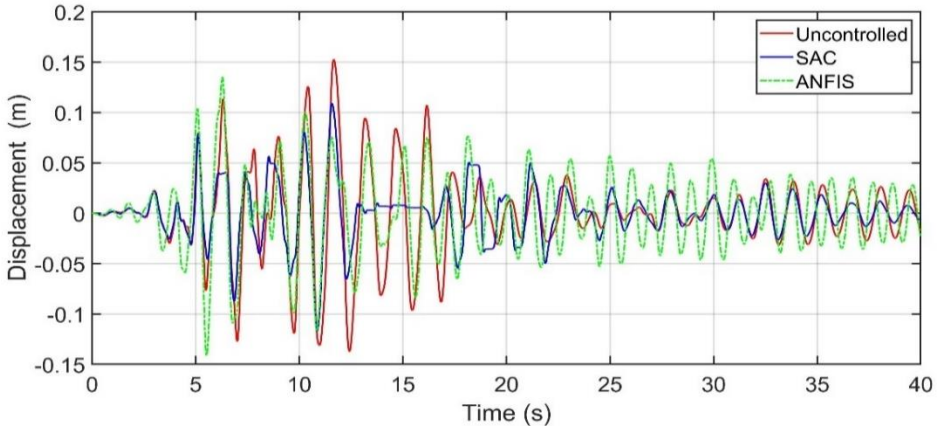

Figure 65: Time histories of the Building 1's top floor displacements under Northridge earthquake: (a) *x*-direction, (b) *y*-direction, and (b) rotation.

(c)

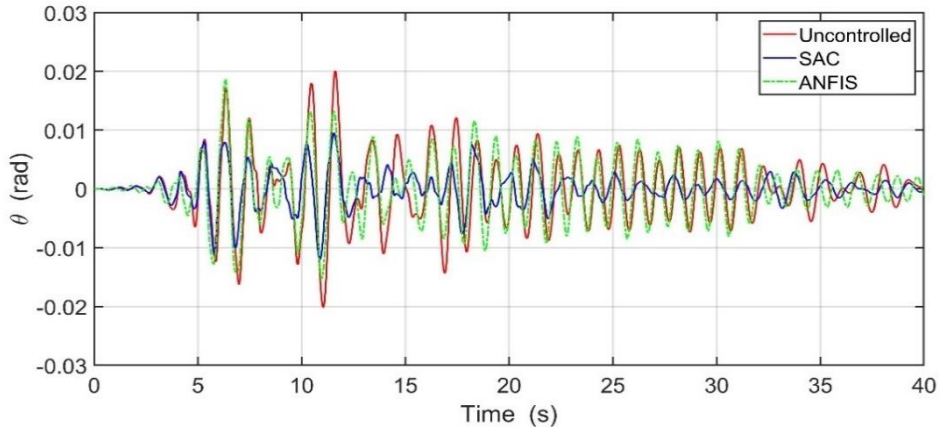

Figure 65: Continued.

(a)

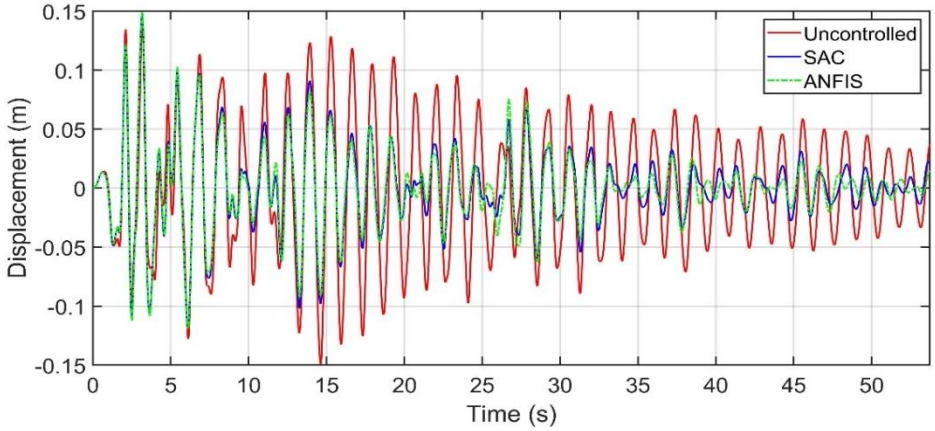

(b)

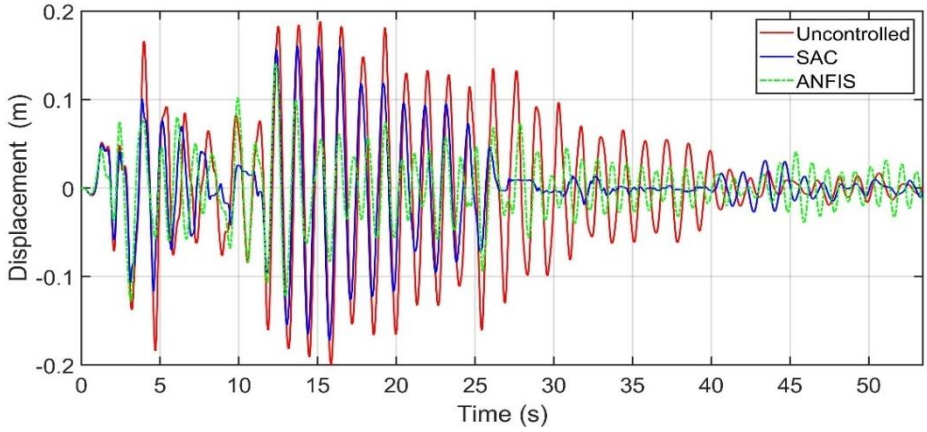

Figure 66: Time histories of the Building 1's top floor displacements under El-Centro earthquake: (a) *x*-direction, (b) *y*-direction, and (b) rotation.

(c)

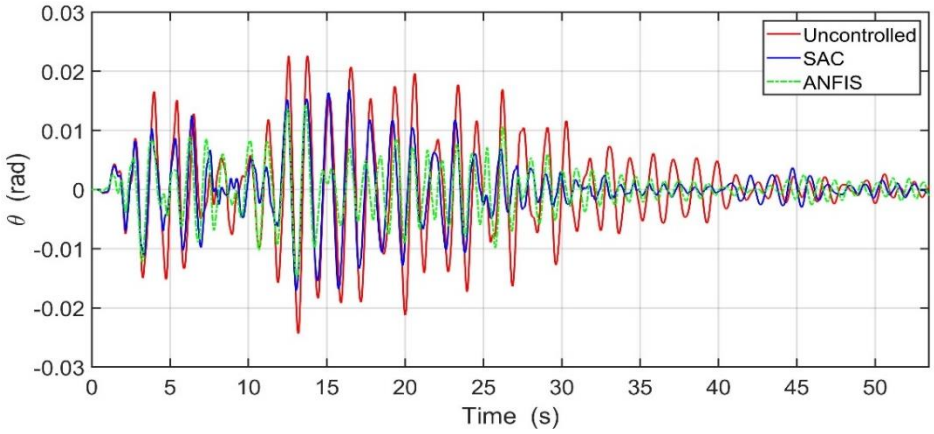

Figure 66: Continued.

The effectiveness of using the adaptive controllers in enhancing the overall seismic performances of both buildings in both directions is also investigated. The RMS responses under each earthquake's component is calculated according to equation (5.27). Figure 67 and Figure 69 depict the RMS of the translational and rotational displacements of Building 1 and 2, respectively. Further, Figure 67 and Figure 69 depict the RMS of the translational accelerations of Building 1 and 2, respectively. These figures show that a significant reduction in the overall displacement and accelerations has been achieved by both ANFIS and SAC, respectively. As an exception, SAC for Building 2 has shown lack of efficiency in mitigating the *y*-displacement under some earthquakes compared to ANFIS as depicted in Figure 67b. Regarding the translational accelerations, both SAC and ANFIS achieve a significant reduction under almost all eleven pairs of earthquakes.

(a)

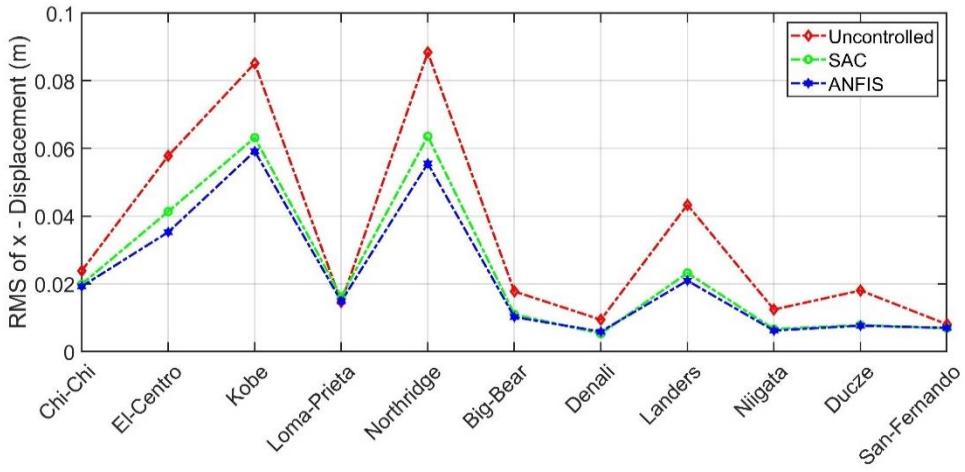

(b)

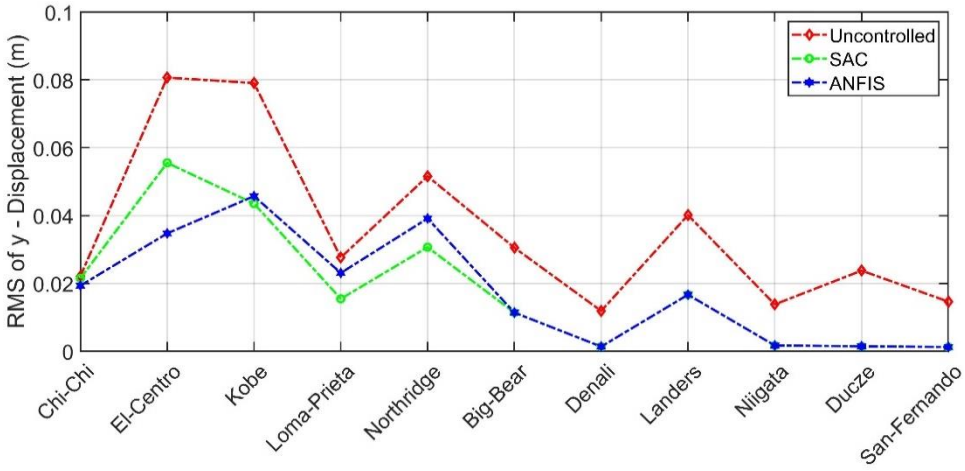

(c)

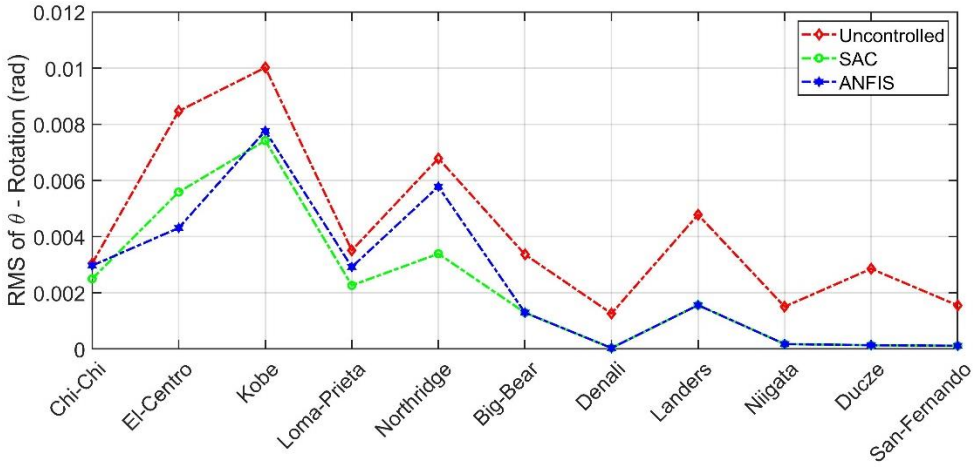

Figure 67: RMS of the displacement responses of symmetrical Building 1 (a) *x*-direction, (b) *y*-direction, and (c) θ-motion.

(a)

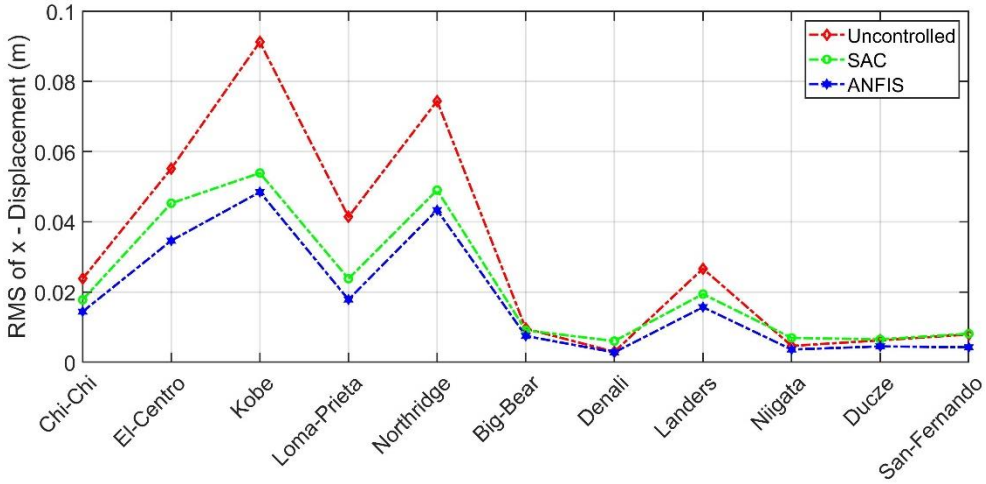

(b)

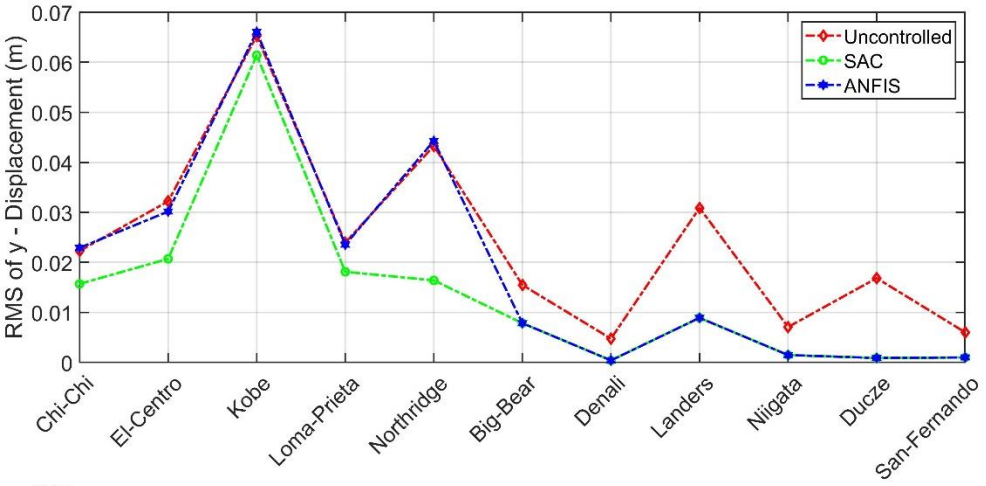

(c)

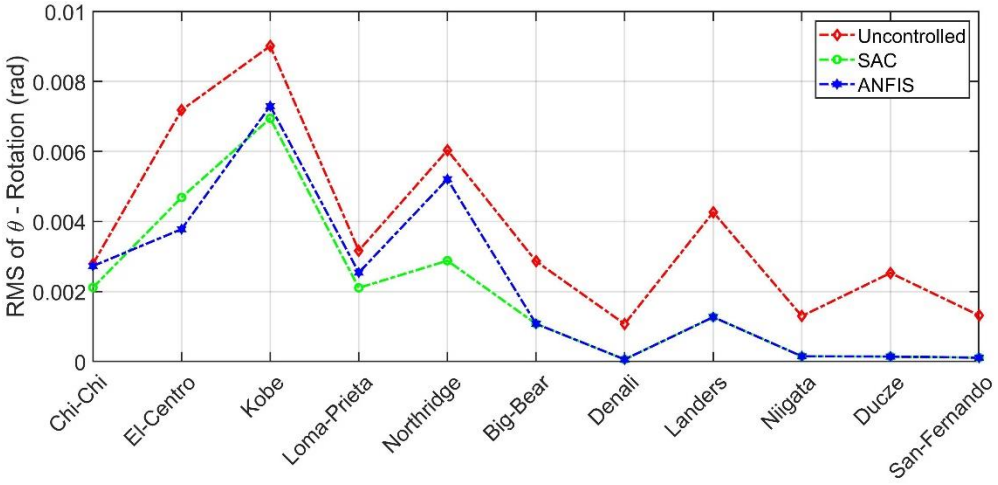

Figure 68: RMS of the displacement responses of symmetrical Building 2 (a) *x*-direction, (b) *y*-direction, and (c) θ-motion.

(a)

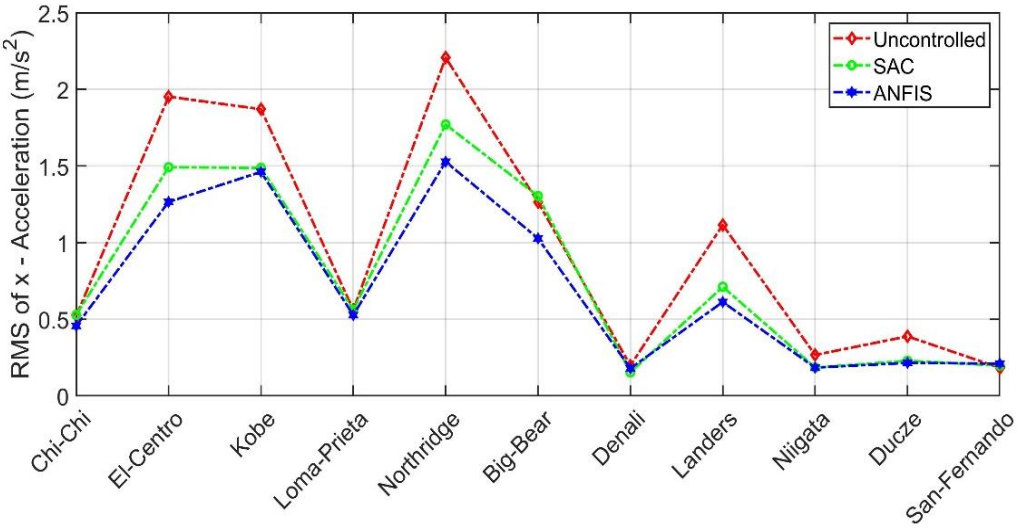

(b)

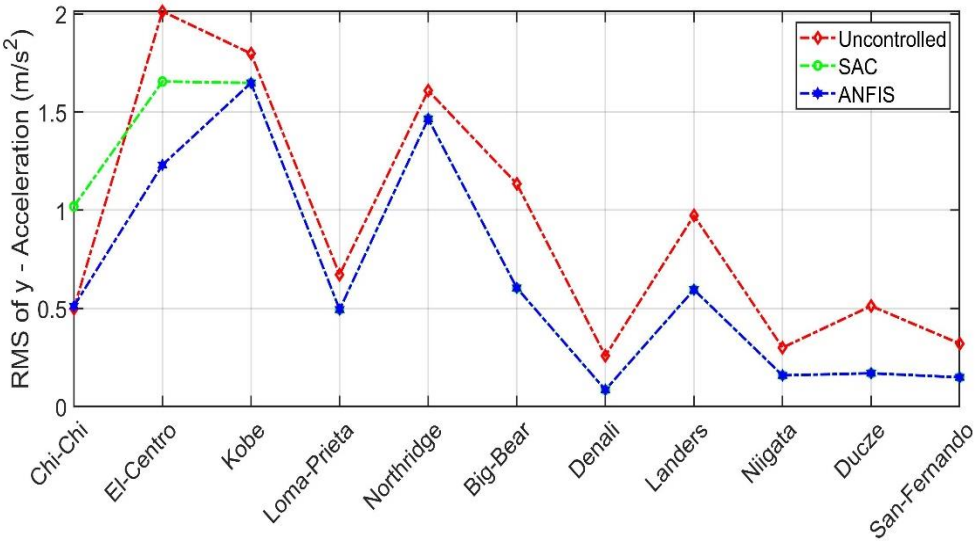

Figure 69: RMS of the acceleration responses of symmetrical Building 1 (a) *x*-direction and (b) *y*-direction.

(a)

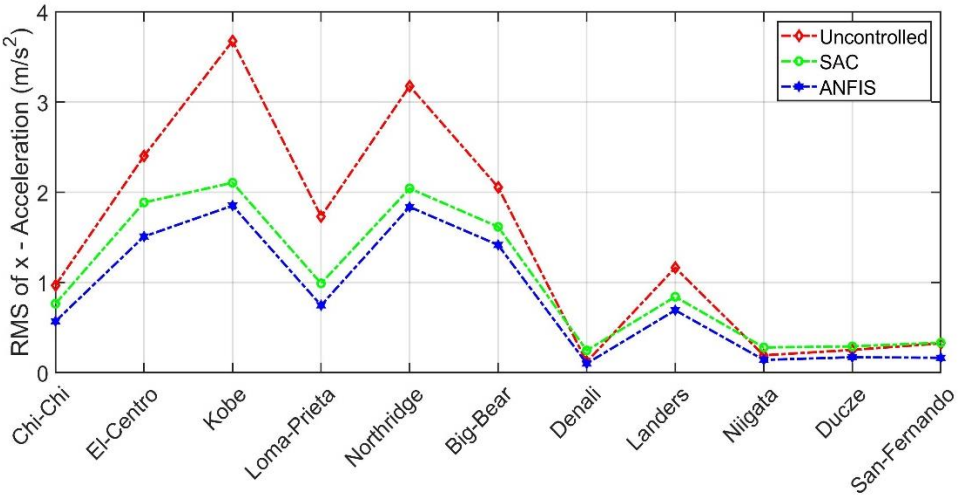

(b)

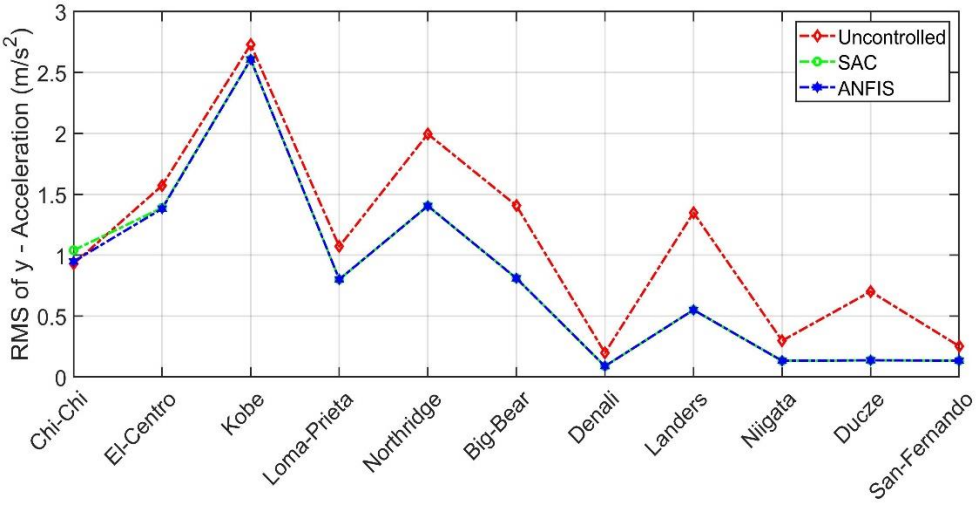

Figure 70: RMS of the acceleration responses of symmetrical Building 2 (a) *x*-direction and (b) *y*-direction.

To generalize the results for the eleven pairs of earthquakes, mean of the RMS displacements and accelerations is calculated in Table 16 and Table 17, respectively. From Table 16, the mean of the RMS displacements of Building 1 along *x*-direction is reduced by 42% and 54% for SAC and ANFIS, respectively. For Building 2, 29% and 41.9% reduction in *x*-displacement for Building 2 using SAC and ANFIS, respectively.

Moreover, the RMS displacements along *y*-direction have been also significantly attenuated equally by 50% for Building 1 and 41.6% and 26.3% for Building 2 using SAC and ANFIS, respectively. Interestingly, the rotational motions of the coupled buildings have been greatly mitigated where 48.8% and 41.8% reductions are achieved for Building 1 by SAC and ANFIS, respectively and 47.4% and 42% for Building 2.

Table 16: Mean values of symmetrical Building 1 RMS responses.

	x-disp. (B#1)	*x*-disp. (B#2)	*y*-disp. (B#1)	*y*-disp. (B#2)	θ-rot. (B#1)	θ-rot. (B#2)
Uncontrolled	0.034	0.031	0.036	0.024	0.0043	0.0038
SAC	0.024	0.022	0.018	0.014	0.0022	0.0020
ANFIS	0.022	0.018	0.018	0.019	0.0025	0.0022

Mean of the translational accelerations along *x* and *y* directions for the top floors of both buildings are also calculated in Table 17. For instance, the acceleration along *x*-direction for Building 1 has been mitigated by 29.4% by SAC and 35% by ANFIS while the absolute *x*-acceleration of the top floor of Building 2 is reduced by 29% and 41.9% using SAC and ANFIS, respectively. Further, SAC and ANFIS achieved 50% reduction in the acceleration along *y*-direction for Building 1 while the absolute *y*-acceleration of the top floor of Building 2 is reduced by 41.6% and 20.8% using SAC and ANFIS, respectively. The rotational acceleration of the coupled system is not considered for the comparison since it is less significant than the translational accelerations.

Table 17: Mean values of symmetrical Building 2's RMS responses.

	x- acceleration (B#1)	*x*- acceleration (B#2)	*y*-acceleration (B#1)	*y*-acceleration (B#2)
Uncontrolled	0.034	0.031	0.036	0.024
SAC	0.024	0.022	0.018	0.014
ANFIS	0.022	0.018	0.018	0.019

Regarding the maximum values of the translational and rotational displacements, a descriptive statistic is used to highlight the performance of the adaptive controllers versus the uncontrolled coupled structure. Both mean and standard deviation (SD) are calculated for both the translational displacements of both buildings. SD is a measure of data dispersion around the mean. Figure 71 and Figure 72 depict mean ± SD values of the *x* and *y*-displacements of all floors for both controlled and uncontrolled buildings. These figures show that the adaptive controllers not only reduce the mean of the peak displacements, but also reduce the data spread around the mean as shown in the error bar in the above figures.

(a)

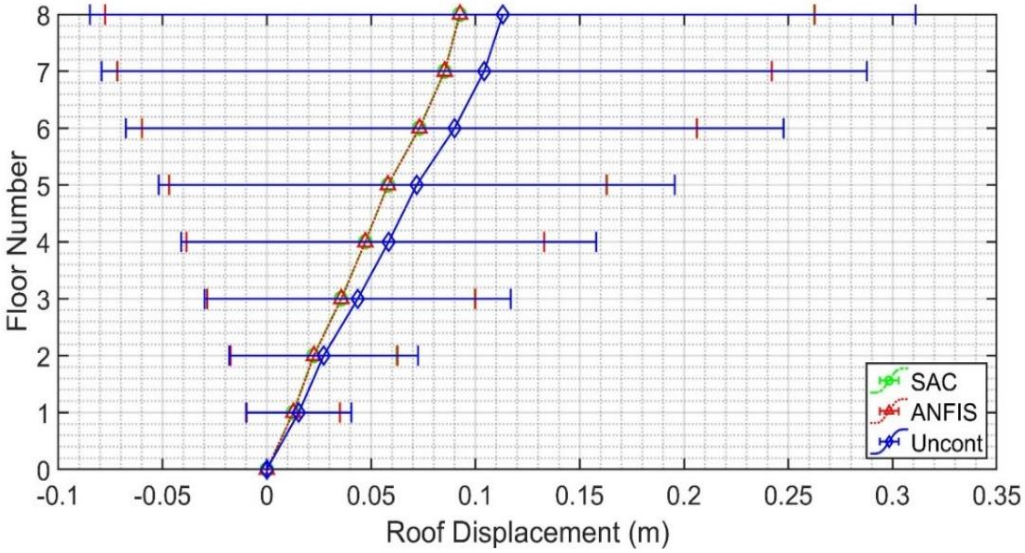

(b)

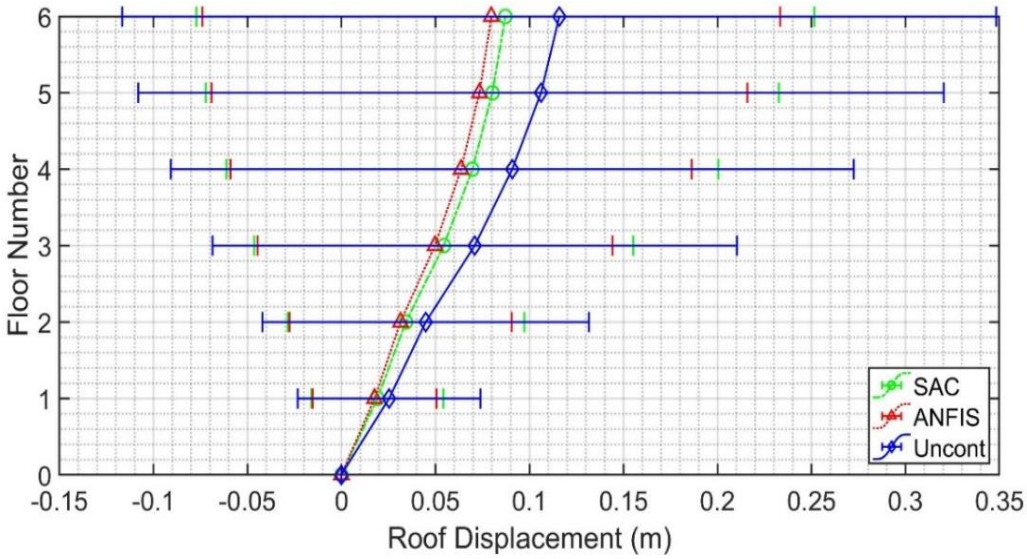

Figure 71: Mean ± SD of peak *x*-displacements of the top floors of uncontrolled, SAC, and ANFIS: (a) Building 1 and (b) Building 2.

(a)

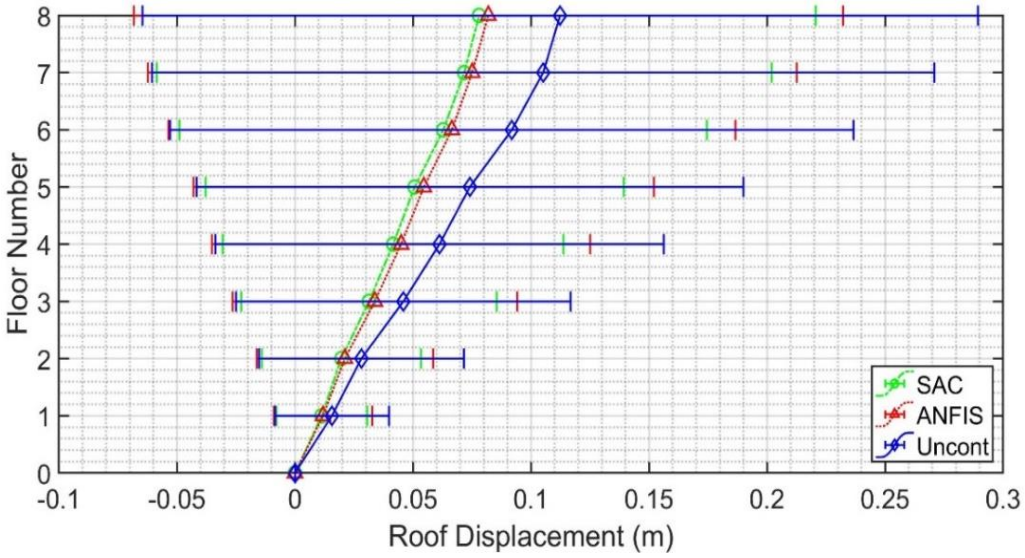

(b)

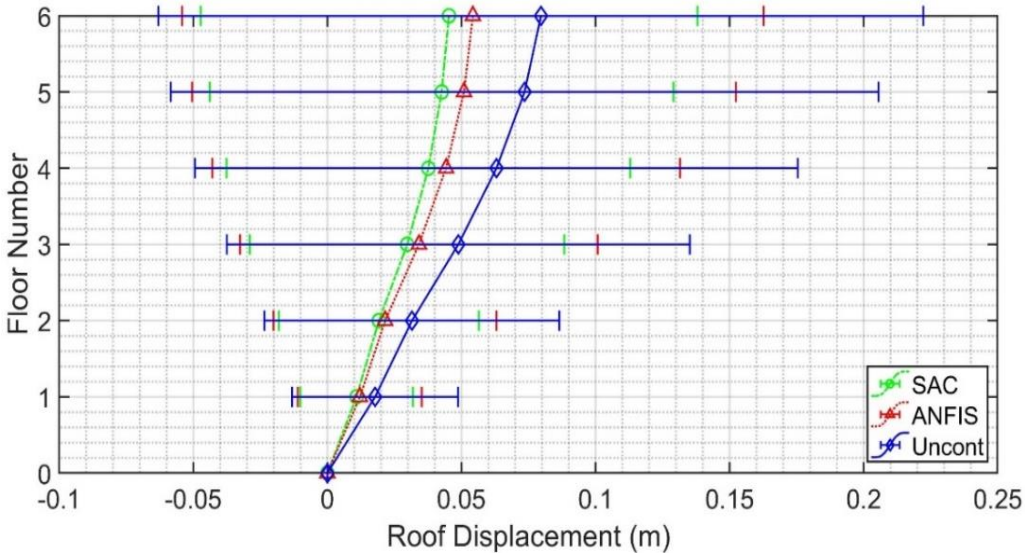

Figure 72: Mean ± SD of peak *y*-displacements of the top floors of uncontrolled, SAC, and ANFIS: (a) Building 1 and (b) Building 2.

6.4.2 Simulations for Asymmetrical Buildings

The asymmetrical individual buildings have a potential to develop torsional responses because of presence of eccentricities. In such systems, an excitation in one direction causes a building to move in all directions and ;therefore, there is independent

motion as in symmetrical building discussed in the previous section. For instance, applying an earthquake along *x*-direction develops translational responses along *x* and *y* directions as well as rotational motion about the vertical axis and vice versa. Figure 73 depicts the results of the displacement time histories when Kobe (N-S component) earthquake applied along *x*-direction only. It is obvious that the responses in all directions. Figure 74 depicts the time history displacements and rotation of the coupled system under Kobe (E-W component) when is applied along *y*-direction only.

Figure 75 through Figure 77 depict the time histories of the Building 1's top floor *x* and *y* translational displacements as well as the rotational ones. These figures prove that the seismic structural responses have been alleviated by the adaptive controllers. Again, the performance might differ from one earthquake to another and from one adaptive controller to another as discussed in the previous section. Surprisingly, the rotational motion of the coupled system is significantly mitigated by placing the control devices along *x* and *y* directions only.

The efficacy of using the adaptive controllers for mitigating the overall seismic performances of both buildings in all directions is also monitored. The RMS response under each earthquake's component is calculated. Figure 78 and Figure 79 depict the RMS of the translational and rotational displacements of both buildings under all the eleven earthquakes. Both figures show that a significant reduction in the overall displacements in all directions has been achieved by both ANFIS and SAC, respectively. Figure 80 and Figure 81 depict the accelerations for both buildings along *x* and *y*-directions, respectively. For the overall *x*-acceleration depicted in Figure 81a, SAC performs better than ANFIS as

the latter exacerbates the acceleration for Building 2. For *y*-acceleration, both SAC and ANFIS reduce the structural acceleration with an exception that ANFIS has two data point off for Building 1.

(a)

(b)

(c)

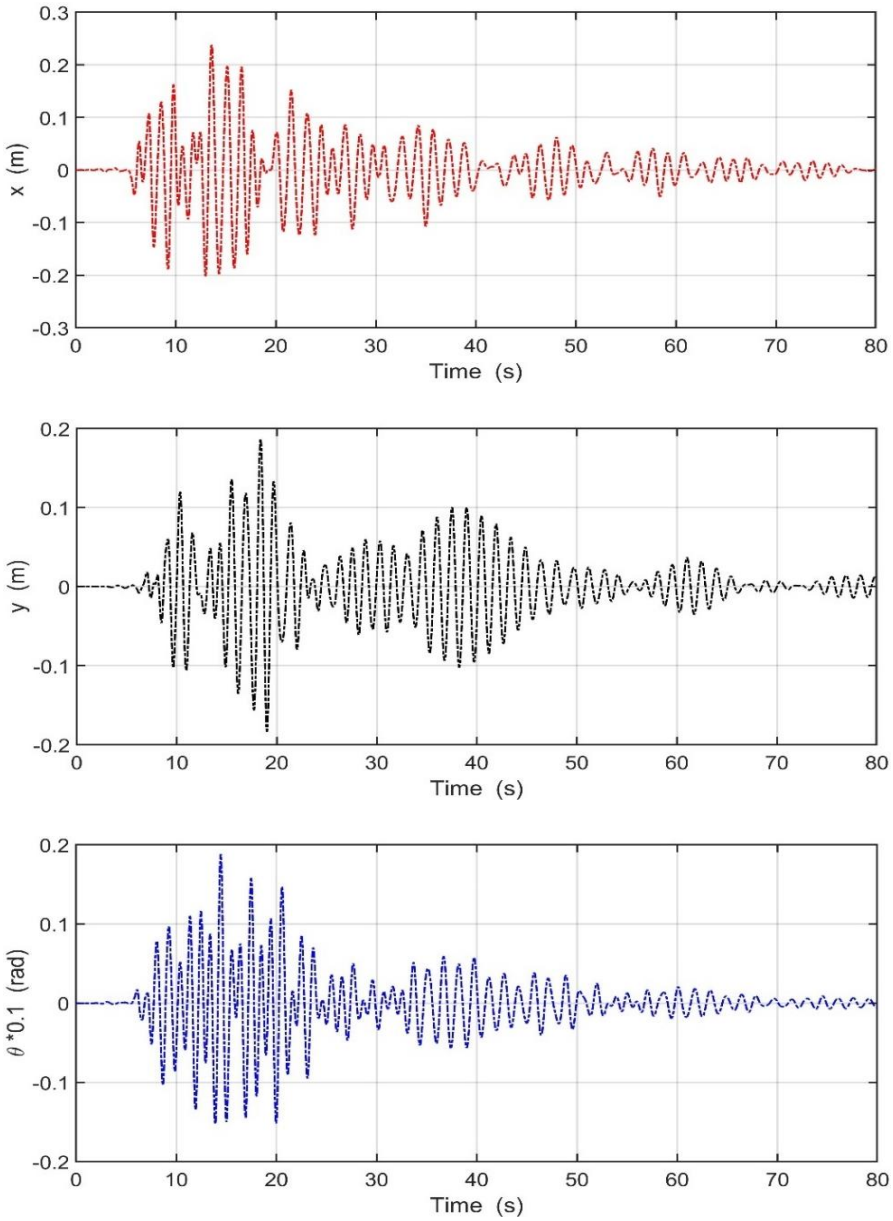

Figure 73: Time histories of the top floor of Building 1 under Kobe N-S component only: (a) *x*-motion, (b) *y*-motion, and (c) *θ*-motion.

(a)

(b)

(c)

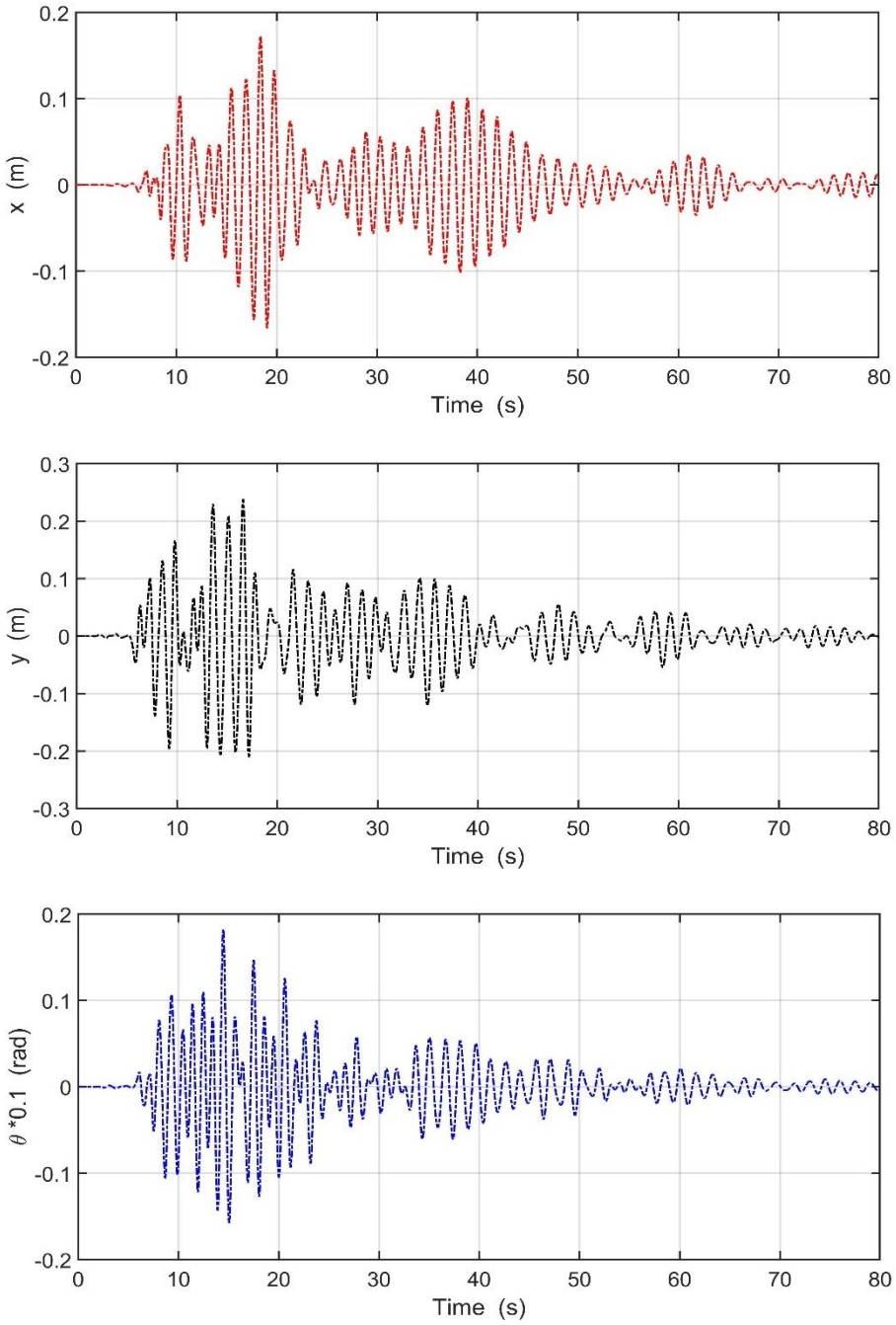

Figure 74: Time histories of the top floor of Building 1 under Kobe E-W component only: (a) *x*-motion, (b) *y*-motion, and (c) θ-motion.

(a)

(b)

(c)

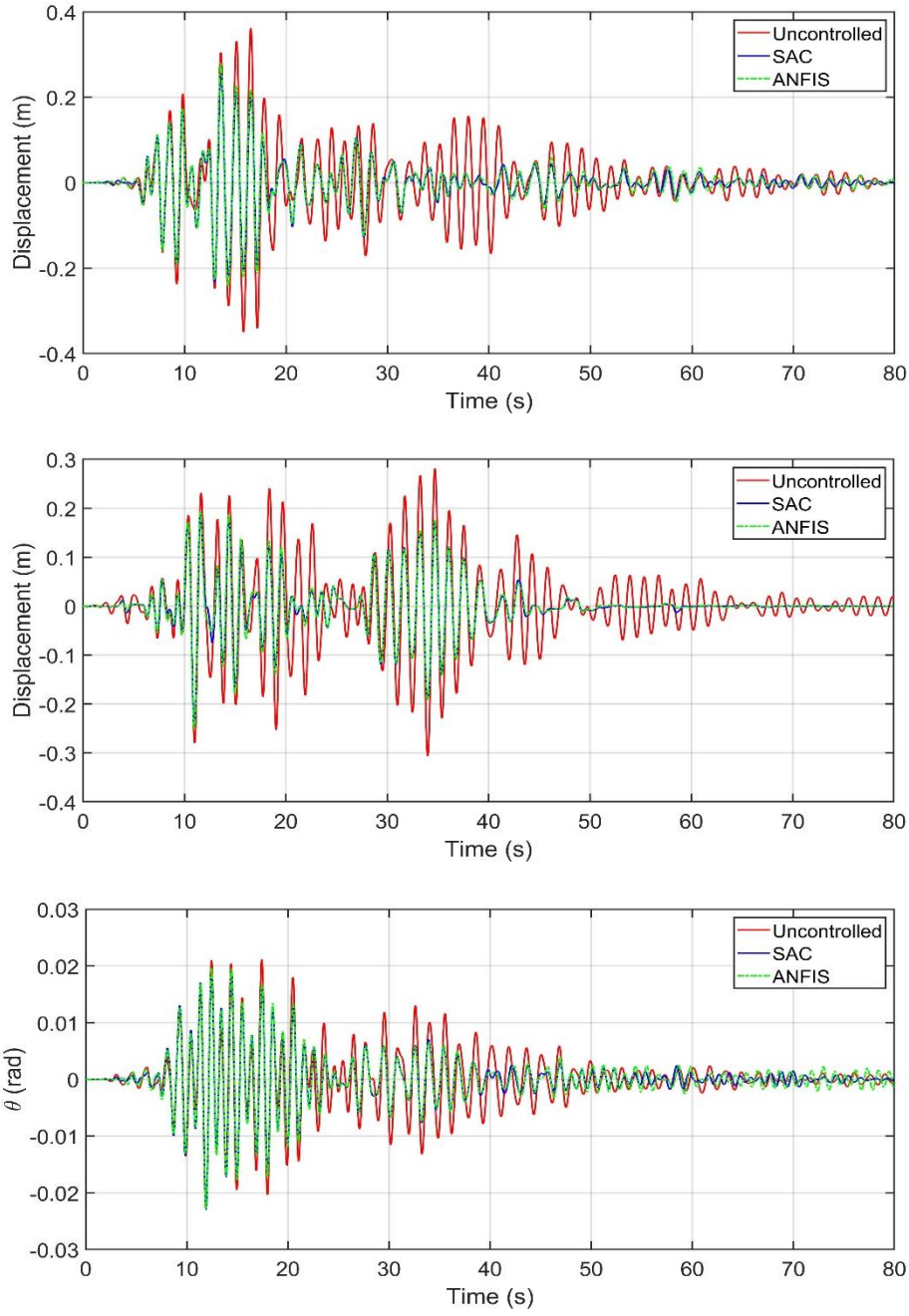

Figure 75: Time histories of the Building 1's top floor responses under Kobe earthquake: (a) *x*-motion, (b) *y*-motion, and (c) θ-motion.

(a)

(b)

(c)

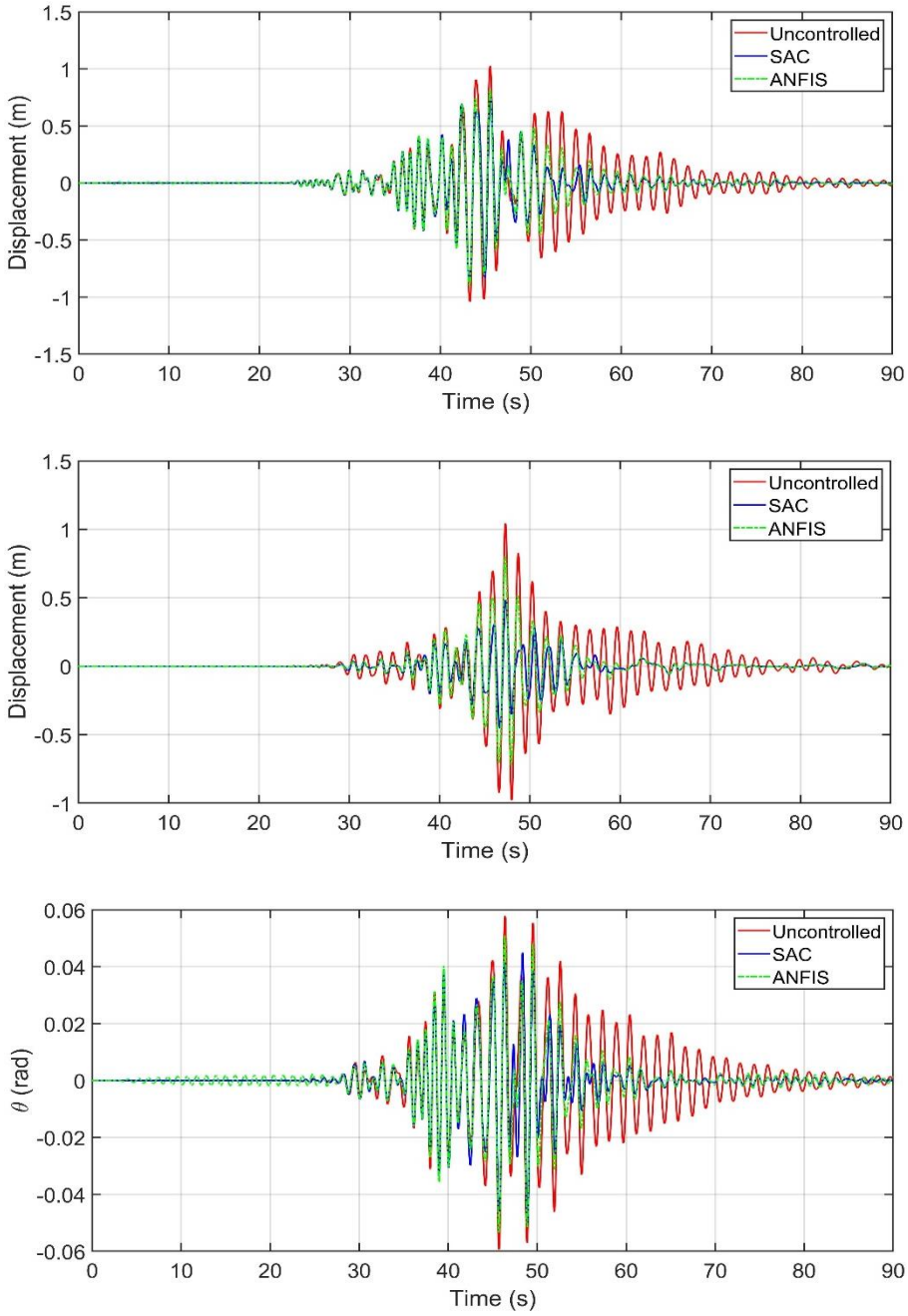

Figure 76: Time histories of the Building 1's top floor responses under Chi-Chi earthquake: (a) *x*-motion, (b) *y*-motion, and (c) θ-motion.

(a)

(b)

(c)

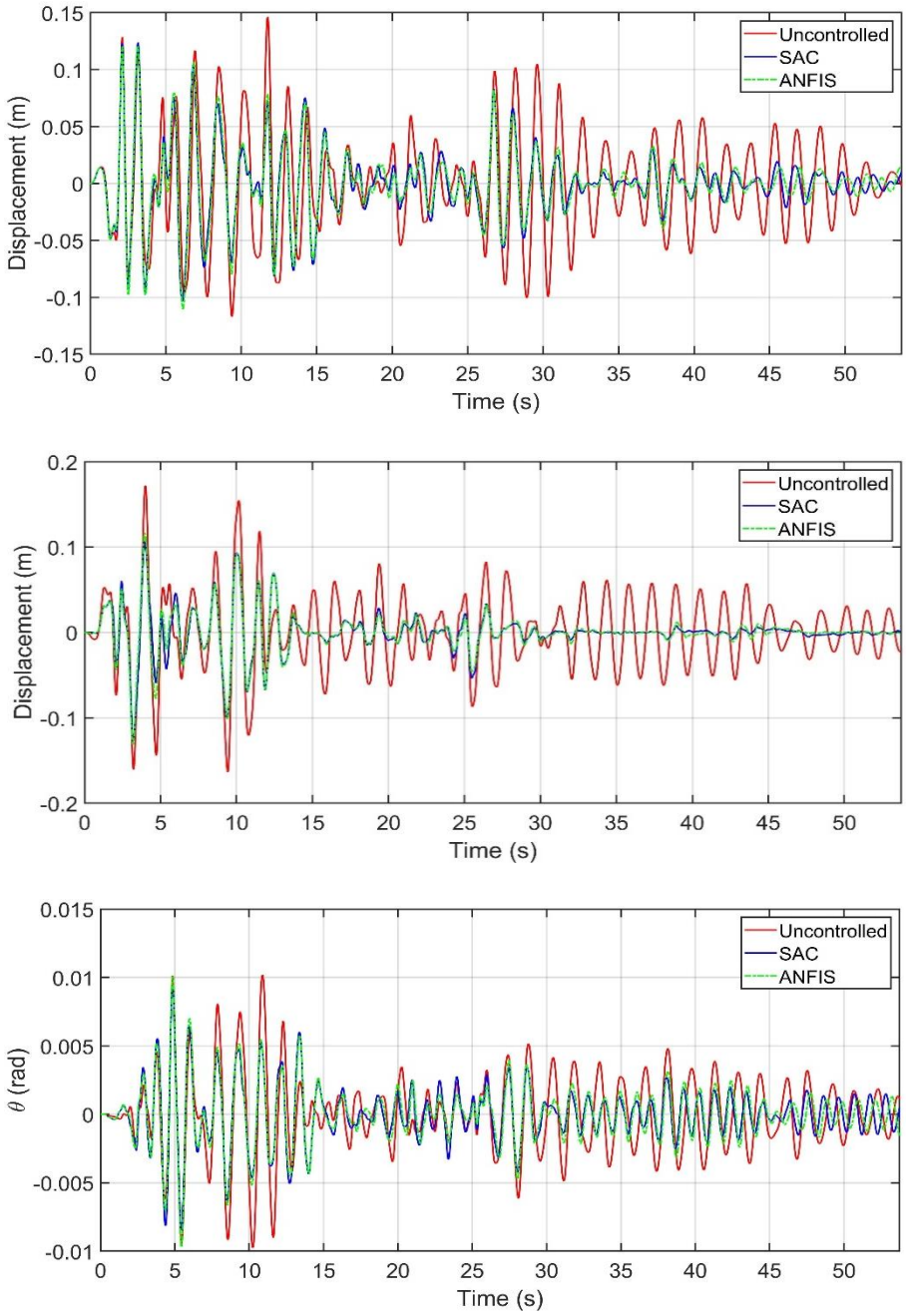

Figure 77: Time histories of the Building 1's top floor responses under El-Centro earthquake: (a) *x*-motion, (b) *y*-motion, and (c) θ-motion.

(a)

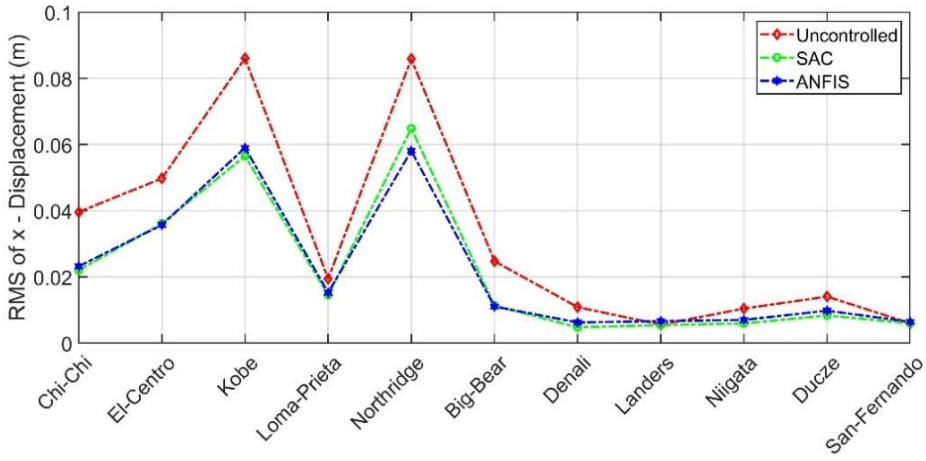

(b)

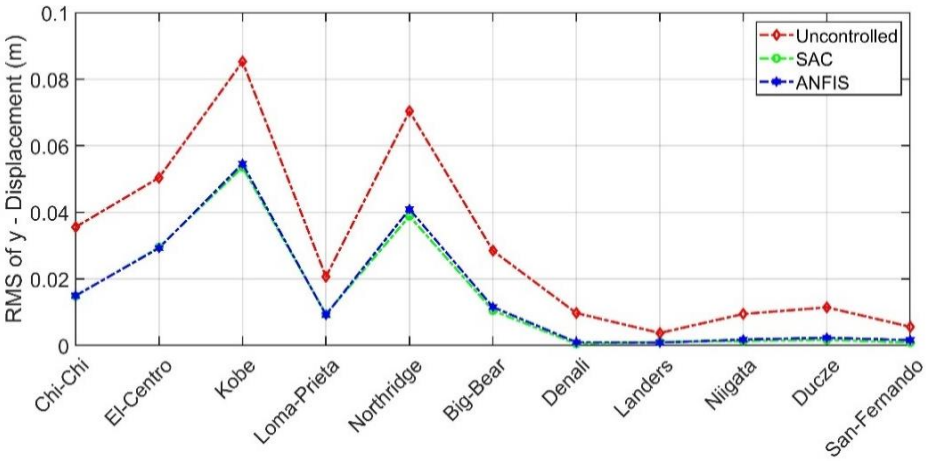

(c)

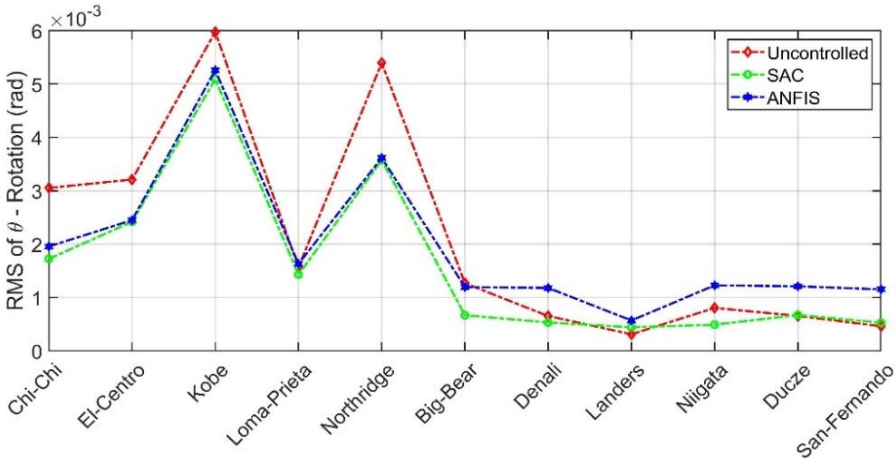

Figure 78: RMS of the structural displacements of asymmetrical Building 1: (a) *x*-direction, (b) *y*- direction, and (c) θ-rotation.

(a)

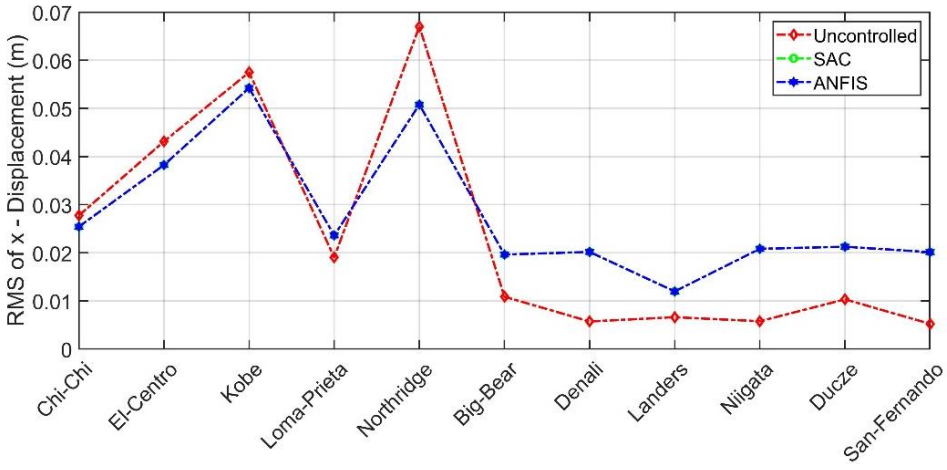

(b)

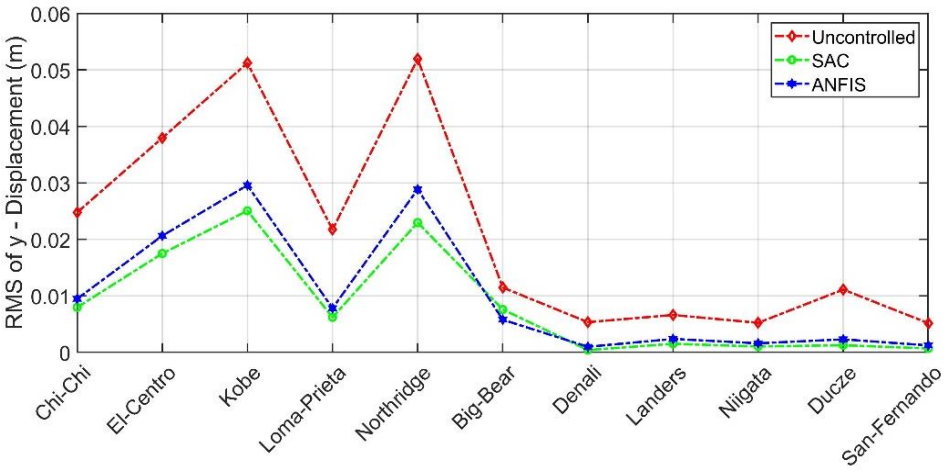

(c)

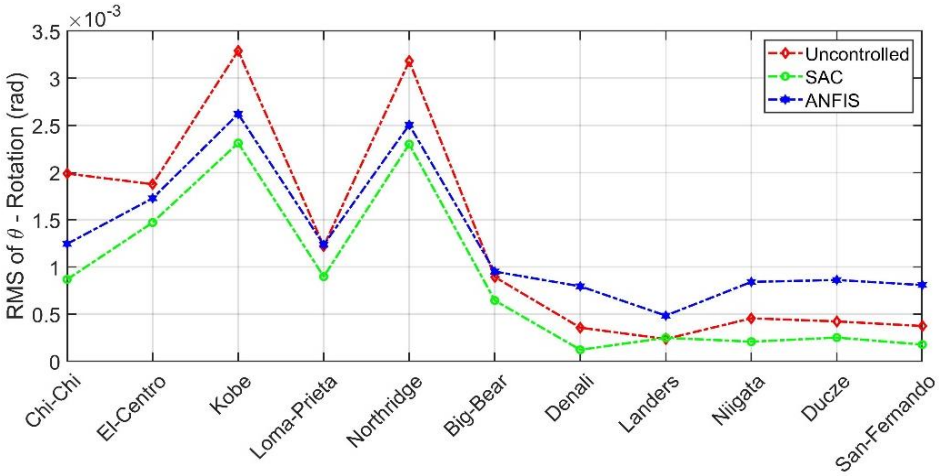

Figure 79: RMS of the structural displacements of asymmetrical Building 2: (a) *x*-direction, (b) *y*- direction, and (c) θ-rotation.

(a)

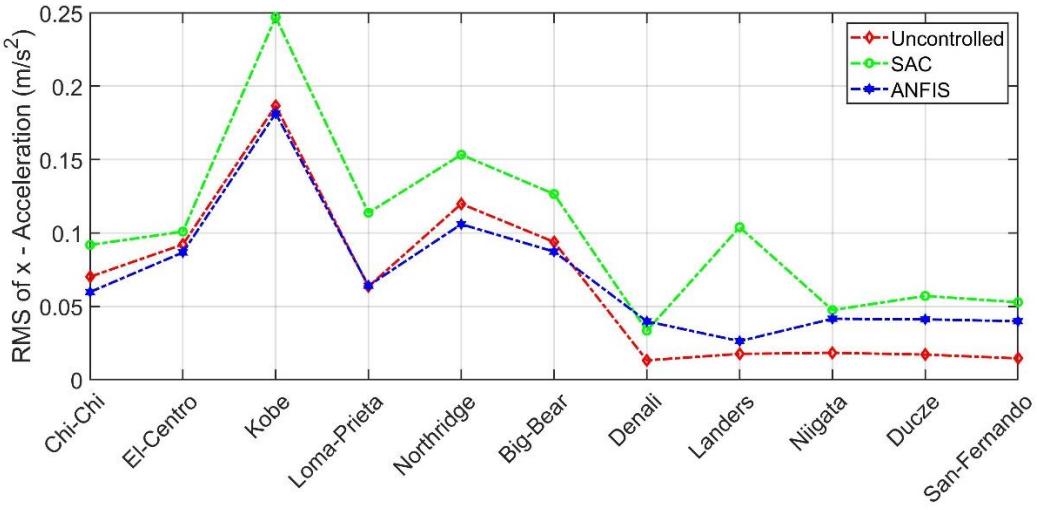

(b)

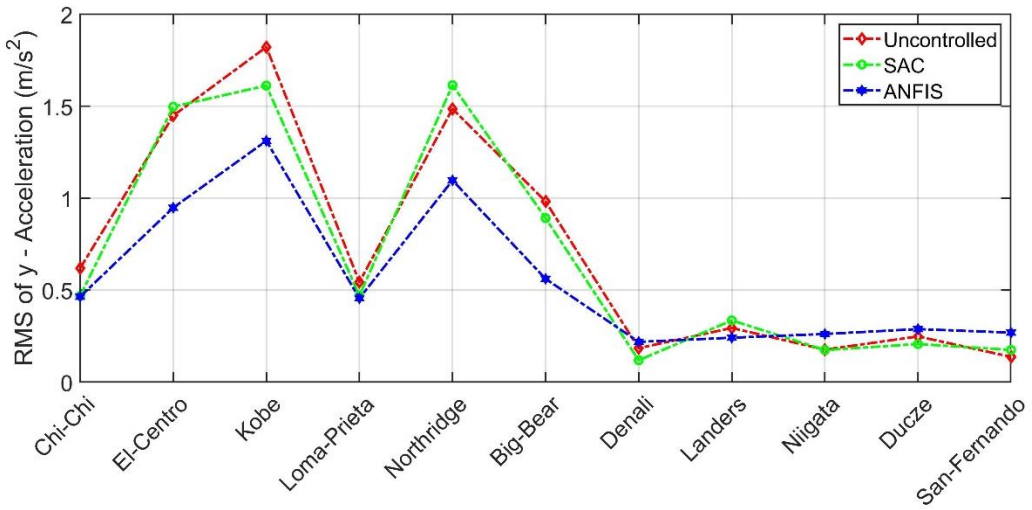

Figure 80: RMS of the structural accelerations of asymmetrical Building 1: (a) *x*-direction, and (b) *y*- direction.

(a)

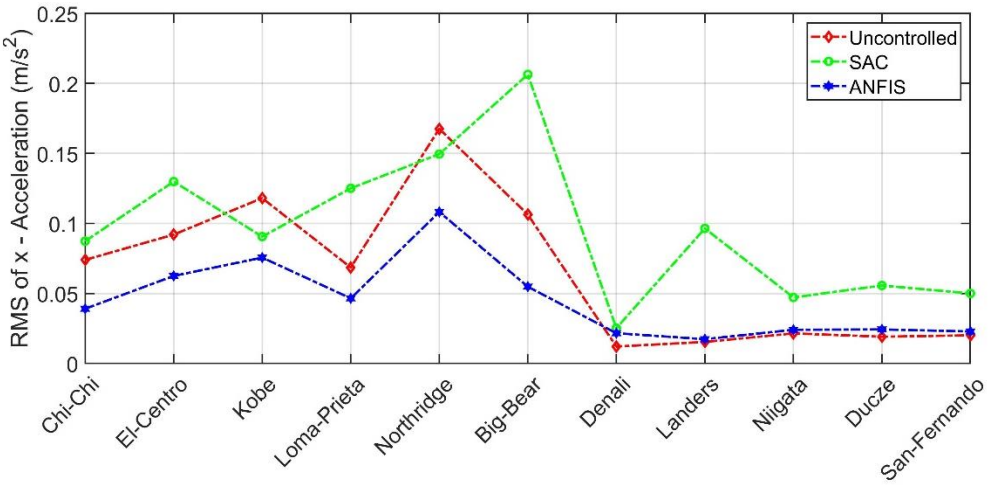

(b)

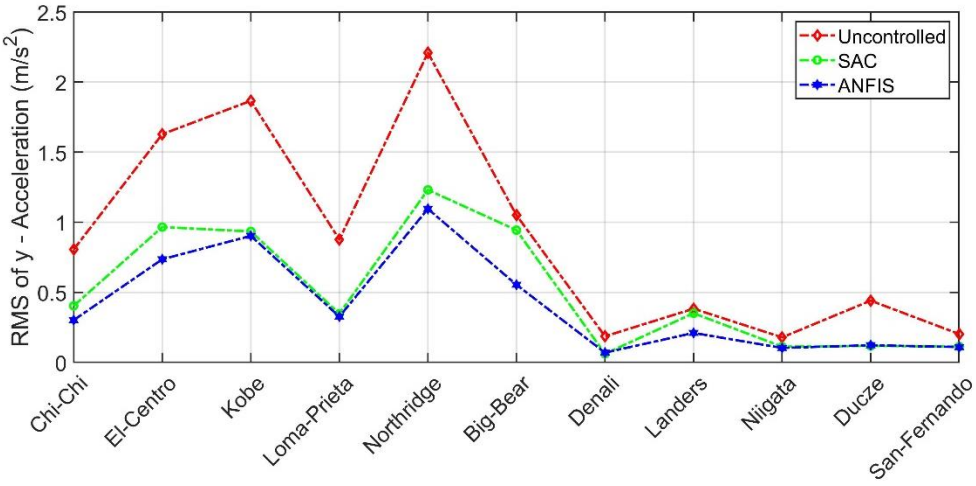

Figure 81: RMS of the structural accelerations of asymmetrical Building 2: (a) *x*-direction, and (b) *y*- direction.

Mean of the RMS displacements and accelerations is calculated in Table 18 and Table 19, respectively. From Table 18, the mean of the RMS displacements of Building 1 along *x*-direction is reduced by 34% and 31% for SAC and ANFIS, respectively. For Building 2, there is an increase in the mean value by 16% for SAC and ANFIS, respectively. Moreover, the RMS displacements along *y*-direction have been also

significantly attenuated equally by 50% for Building 1 and 62% and 55% for Building 2 using SAC and ANFIS, respectively. The rotational motions of the coupled buildings have been greatly mitigated where 24% and 9.5% reductions are achieved for Building 1 by SAC and ANFIS, respectively and 30.7% and 0% for Building 2.

Table 18: Mean values of asymmetrical Building 1 RMS responses.

	x-disp. (B#1)	*x*-disp. (B#2)	*y*-disp. (B#1)	*y*-disp. (B#2)	θ-rot. (B#1)	θ-rot. (B#2)
Uncontrolled	0.032	0.024	0.030	0.021	0.0021	0.0013
SAC	0.021	0.028	0.015	0.008	0.0016	0.0009
ANFIS	0.022	0.028	0.015	0.010	0.0019	0.0013

Mean of the translational accelerations along *x* and *y* directions for the top floors of both buildings are also calculated in Table 19. The acceleration along *x*-direction for Building 1 has been slightly increased by 9.3% by ANFIS, but with 61% by SAC while the absolute *x*-acceleration of the top floor of Building 2 is reduced by 29% and 41.9% using SAC and ANFIS, respectively. Further, SAC and ANFIS achieved 50% reduction in the acceleration along *y*-direction for Building 1 while the absolute *y*-acceleration of the top floor of Building 2 is reduced by 30.7% by ANFIS, but with 49% increase by SAC.

Table 19: Mean values of asymmetrical Building 2 RMS responses.

	x- acceleration (B#1)	*x*- acceleration (B#2)	*y*-acceleration (B#1)	*y*-acceleration (B#2)
Uncontrolled	0.064	0.065	0.722	0.893
SAC	0.103	0.097	0.688	0.507
ANFIS	0.070	0.045	0.556	0.412

Regarding the maximum values of the translational and rotational displacements, both mean and standard deviation (SD) are calculated for both buildings. Figure 82 and Figure 83 depict mean ± SD values of the *x* and *y*-displacements of all floors for both asymmetrical controlled and uncontrolled buildings. These figures show that the adaptive controllers reduce both mean and SD for all floors of both buildings.

(a)

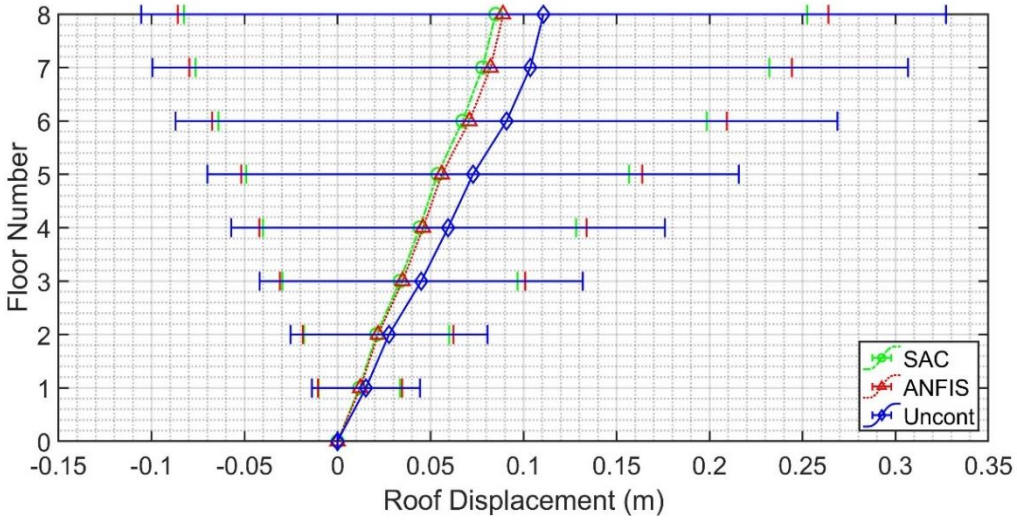

(b)

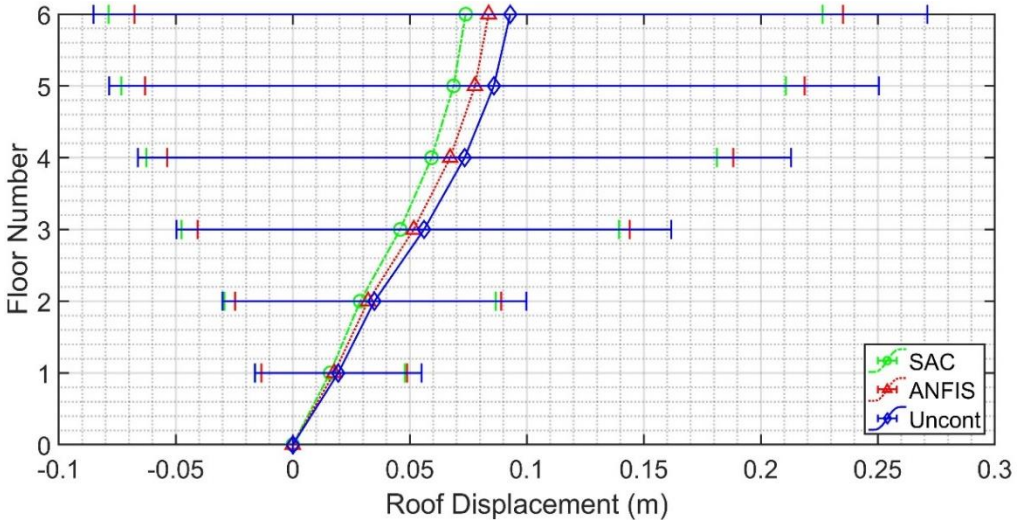

Figure 82: Mean ± SD of peak *x*-displacements of the top floors of uncontrolled, SAC, and ANFIS: (a) Building 1 and (b) Building 2.

(a)

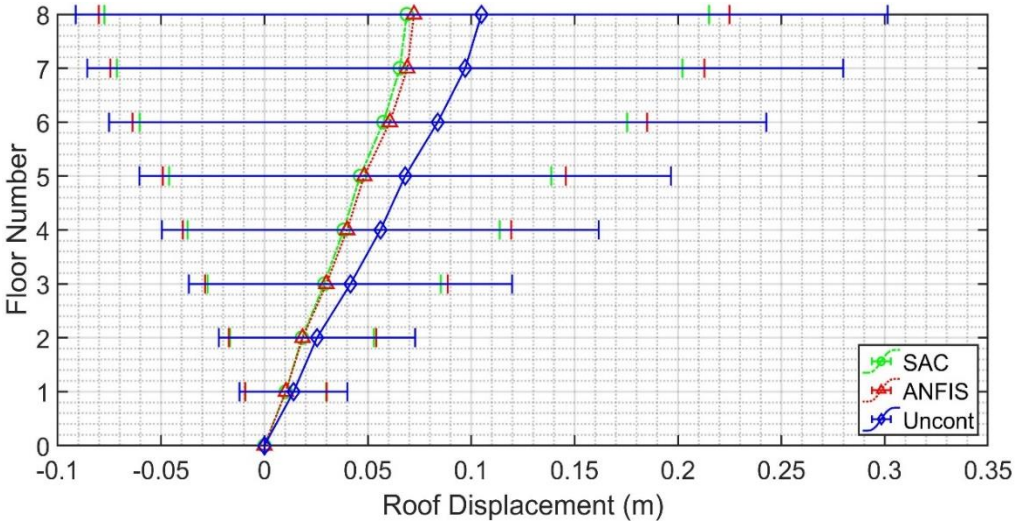

(b)

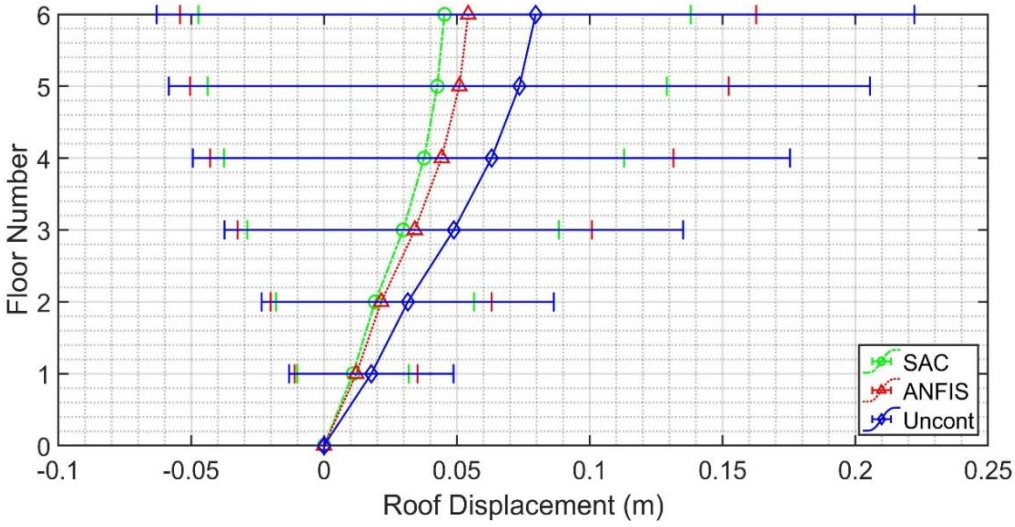

Figure 83: Mean ± SD of peak *y*-displacements of the top floors of uncontrolled, SAC, and ANFIS: (a) Building 1 and (b) Building 2.

6.5 Effect of Link End Connection

Different types of end connections can be designed to connect a skybridge to adjacent buildings. However, the connection type might have an impact on the overall structural performance of the coupled system. On the other hand, some connections eliminate the coupling effect between the buildings as in the case of the roller support.

Study of different connections for fully passive links were conducted few studies (Christenson, 2001, Atheer, 2017). In contrast to the passive, connection types have no effect on the structural performance when the links are provided with MR dampers as shown Figure and Figure. The reason is that when a damper is provided within the link, any effect due to the type of connection is absorbed by the damper keeping the performance almost the same. The following two figures depict the seismic performance of the asymmetrical coupled system under Kobe and El-Centro earthquakes, respectively.

(a)

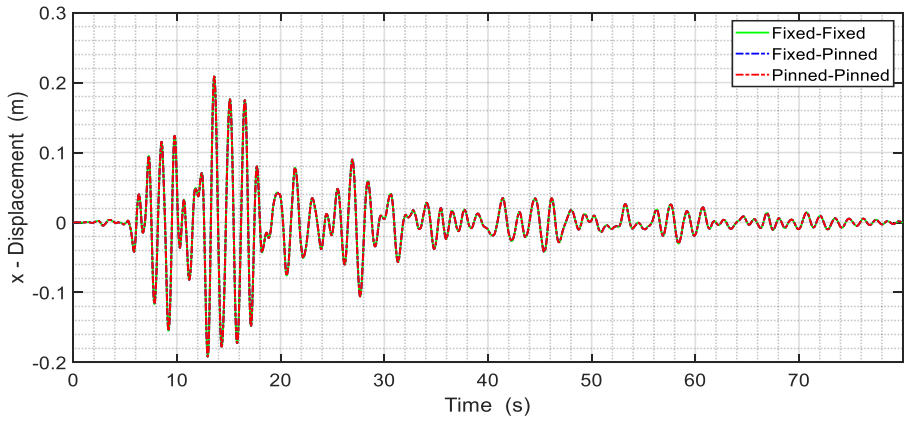

(b)

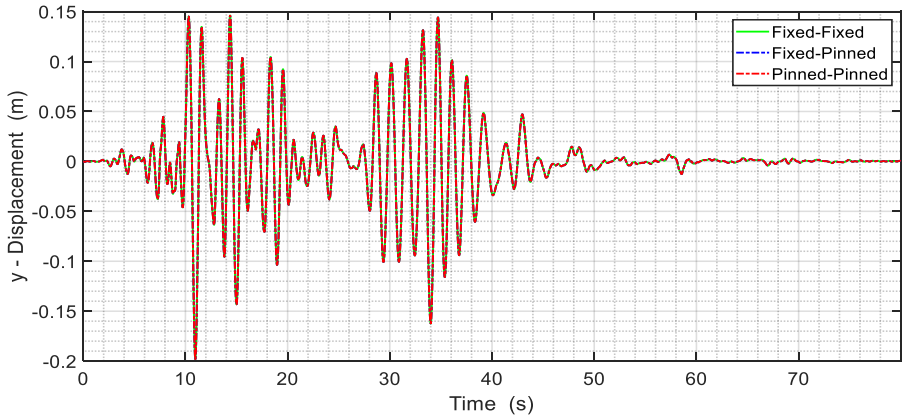

Figure 84: Time histories of the asymmetrical Building 1's responses under Kobe earthquake: (a) *x*-motion, (b) *y*-motion, and (c) θ-motion.

(c)

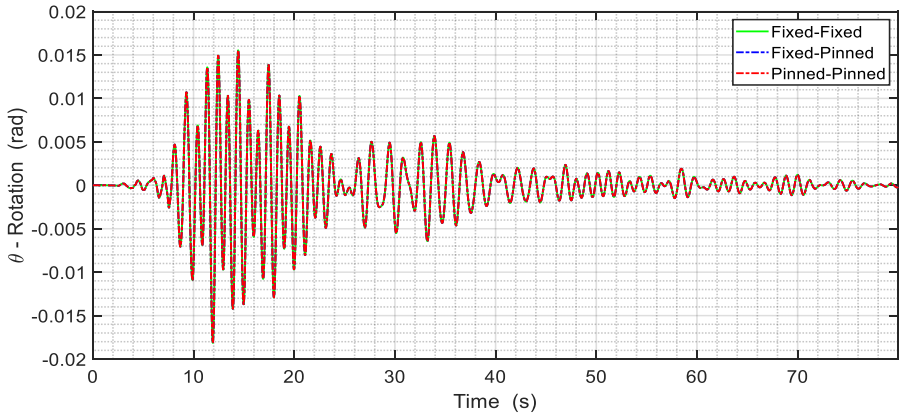

Figure 84: Continued.

(a)

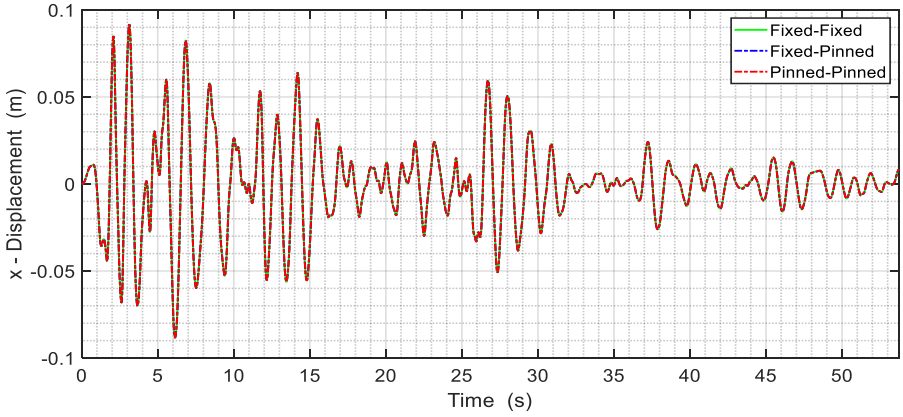

(b)

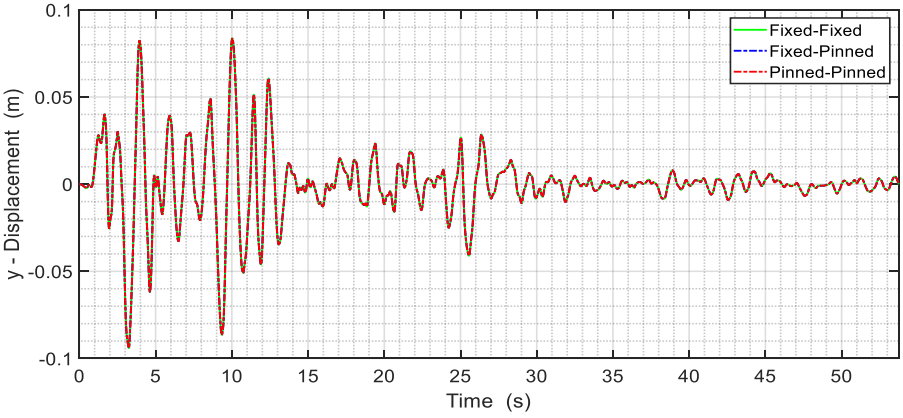

Figure 85: Time histories of the asymmetrical Building 1's responses under El-Centro earthquake: (a) *x*-motion, (b) *y*-motion, and (c) θ-motion.

(c)

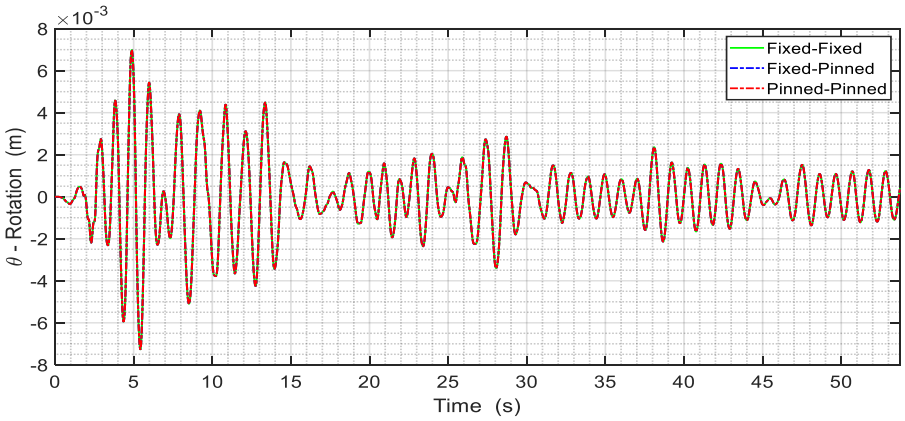

Figure 85: Continued.

6.6 Epilogue

The objective of the current chapter is to investigate the efficacy of two adaptive control methods to mitigate three-dimensional coupled buildings connected by MR dampers and subjected to bi-directional excitations. The adaptive controllers are SAC and ANFIS with displacement feedback. The modeling of the three-dimensional structure was developed for two cases: (1) both buildings are symmetrical and (2) both buildings are asymmetrical. In the first case, it is found that the motion along *x*-direction is uncoupled from the other motions and can be solved independently. It was also found, for the first case, that the rotational motion purely due to coupling is very small and can be neglected. For the asymmetrical buildings case, all the motions need to be considered even when the external disturbance is applied along one direction. It was found that the rotational responses for the asymmetrical buildings can be alleviated by providing control devices along *x* and *y* directions only. The numerical simulations with several pairs of ground motions show that driving MR dampers connecting two adjacent buildings by the adaptive

controllers developed in this chapter can effectively alleviate the seismic responses of the three-dimensional coupled system.

References

Atheer, K., Jumaah. (2017). *Structural Coupling of High-Rise Buildings Linked By Skybridges.* (Master of Science), Texas A&M University,

Chopra, A. K. (2012). *Dynamics of structures : theory and applications to earthquake engineering. 4th ed. Anil K. Chopra*: Boston : Prentice Hall, ©2012.

Christenson, R. E., & Spencer, B. F. (2001). *Semiactive control of civil structures for natural hazard mitigation: analytical and experimental studies.* directed by B. F. Spencer, for the Department of Civil Engineering and Geological Sciences. University of Notre Dame.

Lim, J., Bienkiewicz, B., & Richards, E. (2011). Modeling of structural coupling for assessment of modal properties of twin tall buildings with a skybridge. *Journal of Wind Engineering and Industrial Aerodynamics, 99*(5), 615-623. doi:https://doi.org/10.1016/j.jweia.2011.02.010

Paultre, P. (2013). *Dynamics of structures*: John Wiley & Sons.

Paz, M. (2012). *Structural dynamics: theory and computation*: Springer Science & Business Media.

Song, J., & Tse, K. T. (2014). Dynamic characteristics of wind-excited linked twin buildings based on a 3-dimensional analytical. *Engineering Structures, 79*, 169-181.

CHAPTER VII

SUMMARY, CONCLUSIONS, AND FUTURE STUDIES

7.1 Summary and Conclusions

The current research studied the effectiveness of using adaptive control for enhancing the seismic performance of coupled buildings by semi-active or active devices. The magneto-rheological (MR) damper was used as a semi-active device, while the hydraulic actuator was used as an active device. Very realistic models were used for both devices to capture their actual behavior. The dynamic characteristics of multi-story coupled buildings are modeled and investigated. The simple adaptive control (SAC) method was used throughout this dissertation to drive the control devices connecting two adjacent buildings. Also, the adaptive neuro-fuzzy inference systems (ANFIS) was used as another example of adaptive control. Different models of coupled structures under different earthquake recordings were examined in this research.

In chapter three, two connected linear adjacent buildings with different heights were considered to form the coupled system. SAC was used to regulate these devices under seismic excitations. Both the MR damper and the hydraulic actuator were employed to test the efficacy of SAC with different types of control schemes. SAC with displacement feedback was first utilized to control the coupled system with the original design parameters. Then, SAC was used to control the system in the presence of noise and parameter changes. Change is the structural parameters was reflected as a reduction in the mass and stiffness properties of the original system. The damaged system was considered

to show the potential of the adaptive controller to cope with parameter variations under the seismic actions. Noisy measurements were generated as Gaussian random vibrations and then added to the actual measurements to emulate the situation in real-world applications. The performance of SAC was compared with two semi-active algorithms: optimal control theory and Lyapunov stability theory-based algorithm. A suite of five major earthquakes were selected to perform the dynamic analyses in the time domain. The results showed that SAC has a great potential in attenuating the seismic responses of the coupled system and in dealing with uncertainties and parameter variations. The results also showed that the MR damper was more effective than the hydraulic actuator in reducing the structural responses where the latter exacerbated the responses in some circumstances.

Civil structures usually experience inelastic behavior during earthquakes. Therefore, investigation of the performance of adaptive control for enhancing the inelastic behavior of coupled systems is paramount. In chapter four, nonlinear coupled structure is examined. The coupled system consisting of two buildings with the same height, but with different dynamic characteristics, was considered. The MR dampers controlled by SAC were used to connect the two buildings at three levels. A stable hysteretic behavior of the structural system was considered to capture the variation in flexibility and energy loss under various intensity levels of seismic events. The Bouc-Wen's nonlinear differential equation was used to model the hysteretic behavior of the restoring force-displacement smooth curve of the developed nonlinear structural system. The Bouc-Wen model is capable of mathematically tracking various shapes of the force-displacement curves by

adjusting its own parameters. The proposed nonlinear model was validated through a finite element model. The optimal control theory was also considered for sake of comparison. The results showed that using SAC to drive the MR dampers connecting two adjacent nonlinear buildings can be used to effectively alleviate the seismic responses and significantly reduce the permanent deformations.

The performance of SAC was compared with the adaptive neuro-fuzzy inference systems (ANFIS) in chapter five. ANFIS consists of a fuzzy logic controller provided with a learning algorithm based on adaptive neural networks. The learning algorithm is implemented to adjust the parameters of the fuzzy logic controller such that its outputs track the behavior of predetermined training data. Displacement, velocity, and acceleration feedbacks were employed to investigate the sensitivity of the adaptive controllers to the type of feedback. For the primary fuzzy logic controller, seven Gaussian membership functions were used to map the input (crisp) data into fuzzified values. The Fuzzy Logic Toolbox was used to carry out the numerical analyses. Undamaged and damaged coupled structures were considered in this chapter. The results showed that both SAC and ANFIS were promising in enhancing the structural performance under natural hazards. Specifically, SAC with displacement feedback proved to surpass the other schemes in the presence of parameter variations. Therefore, the displacement feedback was used in the next chapter where a more realistic coupled system was studied.

In chapter six, fully three-dimensional coupled system was considered to identify the sensitivity of the adaptive controllers to modeling. The structural system modeled as two three-dimensional buildings connected by frame elements in which the MR dampers

were implemented. The equations of motions of the three-dimensional model were formulated by assuming that each floor diaphragm is rigid in its own plane but flexible in the vertical plane. Each link is assumed to have three degrees-of-freedom, two translational and one rotational, at its ends. The MR dampers were controlled by adaptive neuro-fuzzy inference systems and simple adaptive control methods. The displacement feedback type is used for both control methods to design the closed-loop action. ANFIS was designed based on Sugeno-type model where seven triangular membership functions were chosen to fuzzify the input (crisp) in the fuzzy logic controller. The training data for ANFIS were generated by utilizing the LQR controller under white-noise excitation. For SAC, LQR was also employed to generate the desired trajectories of the reference-model. Numerical simulations were carried out for both symmetrical and asymmetrical coupled buildings under eleven pairs of major earthquakes. The results showed that both ANFIS and SAC can deal very successfully with modeling complexities. In terms of seismic response reduction, both methods have shown a great potential in enhancing the structural performance under bi-directional earthquakes.

7.2 Future Studies

In the current study, the maximum control force generated by the control devices is saturated to 1000 kN to meet the capacity of the available models. Future research might carry out an optimization study to identify effects of increasing the maximum control force and the corresponding impact on the structural behavior. Moreover, the optimization study can be conducted to determine the number and optimal configuration of the structural links

provided with control devices and driven by an adaptive controller to reach an optimum performance of the coupled systems.

To verify the current results, future studies including experimental testings might be conducted using coupled building models considering in-plane and out-of-plane motions.

The nonlinear coupled system model considered in this research is a shear-type model system. Future studies can consider fully three-dimensional models with fully nonlinear behavior where both materially and geometrical nonlinearities can be considered. Also, developing benchmark coupled buildings would be an interesting choice for future studies to consider quite realistic physical device sizes, force limits, and control constraints.

The tuning parameters within SAC were determined in this research by trial and error. Further investigation can be pursued on finding a guideline for choosing these parameters based on, for example, the structural system properties and the external disturbances.